Vibration Characteristics of Thin-Walled Noncircular Composite Cylinders

Hung-Chieh Lo

Dissertation submitted to the faculty of the Virginia Polytechnic Institute and State University in partial fulfillment of the requirements for the degree of

Doctor of Philosophy

In

Engineering Mechanics

Michael W. Hyer, Chair

Romesh C. Batra

Scott W. Case

Scott L. Hendricks

Kathy Lu

September 10, 2010

Blacksburg, VA

Keywords: Composite, Elliptical Cylinder, Fundamental Frequency

Vibration Characteristics of Thin-Walled Noncircular Composite Cylinders

Hung-Chieh Lo

ABSTRACT

The lowest natural frequencies of thin-walled noncircular fiber-reinforced composite cylinders, specifically cylinders with elliptical cross sections, are investigated. Of interest is the variation of the lowest natural frequency, the so-called fundamental frequency, as a function of wall laminate properties, cross-sectional eccentricity and other cylinder geometric parameters. Both simple and clamped support boundary conditions are investigated. Laminate properties that are uniform with circumferential location and laminate properties that vary with circumferential location, by way of varying laminate fiber angle with circumferential location, are considered. As the radius of curvature of a noncircular cylinder varies with circumferential location, it is logical to consider the influence of circumferentially varying fiber orientation on the fundamental frequency. The analysis for predicting the fundamental frequency is based on Donnell shell theory, linear elastic properties, and the use of Hamilton's Principle in conjunction with the Rayleigh-Ritz technique. By use of a so-called shape factor, the magnitude of cylinder normal displacements are modulated to be larger in the regions of the cross section with the largest radius of curvatures and smaller in the regions with the smallest radius of curvature. The final equations for predicting the fundamental frequency are quite complex, but a series of approximations results in a hierarchy of simpler equations, the simplest being referred to as Lo's approximation. The prediction of the fundamental frequencies is spot checked by comparing the results as predicted by the various levels of approximation with predictions of a shell-based finite element model. Considering uniform laminate properties, comparisons between the developed analysis and the finite element model are good for all levels of simpler equations, and excellent in some cases. The developed analysis is subsequently used for parameter studies. It is found that compared to a circular cylinder of the same circumference and with uniform laminate properties, the fundamental frequency of an elliptical cylinder is always less. Surprisingly, based on the results obtained, it appears that for a given cylinder geometry the fundamental frequency is not

particularly sensitive to wall lamination sequence, though the wave number in the circumferential direction of the mode shape associated with the fundamental frequency is sensitive to lamination sequence. Considering cylinders with circumferentially varying fiber orientation, comparisons between the developed analysis and the finite element model for most of the cases studied are good. However, the developed equations are limited since it is difficult to find a set of known functions to describe the deformation of an arbitrary lamination sequence when applying the Rayleigh-Ritz technique. In general, it can be concluded that the effect of varying fiber orientation on the fundamental frequency is much less than the influence of cylinder aspect ratio. It can also be concluded that the developed analysis would be an excellent tool for design purposes, as the calculation of the fundamental frequency is done quickly, and design trade-offs studies would be easy.

Acknowledgments

I am especially indebted to my advisor Dr. Michael W. Hyer for his guidance and advice. Throughout this part of my academic life, his patience and kindness have been the most important support of my research including this dissertation.

I would like to thank my committee members: Dr. Romesh C. Batra, Dr. Scott W. Case, Dr. Scott L. Hendricks, and Dr. Kathy Lu. I truly appreciate their thoughtful advice regarding to my learning these years and their valuable comments for this study. I am also thankful for the immeasurable help from all the people in Department of Engineering Science and Mechanics.

Finally, my sincerest gratitude is to my family. I would not have had the chance to pursue a degree far away from home without their heartily support and encouragement.

Table of Contents

List of Figures

List of Tables

Chapter 1 Introduction

Thin-walled cylindrical structures are commonly used to withstand varied kinds of loadings, such as axial compression, torsion, internal or external pressure, overall bending, and combinations of these. Practically speaking, circles have been chosen as the cross-sectional shape of the majority of cylindrical structures because of ease of fabrication, analysis, and design. Additionally, a circle has the maximum cross sectional area among the many shapes with the same circumference, implying that in terms of contained volume, a circular cross section may be the most effective. However, the use of a structure with a noncircular cross section may be required to satisfy particular design requirements. For example, in order to accommodate more passengers comfortably, the cross section of an aircraft might be designed to be noncircular. Other payload requirements or dimensional constraints may also dictate a noncircular design. Additionally, for aerodynamic reasons, in the case of aircraft, or hydrodynamic reasons, in the case of submersible vehicles, a noncircular cross section may be desirable. Therefore, it is necessary to be aware of the mechanical characteristics of cylindrical structures with noncircular cross sections.

One characteristic of structures that is important to understand is their vibration response. The low frequency resonance of structures is an issue that should be understood, as resonances often result in annoying vibration or noise. The lowest natural frequency of a structure, the so-called fundamental frequency, is an important factor in determining low frequency response. A low fundamental frequency means a greater response to near-by energy sources, large vibration amplitudes, and even reduced fatigue life. Ellipses are special cases of noncircular cross sections, and the primary interest in this study. In Fig. 1- 1 several elliptical cross sections are illustrated as solid lines, in addition to a circular cross section to the left. Each cross section has the same circumference and the radius of curvature at a generic point around the circumference is denoted as R. The locus of locations of the centers of curvature for the various cross sections are shown as dotted lines, and the maximum radius of curvatures, R_{max}, and the minimum radius of curvatures R_{min} are also illustrated. Considering cylindrical structures with cross sections of the same circumference, it is important to know whether the fundamental frequency of the cylindrical structure with a noncircular cross section is lower than the fundamental frequency of the cylindrical structure with a circular cross section, and if so, by how much less. In the context of cylinders

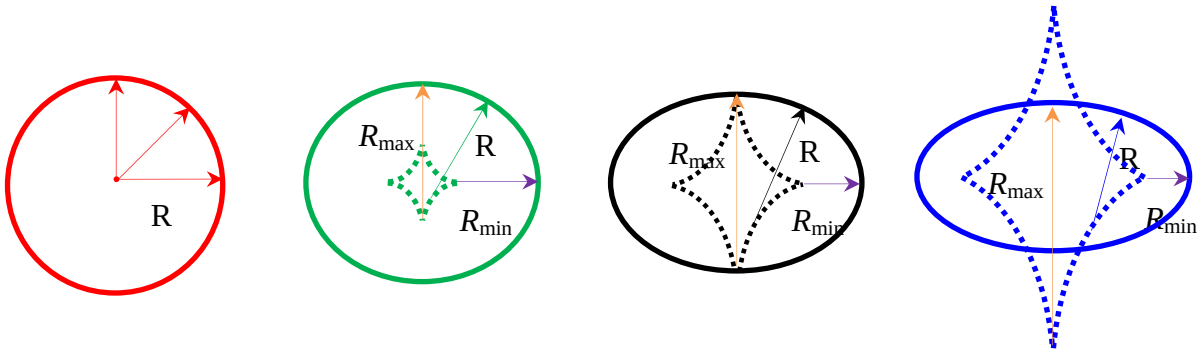

Fig. 1- 1 A circle and three ellipses with the same circumference

constructed of fiber-reinforced composite materials, if a noncircular geometry leads to reduced fundamental frequencies, the question can then be asked as to whether fiber-direction tailoring can be used to increase the fundamental frequency of noncircular cylinder to equal or at least approach the fundamental frequency of the circular cylinder. In particular, there is considerable interest in determining if varying the fiber angle of the composite material with circumferential position has any advantages for noncircular cross sections. In a recent study of the axial buckling characteristics of elliptical composite cylinders [1] it was found that varying the fiber angle with circumferential position compensated for the loss of buckling capacity due to the noncircular geometry. Basically the idea proposed [1] was that since the radius of curvature varied with circumferential position, perhaps varying the fiber angle, and therefore the axial and circumferential stiffness, with circumferential position would mitigate the effects of varying radius of curvature. An overarching objective of the work herein has this concept in mind for vibration response and it will be addressed directly.

Before the concept of varying the fiber angle with circumferential position is investigated, it is necessary to fully understand the effect of noncircular geometries on the vibration characteristics of thin-walled composite cylinders, especially the fundamental frequency, without the potentially complicating issue of variable fiber orientation. Elliptical cross sections are chosen here because of the convenient and well-established analytic representation of the geometry of an ellipse. It is believed, however, that the conclusions reached regarding vibration behavior of cylinders with elliptical cross sections apply to other noncircular geometries, and therefore the results presented

herein are considered general. So, a second overarching objective is to achieve an understanding of the effect various material and geometric parameters have on the fundamental vibration frequency of thin-walled elliptical cylinders.

In the next section, Section 1.1, the essential nomenclature of an elliptical cylindrical composite shell is presented. In Section 1.2 the definition of wave number is presented, and that is followed in Section 1.3 by a brief review of important literature relevant to understanding vibration characteristics of cylindrical shells. In Section 1.4 the objectives of this dissertation are described more specifically. Section 1.5, the last section of this chapter, provides a roadmap to the chapters to follow.

1.1 Geometry and Nomenclature for Description of an Elliptical Cylinder

As observed in Fig. 1- 1, unlike a circle, the radius of curvature of an ellipse is not the same at every location around the circumference. The flattest point of the cross section has the maximum radius of curvature, while the most highly curved point has the minimum radius of curvature. The classic cylindrical coordinate system is therefore not well suited for describing the geometry of the ellipse, rather a curvilinear coordinate system can be utilized when considering a cylindrical structure with an elliptical cross section. In Fig. 1- 2 an elliptical cylinder with length L, wall thickness H, semi-major dimension a, semi-minor dimension b, and circumference C is illustrated. Notice that a and b are distances from the cylinder axis to the mid-thickness location within the wall, hereafter referred to the reference surface location. As the global Cartesian coordinates are denoted by X, Y, and Z, a local curvilinear coordinate system is identified by the x-direction, which coincides with the axial direction of the cylinder, the s-direction, which is tangent to the reference surface, and the z-direction, which is normal to the reference surface. The radius of curvature, R, i.e., the inverse of the curvature, is the distance from the center of curvature to the reference surface and it varies, as mentioned, with circumferential location. For convenience, a circular cross section with the same circumference C as the ellipse is defined to have radius R_0, where

$$R_0 = \frac{C}{2\pi} \qquad \text{Eq. 1- 1}$$

The angle θ denotes the angle between the orientation of the fiber in any particular layer in the wall laminate and the axial direction. The displacements of a point on the reference surface in x-,

s-, and *z*-directions are denoted as *u*°, *v*°, and *w*°, respectively. The rotations about those directions on the reference surface are denoted as ϕ_x°, ϕ_s°, and ϕ_z°, respectively. The eccentricity, *e*, of the cross section can be written in terms of the so-called aspect ratio, *b*/*a*, by the relationship

$$e = \sqrt{1 - \left(\frac{b}{a}\right)^2} \qquad \text{Eq. 1- 2}$$

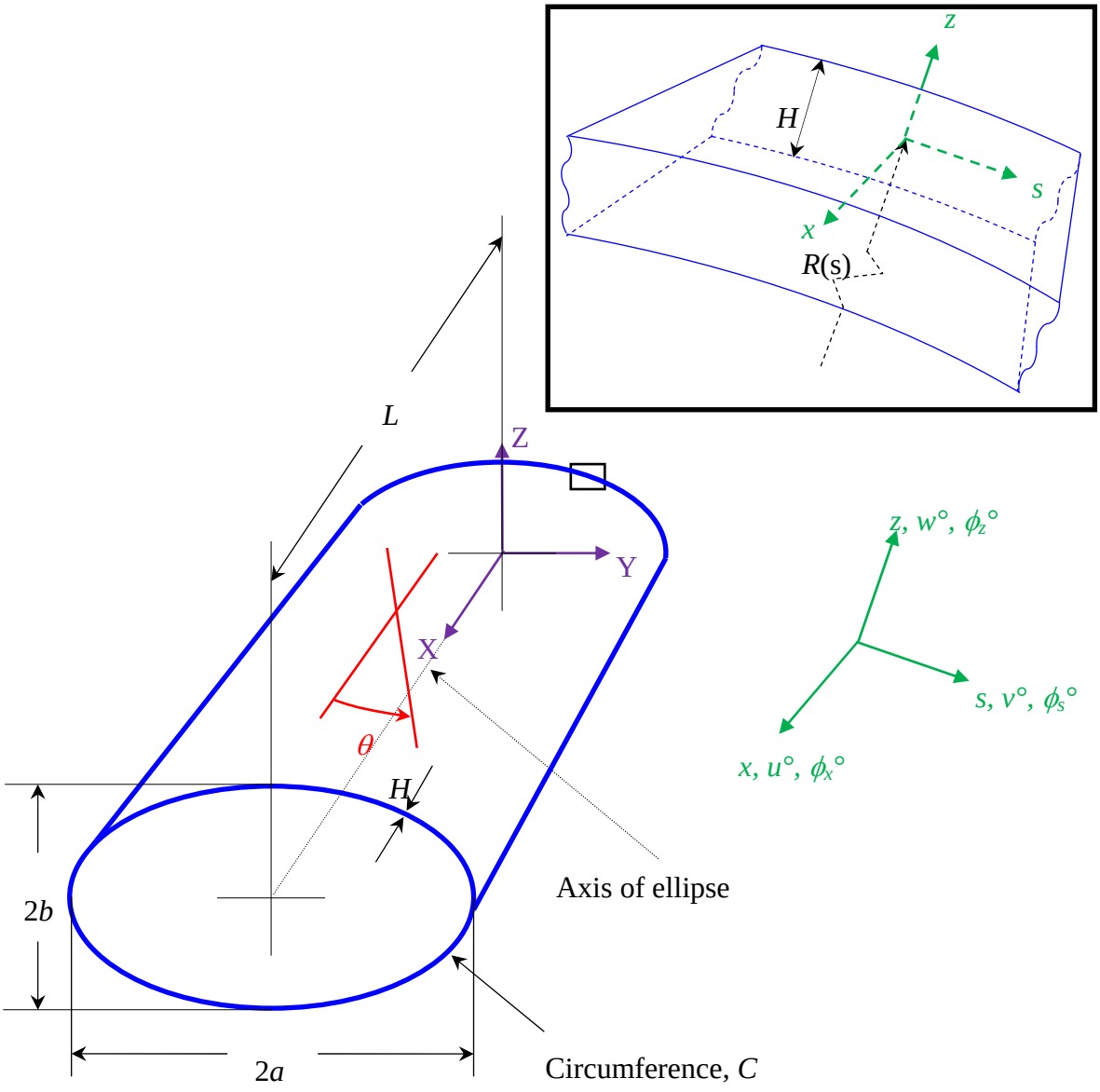

Fig. 1- 2 Cylinder geometry and nomenclature

It is easy to conclude that both eccentricity and aspect ratio of an ellipse are between zero and one. Considering a circular shape, the aspect ratio is unity while the eccentricity is zero. As the circular shape flattens, the eccentricity increases and the aspect ratio becomes smaller. This is illustrated in Table 1- 1, where all the ellipses have the same circumference.

Table 1- 1 Eccentricity and aspect ratio of four ellipses of the same circumference

	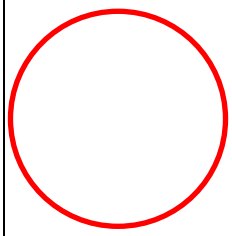	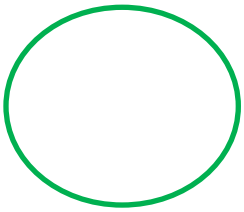	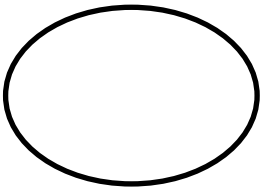	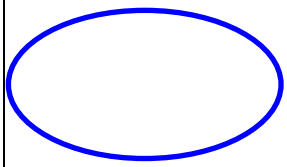
Aspect ratio *b/a*	1.00	0.85	0.70	0.55
Eccentricity *e*	0	0.53	0.71	0.84

Details of an elliptical cross-section are shown in Fig. 1- 3. In terms of global coordinates, the equation of the cross-section is expressed as

$$\left(\frac{\mathrm{Y}}{a}\right)^2 + \left(\frac{\mathrm{Z}}{b}\right)^2 = 1 \qquad \text{Eq. 1- 3}$$

Hyer and Vogl [2] used a parametric representation, with parameter ξ, to define the ellipse as

$$\mathrm{Y} = a \sin \xi \qquad \text{Eq. 1- 4}$$

$$\mathrm{Z} = b \cos \xi \qquad \text{Eq. 1- 5}$$

In terms of the parametric representation, the radius of curvature becomes

$$R(\xi) = \frac{(a^2 \cos^2 \xi + b^2 \sin^2 \xi)^{3/2}}{ab} \qquad \text{Eq. 1- 6}$$

and the curvilinear coordinate *s* becomes

$$s(\xi) = \int_0^{\xi} (a^2\cos^2\zeta + b^2\sin^2\zeta)^{1/2}\,\mathrm{d}\zeta \qquad \text{Eq. 1- 7}$$

The angle corresponding to *s*, defined as ϕ, has the following relationship with ξ,

$$\phi(\xi) = \tan^{-1}\left(\frac{a}{b}\tan(\xi)\right) \qquad \text{Eq. 1- 8}$$

The values of the parameter ξ at key locations around the circumference are indicated in Fig. 1-3, and from Eq. 1- 6 it can be concluded that

$$R_{\max} = \frac{a^2}{b} \qquad \text{Eq. 1- 9}$$

and

$$R_{\min} = \frac{b^2}{a} \qquad \text{Eq. 1- 10}$$

By Eq. 1- 7 it can be concluded that

$$C = s(2\pi) = \int_0^{2\pi} (a^2\cos^2\zeta + b^2\sin^2\zeta)^{1/2}\,\mathrm{d}\zeta \qquad \text{Eq. 1- 11}$$

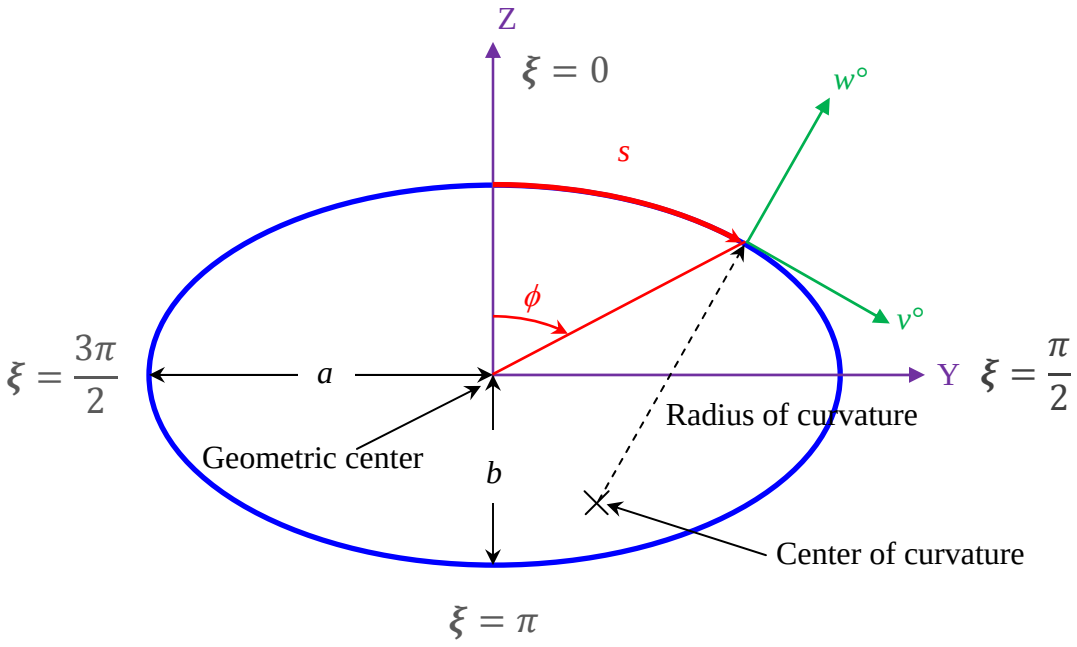

Fig. 1- 3 Cylinder cross-section detail

1.2 Definition of Wave Numbers

As the discussion of some of the papers cited in the literature review refer to wave numbers in the axial and circumferential direction, and since wave number predictions will accompany the predictions of the fundamental frequencies in later chapters, it is appropriate at this point to define the two wave numbers as they are commonly used, which is the way they are used in this work. The wave numbers in axial and circumferential directions are denoted as m and n, respectively. The concept of a wave number can be traced back to the spatially periodic variation of the vibration displacement pattern, or mode shape. The axial wave number m refers to the number of *half* waves of this periodic displacement pattern in the x-direction, while the circumferential wave number n refers to the number of *full* waves in the circumferential direction. In Fig. 1- 4a the blue line represents the periodic character of the mode shape of simply-supported cylinders in the x-direction, whereas the red line represents the periodic character of the mode shape of clamped support cylinders. Both of these mode shapes are referred to as having an $m = 5$ axial wave number. While the axial wave number of the simply-supported cylinder, shown again in Fig. 1- 5a can easily be identified with $m = 5$ in the axial direction, the axial wave number of clamped support cylinder does not exactly refer to half waves. However, in Fig. 1- 5b, it can be claimed that $m = 5$ by considering the number of zero values of displacement in the wave pattern. Fig. 1- 4b shows the circumferential wave number $n = 5$.

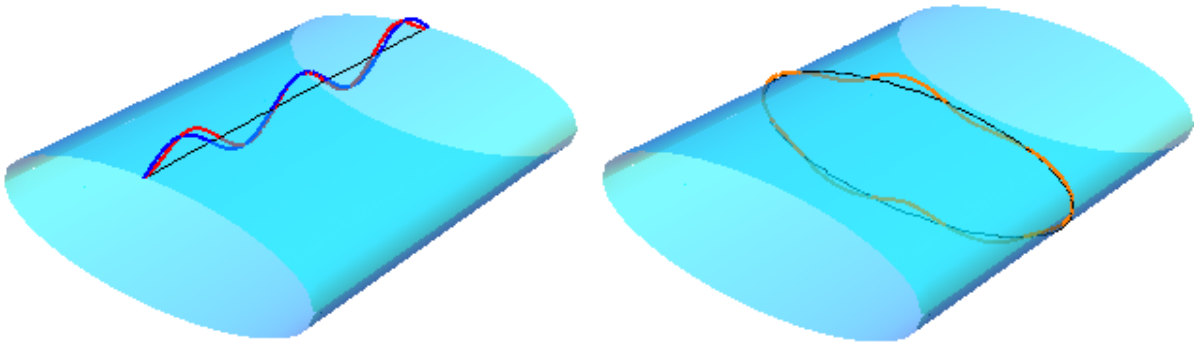

(a) axial wave number (b) circumferential wave number

Fig. 1- 4 Wave patterns in (a) axial and (b) circumferential directions

In Fig. 1- 5c it can be observed that the wave number in circumferential direction is the number of whole waves around the circumference.

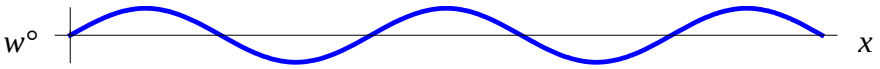

(a) normal displacement at $s = 0$ for $m = 5$ with simple supports

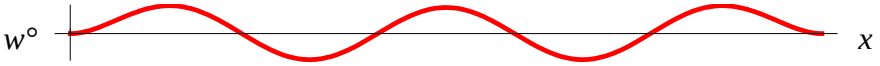

(b) normal displacement at $s = 0$ for $m = 5$ with clamped supports

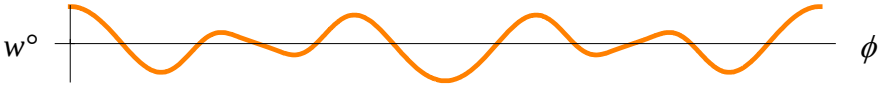

(c) normal displacement at $x = L/2$ for $n = 5$

Fig. 1- 5 Further views of wave patterns in the axial and circumferential directions

1.3 Literature Review

There are hundreds of papers which address the methods of determining the vibration characteristics of cylindrical shells, particular isotropic circular cylinders. Based on types of material and shapes of cross section, herein the research related to the vibration characteristics of cylindrical shells is classified into four areas: circular isotropic cylindrical shells; noncircular isotropic cylindrical shells; circular laminated composite cylindrical shells; noncircular laminated composite cylindrical shells.

In the beginning of this section, 1.3.1, only selected papers for circular isotropic cylindrical shells are presented, as there are many, many publications on the topic. In the second part of this section, section 1.3.2, a review of the vibration characteristics of noncircular isotropic cylindrical shells is followed in section 1.3.3 by a review of the vibration characteristics of circular laminated composite cylindrical shells. The last portion of this section is the review of noncircular laminated composite cylindrical shells.

1.3.1 Vibration Characteristics of Circular Isotropic Cylindrical Shells

Almroth [3] classified the boundary conditions for simply-supported and clamped support cylindrical shells into four types for each support condition. Whichever kind of boundary condition is considered, the shell is assumed to be supported in the normal direction at the edge, that is, the normal displacement is zero at $x = 0$ and $x = L$. There are three additional conditions required on each boundary obtained by selection of one of each of the following three pairs.

$$\frac{\partial w}{\partial x} = 0 \quad \text{or} \quad M_x = 0 \left(\frac{\partial^2 w}{\partial x^2} = 0\right) \qquad \text{Eq. 1- 12}$$

$$u = 0 \quad \text{or} \quad N_x = 0 \qquad \text{Eq. 1- 13}$$

$$v = 0 \quad \text{or} \quad N_{xs} = 0 \qquad \text{Eq. 1- 14}$$

where for isotropic materials the condition in Eq. 1-12 of zero moment reduces to the kinematic condition in parenthesis. The selection as classified by Almroth [3] is listed in Table 1- 2. In the literature of this study simple support is the S2 condition and clamped support is the C2 condition.

Table 1- 2 Almroth [3] classification of boundary conditions for isotropic circular cylinders

S1	$\frac{\partial^2 w}{\partial x^2} = 0$	$u = 0$	$v = 0$
S2	$\frac{\partial^2 w}{\partial x^2} = 0$	$N_x = 0$	$v = 0$
S3	$\frac{\partial^2 w}{\partial x^2} = 0$	$u = 0$	$N_{xs} = 0$
S4	$\frac{\partial^2 w}{\partial x^2} = 0$	$N_x = 0$	$N_{xs} = 0$
C1	$\frac{\partial w}{\partial x} = 0$	$u = 0$	$v = 0$
C2	$\frac{\partial w}{\partial x} = 0$	$N_x = 0$	$v = 0$
C3	$\frac{\partial w}{\partial x} = 0$	$u = 0$	$N_{xs} = 0$
C4	$\frac{\partial w}{\partial x} = 0$	$N_x = 0$	$N_{xs} = 0$

In a very comprehensive compilation on the topic, Leissa [4] reviewed papers regarding vibrations of thin isotropic cylindrical shells and compared these studies with comprehensive shell theories under simply-supported and clamped supports. In the same era, Sharma and Johns [5-6] studied natural frequencies of clamped-free circular cylindrical shells with experiments and a variety of theoretical methods. To test the effect of boundary conditions, Soedel [7] developed a new formula for the natural frequencies of closed circular cylindrical shells with a variety of boundary conditions. However, by applying the Love shell theory, Soedel [8] investigated the natural frequencies of circular isotropic cylindrical shells via Hamilton's principle. Before the end of last century, Callahan and Baruh [9] follow Soedel's[8] study to generate natural frequencies for any known boundary conditions by packages of software based on MATLAB and MAPLE V and found good agreement with former studies.

1.3.2 Vibration Characteristics of Noncircular Isotropic Cylindrical Shells

Soldatos [10] authored a comprehensive review of investigations of noncircular cylindrical shells for vibration and buckling problems. Some of the following summaries are cited from Soldatos' review. Based on membrane theory, Herrman and Mirsky [11] neglected the effect of moments to study natural frequencies of elliptical cylindrical shells and concluded the axial wave number for the lowest natural frequency is one, that is, for simply-supported cylinders the vibration shape is a half wave in the axial direction (see Fig. 1- 4a). Klosner and Pohle [12] and Klosner [13-14] used a perturbation approach by considering the varying curvature of a noncircular cylinder to be

$$\frac{1}{R(s)} = \frac{1}{R_0} + \frac{\varepsilon}{R_0} \cos\left(\frac{4\pi s}{C}\right) \qquad \text{Eq. 1- 15}$$

where ε is the noncircular parameter and also the perturbation parameter. The investigations began with an analysis based on the plane-strain assumption ($u° = 0$) [12], and that analysis was followed [13-14] by including considerations of displacement in x-direction (removing the plane-strain assumption). Torsional and flexural free vibration modes for infinitely long cylinders were investigated. Finite length noncircular cylindrical shells with an elliptical cross section were studied by Sewall *et al.* [15] by applying the Ritz procedure to the energy functional of Sanders' shell theory, and by Culberson and Boyd [16] for cylinders with an oval cross section by applying an analytic approach equivalent to Galerkin's method while considering Donnell and

Love shell theories and concluding that results based on Donnell and Love shell theories are nearly identical. Comparing natural frequencies between the results of Sewall *et al.* [15] and Culberson and Boyd [16] for the same aspect ratio b/a, Culberson and Boyd [16] concluded the difference is less than 1% when $|\varepsilon|$ is less than 0.25 and less than 10% when $|\varepsilon|$ is less than 0.65. Culberson and Boyd [16] also compared their results with Klosner's [14] results and found good agreement when $|\varepsilon|$ is less than 0.5.

Bergman [17] treated a doubly symmetric oval cylindrical shell as two pairs of circular cylindrical panels using the Goldenveizer shell theory. Shirakawa and Morita [18] used the same approach as Bergman [17] to investigate elliptical cylindrical shells with Love's shell theory. The results from the approach agreed well with results of Culberson and Boyd [16].

Boyd and Rao [19] considered the effect of stiffening rings and stringers on natural frequencies of elliptical cylindrical shells with different boundary conditions, including simply-supported, clamped-clamped, free-free, and clamped-free. (Rings stiffen the structure in the circumferential directions, while stringers are parallel to the axial direction.) The results show that whatever the boundary conditions are, rings increase the natural frequency, whereas stringers decrease the natural frequency. Chen and Kempner [20] employed a variational method with Donnell and Sanders shell theories to investigate natural frequencies of oval cylindrical shells with different combinations of simply-supported and clamped boundaries, which were based on the Almroth's classification [3], and concluded that the natural frequencies and vibration modes based on these two different shell theories are in good agreement, though the specification of the boundary conditions is somewhat different. Moreover, the natural frequencies of simply-supported cylinders in Chen and Kempner's [20] study have a good agreement with Culberson and Boyd [16].

Based on Flügge shell theory, Suzuki *et al.* [21] developed an infinite power series to express the square of the variable curvature. However, the coefficients of power series are assumed to be in terms of the displacement components. Considering cylindrical shells with an elliptical cross section under simple supports, the power series are substituted into the Navier-type equations of Flügge shell theory. The method results in a set of recursive formulas for the coefficients of power series of displacement components. Suzuki and Leissa [22] followed the same approach to investigate the natural frequencies of noncircular cylindrical shells with circumferentially varying thickness. Also

based on Flügge shell theory, Koumousis and Armenàkas [23] compared their results with Donnell, Love, and Sanders shell theories in the Culberson and Boyd [16] study with a variety of values for L/R_0, H/R_0, and ε, the noncircular parameters mentioned before. Though there is a large difference in the results between Flügge shell theory and the other three theories for thick, long, and highly noncircular shells, there is still a good agreement for certain ranges of L/R_0, H/R_0, and ε. Following the former study, Koumousis and Armenàkas [24] uncoupled the frequencies for the longitudinal mode from the plane-strain modes by letting L approaching infinity and they concluded that the longitudinal frequencies of Flügge shell theory and other three theories are very close, whereas plane-strain frequencies of Flügge shell theory and other three theories are notably different.

An approximate finite strip method was employed by Kumar and Singh [25-26] to investigate the natural frequencies of noncircular cylindrical shells with circumferentially varying thickness based on Donnell shell theory under simple supports [25] and under clamped-free and clamped-clamped supports [26]. The strips are aligned with the axial direction and the thickness and the radius of curvature of each strip depends on its circumferential location. Compared with other studies, the results of the former study [25] has a good agreement with the results of Culberson and Boyd [16] for constant thickness cylinders, as does Suzuki and Leissa's study [22] for a parabolic variation of thickness.

A transfer matrix approach was employed by Yamada *et al.* [27] and Irie *et al.* [28], however, based on Goldenveizer-Novozhilov shell theory to investigate natural frequencies of cylindrical shells with more complicated noncircular cross sections. Though the interesting cross sections were three-lobed and four-lobed in the study of Yamada *et al.* [27], whereas Irie *et al.* [28] considered the elliptical cylindrical shells with a longitudinal interior plate, Yamada *et al.* [27] and Irie *et al.* [28] both generate the natural frequencies for elliptical cylinders. Both of these two studies have good agreement with Sewall *et al.* [15] when elliptical cross sections are considered.

A mapping method was applied by Chueng *et al.* [29] using Donnell shell theory to investigate the dynamic transient response of isotropic cylindrical shells with simple supports. The mapping method can transform any known noncircular cross section into corresponding circular cross section for cylindrical shells. However, the mapping cannot uncouple the circumferential modes of the mapped circular cylindrical shells, but only addresses the mapping of complicated transverse

sections into circles. The result has a good agreement with the corresponding problems based on a membrane theory [30].

Using Bezier functions, Kumar and Singh [31] studied the free vibration of noncircular cylindrical shells within a circumferentially varying thickness. The study showed the advantages of using Bezier polynomials, including the ability to enforce boundary conditions and economy of computer resources.

1.3.3 Vibration Characteristics of Circular Laminated Composite Cylindrical Shells

Based on Donnell shell theory, Dong [32] and Jones and Morgan [33] derived equations for natural frequencies of circular composite cylindrical shells fabricated with cross-ply laminates. Dong [32] developed an equation valid for simply supported shells and an iterative scheme for any other boundary conditions. Jones and Morgan [33] used the same equation to discuss both the natural frequency and the buckling load. When the same material properties are considered, the results from these two investigations have good agreement.

Love shell theory was employed by Bert *et al.* [34] to determine the free vibration characteristics of circular cylinders with arbitrary laminates, either symmetric or unsymmetric, and simple supports. They discussed the importance of the coupling of bending and stretching for cylinders of boron/epoxy composite with various lamination sequences and obtained a general solution for the axisymmetric modes of an arbitrarily laminated anisotropic cylinder and an approximate solution for the unsymmetric modes of the same general class of shells with simply-supported boundary conditions. Stavsky and Loewy [35] also applied Love shell theory in their study. By comparing with Donnell shell theory, they pointed out for large length-to-radius ratios, say, $L=5R_0$, the lowest natural frequency from Donnell shell theory is about 15% higher than that from Love shell theory, and much higher when the length-radius ratio is larger.

There are other applications based on Love shell theory. For example, Greenberg and Stavsky [36] derived an equation of motion for laminated filament-wound cylinders in which each layer is permitted an arbitrary fiber orientation. They provided a framework of optimization of composite shells. Soedel [37] derived a close-form simplified equation for natural frequency

of orthotropic circular cylinders based on Love shell theory and found good agreement with the solution base on the finite element method and pointed out the effect of neglecting in-plane deflection contribution to the bending strain expressions.

Compared with the ratio of shear modulus to the extensional modulus for an isotropic material, composite materials have a much lower ratio in the fiber direction and a higher ratio perpendicular to the fiber direction. Therefore, Bert and Kumar [38] asserted that thickness-shear flexibility is important for composite materials and then discussed the natural frequencies of circular cross-ply composite cylindrical shells, based on Sanders, Love, and Donnell shell theories. The closed-form equations for shear deformable theory with rotary inertia, shear deformable theory without rotary inertia, and thin-shell theory were presented. In terms of the thin shells they considered, $H/R_0 < 0.01$, the inclusion of thickness-shear deformation, however, sometimes decreases the natural frequencies, while sometimes it increases them, but the variation of the lowest natural frequencies is smaller than 1%. Moreover, the influence of rotary inertia is almost negligible.

Another study for effect of thickness-shear and rotary inertia, conducted by Rao [39], concerned two-layered shells. The author pointed out that the effects of transverse shear and rotary inertia are predominant for $H/R_0 > 0.05$. Considering thickness-radius ratios $H/R_0 = 0.02$, 0.05, 0.1, and 0.2, Kumar and Rao [40] investigated the free vibrations of circular cross-ply laminated composite cylindrical shells by the finite element method and concluded that the higher frequencies are observably affected by transverse shear terms.

Lakshminarayana and Dwarakanath [41] used the commercial finite element software CSA/NASTRAN to investigate the free vibrations of circular cylinders with arbitrary laminates and clamped-free boundaries, and compared the orthotropic cases with former studies, including those of Bert *et al.* [34], with good agreement.

Based on Donnell shell theory plus a shear-deformation theory, Nosier and Reddy [42] obtained an improved analytical procedure for studying free vibration and stability problems of circular cross-ply laminated cylinders with a variety of boundary conditions for situations where the order of governing equations is higher than eight and the number of governing equations is higher than three. The modified theory is asserted to be fairly accurate when isotropic cylinders are concerned.

Ye and Soldatos [43] used fully three-dimensional elasticity considerations to study the free vibrations of cross-ply laminated cylinders having clamped boundaries. A very satisfactory agreement of results was observed with a solution based on a two-dimensional shear-deformation shell theory for thin (H/R_0 = 0.05, 0.1, 0.2) and moderately thick (H/R_0 = 1) cylinders, and another solution based on three dimensional equations of elasticity by the finite element method.

Tizzi [44] investigated the free vibration frequencies and eigenmodes of cylindrical structures with clamped-clamped boundaries and established a simplified numerical model for the analysis of the flexural-torsional and in-plane dynamic behavior. Fiber orientations $\theta = 72$, 52, 32, and 12°, relative to the helicoidal filament winding angle defined by the author, in the laminate sequence $[\theta]_{20}$ are considered. The ratios H/R_0 and L/R_0 of the studied cylinder are 0.0321 and 5.53, respectively. Though the agreement for the larger thickness may be good, the results for smaller values of H/R_0 still have a good agreement with the corresponding finite element method solutions. Later, Tizzi [45] studied the optimization of symmetric, balanced angle-ply laminated composite cylinders with fixed minimum frequency by a Ritz procedure so as to find the lightest weight of the structure. This was accomplished by changing the thickness around the cylinder to maintain the natural frequency to be the same as the reference uniform thickness shells. The varying thickness is considered as a function of x and s and the considered laminate sequences are $[\pm\theta]_S$, for θ = 72, 52, 32, and 12°. The result shows that the varying thickness $[\pm 52]_S$ laminated composite cylindrical shells can save more than 16% of the relative weight of the uniform thickness $[\pm 52]_S$ laminated composite cylindrical shells.

Blom *et al.* [46] conducted modal testing and finite element analysis for two circular composite cylinders. One cylinder was fabricated with a constant fiber angle for each layer, and the other was fabricated with circumferentially varying fiber angles. Modal analysis was carried out using Abaqus, and the corresponding natural frequencies and their modes were compared with the experimental results. According to the finite element analysis, the variation of natural frequencies between these two cylindrical shells was about 15%, implying that for circular cylinders the circumferentially varying fiber angle has minimal effect. There was good agreement between the analytical and experimental results.

1.3.4 Vibration Characteristics of Noncircular Laminated Composite Cylindrical Shells

Based on Donnell shell theory with Kirchhoff-Love assumptions, Soldatos and Tzivanidis [47] investigated the vibration characteristics of noncircular cross-ply laminated cylindrical shells by employing the Galerkin method to solve the differential equations of motion and concluded that for a given number of layers, the eccentricity parameter, ε, does not affect the wave number of the lowest natural frequency, while for a given ε, the number of layers does affect the vibration mode. Later, Soldatos [48], using Flügge shell theory and the same approach, studied the vibrations of noncircular anisotropic laminated cylindrical shells and concluded that the difference between frequencies predicted by Donnell and Flügge shell theories is small, but increases for the large values of L and ε considered. Hui and Du [49] investigated the effects of the axial imperfections on the vibrations of oval cross-ply anti-symmetric cylindrical shells with simple supports based on Donnell shell theory. Though imperfections are another issue, the natural frequencies of the perfect laminated oval shells have a good agreement with the study of Soldatos [48].

Suzuki *et al.* [50] used Hamilton's principle and Love shell theory to investigate the natural frequencies for a set of symmetrically laminated cross-ply elliptical thin cylindrical shells with simple supports. They pointed out the influence of number of layers and stacking sequence on the frequencies. Suzuki *et al.* [51] employed the same approach to survey natural frequencies for a set of thick shells while considering the shear deformation and rotary inertia and evaluated the importance of shear deformation and rotary inertia.

Based on a shell theory which included the effects of shear deformation and rotary inertia, Kumar and Singh [52] employed Bezier functions to investigate the free vibration characteristics of the composite noncircular cylinders composed of layered media of different material properties and with clamped-clamped supports. From the numerical example studied by the authors, it was observed that at higher circumferential wave numbers both the oval and circular cylinders have almost equal values of natural frequencies.

Through use of the finite element method, Ganapathi *et al.* [53] investigated the natural frequencies of noncircular cylindrical shells with cross-ply laminates based on higher-order shear deformation theory, plus the effect of in-plane and rotary inertias, and pointed out that the shape

of cross section can significantly alter the frequency values, depending on thickness-radius and length-radius ratios, H/R_0 and L/R_0, respectively, and the circumferential wave number. They concluded that the eccentricity parameter can affect the wave number corresponding to the fundamental mode, depending on thickness value. Using the same approach, based on higher-order shear deformation theory and first-order shear deformation theory, respectively, Ganapathi and Haboussi [54] and Ganapathi *et al.* [55] studied the free vibration of laminated anisotropic non-circular cylinders. The effect of in-plane and rotary inertias was considered in both studies. Eight-layer and two-layer shells were considered in both studies. The lamination sequences of the eight-layer shells included $[\pm 15]_4$, $[\pm 30]_4$, $[\pm 45]_4$, $[\pm 60]_4$, $[\pm 75]_4$, and $[0/90]_4$, and the lamination sequences of the two-layer shells included [±15], [±30], [±45], [±60], [±75], and [0/90]. Ganapathi and Haboussi [54] concluded that, in general, for both eight-layer and two-layer cylinders, the maximum fundamental frequencies occurred for 45° ply-angle, whereas the minimum fundamental frequencies occurred for 15° ply-angle. Ganapathi *et al.* [55] found that, in general, the lowest natural frequency was predicted for a ply-angle of 15° and the maximum natural frequency occurred for the 45° or 60° cases, for thin shells, depending on H/R_0 and L/R_0. However, Ganapathi *et al.* [55] also found that for thick shells, the maximum fundamental frequencies occurred for a 15° ply-angle, whereas the minimum fundamental frequencies occurred for a 75° ply-angle, which is totally different from the findings for thin shells.

1.4 Objectives, Goals, and Approach

The two overarching objectives of this study were mentioned earlier, the first of which is to investigate whether or not varying the fiber orientation with circumferential position can be used to control any detrimental effects of a noncircular geometry as regards the fundamental frequency. Clearly, the work of Blom *et al.* [46] is relevant to this objective, but the investigation was limited to circular cylinders and only one specific case was studied. Furthermore, the investigation was motivated by designing the variable fiber angle orientation cylinder to better resist bending loads, and the vibration study was conducted to determine what effects the variable fiber orientation had on the vibration characteristics. This is basically the opposite of investigating whether a variable fiber angle orientation can be used to improve vibration characteristics. From the literature review, it appears such a study has not been done, so the first objective of the research

herein is a worthy one. However, the second overarching objective needs to be met first, so the general role of cylinder geometry and material properties, by way of fiber angles in the various layers, is well understood. While some of the past investigations cited above have been conducted in this spirit, often the lamination sequences consider are of limited practical value, e.g., cross-ply, or $[\pm\theta]$ laminates which have no fibers in the axial or circumferential directions. So the objective of this phase of the research is also a worthy one.

Concerning the second overarching objective, the specific goals are to determine the effect on the fundamental frequency of

1. Cylinder size, including circumference and length
2. Cross sectional eccentricity
3. Fiber orientation
4. Boundary conditions

To study the role of the various geometric and material parameters on the fundamental frequency, an analysis based on the Rayleigh-Ritz approach coupled with Hamilton's principle and Donnell shell theory will be developed. To incorporate into the analysis the influence of the noncircular geometry on the modal displacements, a so-called shape factor is introduced, a step that is believed to be unique. The result is a hierarchy of closed-form expressions for the fundamental frequency as a function of the geometric and material parameters, each level of the hierarchy incorporating various levels of simplification. Finite element results will be used to spot-check these results and to lend credibility to the expressions. The same general approach will be used to study the case of circumferentially varying fiber orientation. For the Rayleigh-Ritz approach the algebra is considerably more complicated as, effectively, the elastic properties vary with circumferential location around the ellipse. A simple linear variation is considered, but that still complicates the analysis. Finite element results for the variable fiber orientation will also be used to provide a comparison with the closed-form expressions.

1.5 Overview of Remaining Chapters

A description of the problem studied is given in Chapter 2, including the geometry of a general shell, key assumptions of Donnell shell theory, and the boundary conditions enforced. In

that chapter Hamilton's principle and the Rayleigh-Ritz approach are outlined. The derivation of the Rayleigh-Ritz solution for the fundamental frequencies is presented in Chapter 3. Numerical results are presented in Chapter 4, including results from the various levels of simplification, and comparisons with finite element analyses. In Chapter 5 the work on circumferentially-varying fiber orientation is presented. As the variable fiber orientation adds another dimension to the problem, the variation of other important geometric and material parameters is more limited when presenting numerical results for these cases than with the results for the fixed orientation fibers in Chapter 4. A discussion of the sources of the difference between the prediction of the Rayleigh-Ritz based analysis and finite element results and a discussion of Lo's approximation are presented in Chapter 6. Summaries of the work presented and the conclusions reached make up Chapter 7. The finite element model used to spot check results from the developed analysis is described in Appendix A. The results for fundamental frequencies based on so-called sine-based functions are presented in Appendix B.

Chapter 2 Development of the Analysis

Though Donnell shell theory has its limitations, it is the simplest of all shell theories. It is capable of capturing the first-order effects of geometry and material properties of interest here. So, following a discussion of the geometry of a general shell in Section 2.1, the discussion in Section 2.2 focuses on Donnell shell theory. The limiting assumptions of the theory, the kinematics of deformation, and the corresponding strain-displacement relations, including the definitions of the reference surface strains and curvatures are discussed. In Section 2.3 the stress-strain relations for a fiber-reinforced composite material are discussed whereas in Section 2.4 the definitions of the force and moment resultants are presented. Hamilton's principle and the cylinder boundary conditions consistent with Hamilton's principle are described in Section 2.5. The Rayleigh-Ritz approach is outlined in Sections 2.6.

2.1 Geometry of General Shell

The distance from the origin O to arbitrary point P on what will become the reference surface of a shell can be expressed as

$$\vec{r} = \vec{r}(\alpha, \beta) \qquad \text{Eq. 2- 1}$$

where α and β are independent curvilinear coordinates which are used to represent the surface, as shown in Fig. 2- 1. The distance to a neighboring point P' is expressed as $\vec{r} + \mathrm{d}\vec{r}$ where

$$\mathrm{d}\vec{r} = \frac{\partial \vec{r}}{\partial \alpha}\mathrm{d}\alpha + \frac{\partial \vec{r}}{\partial \beta}\mathrm{d}\beta \qquad \text{Eq. 2- 2}$$

The squared magnitude of the distance between points P and P', called the first fundamental form of the surface, is

$$(\mathrm{d}l)^2 = \mathrm{d}\vec{r} \cdot \mathrm{d}\vec{r} = {A_\alpha}^2(\mathrm{d}\alpha)^2 + 2A_\alpha A_\beta \cos\chi \, \mathrm{d}\alpha\mathrm{d}\beta + {A_\beta}^2(\mathrm{d}\beta)^2 \qquad \text{Eq. 2- 3}$$

where

$$A_\alpha = \left(\frac{\partial \vec{r}}{\partial \alpha} \cdot \frac{\partial \vec{r}}{\partial \alpha}\right)^{\frac{1}{2}} \qquad \text{Eq. 2- 4}$$

$$A_\beta = \left(\frac{\partial \vec{r}}{\partial \beta} \cdot \frac{\partial \vec{r}}{\partial \beta}\right)^{\frac{1}{2}}$$

$$\cos \chi = \frac{1}{A_\alpha A_\beta} \frac{\partial \vec{r}}{\partial \alpha} \cdot \frac{\partial \vec{r}}{\partial \beta}$$

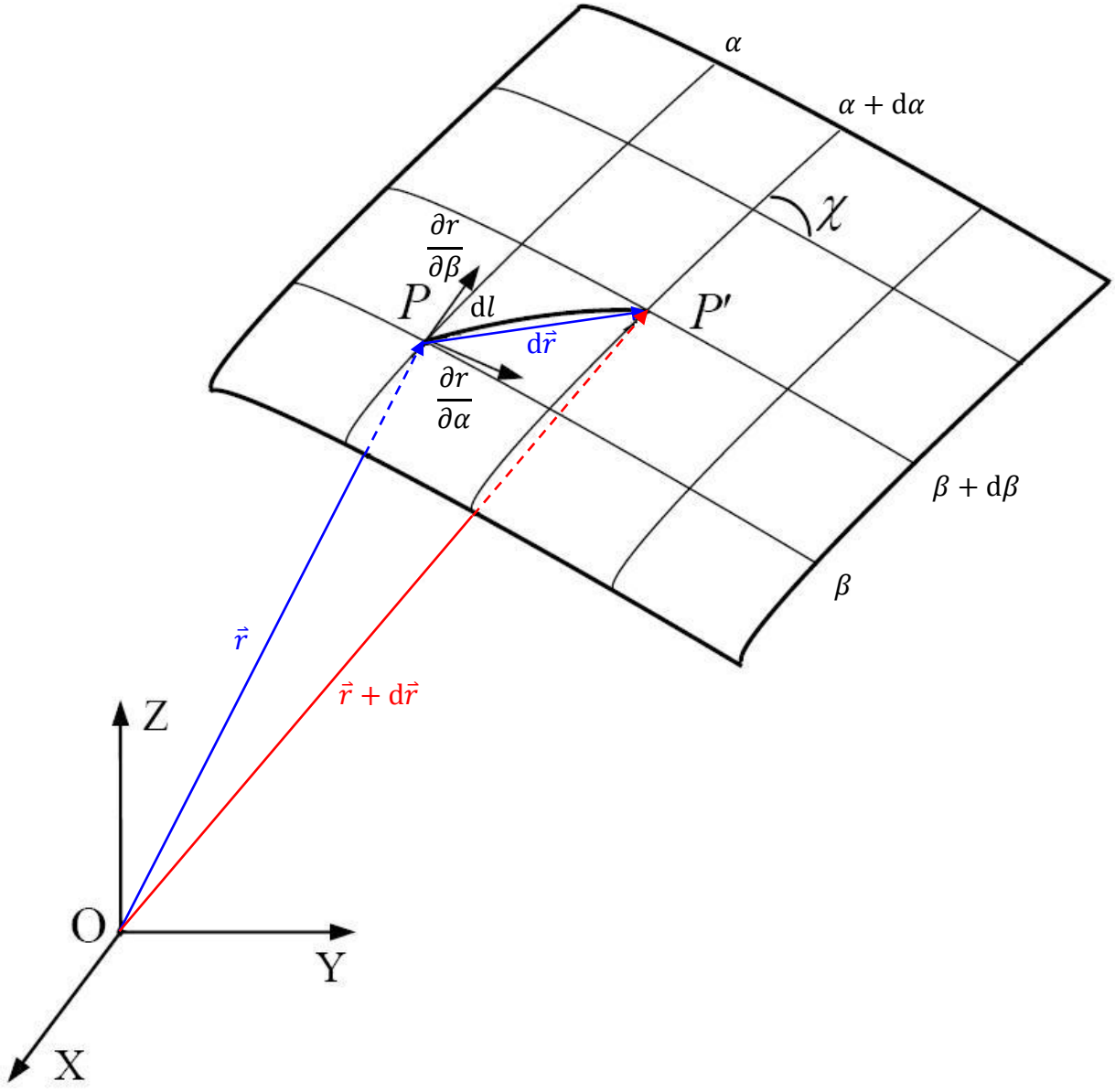

Fig. 2- 1 Geometry of reference point P and point P' on surface

The parameters A_α and A_β are referred to as Lamé parameters and χ is the angle between the coordinate lines α and β. The unit vectors tangential to the surface along with the coordinate lines α and β are, respectively, defined by

$$\hat{t}_\alpha = \frac{1}{A_\alpha}\frac{\partial \vec{r}}{\partial \alpha}$$
$$\hat{t}_\beta = \frac{1}{A_\beta}\frac{\partial \vec{r}}{\partial \beta} \qquad \text{Eq. 2- 5}$$

The unit vector normal to the surface, $\hat{n}$, is defined by

$$\hat{n} = \frac{\frac{\partial \vec{r}}{\partial \alpha} \times \frac{\partial \vec{r}}{\partial \beta}}{\left|\frac{\partial \vec{r}}{\partial \alpha} \times \frac{\partial \vec{r}}{\partial \beta}\right|} = \frac{\hat{t}_\alpha \times \hat{t}_\beta}{\sin\chi} \qquad \text{Eq. 2- 6}$$

Considering arbitrary point P and its neighboring point P' on a surface and the unit vector normal to the surface, $\hat{n}$, the unit vector along the tangent to the curve PP' is

$$\hat{T} = \frac{\mathrm{d}\vec{r}}{\mathrm{d}l} = \frac{\partial \vec{r}}{\partial \alpha}\frac{\mathrm{d}\alpha}{\mathrm{d}l} + \frac{\partial \vec{r}}{\partial \beta}\frac{\mathrm{d}\beta}{\mathrm{d}l} \qquad \text{Eq. 2- 7}$$

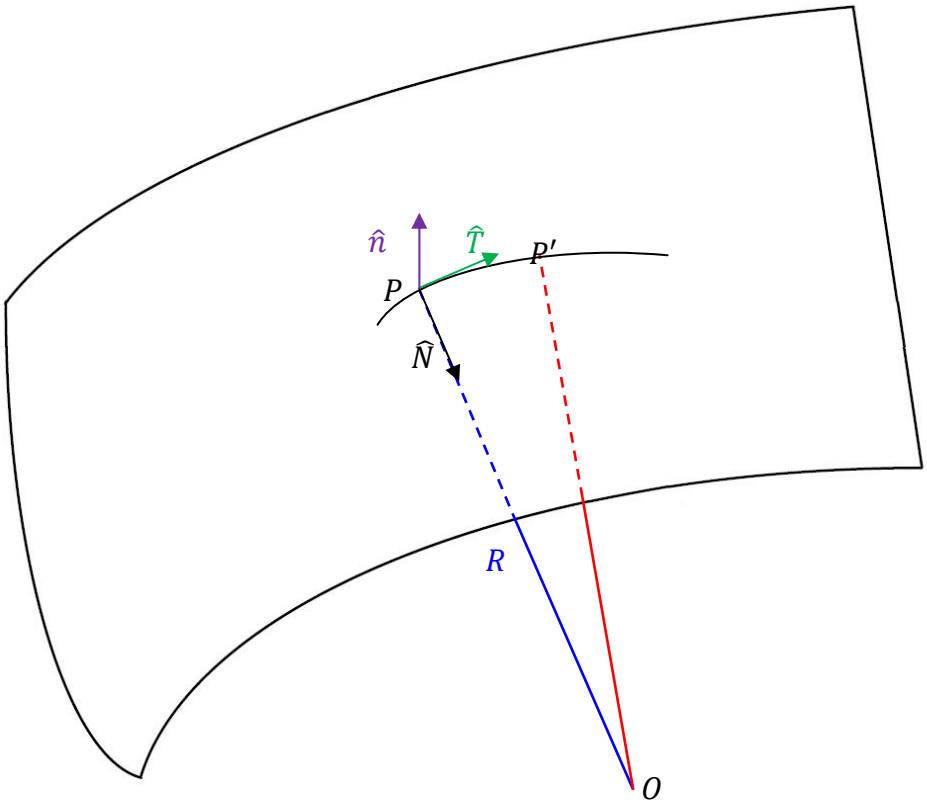

Fig. 2- 2 Curvature of a surface

As shown in Fig. 2- 2, by Frenet's formula,

$$\frac{\mathrm{d}\hat{T}}{\mathrm{d}l} = \frac{\mathrm{d}^2\vec{r}}{\mathrm{d}l^2} = \frac{\widehat{N}}{R} \qquad \text{Eq. 2- 8}$$

where R is the radius of curvature of the curve PP' at point P, point O is the center of curvature of that, and $\widehat{N}$ is the unit vector along the principal normal to the curve PP'. Substituting Eq. 2- 7 into Eq. 2- 8, the expression for the curvature becomes

$$\frac{\widehat{N}}{R} = \frac{\partial^2\vec{r}}{\partial\alpha^2}\left(\frac{\mathrm{d}\alpha}{\mathrm{d}l}\right)^2 + \frac{\partial\vec{r}}{\partial\alpha}\frac{\mathrm{d}^2\alpha}{\mathrm{d}l^2} + 2\frac{\partial^2\vec{r}}{\partial\alpha\partial\beta}\frac{\mathrm{d}\alpha}{\mathrm{d}l}\frac{\mathrm{d}\beta}{\mathrm{d}l} + \frac{\partial^2\vec{r}}{\partial\beta^2}\left(\frac{\mathrm{d}\beta}{\mathrm{d}l}\right)^2 + \frac{\partial\vec{r}}{\partial\beta}\frac{\mathrm{d}^2\beta}{\mathrm{d}l^2} \qquad \text{Eq. 2- 9}$$

Using the orthogonal characteristic of $\hat{t}_\alpha$ and $\hat{n}$, as well as that of $\hat{t}_\beta$ and $\hat{n}$, Eq. 2- 9 becomes

$$\frac{\widehat{N}}{R}\cdot\hat{n} = \frac{\partial^2\vec{r}}{\partial\alpha^2}\cdot\hat{n}\left(\frac{\mathrm{d}\alpha}{\mathrm{d}l}\right)^2 + 2\frac{\partial^2\vec{r}}{\partial\alpha\partial\beta}\cdot\hat{n}\frac{\mathrm{d}\alpha}{\mathrm{d}l}\frac{\mathrm{d}\beta}{\mathrm{d}l} + \frac{\partial^2\vec{r}}{\partial\beta^2}\cdot\hat{n}\left(\frac{\mathrm{d}\beta}{\mathrm{d}l}\right)^2 \qquad \text{Eq. 2- 10}$$

Denoting

$$\mathrm{L} = \frac{\partial^2\vec{r}}{\partial\alpha^2}\cdot\hat{n} = \frac{\partial}{\partial\alpha}\left(\frac{\partial\vec{r}}{\partial\alpha}\cdot\hat{n}\right) - \frac{\partial\vec{r}}{\partial\alpha}\cdot\frac{\partial\hat{n}}{\partial\alpha} = -\frac{\partial\vec{r}}{\partial\alpha}\cdot\frac{\partial\hat{n}}{\partial\alpha} = -A_\alpha\hat{t}_\alpha\cdot\frac{\partial\hat{n}}{\partial\alpha}$$

$$\mathrm{M} = \frac{\partial^2\vec{r}}{\partial\alpha\partial\beta}\cdot\hat{n} = -\frac{\partial\vec{r}}{\partial\alpha}\cdot\frac{\partial\hat{n}}{\partial\beta} = -\frac{\partial\vec{r}}{\partial\beta}\cdot\frac{\partial\hat{n}}{\partial\alpha} = -A_\beta\hat{t}_\beta\cdot\frac{\partial\hat{n}}{\partial\alpha} \qquad \text{Eq. 2- 11}$$

$$\mathrm{N} = \frac{\partial^2\vec{r}}{\partial\beta^2}\cdot\hat{n} = -\frac{\partial\vec{r}}{\partial\beta}\cdot\frac{\partial\hat{n}}{\partial\beta} = -A_\beta\hat{t}_\beta\cdot\frac{\partial\hat{n}}{\partial\beta}$$

Equation 2- 10 becomes

$$\frac{\widehat{N}}{R}\cdot\hat{n} = \frac{\mathrm{L}(\mathrm{d}\alpha)^2 + 2\mathrm{M}\mathrm{d}\alpha\mathrm{d}\beta + \mathrm{N}(\mathrm{d}\beta)^2}{(\mathrm{d}l)^2} \qquad \text{Eq. 2- 12}$$

The denominator of the right hand side of Eq. 2- 12 is the first fundamental form of the surface, whereas the numerator of the right hand side of Eq. 2- 12 is the second fundamental form. When $\widehat{N} = -\hat{n}$, the normal curvature κ becomes

$$-\kappa = -\frac{1}{R} = \frac{\mathrm{L}(\mathrm{d}\alpha)^2 + 2\mathrm{M}\mathrm{d}\alpha\mathrm{d}\beta + \mathrm{N}(\mathrm{d}\beta)^2}{{A_\alpha}^2(\mathrm{d}\alpha)^2 + 2A_\alpha A_\beta\cos\chi\,\mathrm{d}\alpha\mathrm{d}\beta + {A_\beta}^2(\mathrm{d}\beta)^2} \qquad \text{Eq. 2- 13}$$

The minus sign means the outer normal of the curve is chosen to be the positive normal to the surface. Substituting $\mathrm{d}\beta = 0$ and $\mathrm{d}\alpha = 0$ into Eq. 2- 13, respectively, the curvatures along α and β can be obtained as

$$-\kappa_\alpha = -\frac{1}{R_\alpha} = \frac{\mathrm{L}}{{A_\alpha}^2} \qquad \text{Eq. 2- 14}$$

$$-\kappa_\beta = -\frac{1}{R_\beta} = \frac{\mathrm{N}}{{A_\beta}^2}$$

The twist curvature of the surface is defined as

$$-\kappa_{\alpha\beta} = -\frac{1}{R_{\alpha\beta}} = \frac{\mathrm{M}}{A_\alpha A_\beta} \qquad \text{Eq. 2- 15}$$

However, $\cos\chi$ and M are zero for an orthogonal coordinate system [57]. In that regard, because of the problem of interest herein, all that follows is based on an orthogonal coordinate system, such as a Cartesian, cylindrical, or spherical coordinate system.

Considering the first derivatives of $\hat{n}$, the derivatives must lie in the plane of $\hat{t}_\alpha$ and $\hat{t}_\beta$, that is,

$$\frac{\partial \hat{n}}{\partial \alpha} = \hat{t}_\alpha \cdot \frac{\partial \hat{n}}{\partial \alpha}\hat{t}_\alpha + \hat{t}_\beta \cdot \frac{\partial \hat{n}}{\partial \alpha}\hat{t}_\beta = -\frac{\mathrm{L}}{A_\alpha}\hat{t}_\alpha - \frac{\mathrm{M}}{A_\beta}\hat{t}_\beta = -\frac{\mathrm{L}}{A_\alpha}\hat{t}_\alpha = \frac{A_\alpha}{R_\alpha}\hat{t}_\alpha \qquad \text{Eq. 2- 16}$$

Similarly,

$$\frac{\partial \hat{n}}{\partial \beta} = \frac{A_\beta}{R_\beta}\hat{t}_\beta \qquad \text{Eq. 2- 17}$$

For continuous $\vec{r}$, $\hat{n}$, and $\hat{t}_\alpha$, it must be true that

$$\frac{\partial^2 \vec{r}}{\partial\alpha\partial\beta} = \frac{\partial^2 \vec{r}}{\partial\beta\partial\alpha} \qquad \text{Eq. 2- 18}$$

$$\frac{\partial^2 \hat{n}}{\partial\alpha\partial\beta} = \frac{\partial^2 \hat{n}}{\partial\beta\partial\alpha} \qquad \text{Eq. 2- 19}$$

$$\frac{\partial^2 \hat{t}_\alpha}{\partial\alpha\partial\beta} = \frac{\partial^2 \hat{t}_\alpha}{\partial\beta\partial\alpha} \qquad \text{Eq. 2- 20}$$

Equation 2- 18 leads to

$$\frac{\partial A_\alpha \hat{t}_\alpha}{\partial\beta} = \frac{\partial A_\beta \hat{t}_\beta}{\partial\alpha}$$

$$A_\alpha \frac{\partial \hat{t}_\alpha}{\partial\beta} + \hat{t}_\alpha \frac{\partial A_\alpha}{\partial\beta} = A_\beta \frac{\partial \hat{t}_\beta}{\partial\alpha} + \hat{t}_\beta \frac{\partial A_\beta}{\partial\alpha}$$

$$\frac{\partial \hat{t}_\beta}{\partial\alpha} = \frac{1}{A_\beta}\left(A_\alpha \frac{\partial \hat{t}_\alpha}{\partial\beta} + \hat{t}_\alpha \frac{\partial A_\alpha}{\partial\beta} - \hat{t}_\beta \frac{\partial A_\beta}{\partial\alpha}\right) \qquad \text{Eq. 2- 21}$$

Considering the first derivatives of $\hat{t}_\alpha$ in α, the derivative must lie in the plane of $\hat{n}$ and $\hat{t}_\beta$, that is,

$$\frac{\partial \hat{t}_\alpha}{\partial \alpha} = \hat{n} \cdot \frac{\partial \hat{t}_\alpha}{\partial \alpha}\hat{n} + \hat{t}_\beta \cdot \frac{\partial \hat{t}_\alpha}{\partial \alpha}\hat{t}_\beta = -\hat{t}_\alpha \cdot \frac{\partial \hat{n}}{\partial \alpha}\hat{n} - \hat{t}_\alpha \cdot \frac{\partial \hat{t}_\beta}{\partial \alpha}\hat{t}_\beta = -\frac{A_\alpha}{R_\alpha}\hat{n} - \frac{1}{A_\beta}\frac{\partial A_\alpha}{\partial \beta}\hat{t}_\beta \quad \text{Eq. 2- 22}$$

Similarly,

$$\frac{\partial \hat{t}_\alpha}{\partial \beta} = \frac{1}{A_\alpha}\frac{\partial A_\beta}{\partial \alpha}\hat{t}_\beta \quad \text{Eq. 2- 23}$$

$$\frac{\partial \hat{t}_\beta}{\partial \alpha} = \frac{1}{A_\beta}\frac{\partial A_\alpha}{\partial \beta}\hat{t}_\alpha \quad \text{Eq. 2- 24}$$

$$\frac{\partial \hat{t}_\beta}{\partial \beta} = -\frac{A_\beta}{R_\beta}\hat{n} - \frac{1}{A_\alpha}\frac{\partial A_\beta}{\partial \alpha}\hat{t}_\alpha \quad \text{Eq. 2- 25}$$

Equation 2- 19 leads to

$$\frac{\partial}{\partial \beta}\left(\frac{A_\alpha}{R_\alpha}\hat{t}_\alpha\right) = \frac{\partial}{\partial \alpha}\left(\frac{A_\beta}{R_\beta}\hat{t}_\beta\right)$$

$$\left(\frac{\partial}{\partial \beta}\frac{A_\alpha}{R_\alpha}\right)\hat{t}_\alpha + \frac{1}{R_\alpha}\frac{\partial A_\beta}{\partial \alpha}\hat{t}_\beta = \left(\frac{\partial}{\partial \alpha}\frac{A_\beta}{R_\beta}\right)\hat{t}_\beta + \frac{1}{R_\beta}\frac{\partial A_\alpha}{\partial \beta}\hat{t}_\alpha \quad \text{Eq. 2- 26}$$

That means

$$\frac{1}{R_\beta}\frac{\partial A_\alpha}{\partial \beta} = \left(\frac{\partial}{\partial \beta}\frac{A_\alpha}{R_\alpha}\right) \quad \text{Eq. 2- 27}$$

$$\frac{1}{R_\alpha}\frac{\partial A_\beta}{\partial \alpha} = \left(\frac{\partial}{\partial \alpha}\frac{A_\beta}{R_\beta}\right) \quad \text{Eq. 2- 28}$$

Equations 2- 27 and 2- 28 are the so-called Codazzi conditions. Equation 2- 20 leads to

$$\frac{\partial}{\partial \beta}\left(-\frac{A_\alpha}{R_\alpha}\hat{n} - \frac{1}{A_\beta}\frac{\partial A_\alpha}{\partial \beta}\hat{t}_\beta\right) = \frac{\partial}{\partial \alpha}\left(\frac{1}{A_\alpha}\frac{\partial A_\beta}{\partial \alpha}\hat{t}_\beta\right)$$

$$-\frac{A_\alpha}{R_\alpha}\frac{A_\beta}{R_\beta}\hat{t}_\beta - \frac{\partial}{\partial \beta}\left(\frac{1}{A_\beta}\frac{\partial A_\alpha}{\partial \beta}\right)\hat{t}_\beta = \frac{\partial}{\partial \alpha}\left(\frac{1}{A_\alpha}\frac{\partial A_\beta}{\partial \alpha}\right)\hat{t}_\beta \quad \text{Eq. 2- 29}$$

which means

$$\frac{\partial}{\partial \alpha}\left(\frac{1}{A_\alpha}\frac{\partial A_\beta}{\partial \alpha}\right) + \frac{\partial}{\partial \beta}\left(\frac{1}{A_\beta}\frac{\partial A_\alpha}{\partial \beta}\right) = -\frac{A_\alpha}{R_\alpha}\frac{A_\beta}{R_\beta} \quad \text{Eq. 2- 30}$$

Equation 2- 30 is the so-called Gauss condition. For an elliptical cylindrical shell with $\alpha = x$ and $\beta = s$ as shown in Fig. 1- 2, A_α and A_β are unity, $\partial A_\alpha/\partial \beta$ and $\partial A_\beta/\partial \alpha$ are zero, and R_α approaches to infinity (Donnell, 1976). These relations will be used shortly.

2.2 Assumptions of Donnell Shell Theory

While the geometry of a cylinder has been shown in Fig. 1- 2, there are a number of major assumptions regarding the geometry and kinematics that are intrinsic to Donnell shell theory, and, which, of course, lead to limitations of the theory. These primary assumptions of Donnell shell theory for the problem at hand are [58]:

(1) The shell is sufficiently thin, i.e., the ratio of wall thickness to radius, H/R, is small compared to unity.

(2) The strains are sufficiently small compared to unity.

(3) The material obeys Hooke's law

(4) The Kirchhoff hypothesis is assumed valid. That is, straight lines normal to the undeformed reference surface remain straight and normal to the deformed reference surface, and the length of the normal remains unchanged.

(5) The normal and shear stresses acting in the direction normal to the reference surface may be neglected in comparison with the stresses acting in the direction parallel to the reference surface, i.e., the cylinder wall is in a state of plane stress.

(6) The displacements in the x- and s-directions, $u(x,s)$ and $v(x,s)$, are infinitesimal, whereas the displacements in the z-direction, $w(x,s)$, can be of the same order as the wall thickness.

(7) The derivatives of $w(x,s)$ in the x- and s-directions are small compared to unity.

(8) Curvature changes are small and can be represented by linear functions of $w(x,s)$.

Assumption (6) limits the theory to those cases where the major component of the vibration mode is the displacement component normal to the cylinder wall. Assumption (7) limits the number of circumferential and axial waves in the displacement component normal to the cylinder wall. Based on the above assumptions, the details of the deformation of a differential element of cylinder wall are shown schematically in Fig. 2.3. The figure represents the displacement of an element of cylinder wall as seen looking toward the xz plane and sz planes. The blue lines represent the undeformed differential element and the red lines represent the deformed differential element. The solid lines are the inner and outer surfaces of the cylinder wall, while the dotted lines are the reference surface, which, as mentioned earlier, is the mid-surface of the wall. The dash lines are the straight lines normal to the reference surface and as shown, those lines remain straight.

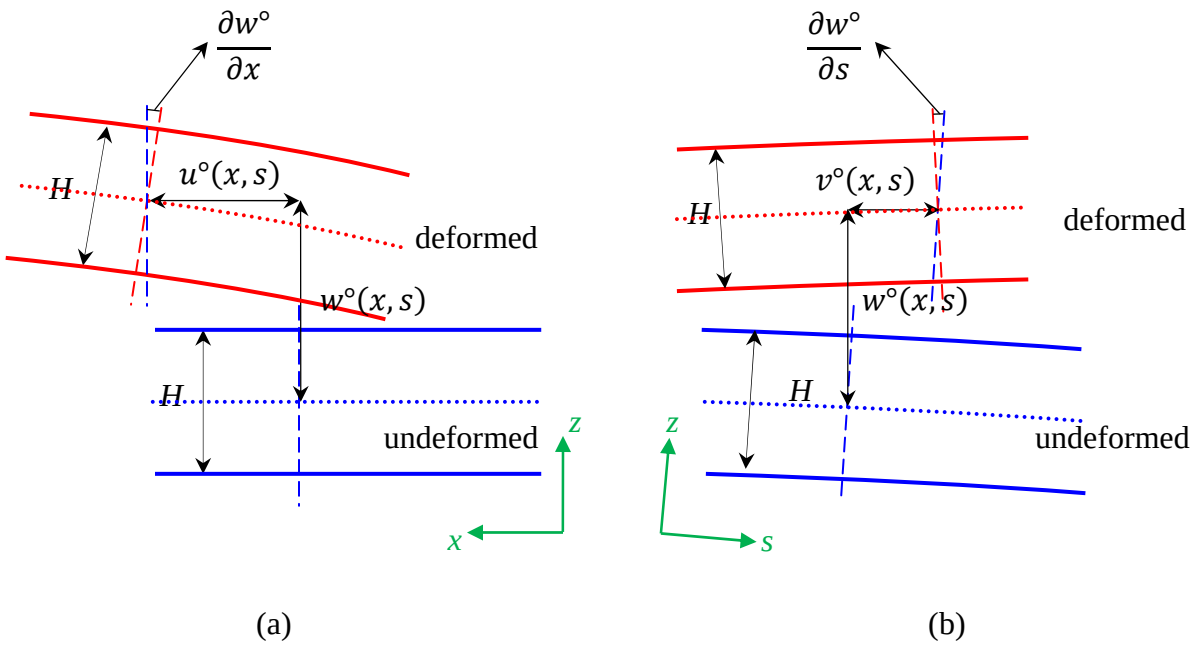

(a) (b)

Fig. 2- 3 Kinematics of deformation (a) in *xz*-plane, and (b) in *sz*-plane

The coordinate systems shown in green coincide with the reference surface and the straight normal lines. Keeping with assumption (4), there is no normal strain in *z*-direction. The displacements of a point on the reference surface in *x*-, *s*-, and *z*-directions are, respectively, u°, v° and w°, as denoted in the last chapter. In Fig. 2- 3a a clockwise rotation of the segment in the *xz* plane is $\phi_s^\circ = -\partial w^\circ / \partial x$, whereas the counterclockwise rotation of the segment in the *sz* plane is $\phi_x^\circ = \partial w^\circ / \partial s$, as seen in Fig. 2- 3b and as illustrated in Fig. 1- 2.

As a result of the translations and rotations illustrated in Fig. 2- 3, by the Kirchhoff hypothesis, assumption (4), the displacements in *x*-, *s*-, and *z*-directions of an arbitrary point in the cylinder wall, denoted as *u*, *v*, and *w*, respectively, are

$$u(x,s,z) = u^\circ(x,s) - z\frac{\partial w^\circ(x,s)}{\partial x}$$

$$v(x,s,z) = v^\circ(x,s) - z\frac{\partial w^\circ(x,s)}{\partial s} \qquad \text{Eq. 2- 31}$$

$$w(x,s,z) = w^\circ(x,s)$$

Denoting the normal strains in *x*- and *s*-directions and the shear strain in *xs* plane, ε_x, ε_s, and γ_{xs}, respectively, then the strains at a general point within the cylinder wall a distance *z* from the reference surface can be expressed in terms of the reference surface strains $\varepsilon_x{}^\circ$, $\varepsilon_s{}^\circ$, and $\gamma_{xs}{}^\circ$, and the reference surface bending and twist curvatures at that point $\kappa_x{}^\circ$, $\kappa_s{}^\circ$, and $\kappa_{xs}{}^\circ$ as

$$\begin{aligned}\varepsilon_x(x,s,z) &= \varepsilon_x{}^\circ(x,s) + z\kappa_x{}^\circ(x,s)\\ \varepsilon_s(x,s,z) &= \varepsilon_s{}^\circ(x,s) + z\kappa_s{}^\circ(x,s)\\ \gamma_{xs}(x,s,z) &= \gamma_{xs}{}^\circ(x,s) + z\kappa_{xs}{}^\circ(x,s)\end{aligned} \qquad \text{Eq. 2- 32}$$

Considering the reference surface strains and curvatures, based on the Donnell shallow shell theory the kinematics of infinitesimal deformations on the reference surface are

$$\begin{aligned}\varepsilon_\alpha{}^\circ &= \frac{1}{A_\alpha}\frac{\partial u^\circ}{\partial \alpha} + \frac{1}{A_\alpha A_\beta}\frac{\partial A_\alpha}{\partial \beta}v^\circ + \frac{w^\circ}{R_\alpha}\\ \varepsilon_\beta{}^\circ &= \frac{1}{A_\beta}\frac{\partial v^\circ}{\partial \beta} + \frac{1}{A_\alpha A_\beta}\frac{\partial A_\beta}{\partial \alpha}u^\circ + \frac{w^\circ}{R_\beta}\\ \gamma_{\alpha\beta}{}^\circ &= \frac{A_\alpha}{A_\beta}\frac{\partial}{\partial \beta}\left(\frac{u^\circ}{A_\alpha}\right) + \frac{A_\beta}{A_\alpha}\frac{\partial A_\beta}{\partial \alpha}\left(\frac{v^\circ}{A_\beta}\right)\end{aligned} \qquad \text{Eq. 2- 33}$$

and the reference surface curvature changes are

$$\begin{aligned}\kappa_\alpha{}^\circ &= \frac{1}{A_\alpha}\frac{\partial \phi_\alpha{}^\circ}{\partial \alpha} + \frac{1}{A_\alpha A_\beta}\frac{\partial A_\alpha}{\partial \beta}\phi_\beta{}^\circ\\ \kappa_\beta{}^\circ &= \frac{1}{A_\beta}\frac{\partial \phi_\beta{}^\circ}{\partial \beta} + \frac{1}{A_\alpha A_\beta}\frac{\partial A_\beta}{\partial \alpha}\phi_\alpha{}^\circ\\ \kappa_{\alpha\beta}{}^\circ &= \frac{1}{A_\alpha}\frac{\partial \phi_\beta{}^\circ}{\partial \alpha} + \frac{1}{A_\beta}\frac{\partial \phi_\alpha{}^\circ}{\partial \beta} - \frac{1}{A_\alpha A_\beta}\left(\phi_\alpha{}^\circ\frac{\partial A_\alpha}{\partial \beta} + \phi_\beta{}^\circ\frac{\partial A_\beta}{\partial \alpha}\right)\end{aligned} \qquad \text{Eq. 2- 34}$$

where the rotations about the α and β directions are, respectively,

$$\begin{aligned}\phi_\alpha{}^\circ &= -\frac{1}{A_\alpha}\frac{\partial w^\circ}{\partial \alpha} + \frac{u^\circ}{R_\alpha}\\ \phi_\beta{}^\circ &= -\frac{1}{A_\beta}\frac{\partial w^\circ}{\partial \beta} + \frac{v^\circ}{R_\beta}\end{aligned} \qquad \text{Eq. 2- 35}$$

Ignoring the effect of u° and v° in $\phi_\alpha{}^\circ$ and $\phi_\beta{}^\circ$, the rotation terms become

$$\begin{aligned}\phi_\alpha{}^\circ &= -\frac{1}{A_\alpha}\frac{\partial w^\circ}{\partial \alpha}\\ \phi_\beta{}^\circ &= -\frac{1}{A_\beta}\frac{\partial w^\circ}{\partial \beta}\end{aligned} \qquad \text{Eq. 2- 36}$$

and the curvature changes become

$$\kappa_\alpha{}^\circ = -\frac{1}{A_\alpha}\frac{\partial}{\partial\alpha}\left(\frac{1}{A_\alpha}\frac{\partial w^\circ}{\partial\alpha}\right) - \frac{1}{A_\alpha A_\beta}\frac{1}{A_\beta}\frac{\partial w^\circ}{\partial\beta}\frac{\partial A_\alpha}{\partial\beta}$$

$$\kappa_\beta{}^\circ = -\frac{1}{A_\beta}\frac{\partial}{\partial\beta}\left(\frac{1}{A_\beta}\frac{\partial w^\circ}{\partial\beta}\right) - \frac{1}{A_\alpha A_\beta}\frac{1}{A_\alpha}\frac{\partial w^\circ}{\partial\alpha}\frac{\partial A_\beta}{\partial\alpha} \qquad \text{Eq. 2- 37}$$

$$\kappa_{\alpha\beta}{}^\circ = -\frac{1}{A_\alpha}\frac{\partial}{\partial\alpha}\left(\frac{1}{A_\beta}\frac{\partial w^\circ}{\partial\beta}\right) - \frac{1}{A_\beta}\frac{\partial}{\partial\beta}\left(\frac{1}{A_\alpha}\frac{\partial w^\circ}{\partial\alpha}\right) + \frac{1}{A_\alpha A_\beta}\left(\frac{1}{A_\alpha}\frac{\partial w^\circ}{\partial\alpha}\frac{\partial A_\alpha}{\partial\beta} + \frac{1}{A_\beta}\frac{\partial w^\circ}{\partial\beta}\frac{\partial A_\beta}{\partial\alpha}\right)$$

Considering the *xsz* curvilinear coordinate system, the strain-displacement relations for a cylindrical shell reference surface can be expressed as

$$\begin{aligned}
\varepsilon_x{}^\circ(x,s) &= \frac{\partial u^\circ(x,s)}{\partial x} \\
\varepsilon_s{}^\circ(x,s) &= \frac{\partial v^\circ(x,s)}{\partial s} + \frac{w^\circ(x,s)}{R(s)} \\
\gamma_{xs}{}^\circ(x,s) &= \frac{\partial u^\circ(x,s)}{\partial s} + \frac{\partial v^\circ(x,s)}{\partial x} \\
\kappa_x{}^\circ(x,s) &= -\frac{\partial^2 w^\circ(x,s)}{\partial x^2} \\
\kappa_s{}^\circ(x,s) &= -\frac{\partial^2 w^\circ(x,s)}{\partial s^2} \\
\kappa_{xs}{}^\circ(x,s) &= -2\frac{\partial^2 w^\circ(x,s)}{\partial x \partial s}
\end{aligned} \qquad \text{Eq. 2- 38}$$

2.3 Constitutive Behavior

For the state of plane stress within the cylinder wall, the transversely isotropic engineering properties of importance for a layer of fiber-reinforced material are: the extensional modulus in the fiber orientation, E_1; the extensional modulus in any direction which is perpendicular to the fiber direction, E_2; the shear modulus in the plane of the layer G_{12}; and the major Poisson's ratio υ_{12}. Following normal convention [59], the 1-direction is in the fiber direction and the 2-

direction is perpendicular to the fiber direction. The 3-direction, not discussed here, is perpendicular to the 1- and 2-directions, is oriented by the right hand rule, and coincides with the *z* direction, the direction normal to the wall. This 123 coordinate system is referred to as the principal material coordinate system. However, for the finite element analysis to be described in Appendix A, which utilizes an element that enforces the Kirchhoff hypothesis as the element becomes thinner and thinner, the through-thickness shear moduli in the principal material coordinate system, G_{13} and G_{23}, are also needed.

Hooke's law for a point within a layer of the cylinder wall can be written as

$$\begin{Bmatrix} \varepsilon_1 \\ \varepsilon_2 \\ \varepsilon_3 \\ \gamma_{23} \\ \gamma_{13} \\ \gamma_{12} \end{Bmatrix} = \begin{bmatrix} \mathrm{S}_{11} & \mathrm{S}_{12} & \mathrm{S}_{13} & 0 & 0 & 0 \\ \mathrm{S}_{21} & \mathrm{S}_{22} & \mathrm{S}_{23} & 0 & 0 & 0 \\ \mathrm{S}_{31} & \mathrm{S}_{32} & \mathrm{S}_{33} & 0 & 0 & 0 \\ 0 & 0 & 0 & \mathrm{S}_{44} & 0 & 0 \\ 0 & 0 & 0 & 0 & \mathrm{S}_{55} & 0 \\ 0 & 0 & 0 & 0 & 0 & \mathrm{S}_{66} \end{bmatrix} \cdot \begin{Bmatrix} \sigma_1 \\ \sigma_2 \\ \sigma_3 \\ \tau_{23} \\ \tau_{13} \\ \tau_{12} \end{Bmatrix} \qquad \text{Eq. 2- 39}$$

where, because of the assumed transverse isotropy,

$$\begin{gathered} \mathrm{S}_{11} = \frac{1}{E_1} \\ \mathrm{S}_{12} = \mathrm{S}_{21} = \mathrm{S}_{13} = \mathrm{S}_{31} = \frac{-\upsilon_{21}}{E_2} = \frac{-\upsilon_{12}}{E_1} \\ \mathrm{S}_{22} = \mathrm{S}_{33} = \frac{1}{E_2} \\ \mathrm{S}_{23} = \mathrm{S}_{32} = \frac{-\upsilon_{23}}{E_2} \\ \mathrm{S}_{44} = \frac{1}{G_{23}} \\ \mathrm{S}_{55} = \mathrm{S}_{66} = \frac{1}{G_{12}} \end{gathered} \qquad \text{Eq. 2- 40}$$

Moreover, considering the condition of plane stress within the cylinder wall, $\sigma_3 = 0, \tau_{23} = 0, \tau_{13} = 0$, Eq. 2- 39 can be reduced into

$$\begin{gathered} \varepsilon_1 = \frac{\sigma_1}{E_1} - \frac{\upsilon_{21}\sigma_2}{E_2} \\ \varepsilon_2 = \frac{\sigma_2}{E_2} - \frac{\upsilon_{12}\sigma_1}{E_1} \end{gathered} \qquad \text{Eq. 2- 41}$$

$$\gamma_{12} = \frac{\tau_{12}}{G_{12}}$$

Based on Eq. 2- 41 for a layer of composite material in a state of plane stress, the Q matrix, with components Q_{11}, Q_{12}, Q_{22}, and Q_{66}, can be employed to express the plane-stress stress-strain relationship in the principle material coordinate system. That relationship can be written as

$$\begin{Bmatrix} \sigma_1 \\ \sigma_2 \\ \tau_{12} \end{Bmatrix} = \begin{bmatrix} \mathrm{Q}_{11} & \mathrm{Q}_{12} & 0 \\ \mathrm{Q}_{12} & \mathrm{Q}_{22} & 0 \\ 0 & 0 & \mathrm{Q}_{66} \end{bmatrix} \cdot \begin{Bmatrix} \varepsilon_1 \\ \varepsilon_2 \\ \gamma_{12} \end{Bmatrix} \qquad \text{Eq. 2- 42}$$

where σ_1, σ_2, and τ_{12} are, respectively, the normal stress in fiber direction, the normal stress perpendicular to the fiber direction, the shear stress in the plane of the layer, whereas ε_1, ε_2, and γ_{12} are the axial strain in fiber direction, the axial strain perpendicular to the fiber direction, and the shear strain in the plane of the layer, respectively. The components of Q matrix are

$$\begin{aligned} \mathrm{Q}_{11} &= \frac{E_1}{1 - \upsilon_{12}\upsilon_{21}} \\ \mathrm{Q}_{12} &= \frac{\upsilon_{12}E_2}{1 - \upsilon_{12}\upsilon_{21}} = \frac{\upsilon_{21}E_1}{1 - \upsilon_{12}\upsilon_{21}} \\ \mathrm{Q}_{22} &= \frac{E_2}{1 - \upsilon_{12}\upsilon_{21}} \\ \mathrm{Q}_{66} &= G_{12} \end{aligned} \qquad \text{Eq. 2- 43}$$

where υ_{21} is determined by the reciprocity relation

$$\frac{\upsilon_{21}}{E_2} = \frac{\upsilon_{12}}{E_1} \qquad \text{Eq. 2- 44}$$

In terms of the curvilinear *xsz* coordinate-system shown in Figs. 1- 2 and 1- 3, σ_x, σ_s, and τ_{xs} are the normal stress in *x*-direction, the normal stress in *s*-direction, the shear stress in *xs*-plane, respectively, whereas ε_x, ε_s, and γ_{xs} are the axial strain in *x*-direction, the axial strain in *s*-direction, and the shear strain in the *xs*-plane, respectively. Assuming, as in Fig. 1- 2, that the fiber direction, i.e., the 1-direction, is oriented at an angle θ relative to the axial *x*-direction, and transforming the stress-strain relation of Eq. 2- 39 into the curvilinear *xsz* coordinate system results in

$$\begin{Bmatrix} \sigma_x \\ \sigma_s \\ \tau_{xs} \end{Bmatrix} = \begin{bmatrix} \overline{\mathrm{Q}}_{11} & \overline{\mathrm{Q}}_{12} & \overline{\mathrm{Q}}_{16} \\ \overline{\mathrm{Q}}_{12} & \overline{\mathrm{Q}}_{22} & \overline{\mathrm{Q}}_{26} \\ \overline{\mathrm{Q}}_{16} & \overline{\mathrm{Q}}_{26} & \overline{\mathrm{Q}}_{66} \end{bmatrix} \cdot \begin{Bmatrix} \varepsilon_x \\ \varepsilon_s \\ \gamma_{xs} \end{Bmatrix} \qquad \text{Eq. 2- 45}$$

where

$$\begin{aligned}
\overline{\mathrm{Q}}_{11} &= \mathrm{Q}_{11}\cos^4\theta + 2(\mathrm{Q}_{12}+2\mathrm{Q}_{66})\cos^2\theta\sin^2\theta + \mathrm{Q}_{22}\sin^4\theta \\
\overline{\mathrm{Q}}_{12} &= (\mathrm{Q}_{11}+\mathrm{Q}_{22}-4\mathrm{Q}_{66})\cos^2\theta\sin^2\theta + \mathrm{Q}_{12}(\cos^4\theta+\sin^4\theta) \\
\overline{\mathrm{Q}}_{16} &= (\mathrm{Q}_{11}-\mathrm{Q}_{12}-2\mathrm{Q}_{66})\cos^3\theta\sin\theta + (\mathrm{Q}_{12}-\mathrm{Q}_{22}+2\mathrm{Q}_{66})\cos\theta\sin^3\theta \\
\overline{\mathrm{Q}}_{22} &= \mathrm{Q}_{11}\sin^4\theta + 2(\mathrm{Q}_{12}+2\mathrm{Q}_{66})\cos^2\theta\sin^2\theta + \mathrm{Q}_{22}\cos^4\theta \\
\overline{\mathrm{Q}}_{26} &= (\mathrm{Q}_{11}-\mathrm{Q}_{12}-2\mathrm{Q}_{66})\cos\theta\sin^3\theta + (\mathrm{Q}_{12}-\mathrm{Q}_{22}+2\mathrm{Q}_{66})\cos^3\theta\sin\theta \\
\overline{\mathrm{Q}}_{66} &= (\mathrm{Q}_{11}+\mathrm{Q}_{22}-2\mathrm{Q}_{12}-2\mathrm{Q}_{66})\cos^2\theta\sin^2\theta + \mathrm{Q}_{66}(\cos^4\theta+\sin^4\theta)
\end{aligned} \qquad \text{Eq. 2- 46}$$

Substituting Eq. 2- 32 into Eq. 2- 45, the stress-strain relationship can be written in terms of the reference surface strains and curvatures as

$$\begin{aligned}
\sigma_x &= \overline{\mathrm{Q}}_{11}\varepsilon_x{}^\circ + \overline{\mathrm{Q}}_{12}\varepsilon_s{}^\circ + \overline{\mathrm{Q}}_{16}\gamma_{xs}{}^\circ + \overline{\mathrm{Q}}_{11} z\,\kappa_x{}^\circ + \overline{\mathrm{Q}}_{12} z\,\kappa_s{}^\circ + \overline{\mathrm{Q}}_{16} z\,\kappa_{xs}{}^\circ \\
\sigma_s &= \overline{\mathrm{Q}}_{12}\varepsilon_x{}^\circ + \overline{\mathrm{Q}}_{22}\varepsilon_s{}^\circ + \overline{\mathrm{Q}}_{26}\gamma_{xs}{}^\circ + \overline{\mathrm{Q}}_{12} z\,\kappa_x{}^\circ + \overline{\mathrm{Q}}_{22} z\,\kappa_s{}^\circ + \overline{\mathrm{Q}}_{26} z\,\kappa_{xs}{}^\circ \\
\tau_{xs} &= \overline{\mathrm{Q}}_{16}\varepsilon_x{}^\circ + \overline{\mathrm{Q}}_{26}\varepsilon_s{}^\circ + \overline{\mathrm{Q}}_{66}\gamma_{xs}{}^\circ + \overline{\mathrm{Q}}_{16} z\,\kappa_x{}^\circ + \overline{\mathrm{Q}}_{26} z\,\kappa_s{}^\circ + \overline{\mathrm{Q}}_{66} z\,\kappa_{xs}{}^\circ
\end{aligned} \qquad \text{Eq. 2- 47}$$

2.4 Stress Resultants

The force resultants N_x, N_s, and N_{xs} are the normal force resultant in *x*-direction, the normal force resultant in the *s*-direction, and shear force resultant in *xs*-plane, respectively. The positive sense of these resultants is illustrated in Fig. 2- 4a. The moment resultants M_x and M_s are referred to as bending moment resultants and M_{xs} is referred to as the twisting moment resultant, as illustrated in Fig. 2- 4b. The force resultants N_x, N_s, and N_{xs} are defined as

$$\begin{aligned}
N_x &\equiv \int_{-H/2}^{H/2} \sigma_x \,\mathrm{dz} \\
N_s &\equiv \int_{-H/2}^{H/2} \sigma_s \,\mathrm{dz} \\
N_{xs} &\equiv \int_{-H/2}^{H/2} \tau_{xs} \,\mathrm{dz}
\end{aligned} \qquad \text{Eq. 2- 48}$$

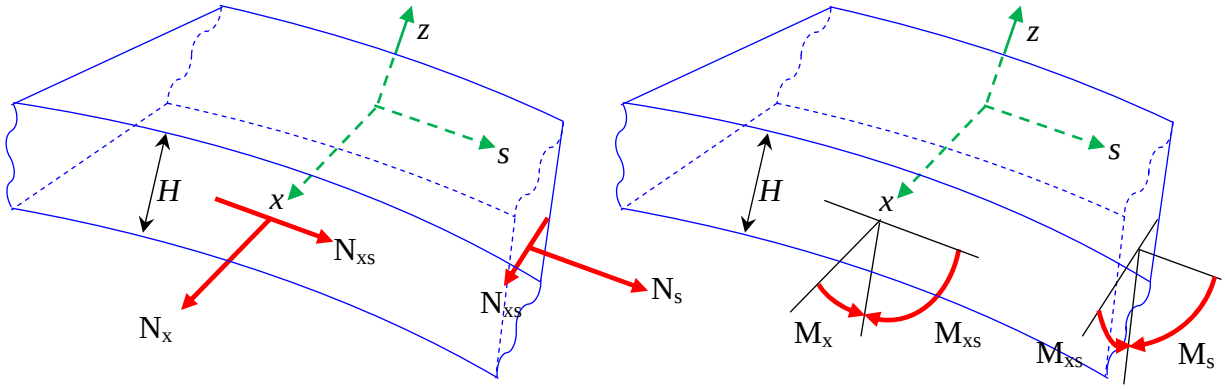

(a) (b)

Fig. 2- 4 (a) Force resultants and (b) moment resultants

The moment resultants M_x, M_s, and M_{xs}, are defined as:

$$M_x \equiv \int_{-H/2}^{H/2} \sigma_x \, z \mathrm{d}z$$

$$M_s \equiv \int_{-H/2}^{H/2} \sigma_s \, z \mathrm{d}z \qquad \text{Eq. 2- 49}$$

$$M_{xs} \equiv \int_{-H/2}^{H/2} \tau_{xs} \, z \mathrm{d}z$$

By substituting Eq. 2- 47 into Eq. 2- 48 and Eq. 2- 49 and carrying out the integration in the z-direction, the force and moment resultants can be expressed in terms of reference strains and reference curvatures as follows:

$$\begin{Bmatrix} N_x \\ N_s \\ N_{xs} \\ M_x \\ M_s \\ M_{xs} \end{Bmatrix} = \begin{bmatrix} \mathrm{A}_{11} & \mathrm{A}_{12} & \mathrm{A}_{16} & \mathrm{B}_{11} & \mathrm{B}_{12} & \mathrm{B}_{16} \\ \mathrm{A}_{12} & \mathrm{A}_{22} & \mathrm{A}_{26} & \mathrm{B}_{12} & \mathrm{B}_{22} & \mathrm{B}_{26} \\ \mathrm{A}_{16} & \mathrm{A}_{26} & \mathrm{A}_{66} & \mathrm{B}_{16} & \mathrm{B}_{26} & \mathrm{B}_{66} \\ \mathrm{B}_{11} & \mathrm{B}_{12} & \mathrm{B}_{16} & \mathrm{D}_{11} & \mathrm{D}_{12} & \mathrm{D}_{16} \\ \mathrm{B}_{12} & \mathrm{B}_{22} & \mathrm{B}_{26} & \mathrm{D}_{12} & \mathrm{D}_{22} & \mathrm{D}_{26} \\ \mathrm{B}_{16} & \mathrm{B}_{26} & \mathrm{B}_{66} & \mathrm{D}_{16} & \mathrm{D}_{26} & \mathrm{D}_{66} \end{bmatrix} \begin{Bmatrix} \varepsilon_x{}^\circ \\ \varepsilon_s{}^\circ \\ \gamma_{xs}{}^\circ \\ \kappa_x{}^\circ \\ \kappa_s{}^\circ \\ \kappa_{xs}{}^\circ \end{Bmatrix} \qquad \text{Eq. 2- 50}$$

where

$$\mathrm{A}_{ij} = \int_{-H/2}^{H/2} \overline{\mathrm{Q}}_{ij} \, \mathrm{d}z \qquad \text{for i, j = 1, 2, 6}$$

$$B_{ij} = \int_{-H/2}^{H/2} \overline{Q}_{ij} z \, dz \qquad \text{for i, j = 1, 2, 6} \qquad \text{Eq. 2- 51}$$

$$D_{ij} = \int_{-H/2}^{H/2} \overline{Q}_{ij} \, z^2 dz \qquad \text{for i, j = 1, 2, 6}$$

Equation 2- 50 is essentially the constitutive equation for the cylinder wall laminate.

2.5 Hamilton's Principle

Hamilton's principle, used in conjunction with the Rayleigh-Ritz method, is an established means for estimating the natural frequencies, in particular, of the cylinders of interest here. Hamilton's principle for a vibratory problem is given as

$$\delta A = \delta \int_{t_0}^{\frac{2\pi}{\omega}+t_0} \left(\widetilde{K} - \widetilde{\Pi}\right) dt = 0 \qquad \text{Eq. 2- 52}$$

where A is the action integral, $\widetilde{\Pi}$ is the potential energy, $\widetilde{K}$ is the kinetic energy, ω is the natural frequency of interest, and δ, treated here mathematically like a differential operator, is the variational operator. The time interval of integration is one complete period of natural oscillation. The time-dependent deformations in *x*-, *s*-, and *z*-directions are denoted as $\widetilde{U}$, $\tilde{V}$ and $\widetilde{W}$, respectively. Displacements $\widetilde{U}$, $\tilde{V}$, and $\widetilde{W}$ are written in the form of Eq. 2- 31 as

$$\widetilde{U}(x,s,z,t) = \widetilde{U}^{\circ}(x,s,t) - z\frac{\partial \widetilde{W}^{\circ}(x,s,t)}{\partial x}$$

$$\tilde{V}(x,s,z,t) = \tilde{V}^{\circ}(x,s,t) - z\frac{\partial \widetilde{W}^{\circ}(x,s,t)}{\partial s} \qquad \text{Eq. 2- 53}$$

$$\widetilde{W}(x,s,z,t) = \widetilde{W}^{\circ}(x,s,t)$$

where $\widetilde{U}^{\circ}$, $\tilde{V}^{\circ}$ and $\widetilde{W}^{\circ}$ are the time-dependent deformations in *x*-, *s*-, and *z*-directions of the reference surface, respectively. The contribution to the action integral of the kinetic energy is

$$A_K = \int_{t_0}^{\frac{2\pi}{\omega}+t_0} \widetilde{K} \, dt = \frac{1}{2}\rho \int_{t_0}^{\frac{2\pi}{\omega}+t_0} \int_0^C \int_0^L \int_{-H/2}^{H/2} \left(\dot{\widetilde{U}}^2 + \dot{\tilde{V}}^2 + \dot{\widetilde{W}}^2\right) dz dx ds dt \qquad \text{Eq. 2- 54}$$

where $\dot{\widetilde{U}}$, $\dot{\tilde{V}}$, and $\dot{\widetilde{W}}$ are partial time derivatives of $\widetilde{U}$, $\tilde{V}$ and $\widetilde{W}$, respectively, and ρ is the mass density. Substituting Eq. 2- 53 into Eq. 2- 54, the contribution to the action integral of the kinetic energy becomes

$$\mathrm{A_K} = \frac{1}{2}\rho \int_{t_0}^{\frac{2\pi}{\omega}+t_0} \int_0^C \int_0^L \int_{-H/2}^{H/2} \left(\dot{\tilde{U}}^{\circ 2} + \dot{\tilde{V}}^{\circ 2} + \dot{\tilde{W}}^{\circ 2} - 2\left(\dot{\tilde{U}}^{\circ} z \frac{\partial \dot{\tilde{W}}^{\circ}}{\partial x} + \dot{\tilde{V}}^{\circ} z \frac{\partial \dot{\tilde{W}}^{\circ}}{\partial s} \right) + z^2 \left(\left(\frac{\partial \dot{\tilde{W}}^{\circ}}{\partial x} \right)^2 + \left(\frac{\partial \dot{\tilde{W}}^{\circ}}{\partial s} \right)^2 \right) \right) \mathrm{d}z\mathrm{d}x\mathrm{d}s\mathrm{d}t$$

Based on the assumptions of the Donnell shell theory, the terms with the first-order spatial derivatives of $\dot{\tilde{W}}^{\circ}$ are ignored and the contribution to the action integral from the kinetic energy becomes

$$\mathrm{A_K} = \frac{1}{2}\rho \int_{t_0}^{\frac{2\pi}{\omega}+t_0} \int_0^C \int_0^L \int_{-\frac{H}{2}}^{\frac{H}{2}} \left(\dot{\tilde{U}}^{\circ 2} + \dot{\tilde{V}}^{\circ 2} + \dot{\tilde{W}}^{\circ 2} \right) \mathrm{d}z\mathrm{d}x\mathrm{d}s\mathrm{d}t$$

$$\mathrm{A_K} = \frac{1}{2}\rho H \int_{t_0}^{\frac{2\pi}{\omega}+t_0} \int_0^C \int_0^L \left(\dot{\tilde{U}}^{\circ 2} + \dot{\tilde{V}}^{\circ 2} + \dot{\tilde{W}}^{\circ 2} \right) \mathrm{d}x\mathrm{d}s\mathrm{d}t \qquad \text{Eq. 2- 55}$$

The contribution to the action integral from the potential energy is

$$\mathrm{A_P} = \int_{t_0}^{\frac{2\pi}{\omega}+t_0} \tilde{\Pi}\, \mathrm{d}t = \frac{1}{2} \int_{t_0}^{\frac{2\pi}{\omega}+t_0} \int_0^C \int_0^L \int_{-H/2}^{H/2} \left(\tilde{\sigma}_x \tilde{\varepsilon}_x + \tilde{\sigma}_s \tilde{\varepsilon}_s + \tilde{\tau}_{xs} \tilde{\gamma}_{xs} \right) \mathrm{d}z\mathrm{d}x\mathrm{d}s\mathrm{d}t \qquad \text{Eq. 2- 56}$$

where $\tilde{\sigma}_x$, $\tilde{\sigma}_s$, and $\tilde{\tau}_{xs}$ are the time-dependent normal stress in *x*-direction, the time-dependent normal stress in *s*-direction, and the time-dependent shear stress in *xs*-plane, respectively, and $\tilde{\varepsilon}_x$, $\tilde{\varepsilon}_s$, $\tilde{\gamma}_{xs}$, are the time-dependent normal strain in *x*-direction, the time-dependent normal strain in *s*-direction, and the time-dependent shear strain in *xs*-plane, respectively. Due to the assumed functional form of Eq. 2- 53, the time-dependent strains have the same relations as Eq. 2- 32 with the corresponding time-dependent strains and curvatures as follows:

$$\begin{aligned} \tilde{\varepsilon}_x(x,s,z,t) &= \tilde{\varepsilon}_x{}^{\circ}(x,s,t) + z\tilde{\kappa}_x{}^{\circ}(x,s,t) \\ \tilde{\varepsilon}_s(x,s,z,t) &= \tilde{\varepsilon}_s{}^{\circ}(x,s,t) + z\tilde{\kappa}_s{}^{\circ}(x,s,t) \\ \tilde{\gamma}_{xs}(x,s,z,t) &= \tilde{\gamma}_{xs}{}^{\circ}(x,s,t) + z\tilde{\kappa}_{xs}{}^{\circ}(x,s,t) \end{aligned} \qquad \text{Eq. 2- 57}$$

where $\tilde{\varepsilon}_x{}^{\circ}$, $\tilde{\varepsilon}_s{}^{\circ}$, and $\tilde{\gamma}_{xs}{}^{\circ}$ are the time-dependent strains of the reference surface and $\tilde{\kappa}_x{}^{\circ}$, $\tilde{\kappa}_s{}^{\circ}$, and $\tilde{\kappa}_{xs}{}^{\circ}$ are the time-dependent curvatures, and the time-dependent strain-displacement relations are from Eq. 2- 38

$$\tilde{\varepsilon}_x{}^{\circ}(x,s,t) = \frac{\partial \tilde{U}^{\circ}(x,s,t)}{\partial x}$$

$$\tilde{\varepsilon}_s{}^{\circ}(x,s,t) = \frac{\partial \tilde{V}^{\circ}(x,s,t)}{\partial s} + \frac{\tilde{W}^{\circ}(x,s,t)}{\tilde{R}(s,t)}$$

$$\tilde{\gamma}_{xs}{}^{\circ}(x,s,t) = \frac{\partial \tilde{U}^{\circ}(x,s,t)}{\partial s} + \frac{\partial \tilde{V}^{\circ}(x,s,t)}{\partial x}$$
$$\tilde{\kappa}_{x}{}^{\circ}(x,s,t) = -\frac{\partial^2 \tilde{W}^{\circ}(x,s,t)}{\partial x^2}$$
$$\tilde{\kappa}_{s}{}^{\circ}(x,s,t) = -\frac{\partial^2 \tilde{W}^{\circ}(x,s,t)}{\partial s^2}$$
$$\tilde{\kappa}_{xs}{}^{\circ}(x,s,t) = -2\frac{\partial^2 \tilde{W}^{\circ}(x,s,t)}{\partial x \partial s}$$

Eq. 2- 58

As a result, the time-dependent stresses have relations with the corresponding time-dependent strains and curvatures from Eq. 2- 47 as

$$\tilde{\sigma}_x = \overline{\mathrm{Q}}_{11}\tilde{\varepsilon}_x{}^{\circ} + \overline{\mathrm{Q}}_{12}\tilde{\varepsilon}_s{}^{\circ} + \overline{\mathrm{Q}}_{16}\tilde{\gamma}_{xs}{}^{\circ} + \overline{\mathrm{Q}}_{11} z\,\tilde{\kappa}_x{}^{\circ} + \overline{\mathrm{Q}}_{12} z\,\tilde{\kappa}_s{}^{\circ} + \overline{\mathrm{Q}}_{16} z\,\tilde{\kappa}_{xs}{}^{\circ}$$
$$\tilde{\sigma}_s = \overline{\mathrm{Q}}_{12}\tilde{\varepsilon}_x{}^{\circ} + \overline{\mathrm{Q}}_{22}\tilde{\varepsilon}_s{}^{\circ} + \overline{\mathrm{Q}}_{26}\tilde{\gamma}_{xs}{}^{\circ} + \overline{\mathrm{Q}}_{12} z\,\tilde{\kappa}_x{}^{\circ} + \overline{\mathrm{Q}}_{22} z\,\tilde{\kappa}_s{}^{\circ} + \overline{\mathrm{Q}}_{26} z\,\tilde{\kappa}_{xs}{}^{\circ}$$
$$\tilde{\tau}_{xs} = \overline{\mathrm{Q}}_{16}\tilde{\varepsilon}_x{}^{\circ} + \overline{\mathrm{Q}}_{26}\tilde{\varepsilon}_s{}^{\circ} + \overline{\mathrm{Q}}_{66}\tilde{\gamma}_{xs}{}^{\circ} + \overline{\mathrm{Q}}_{16} z\,\tilde{\kappa}_x{}^{\circ} + \overline{\mathrm{Q}}_{26} z\,\tilde{\kappa}_s{}^{\circ} + \overline{\mathrm{Q}}_{66} z\,\tilde{\kappa}_{xs}{}^{\circ}$$

Eq. 2- 59

As a result of Eq. 2- 48 and Eq. 2- 49, the time-dependent force and moment resultants are denoted as

$$\tilde{N}_x \equiv \int_{-H/2}^{H/2} \tilde{\sigma}_x \,\mathrm{dz}$$
$$\tilde{N}_s \equiv \int_{-H/2}^{H/2} \tilde{\sigma}_s \,\mathrm{dz}$$
$$\tilde{N}_{xs} \equiv \int_{-H/2}^{H/2} \tilde{\tau}_{xs} \,\mathrm{dz}$$
$$\tilde{M}_x \equiv \int_{-H/2}^{H/2} \tilde{\sigma}_x \, z\mathrm{dz}$$
$$\tilde{M}_s \equiv \int_{-H/2}^{H/2} \tilde{\sigma}_s \, z\mathrm{dz}$$
$$\tilde{M}_{xs} \equiv \int_{-H/2}^{H/2} \tilde{\tau}_{xs} \, z\mathrm{dz}$$

Eq. 2- 60

Based on Eq. 2- 50, the time-dependent force and moment resultants can be written as

$$\begin{Bmatrix} \widetilde{N}_x \\ \widetilde{N}_s \\ \widetilde{N}_{xs} \\ \widetilde{M}_x \\ \widetilde{M}_s \\ \widetilde{M}_{xs} \end{Bmatrix} = \begin{bmatrix} \mathrm{A}_{11} & \mathrm{A}_{12} & \mathrm{A}_{16} & \mathrm{B}_{11} & \mathrm{B}_{12} & \mathrm{B}_{16} \\ \mathrm{A}_{12} & \mathrm{A}_{22} & \mathrm{A}_{26} & \mathrm{B}_{12} & \mathrm{B}_{22} & \mathrm{B}_{26} \\ \mathrm{A}_{16} & \mathrm{A}_{26} & \mathrm{A}_{66} & \mathrm{B}_{16} & \mathrm{B}_{26} & \mathrm{B}_{66} \\ \mathrm{B}_{11} & \mathrm{B}_{12} & \mathrm{B}_{16} & \mathrm{D}_{11} & \mathrm{D}_{12} & \mathrm{D}_{16} \\ \mathrm{B}_{12} & \mathrm{B}_{22} & \mathrm{B}_{26} & \mathrm{D}_{12} & \mathrm{D}_{22} & \mathrm{D}_{26} \\ \mathrm{B}_{16} & \mathrm{B}_{26} & \mathrm{B}_{66} & \mathrm{D}_{16} & \mathrm{D}_{26} & \mathrm{D}_{66} \end{bmatrix} \begin{Bmatrix} \tilde{\varepsilon}_x{}^\circ \\ \tilde{\varepsilon}_s{}^\circ \\ \tilde{\gamma}_{xs}{}^\circ \\ \tilde{\kappa}_x{}^\circ \\ \tilde{\kappa}_s{}^\circ \\ \tilde{\kappa}_{xs}{}^\circ \end{Bmatrix} \qquad \text{Eq. 2- 61}$$

Substituting Eq. 2- 57 and Eq. 2- 60 into Eq. 2- 56, the contribution to the action integral from the potential energy becomes

$$\mathrm{A_P} = \frac{1}{2}\int_{t_0}^{\frac{2\pi}{\omega}+t_0}\int_0^C\int_0^L \big(\widetilde{N}_x\tilde{\varepsilon}_x{}^\circ + \widetilde{N}_s\tilde{\varepsilon}_s{}^\circ + \widetilde{N}_{xs}\tilde{\gamma}_{xs}{}^\circ + \widetilde{M}_x\tilde{\kappa}_x{}^\circ + \widetilde{M}_s\tilde{\kappa}_s{}^\circ + \widetilde{M}_{xs}\tilde{\kappa}_{xs}{}^\circ\big)\mathrm{d}x\mathrm{d}s\mathrm{d}t \qquad \text{Eq. 2- 62}$$

Considering Eq. 2- 52,

$$\delta A = \delta\mathrm{A_K} - \delta\mathrm{A_P} = 0 \qquad \text{Eq. 2- 63}$$

Using Eq. 2- 55, $\delta\mathrm{A_K}$ becomes

$$\begin{aligned}\delta\mathrm{A_K} &= \rho H\int_{t_0}^{\frac{2\pi}{\omega}+t_0}\int_0^C\int_0^L \left(\dot{\tilde{U}}^\circ\delta\dot{\tilde{U}}^\circ + \dot{\tilde{V}}^\circ\delta\dot{\tilde{V}}^\circ + \dot{\widetilde{W}}^\circ\delta\dot{\widetilde{W}}^\circ\right)\mathrm{d}x\mathrm{d}s\mathrm{d}t \\ &= \rho H\int_0^C\int_0^L\int_{t_0}^{\frac{2\pi}{\omega}+t_0} \left(\dot{\tilde{U}}^\circ\delta\dot{\tilde{U}}^\circ + \dot{\tilde{V}}^\circ\delta\dot{\tilde{V}}^\circ + \dot{\widetilde{W}}^\circ\delta\dot{\widetilde{W}}^\circ\right)\mathrm{d}t\mathrm{d}x\mathrm{d}s\end{aligned} \qquad \text{Eq. 2- 64}$$

Considering integration of the first term by parts as follows,

$$\int_{t_0}^{\frac{2\pi}{\omega}+t_0}\dot{\tilde{U}}^\circ\delta\dot{\tilde{U}}^\circ\mathrm{d}t = \dot{\tilde{U}}^\circ\delta\tilde{U}^\circ\Big|_{t=t_0}^{t=\frac{2\pi}{\omega}+t_0} - \int_{t_0}^{\frac{2\pi}{\omega}+t_0}\ddot{\tilde{U}}^\circ\delta\tilde{U}^\circ\mathrm{d}t \qquad \text{Eq. 2- 65}$$

where $\ddot{\tilde{U}}^\circ$ is the second-order time derivative of $\tilde{U}^\circ$, and doing likewise for the other two terms, Eq. 2- 64 can be rewritten as

$$\begin{aligned}\delta\mathrm{A_K} &= \int_0^C\int_0^L \left(\dot{\tilde{U}}^\circ\delta\tilde{U}^\circ + \dot{\tilde{V}}^\circ\delta\tilde{V}^\circ + \dot{\widetilde{W}}^\circ\delta\widetilde{W}^\circ\right)\mathrm{d}x\mathrm{d}s\Big|_{t=t_0}^{t=\frac{2\pi}{\omega}+t_0} \\ &-\rho H\int_0^C\int_0^L\int_{t_0}^{\frac{2\pi}{\omega}+t_0} \left(\ddot{\tilde{U}}^\circ\delta\tilde{U}^\circ + \ddot{\tilde{V}}^\circ\delta\tilde{V}^\circ + \ddot{\widetilde{W}}^\circ\delta\widetilde{W}^\circ\right)\mathrm{d}t\mathrm{d}x\mathrm{d}s\end{aligned} \qquad \text{Eq. 2- 66}$$

where $\ddot{\tilde{V}}^\circ$ and $\ddot{\widetilde{W}}^\circ$ are the second-order derivatives of $\tilde{V}^\circ$ and $\widetilde{W}^\circ$. Considering that the time-dependent displacements are harmonic in time, $\delta\mathrm{A_K}$ becomes

$$\delta\mathrm{A_K} = -\rho H\int_0^C\int_0^L\int_{t_0}^{\frac{2\pi}{\omega}+t_0} \left(\ddot{\tilde{U}}^\circ\delta\tilde{U}^\circ + \ddot{\tilde{V}}^\circ\delta\tilde{V}^\circ + \ddot{\widetilde{W}}^\circ\delta\widetilde{W}^\circ\right)\mathrm{d}t\mathrm{d}x\mathrm{d}s \qquad \text{Eq. 2- 67}$$

Substituting Eq. 2- 58 into Eq. 2- 62, $\delta\mathrm{A_P}$ becomes

$$\delta \mathrm{A_P} = \int_{t_0}^{\frac{2\pi}{\omega}+t_0} \int_0^C \int_0^L \left(\widetilde{N}_x \delta \tilde{\varepsilon}_x{}^\circ + \widetilde{N}_s \delta \tilde{\varepsilon}_s{}^\circ + \widetilde{N}_{xs} \delta \tilde{\gamma}_{xs}{}^\circ \right.$$
$$\left. + \widetilde{M}_x \delta \tilde{\kappa}_x{}^\circ + \widetilde{M}_s \delta \tilde{\kappa}_s{}^\circ + \widetilde{M}_{xs} \delta \tilde{\kappa}_{xs}{}^\circ \right) \mathrm{d}x\mathrm{d}s\mathrm{d}t$$
$$= \int_{t_0}^{\frac{2\pi}{\omega}+t_0} \int_0^C \int_0^L \left(\widetilde{N}_x \frac{\partial \delta \widetilde{U}^\circ}{\partial x} + \widetilde{N}_s \frac{\partial \delta \widetilde{V}^\circ}{\partial s} + \widetilde{N}_s \delta \frac{\widetilde{W}}{R} + \widetilde{N}_{xs} \frac{\partial \delta \widetilde{U}^\circ}{\partial s} + \widetilde{N}_{xs} \frac{\partial \delta \widetilde{V}^\circ}{\partial x} \right.$$
$$\left. - \widetilde{M}_x \frac{\partial^2 \delta \widetilde{W}^\circ}{\partial x^2} - \widetilde{M}_s \frac{\partial^2 \delta \widetilde{W}^\circ}{\partial s^2} - 2\widetilde{M}_{xs} \frac{\partial^2 \delta \widetilde{W}^\circ}{\partial x \partial s} \right) \mathrm{d}x\mathrm{d}s\mathrm{d}t \qquad \text{Eq. 2- 68}$$

Considering integration by parts once, for example, as follows

$$\int_0^L \widetilde{N}_x \frac{\partial \delta \widetilde{U}^\circ}{\partial x} \mathrm{d}x = \widetilde{N}_x \delta \widetilde{U}^\circ \Big|_{x=0}^{x=L} - \int_0^L \frac{\partial \widetilde{N}_x}{\partial x} \delta \widetilde{U}^\circ \mathrm{d}x \qquad \text{Eq. 2- 69}$$

and integration by parts twice, for example, as follows,

$$\int_0^L \widetilde{M}_x \frac{\partial^2 \delta \widetilde{W}^\circ}{\partial x^2} \mathrm{d}x = \widetilde{M}_x \frac{\partial \delta \widetilde{W}^\circ}{\partial x}\Big|_{x=0}^{x=L} - \int_0^L \frac{\partial \widetilde{M}_x}{\partial x} \frac{\partial \delta \widetilde{W}^\circ}{\partial x} \mathrm{d}x$$
$$= \left(\widetilde{M}_x \delta \frac{\partial \widetilde{W}^\circ}{\partial x} - \frac{\partial \widetilde{M}_x}{\partial x} \delta \widetilde{W}^\circ \right)\Big|_{x=0}^{x=L} + \int_0^L \frac{\partial^2 \widetilde{M}_x}{\partial x^2} \delta \widetilde{W}^\circ \, \mathrm{d}x \qquad \text{Eq. 2- 70}$$

$\delta \mathrm{A_P}$ becomes

$$\delta \mathrm{A_P} = \int_{t_0}^{\frac{2\pi}{\omega}+t_0} \int_0^C \widetilde{N}_x \delta \widetilde{U}^\circ \, \mathrm{d}s\mathrm{d}t \Big|_{x=0}^{x=L} - \int_{t_0}^{\frac{2\pi}{\omega}+t_0} \int_0^C \int_0^L \frac{\partial \widetilde{N}_x}{\partial x} \delta \widetilde{U}^\circ \, \mathrm{d}x\mathrm{d}s\,\mathrm{d}t$$
$$+ \int_{t_0}^{\frac{2\pi}{\omega}+t_0} \int_0^L \widetilde{N}_s \delta \widetilde{V}^\circ \, \mathrm{d}x\mathrm{d}t \Big|_{s=0}^{s=C} - \int_{t_0}^{\frac{2\pi}{\omega}+t_0} \int_0^C \int_0^L \frac{\partial \widetilde{N}_s}{\partial s} \delta \widetilde{V}^\circ \, \mathrm{d}x\mathrm{d}s\mathrm{d}t$$
$$+ \int_{t_0}^{\frac{2\pi}{\omega}+t_0} \int_0^C \int_0^L \widetilde{N}_s \delta \frac{\widetilde{W}^\circ}{R} \, \mathrm{d}x\mathrm{d}s\mathrm{d}t \qquad \text{Eq. 2- 71}$$
$$+ \int_{t_0}^{\frac{2\pi}{\omega}+t_0} \int_0^L \widetilde{N}_{xs} \delta \widetilde{U}^\circ \, \mathrm{d}x\mathrm{d}t \Big|_{s=0}^{s=C} - \int_{t_0}^{\frac{2\pi}{\omega}+t_0} \int_0^C \int_0^L \frac{\partial \widetilde{N}_{xs}}{\partial s} \delta \widetilde{U}^\circ \, \mathrm{d}x\mathrm{d}s\mathrm{d}t$$
$$+ \int_{t_0}^{\frac{2\pi}{\omega}+t_0} \int_0^C \widetilde{N}_{xs} \delta \widetilde{V}^\circ \, \mathrm{d}s\mathrm{d}t \Big|_{x=0}^{x=L} - \int_{t_0}^{\frac{2\pi}{\omega}+t_0} \int_0^C \int_0^L \frac{\partial \widetilde{N}_{xs}}{\partial x} \delta \widetilde{V}^\circ \, \mathrm{d}x\mathrm{d}s\mathrm{d}t$$
$$- \int_{t_0}^{\frac{2\pi}{\omega}+t_0} \int_0^C \left(\widetilde{M}_x \delta \frac{\partial \widetilde{W}^\circ}{\partial x} - \frac{\partial \widetilde{M}_x}{\partial x} \delta \widetilde{W}^\circ \right) \mathrm{d}s\mathrm{d}t \Big|_{x=0}^{x=L} - \int_{t_0}^{\frac{2\pi}{\omega}+t_0} \int_0^C \int_0^L \frac{\partial^2 \widetilde{M}_x}{\partial x^2} \delta \widetilde{W}^\circ \, \mathrm{d}x\mathrm{d}s\mathrm{d}t$$

$$-\int_{t_0}^{\frac{2\pi}{\omega}+t_0}\int_0^L\left(\widetilde{M}_s\delta\frac{\partial\widetilde{W}^\circ}{\partial s}-\frac{\partial\widetilde{M}_s}{\partial s}\delta\widetilde{W}^\circ\right)\mathrm{d}x\mathrm{d}t\Bigg|_{s=0}^{s=C}-\int_{t_0}^{\frac{2\pi}{\omega}+t_0}\int_0^C\int_0^L\frac{\partial^2\widetilde{M}_s}{\partial s^2}\delta\widetilde{W}^\circ\ \mathrm{d}x\mathrm{d}s\mathrm{d}t$$

$$-2\int_{t_0}^{\frac{2\pi}{\omega}+t_0}\widetilde{M}_{xs}\delta\widetilde{W}^\circ\mathrm{d}t\Bigg|_{x=0}^{x=L}\Bigg|_{s=0}^{s=C}+2\int_{t_0}^{\frac{2\pi}{\omega}+t_0}\int_0^C\frac{\partial\widetilde{M}_{xs}}{\partial x}\delta\widetilde{W}^\circ\,\mathrm{d}s\mathrm{d}t\Bigg|_{s=0}^{s=C}$$

$$+2\int_{t_0}^{\frac{2\pi}{\omega}+t_0}\int_0^C\frac{\partial\widetilde{M}_{xs}}{\partial s}\delta\widetilde{W}^\circ\,\mathrm{d}s\mathrm{d}t\Bigg|_{x=0}^{x=L}-2\int_{t_0}^{\frac{2\pi}{\omega}+t_0}\int_0^C\int_0^L\frac{\partial^2\widetilde{M}_{xs}}{\partial x\partial s}\delta\widetilde{W}^\circ\ \mathrm{d}x\mathrm{d}s\mathrm{d}t$$

Considering a closed cylinder so that all the values are identical at $s = 0$ and C, $\delta\mathrm{A_P}$ becomes

$$\begin{aligned}\delta\mathrm{A_P}=&\int_{t_0}^{\frac{2\pi}{\omega}+t_0}\int_0^C\left(\widetilde{N}_x\delta\widetilde{U}^\circ+\widetilde{N}_{xs}\delta\widetilde{V}^\circ-\widetilde{M}_x\delta\frac{\partial\widetilde{W}^\circ}{\partial x}\right)\mathrm{d}s\mathrm{d}t\Bigg|_{x=0}^{x=L}\\&+\int_{t_0}^{\frac{2\pi}{\omega}+t_0}\int_0^C\left(\frac{\partial\widetilde{M}_x}{\partial x}+2\frac{\partial\widetilde{M}_{xs}}{\partial s}\right)\delta\widetilde{W}^\circ\mathrm{d}s\mathrm{d}t\Bigg|_{x=0}^{x=L}\\&-\int_{t_0}^{\frac{2\pi}{\omega}+t_0}\int_0^C\int_0^L\left(\left(\frac{\partial\widetilde{N}_x}{\partial x}+\frac{\partial\widetilde{N}_{xs}}{\partial s}\right)\delta\widetilde{U}^\circ+\left(\frac{\partial\widetilde{N}_s}{\partial s}+\frac{\partial\widetilde{N}_{xs}}{\partial x}\right)\delta\widetilde{V}^\circ-\widetilde{N}_s\delta\frac{\widetilde{W}^\circ}{R}\right.\\&\qquad\left.+\left(\frac{\partial^2\widetilde{M}_x}{\partial x^2}+\frac{\partial^2\widetilde{M}_s}{\partial s^2}+2\frac{\partial^2\widetilde{M}_{xs}}{\partial x\partial s}\right)\delta\widetilde{W}^\circ\right)\mathrm{d}x\mathrm{d}s\mathrm{d}t\end{aligned}\qquad\text{Eq. 2- 72}$$

Substituting Eq. 2- 67 and Eq. 2- 72 into Eq. 2- 63, the boundary conditions at $x = 0$ and $x = L$ are obtained as

$$\begin{aligned}&\text{either}\quad\widetilde{N}_x=0\quad\text{or}\quad\delta\widetilde{U}^\circ=0\\&\text{either}\quad\widetilde{N}_{xs}=0\quad\text{or}\quad\delta\widetilde{V}^\circ=0\\&\text{either}\quad\frac{\partial\widetilde{M}_x}{\partial x}+2\frac{\partial\widetilde{M}_{xs}}{\partial s}=0\quad\text{or}\quad\delta\widetilde{W}^\circ=0\\&\text{either}\quad\widetilde{M}_x=0\quad\text{or}\quad\delta\frac{\partial\widetilde{W}^\circ}{\partial x}=0\end{aligned}\qquad\text{Eq. 2- 73}$$

and the governing equations are

$$\int_{t_0}^{\frac{2\pi}{\omega}+t_0}\int_0^C\int_0^L\left(\left(\frac{\partial\widetilde{N}_x}{\partial x}+\frac{\partial\widetilde{N}_{xs}}{\partial s}\right)-\rho H\ddot{\widetilde{U}}^\circ\right)\delta\widetilde{U}^\circ\,\mathrm{d}x\mathrm{d}s\mathrm{d}t=0$$

$$\int_{t_0}^{\frac{2\pi}{\omega}+t_0}\int_0^C\int_0^L\left(\left(\frac{\partial \widetilde{N}_s}{\partial s}+\frac{\partial \widetilde{N}_{xs}}{\partial x}\right)-\rho H\ddot{\widetilde{V}}^\circ\right)\delta\widetilde{V}^\circ \mathrm{d}x\mathrm{d}s\mathrm{d}t=0 \qquad \text{Eq. 2- 74}$$

$$\int_{t_0}^{\frac{2\pi}{\omega}+t_0}\int_0^C\int_0^L\left(\left(\frac{\partial^2 \widetilde{M}_x}{\partial x^2}+\frac{\partial^2 \widetilde{M}_s}{\partial s^2}+2\frac{\partial^2 \widetilde{M}_{xs}}{\partial x\partial s}-\rho H\ddot{\widetilde{W}}^\circ\right)\delta\widetilde{W}^\circ - \widetilde{N}_s\delta\frac{\widetilde{W}^\circ}{R}\right)\mathrm{d}x\mathrm{d}s\mathrm{d}t=0$$

For the natural frequency problem, a separable, harmonic function of time is employed. That is, the time-dependent deformations are as assumed to be the form

$$\begin{aligned}\widetilde{U}(x,s,z,t) &= u(x,s,z)\cos(\omega_k t+\eta)\\ \widetilde{V}(x,s,z,t) &= v(x,s,z)\cos(\omega_k t+\eta)\\ \widetilde{W}(x,s,z,t) &= w(x,s,z)\cos(\omega_k t+\eta)\end{aligned} \qquad \text{Eq. 2- 75}$$

where ω_k is referred to as the natural frequency of the k-th vibration mode, and η is a phase angle. Therefore, the time-dependent deformations on the reference surface are

$$\begin{aligned}\widetilde{U}^\circ(x,s,t) &= u^\circ(x,s)\cos(\omega_k t+\eta)\\ \widetilde{V}^\circ(x,s,t) &= v^\circ(x,s)\cos(\omega_k t+\eta)\\ \widetilde{W}^\circ(x,s,t) &= w^\circ(x,s)\cos(\omega_k t+\eta)\end{aligned} \qquad \text{Eq. 2- 76}$$

The force and moment resultants are then of the form

$$\begin{aligned}\widetilde{N}_x(x,s,t) &= N_x(x,s)\cos(\omega_k t+\eta)\\ \widetilde{N}_s(x,s,t) &= N_s(x,s)\cos(\omega_k t+\eta)\\ \widetilde{N}_{xs}(x,s,t) &= N_{xs}(x,s)\cos(\omega_k t+\eta)\\ \widetilde{M}_x(x,s,t) &= M_x(x,s)\cos(\omega_k t+\eta)\\ \widetilde{M}_s(x,s,t) &= M_s(x,s)\cos(\omega_k t+\eta)\\ \widetilde{M}_{xs}(x,s,t) &= M_{xs}(x,s)\cos(\omega_k t+\eta)\end{aligned} \qquad \text{Eq. 2- 77}$$

Then the governing equations now become

$$\int_0^C\int_0^L\left(\left(\frac{\partial N_x}{\partial x}+\frac{\partial N_{xs}}{\partial s}\right)+\rho H u^\circ {\omega_k}^2\right)\delta u^\circ \mathrm{d}x\mathrm{d}s=0$$

$$\int_0^C\int_0^L\left(\left(\frac{\partial N_s}{\partial s}+\frac{\partial N_{xs}}{\partial x}\right)+\rho H v^\circ {\omega_k}^2\right)\delta v^\circ \mathrm{d}x\mathrm{d}s=0 \qquad \text{Eq. 2- 78}$$

$$\int_0^C \int_0^L \left(\left(\frac{\partial^2 M_x}{\partial x^2} + \frac{\partial^2 M_s}{\partial s^2} + 2\frac{\partial^2 M_{xs}}{\partial x \partial s} + \rho H w^\circ {\omega_k}^2 \right) \delta w^\circ - N_s \delta \frac{w^\circ}{R} \right) \mathrm{d}x\mathrm{d}s = 0$$

For a symmetric, balanced lamination sequence, the governing equations become

$$\int_0^C \int_0^L \left(\mathrm{A}_{11} \frac{\partial^2 u^\circ}{\partial x^2} + \mathrm{A}_{66} \frac{\partial^2 u^\circ}{\partial s^2} + (\mathrm{A}_{12} + \mathrm{A}_{66}) \frac{\partial^2 v^\circ}{\partial x \, \partial s} + \mathrm{A}_{12} \frac{\partial}{\partial x} \frac{w^\circ}{R} + \rho H u^\circ {\omega_k}^2 \right) \delta u^\circ \mathrm{d}x\mathrm{d}s = 0$$

$$\int_0^C \int_0^L \left((\mathrm{A}_{12} + \mathrm{A}_{66}) \frac{\partial^2 u^\circ}{\partial x \, \partial s} + \mathrm{A}_{66} \frac{\partial^2 v^\circ}{\partial x^2} + \mathrm{A}_{22} \frac{\partial^2 v^\circ}{\partial s^2} + \mathrm{A}_{22} \frac{\partial}{\partial s} \frac{w^\circ}{R} + \rho H v^\circ {\omega_k}^2 \right) \delta v^\circ \mathrm{d}x\mathrm{d}s = 0 \qquad \text{Eq. 2- 79}$$

$$\int_0^C \int_0^L \left(\delta \frac{w^\circ}{R} \left(\mathrm{A}_{12} \frac{\partial u^\circ}{\partial x} + \mathrm{A}_{22} \frac{\partial v^\circ}{\partial s} + \mathrm{A}_{22} \frac{w^\circ}{R} \right) + \delta w^\circ \left(\mathrm{D}_{11} \frac{\partial^4 w^\circ}{\partial x^4} + \mathrm{D}_{22} \frac{\partial^4 w^\circ}{\partial s^4} + 4\mathrm{D}_{16} \frac{\partial^4 w^\circ}{\partial x^3 \, \partial s} + 4\mathrm{D}_{26} \frac{\partial^4 w^\circ}{\partial x \partial s^3} + (2\mathrm{D}_{12} + 4\mathrm{D}_{66}) \frac{\partial^4 w^\circ}{\partial x^2 \partial s^2} - \rho H w^\circ {\omega_k}^2 \right) \right) \mathrm{d}x\mathrm{d}s = 0$$

Similarly, in terms of time-independent deformations, $\mathrm{A_K}$ becomes

$$\mathrm{A_K} = \frac{\pi}{2\omega} \rho H {\omega_k}^2 \int_0^C \int_0^L (u^{\circ 2} + v^{\circ 2} + w^{\circ 2}) \, \mathrm{d}x\mathrm{d}s \qquad \text{Eq. 2- 80}$$

and $\mathrm{A_P}$ becomes

$$\begin{aligned} \mathrm{A_P} &= \frac{\pi}{2\omega} \int_0^C \int_0^L (N_x {\varepsilon_x}^\circ + N_s {\varepsilon_s}^\circ + N_{xs} {\gamma_{xs}}^\circ + M_x {\kappa_x}^\circ + M_s {\kappa_s}^\circ + M_{xs} {\kappa_{xs}}^\circ) \, \mathrm{d}x\mathrm{d}s \\ &= \frac{\pi}{2\omega} \int_0^C \int_0^L (\mathrm{A}_{11} {\varepsilon_x}^{\circ 2} + 2\mathrm{A}_{12} {\varepsilon_x}^\circ {\varepsilon_s}^\circ + \mathrm{A}_{22} {\varepsilon_s}^{\circ 2} + 2\mathrm{A}_{16} {\varepsilon_x}^\circ {\gamma_{xs}}^\circ + 2\mathrm{A}_{26} {\gamma_{xs}}^\circ {\varepsilon_s}^\circ \\ &\quad + \mathrm{A}_{66} {\gamma_{xs}}^{\circ 2} + 2\mathrm{B}_{11} {\varepsilon_x}^\circ {\kappa_x}^\circ + 2\mathrm{B}_{12} {\varepsilon_s}^\circ {\kappa_x}^\circ + 2\mathrm{B}_{12} {\varepsilon_x}^\circ {\kappa_s}^\circ + 2\mathrm{B}_{22} {\varepsilon_s}^\circ {\kappa_s}^\circ \\ &\quad + 2\mathrm{B}_{16} {\varepsilon_x}^\circ {\kappa_{xs}}^\circ + 2\mathrm{B}_{16} {\gamma_{xs}}^\circ {\kappa_x}^\circ + 2\mathrm{B}_{26} {\varepsilon_s}^\circ {\kappa_{xs}}^\circ + 2\mathrm{B}_{26} {\gamma_{xs}}^\circ {\kappa_s}^\circ \\ &\quad + 2\mathrm{B}_{66} {\gamma_{xs}}^\circ {\kappa_{xs}}^\circ + \mathrm{D}_{11} {\kappa_x}^{\circ 2} + 2\mathrm{D}_{12} {\kappa_x}^\circ {\kappa_s}^\circ + 2\mathrm{D}_{16} {\kappa_x}^\circ {\kappa_{xs}}^\circ + \mathrm{D}_{22} {\kappa_s}^{\circ 2} \\ &\quad + 2\mathrm{D}_{26} {\kappa_s}^\circ {\kappa_{xs}}^\circ + \mathrm{D}_{66} {\kappa_{xs}}^{\circ 2}) \, \mathrm{d}x\mathrm{d}s \end{aligned} \qquad \text{Eq. 2- 81}$$

For a symmetric, balanced lamination sequence, A_P becomes

$$A_P = \frac{\pi}{2\omega}\int_0^C \int_0^L (A_{11}{\varepsilon_x}^{\circ 2} + 2A_{12}\varepsilon_x{}^{\circ}\varepsilon_s{}^{\circ} + A_{22}{\varepsilon_s}^{\circ 2} + A_{66}{\gamma_{xs}}^{\circ 2} + D_{11}{\kappa_x}^{\circ 2} + D_{22}{\kappa_s}^{\circ 2}$$

$$+2D_{12}\,\kappa_x{}^{\circ}\kappa_s{}^{\circ} + 2D_{16}\kappa_x{}^{\circ}\kappa_{xs}{}^{\circ} + 2D_{26}\,\kappa_s{}^{\circ}\kappa_{xs}{}^{\circ} + D_{66}{\kappa_{xs}}^{\circ 2})\,dx ds \quad \text{Eq. 2- 82}$$

Substituting Eq. 2- 80 and Eq. 2- 82 into Eq. 2- 63, Hamilton's principle is rewritten as

$$\delta A = \frac{\pi}{\omega}\delta K - \frac{\pi}{\omega}\delta \Pi = \frac{\pi}{\omega}(\delta K - \delta \Pi) = 0 \quad \text{Eq. 2- 83}$$

where K is the kinetic energy and

$$K = \frac{1}{2}\rho H {\omega_k}^2 \int_0^C \int_0^L (u^{\circ 2} + v^{\circ 2} + w^{\circ 2})\,dx ds \quad \text{Eq. 2- 84}$$

and Π is the potential energy and

$$\Pi = \frac{1}{2}\int_0^C \int_0^L (A_{11}{\varepsilon_x}^{\circ 2} + 2A_{12}\varepsilon_x{}^{\circ}\varepsilon_s{}^{\circ} + A_{22}{\varepsilon_s}^{\circ 2} + A_{66}{\gamma_{xs}}^{\circ 2} + D_{11}{\kappa_x}^{\circ 2} + D_{22}{\kappa_s}^{\circ 2}$$

$$+2D_{12}\,\kappa_x{}^{\circ}\kappa_s{}^{\circ} + 2D_{16}\kappa_x{}^{\circ}\kappa_{xs}{}^{\circ} + 2D_{26}\,\kappa_s{}^{\circ}\kappa_{xs}{}^{\circ} + D_{66}{\kappa_{xs}}^{\circ 2})\,dx ds \quad \text{Eq. 2- 85}$$

For simply-supported cylinders, the boundary conditions are chosen from Eq. 2- 73 as

$$\begin{gathered} N_x(0,s) = 0 \\ N_x(L,s) = 0 \\ v^{\circ}(0,s) = 0 \\ v^{\circ}(L,s) = 0 \\ w^{\circ}(0,s) = 0 \\ w^{\circ}(L,s) = 0 \\ M_x(0,s) = 0 \\ M_x(L,s) = 0 \end{gathered} \quad \text{Eq. 2- 86}$$

and for clamped support cylinder, the boundary conditions are chosen as

$$\begin{gathered} u^{\circ}(0,s) = 0 \\ u^{\circ}(L,s) = 0 \\ v^{\circ}(0,s) = 0 \\ v^{\circ}(L,s) = 0 \\ w^{\circ}(0,s) = 0 \\ w^{\circ}(L,s) = 0 \end{gathered} \quad \text{Eq. 2- 87}$$

$$\frac{\partial w^{\circ}}{\partial x}(0,s) = 0$$
$$\frac{\partial w^{\circ}}{\partial x}(L,s) = 0$$

2.6 The Rayleigh-Ritz Technique

The separation of time and space variables was assumed in the formulation of Hamilton's principle in the previous section. In this section, to continue with the development of the analysis by introducing the Rayleigh-Ritz technique, it is assumed that the functional dependence of the displacement variables on the spatial coordinates can be further separated and the three components of reference surface displacements are taken to be in the forms of double infinite series as

$$u^{\circ} = \sum_{m=0}^{\infty}\sum_{n=0}^{\infty} \mathrm{U}_{mn} X_m^u(x)\Phi_n^u(s)$$
$$v^{\circ} = \sum_{m=0}^{\infty}\sum_{n=0}^{\infty} \mathrm{V}_{mn} X_m^v(x)\Phi_n^v(s) \qquad \text{Eq. 2- 88}$$
$$w^{\circ} = \sum_{m=0}^{\infty}\sum_{n=0}^{\infty} \mathrm{W}_{mn} X_m^w(x)\Phi_n^w(s)$$

where $X_m^u(x)$, $X_m^v(x)$, and $X_m^w(x)$ are functions of x for displacements in x-, s-, and z-direction, respectively, and $\Phi_n^u(s)$, $\Phi_n^v(s)$, and $\Phi_n^w(s)$ are functions of s. The coefficients U_{mn}, V_{mn} and W_{mn} are undetermined. The functions $X_m^u(x)$, $X_m^v(x)$, $X_m^w(x)$, $\Phi_n^u(s)$, $\Phi_n^v(s)$, and $\Phi_n^w(s)$ are selected to each satisfy the simple support or fixed boundary condition of the cylinder. The integers m and n are associated with the wave numbers in the axial and circumferential directions, respectively. Therefore, the subscript k in governing equations should be replaced by the subscript mn. The Rayleigh-Ritz technique consists of substitutive the displacement form of Eq. 2- 88 into the various components of Eq. 2- 83. The variational process then reduces to the variation of the undetermined coefficients, i.e., $\delta\mathrm{U}_{mn}$, $\delta\mathrm{V}_{mn}$, $\delta\mathrm{W}_{mn}$, ultimately leading to an eigenvalue problem for the cylinder natural frequency ω_{mn}. Application of the Rayleigh-Ritz technique to circular and noncircular cylinders is presented in the next chapter, the results being expressions for the natural frequencies of the cylinders.

Chapter 3 Development of Equations for Natural Frequencies

Using Hamilton's principle and the Rayleigh-Ritz technique, as presented in Section 2.5 and Section 2.6, the equations for natural frequencies of circular and noncircular composite cylinders are derived in this chapter. In Section 3.1 the equations for simply-supported and clamped support circular cylindrical shells are developed. In Section 3.2 the concept of shape factor for use with noncircular cylinders is introduced. In Section 3.3 the equations for the natural frequency of noncircular cylindrical shells are developed by employing the shape factor concept.

3.1 Natural Frequency Equation for Circular Cylinders

There are two subsections to follow: simply-supported cylinders are addressed in the first section, while clamped support cylinders are addressed in the second. In each subsection an equation for natural frequency with consideration of axial, circumferential, and radial inertia is developed. Then, a simplified equation obtained by only considering radial inertia is presented. Finally, other simplifications are made to develop yet other equations for the natural frequency.

3.1.1 Simply-Supported Cylinders

Referring to Eq. 2- 88, the assumed forms of the spatial dependence of the displacements for the application of the Rayleigh-Ritz technique for simply-supported cylinders are taken to be:

$$u^\circ = \sum_{m=0}^{\infty}\sum_{n=0}^{\infty} \mathrm{U}_{mn}\cos\left(\frac{m\pi x}{L}\right)\cos\left(\frac{2n\pi s}{C}\right)$$

$$v^\circ = \sum_{m=0}^{\infty}\sum_{n=0}^{\infty} \mathrm{V}_{mn}\sin\left(\frac{m\pi x}{L}\right)\sin\left(\frac{2n\pi s}{C}\right) \qquad \text{Eq. 3- 1}$$

$$w^\circ = \sum_{m=0}^{\infty}\sum_{n=0}^{\infty} \mathrm{W}_{mn}\sin\left(\frac{m\pi x}{L}\right)\cos\left(\frac{2n\pi s}{C}\right)$$

Considering $m = 0$ case, the assumed displacements become

$$u^\circ = \sum_{n=0}^{\infty} \mathrm{U}_{0n} \cos\left(\frac{2n\pi s}{C}\right)$$

$$v^\circ = 0 \qquad \text{Eq. 3- 2}$$

$$w^\circ = 0$$

for which there is only axial motion in a shearing-type motion. Considering $m > 0$ case, the assumed displacements become

$$u^\circ = \sum_{m=1}^{\infty}\sum_{n=0}^{\infty} \mathrm{U}_{mn} \cos\left(\frac{m\pi x}{L}\right)\cos\left(\frac{2n\pi s}{C}\right)$$

$$v^\circ = \sum_{m=1}^{\infty}\sum_{n=0}^{\infty} \mathrm{V}_{mn} \sin\left(\frac{m\pi x}{L}\right)\sin\left(\frac{2n\pi s}{C}\right) \qquad \text{Eq. 3- 3}$$

$$w^\circ = \sum_{m=1}^{\infty}\sum_{n=0}^{\infty} \mathrm{W}_{mn} \sin\left(\frac{m\pi x}{L}\right)\cos\left(\frac{2n\pi s}{C}\right)$$

Substituting Eq. 3- 2 into Eq. 2- 38, for $m = 0$, the spatial dependence of the reference strains and reference curvatures become

$$\varepsilon_x{}^\circ = 0$$

$$\varepsilon_s{}^\circ = 0$$

$$\gamma_{xs}{}^\circ = -\sum_{n=0}^{\infty} \mathrm{U}_{0n} \frac{2n\pi}{C} \sin\left(\frac{2n\pi s}{C}\right) \qquad \text{Eq. 3- 4}$$

$$\kappa_x{}^\circ = 0$$

$$\kappa_s{}^\circ = 0$$

$$\kappa_{xs}{}^\circ = 0$$

The corresponding potential energy becomes

$$\Pi = \frac{LC}{8} \mathrm{A}_{66} \left(\mathrm{U}_{0n} \frac{2n\pi}{C}\right)^2 \qquad \text{Eq. 3- 5}$$

and the corresponding kinetic energy is

$$\mathrm{K} = \frac{LC}{8}\rho H{\omega_{0n}}^2\left({\mathrm{U}_{0n}}^2\right) \qquad \text{Eq. 3- 6}$$

Substituting Eq. 3- 5 and Eq. 3- 6 into Eq. 2- 83, the equation for the natural frequency at $m = 0$ is obtained as

$$\rho H{\omega_{0n}}^2 = \left(\frac{2n\pi}{C}\right)^2 \mathrm{A}_{66} \qquad \text{Eq. 3- 7}$$

Though not shown explicitly, the $m = 0$ case results in frequencies much higher than the fundamental frequency, which is the interest here.

For $m > 0$, substituting Eq. 3- 3 into Eq. 2- 38, the spatial dependence of the reference strains and reference curvatures become

$$\begin{aligned}
{\varepsilon_x}^\circ &= -\sum_{m=1}^{\infty}\sum_{n=0}^{\infty}\mathrm{U}_{mn}\frac{m\pi}{L}\sin\left(\frac{m\pi x}{L}\right)\cos\left(\frac{2n\pi s}{C}\right)\\
{\varepsilon_s}^\circ &= \sum_{m=1}^{\infty}\sum_{n=0}^{\infty}\left(\mathrm{V}_{mn}\frac{2n\pi}{C}+\frac{\mathrm{W}_{mn}}{R}\right)\sin\left(\frac{m\pi x}{L}\right)\cos\left(\frac{2n\pi s}{C}\right)\\
{\gamma_{xs}}^\circ &= \sum_{m=1}^{\infty}\sum_{n=0}^{\infty}\left(\mathrm{V}_{mn}\frac{m\pi}{L}-\mathrm{U}_{mn}\frac{2n\pi}{C}\right)\cos\left(\frac{m\pi x}{L}\right)\sin\left(\frac{2n\pi s}{C}\right)\\
{\kappa_x}^\circ &= \sum_{m=1}^{\infty}\sum_{n=0}^{\infty}\mathrm{W}_{mn}\left(\frac{m\pi}{L}\right)^2\sin\left(\frac{m\pi x}{L}\right)\cos\left(\frac{2n\pi s}{C}\right)\\
{\kappa_s}^\circ &= \sum_{m=1}^{\infty}\sum_{n=0}^{\infty}\mathrm{W}_{mn}\left(\frac{2n\pi}{C}\right)^2\sin\left(\frac{m\pi x}{L}\right)\cos\left(\frac{2n\pi s}{C}\right)\\
{\kappa_{xs}}^\circ &= 2\sum_{m=1}^{\infty}\sum_{n=0}^{\infty}\mathrm{W}_{mn}\left(\frac{m\pi}{L}\right)\left(\frac{2n\pi}{C}\right)\cos\left(\frac{m\pi x}{L}\right)\sin\left(\frac{2n\pi s}{C}\right)
\end{aligned} \qquad \text{Eq. 3- 8}$$

Substituting Eq. 3- 8 into Eq. 2- 85, the potential energy becomes

$$\begin{aligned}
\Pi = \frac{LC}{8}\Bigg(&\mathrm{A}_{11}\left(\mathrm{U}_{mn}\frac{m\pi}{L}\right)^2 - 2\mathrm{A}_{12}\left(\mathrm{U}_{mn}\frac{m\pi}{L}\right)\left(\mathrm{V}_{mn}\frac{2n\pi}{C}+\frac{\mathrm{W}_{mn}}{R}\right)\\
&+\mathrm{A}_{22}\left(\mathrm{V}_{mn}\frac{2n\pi}{C}+\frac{\mathrm{W}_{mn}}{R}\right)^2 + \mathrm{A}_{66}\left(\mathrm{V}_{mn}\frac{m\pi}{L}-\mathrm{U}_{mn}\frac{2n\pi}{C}\right)^2\\
&+\mathrm{D}_{11}{\mathrm{W}_{mn}}^2\left(\frac{m\pi}{L}\right)^4 + 2\mathrm{D}_{12}\,{\mathrm{W}_{mn}}^2\left(\frac{m\pi}{L}\right)^2\left(\frac{2n\pi}{C}\right)^2\\
&+\mathrm{D}_{22}{\mathrm{W}_{mn}}^2\left(\frac{2n\pi}{C}\right)^4 + 4\mathrm{D}_{66}{\mathrm{W}_{mn}}^2\left(\frac{m\pi}{L}\right)^2\left(\frac{2n\pi}{C}\right)^2\Bigg)
\end{aligned} \qquad \text{Eq. 3- 9}$$

Substituting Eq. 3- 1 into Eq. 2- 84, the kinetic energy becomes

$$\mathrm{K} = \frac{LC}{8}\rho H\omega_{mn}{}^{2}\left(\mathrm{U}_{mn}{}^{2} + \mathrm{V}_{mn}{}^{2} + \mathrm{W}_{mn}{}^{2}\right) \qquad \text{Eq. 3- 10}$$

Unlike the m = 0 case, which has only one undecided coefficient, U_{0n}, so that the natural frequency can be solved directly by eliminating U_{0n} in both the potential and kinetic energies, as in Eq. 3- 7, the $m > 0$ case has three coefficients. Since Hamilton's principle stipulates that $\delta(\mathrm{K} - \Pi) = 0$, and U_{mn}, V_{mn} and W_{mn} are common undetermined coefficients in both the potential energy and the kinetic energy expressions, the simultaneous equations resulting from application of Hamilton's principle are expressed as

$$\begin{aligned} \frac{\partial(\Pi - \mathrm{K})}{\partial \mathrm{U}_{mn}} &= 0 \\ \frac{\partial(\Pi - \mathrm{K})}{\partial \mathrm{V}_{mn}} &= 0 \\ \frac{\partial(\Pi - \mathrm{K})}{\partial \mathrm{W}_{mn}} &= 0 \end{aligned} \qquad \text{Eq. 3- 11}$$

These three equations can be rewritten in matrix form as

$$\begin{bmatrix} \mathrm{T}_{11} - \rho H\omega_{mn}{}^{2} & \mathrm{T}_{12} & \mathrm{T}_{13} \\ \mathrm{T}_{12} & \mathrm{T}_{22} - \rho H\omega_{mn}{}^{2} & \mathrm{T}_{23} \\ \mathrm{T}_{13} & \mathrm{T}_{23} & \mathrm{T}_{33} - \rho H\omega_{mn}{}^{2} \end{bmatrix} \begin{Bmatrix} \mathrm{U}_{mn} \\ \mathrm{V}_{mn} \\ \mathrm{W}_{mn} \end{Bmatrix} = \begin{Bmatrix} 0 \\ 0 \\ 0 \end{Bmatrix} \qquad \text{Eq. 3- 12}$$

where

$$\begin{aligned} \mathrm{T}_{11} &= \mathrm{A}_{11}\left(\frac{m\pi}{L}\right)^{2} + \mathrm{A}_{66}\left(\frac{2n\pi}{C}\right)^{2} \\ \mathrm{T}_{12} &= -(\mathrm{A}_{12} + \mathrm{A}_{66})\left(\frac{m\pi}{L}\right)\left(\frac{2n\pi}{C}\right) \\ \mathrm{T}_{13} &= -\mathrm{A}_{12}\frac{1}{R}\left(\frac{m\pi}{L}\right) \\ \mathrm{T}_{22} &= \mathrm{A}_{66}\left(\frac{m\pi}{L}\right)^{2} + \mathrm{A}_{22}\left(\frac{2n\pi}{C}\right)^{2} \\ \mathrm{T}_{23} &= \mathrm{A}_{22}\frac{1}{R}\left(\frac{2n\pi}{C}\right) \end{aligned} \qquad \text{Eq. 3- 13}$$

and

$$\mathrm{T}_{33} = \mathrm{T}_{33}^{\mathrm{A}} + \mathrm{T}_{33}^{\mathrm{D}} \qquad \text{Eq. 3- 14}$$

where

$$T_{33}^{A} = A_{22}\left(\frac{1}{R}\right)^2 \qquad \text{Eq. 3- 15}$$

$$T_{33}^{D} = D_{11}\left(\frac{m\pi}{L}\right)^4 + (2D_{12} + 4D_{66})\left(\frac{m\pi}{L}\right)^2\left(\frac{2n\pi}{C}\right)^2 + D_{22}\left(\frac{2n\pi}{C}\right)^4 \qquad \text{Eq. 3- 16}$$

Since U_{mn}, V_{mn}, and W_{mn} are independent, the determinant of the three-by-three matrix of coefficients in Eq. 3- 12 must equal zero for there to be a nontrivial solution to the problem. Accordingly, the equation for the natural frequency resulting from equating the determinant to zero is expressed as a sixth degree polynomial in ω_{mn} as

$$\left(\rho H {\omega_{mn}}^2\right)^3 - P_4^s\left(\rho H {\omega_{mn}}^2\right)^2 + P_2^s\left(\rho H {\omega_{mn}}^2\right) - P_0^s = 0 \qquad \text{Eq. 3- 17}$$

where

$$\begin{aligned} P_4^s &= (T_{11} + T_{22} + T_{33}) \\ P_2^s &= \left(T_{11}T_{22} + T_{22}T_{33} + T_{33}T_{11} - {T_{12}}^2 - {T_{23}}^2 - {T_{13}}^2\right) \\ P_0^s &= \left(T_{11}T_{22}T_{33} + 2T_{12}T_{23}T_{13} - T_{33}{T_{12}}^2 - T_{11}{T_{23}}^2 - T_{22}{T_{13}}^2\right) \end{aligned} \qquad \text{Eq. 3- 18}$$

The lowest root, from which the fundamental frequency is derived, is given as

$$\rho H {\omega_{mn}}^2 = \frac{P_4^s}{3} - \frac{1}{3}\sqrt[3]{\frac{RT + \sqrt{RT^2 - 4\left(P_4^{s2} - 3P_2^s\right)^3}}{2}} - \frac{1}{3}\sqrt[3]{\frac{RT - \sqrt{RT^2 - 4\left(P_4^{s2} - 3P_2^s\right)^3}}{2}} \qquad \text{Eq. 3- 19}$$

where

$$RT = -2P_4^{s3} + 9P_4^sP_2^s - 27P_0^s \qquad \text{Eq. 3- 20}$$

The above equation is a bit complicated. It is hypothesized that the vibration mode corresponding to the fundamental frequency is dominated by the normal displacement. Therefore, a simplified equation for natural frequency is derived by ignoring the inertia terms in axial and circumferential directions in Eq. 3- 12. That simplified equation has the form

$$\begin{bmatrix} T_{11} & T_{12} & T_{13} \\ T_{12} & T_{22} & T_{23} \\ T_{13} & T_{23} & T_{33} - \rho H {\omega_{mn}}^2 \end{bmatrix}\begin{Bmatrix} U_{mn} \\ V_{mn} \\ W_{mn} \end{Bmatrix} = \begin{Bmatrix} 0 \\ 0 \\ 0 \end{Bmatrix} \qquad \text{Eq. 3- 21}$$

The simplified natural frequency equation is given by the less complex form

$$\rho H \omega_{mn}{}^2 = \mathrm{T}_{33}^{\mathrm{D}} + \frac{\mathrm{A}_{66}}{R^2}\left(\frac{m\pi}{L}\right)^4 \frac{\mathrm{A}_{11}\mathrm{A}_{22} - \mathrm{A}_{12}{}^2}{\mathrm{T}_{11}\mathrm{T}_{22} - \mathrm{T}_{12}{}^2} \qquad \text{Eq. 3- 22}$$

Equation 3- 22 matches Dong's natural frequency equation for circular cylinder with simple supports [32].

3.1.2 Clamped Support Cylinders

To use the Rayleigh-Ritz approach for the cylinders with clamped supports, the functional dependence of the assumed displacements on the axial coordinate needs to be carefully considered. The vibration mode in the axial direction is assumed to contain only a wave number-to-cylinder length ratio in each vibration mode. According to this assumption, a common form for $X_m^v(x)$ and $X_m^w(x)$ is written as

$$X_m^0(x) = \chi_1 \sin\left(\frac{\lambda_m x}{L}\right) + \chi_2 \cos\left(\frac{\lambda_m x}{L}\right) + \chi_3 \sinh\left(\frac{\lambda_m x}{L}\right) + \chi_4 \cosh\left(\frac{\lambda_m x}{L}\right) \qquad \text{Eq. 3- 23}$$

This equation was adopted from the solution for the displacement of a vibrating clamped Euler-Bernoulli beam. Because the displacement and rotation of the cylinder are zero at $x = 0$, the function must be modified as

$$X_m^0(x) = \chi_1 \sin\left(\frac{\lambda_m x}{L}\right) + \chi_2 \cos\left(\frac{\lambda_m x}{L}\right) - \chi_1 \sinh\left(\frac{\lambda_m x}{L}\right) - \chi_2 \cosh\left(\frac{\lambda_m x}{L}\right) \qquad \text{Eq. 3- 24}$$

For these two boundary conditions to also be satisfied at $x = L$ the function must satisfy

$$\begin{bmatrix} \sin(\lambda_m) - \sinh(\lambda_m) & \cos(\lambda_m) - \cosh(\lambda_m) \\ \cos(\lambda_m) - \cosh(\lambda_m) & -\sin(\lambda_m) - \sinh(\lambda_m) \end{bmatrix} \begin{Bmatrix} \chi_1 \\ \chi_2 \end{Bmatrix} = \begin{Bmatrix} 0 \\ 0 \end{Bmatrix} \qquad \text{Eq. 3- 25}$$

To obtain a nontrivial solution of χ_1 and χ_2, the determinant of the matrix in Eq. 3- 25 should be zero, that is, λ_m must satisfy

$$\cos\lambda_m \cosh\lambda_m = 1 \qquad \text{Eq. 3- 26}$$

resulting in $\lambda_0 = 0$, $\lambda_1 = 4.73$ with χ_1 and χ_2 the corresponding eigenvector components. Therefore, the form of the displacement components for clamped support cylinders are taken to be

$$u^\circ = \sum_{m=0}^{\infty}\sum_{n=0}^{\infty} \mathrm{U}_{mn} X_m^1(x) \cos\left(\frac{2n\pi s}{C}\right)$$

$$v^\circ = \sum_{m=0}^{\infty}\sum_{n=0}^{\infty} \mathrm{V}_{mn} X_m^0(x) \sin\left(\frac{2n\pi s}{C}\right) \qquad \text{Eq. 3- 27}$$

$$w^\circ = \sum_{m=0}^{\infty}\sum_{n=0}^{\infty} \mathrm{W}_{mn} X_m^0(x) \cos\left(\frac{2n\pi s}{C}\right)$$

where

$$X_m^1(x) = \frac{dX_m^0(x)}{dx} \qquad \text{Eq. 3- 28}$$

Considering the m = 0 case, the displacement components become trivial. Therefore, it is only necessary to consider the m > 0 case. Substituting Eq. 3- 27 into Eq. 2- 38, the spatial dependences of the reference strains and reference curvatures become

$$\begin{aligned}
\varepsilon_x{}^\circ &= \sum_{m=1}^{\infty}\sum_{n=0}^{\infty} \mathrm{U}_{mn} X_m^2(x) \cos\left(\frac{2n\pi s}{C}\right) \\
\varepsilon_s{}^\circ &= \sum_{m=1}^{\infty}\sum_{n=0}^{\infty} \left(\mathrm{V}_{mn}\frac{2n\pi}{C} + \frac{\mathrm{W}_{mn}}{R}\right) X_m^0(x) \cos\left(\frac{2n\pi s}{C}\right) \\
\gamma_{xs}{}^\circ &= \sum_{m=1}^{\infty}\sum_{n=0}^{\infty} \left(\mathrm{V}_{mn} - \mathrm{U}_{mn}\frac{2n\pi}{C}\right) X_m^1(x) \sin\left(\frac{2n\pi s}{C}\right) \\
\kappa_x{}^\circ &= -\sum_{m=1}^{\infty}\sum_{n=0}^{\infty} \mathrm{W}_{mn} X_m^2(x) \cos\left(\frac{2n\pi s}{C}\right) \\
\kappa_s{}^\circ &= \sum_{m=1}^{\infty}\sum_{n=0}^{\infty} \mathrm{W}_{mn} \left(\frac{2n\pi}{C}\right)^2 X_m^0(x) \cos\left(\frac{2n\pi s}{C}\right) \\
\kappa_{xs}{}^\circ &= 2\sum_{m=1}^{\infty}\sum_{n=0}^{\infty} \mathrm{W}_{mn} \left(\frac{2n\pi}{C}\right) X_m^1(x) \sin\left(\frac{2n\pi s}{C}\right)
\end{aligned} \qquad \text{Eq. 3- 29}$$

where

$$X_m^2(x) = \frac{dX_m^1(x)}{dx} \qquad \text{Eq. 3- 30}$$

The potential energy becomes

$$\Pi = \frac{C}{4}\Big(\mathrm{A}_{11}\mathrm{U}_{mn}{}^{2}\mathrm{I}_{1m} + 2\mathrm{A}_{12}\mathrm{U}_{mn}\left(\mathrm{V}_{mn}\frac{2n\pi}{C} + \frac{\mathrm{W}_{mn}}{R}\right)\mathrm{I}_{2m} + \mathrm{A}_{22}\left(\mathrm{V}_{mn}\frac{2n\pi}{C} + \frac{\mathrm{W}_{mn}}{R}\right)^{2}\mathrm{I}_{3m} + \mathrm{A}_{66}\left(\mathrm{V}_{mn} - \mathrm{U}_{mn}\frac{2n\pi}{C}\right)^{2}\mathrm{I}_{4m} + \mathrm{D}_{11}\mathrm{W}_{mn}{}^{2}\mathrm{I}_{1m} - 2\mathrm{D}_{12}\,\mathrm{W}_{mn}{}^{2}\left(\frac{2n\pi}{C}\right)^{2}\mathrm{I}_{2m} + \mathrm{D}_{22}\mathrm{W}_{mn}{}^{2}\left(\frac{2n\pi}{C}\right)^{4}\mathrm{I}_{3m} + 4\mathrm{D}_{66}\mathrm{W}_{mn}{}^{2}\left(\frac{2n\pi}{C}\right)^{2}\mathrm{I}_{4m}\Big) \quad \text{Eq. 3- 31}$$

and the kinetic energy is

$$\mathrm{K} = \frac{C}{4}\rho H\omega_{mn}{}^{2}\left(\mathrm{U}_{mn}{}^{2}\,\mathrm{I}_{4m} + \mathrm{V}_{mn}{}^{2}\,\mathrm{I}_{3m} + \mathrm{W}_{mn}{}^{2}\,\mathrm{I}_{3m}\right) \quad \text{Eq. 3- 32}$$

where

$$\mathrm{I}_{1m} = \int_0^L (X_m^2(x))^2\,\mathrm{d}x$$

$$\mathrm{I}_{2m} = \int_0^L (X_m^0(x)X_m^2(x))\,\mathrm{d}x$$

$$\mathrm{I}_{3m} = \int_0^L (X_m^0(x))^2\,\mathrm{d}x \quad \text{Eq. 3- 33}$$

$$\mathrm{I}_{4m} = \int_0^L (X_m^1(x))^2\,\mathrm{d}x$$

Substituting the potential energy and the kinetic energy into Eq. 3- 11, the matrix form of the natural frequency equation becomes

$$\begin{bmatrix} \mathrm{T}_{11}{}' - \mathrm{I}_{4m}\rho H\omega_{mn}{}^{2} & \mathrm{T}_{12}{}' & \mathrm{T}_{13}{}' \\ \mathrm{T}_{12}{}' & \mathrm{T}_{22}{}' - \mathrm{I}_{3m}\rho H\omega_{mn}{}^{2} & \mathrm{T}_{23}{}' \\ \mathrm{T}_{13}{}' & \mathrm{T}_{23}{}' & \mathrm{T}_{33}{}' - \mathrm{I}_{3m}\rho H\omega_{mn}{}^{2} \end{bmatrix}\begin{Bmatrix} \mathrm{U}_{mn} \\ \mathrm{V}_{mn} \\ \mathrm{W}_{mn} \end{Bmatrix} = \begin{Bmatrix} 0 \\ 0 \\ 0 \end{Bmatrix} \quad \text{Eq. 3- 34}$$

where

$$\mathrm{T}_{11}{}' = \mathrm{A}_{11}\mathrm{I}_{1m} + \mathrm{A}_{66}\mathrm{I}_{4m}\left(\frac{2n\pi}{C}\right)^{2}$$

$$\mathrm{T}_{12}{}' = (\mathrm{A}_{12}\mathrm{I}_{2m} - \mathrm{A}_{66}\mathrm{I}_{4m})\left(\frac{2n\pi}{C}\right)$$

$$\mathrm{T}_{13}{}' = \frac{\mathrm{A}_{12}\mathrm{I}_{2m}}{R} \quad \text{Eq. 3- 35}$$

$$T_{22}' = A_{66}I_{4m} + A_{22}I_{3m}\left(\frac{2n\pi}{C}\right)^2$$

$$T_{23}' = \frac{A_{22}I_{3m}}{R}\left(\frac{2n\pi}{C}\right)$$

and

$$T_{33}' = T_{33}^{A}{}' + T_{33}^{D}{}', \qquad \text{Eq. 3- 36}$$

where

$$T_{33}^{A}{}' = A_{22}I_{3m}\left(\frac{1}{R}\right)^2 \qquad \text{Eq. 3- 37}$$

$$T_{33}^{D}{}' = D_{11}I_{1m} - (2D_{12}I_{2m} - 4D_{66}I_{4m})\left(\frac{2n\pi}{C}\right)^2 + D_{22}I_{3m}\left(\frac{2n\pi}{C}\right)^4 \qquad \text{Eq. 3- 38}$$

As with the simple support case, the equation for natural frequency is expressed as a sixth degree polynomial in ω_{mn} as

$$\left(\rho H {\omega_{mn}}^2\right)^3 - P_4^f\left(\rho H {\omega_{mn}}^2\right)^2 + P_2^f\left(\rho H {\omega_{mn}}^2\right) - P_0^f = 0 \qquad \text{Eq. 3- 39}$$

where

$$P_4^f = \left(\frac{T_{11}'}{I_{4m}} + \frac{T_{22}'}{I_{3m}} + \frac{T_{33}'}{I_{3m}}\right)$$

$$P_2^f = \left(\frac{T_{11}'T_{22}'}{I_{3m}I_{4m}} + \frac{T_{22}'T_{33}'}{{I_{3m}}^2} + \frac{T_{33}'T_{11}'}{I_{3m}I_{4m}} - \frac{{T_{12}'}^2}{I_{3m}I_{4m}} - \frac{{T_{23}'}^2}{{I_{3m}}^2} - \frac{{T_{13}'}^2}{{I_{3m}}^2}\right) \qquad \text{Eq. 3- 40}$$

$$P_0^f = \frac{T_{11}'T_{22}'T_{33}' + 2T_{12}'T_{23}'T_{13}' - T_{33}'{T_{12}'}^2 - T_{11}'{T_{23}'}^2 - T_{22}'{T_{13}'}^2}{{I_{3m}}^2 I_{4m}}$$

Again, the lowest root, from which the fundamental frequency is derived, is given as

$$\rho H {\omega_{mn}}^2 = \frac{P_4^f}{3} - \frac{1}{3}\sqrt[3]{\frac{RT + \sqrt{RT^2 - 4\left({P_4^f}^2 - 3P_2^f\right)^3}}{2}} - \frac{1}{3}\sqrt[3]{\frac{RT - \sqrt{RT^2 - 4\left({P_4^f}^2 - 3P_2^f\right)^3}}{2}} \qquad \text{Eq. 3- 41}$$

where

$$RT = -2{P_4^f}^3 + 9P_4^f P_2^f - 27P_0^f \qquad \text{Eq. 3- 42}$$

As with the simply-supported case, a simplified equation based on ignoring inertia effects in axial and circumferential directions is derivable from the matrix form

$$\begin{bmatrix} \mathrm{T_{11}}' & \mathrm{T_{12}}' & \mathrm{T_{13}}' \\ \mathrm{T_{12}}' & \mathrm{T_{22}}' & \mathrm{T_{23}}' \\ \mathrm{T_{13}}' & \mathrm{T_{23}}' & \mathrm{T_{33}}' - \mathrm{I_{3m}}\rho H{\omega_{mn}}^2 \end{bmatrix} \begin{Bmatrix} \mathrm{U}_{mn} \\ \mathrm{V}_{mn} \\ \mathrm{W}_{mn} \end{Bmatrix} = \begin{Bmatrix} 0 \\ 0 \\ 0 \end{Bmatrix} \qquad \text{Eq. 3- 43}$$

The corresponding equation is

$$\rho H{\omega_{mn}}^2 \mathrm{I_{3m}} = \mathrm{T_{33}^{D}}' + \frac{\mathrm{A_{66}I_{4m}}}{{R_0}^2} \frac{\mathrm{A_{11}I_{1m}A_{22}I_{3m}} - (\mathrm{A_{12}I_{2m}})^2}{\mathrm{T_{11}}'\,\mathrm{T_{22}}' - \mathrm{T_{12}}'^2} \qquad \text{Eq. 3- 44}$$

The frequency equations for circular cylindrical shells with simple and clamped supports have been presented with and without considerations of inertia in axial and circumferential directions. Attention now turns to the noncircular cylinders.

3.2 Shape Factor for Noncircular Cylinders

The analysis of the vibration characteristics for noncircular cylinders is different than the analysis for circular cylinders. For the circular cylinders the Rayleigh-Ritz approach employed functions for $\Phi_n^v(s)$ and $\Phi_n^w(s)$ that were orthogonal, specifically, $\cos(2n\pi s/C)$ and $\sin(2n\pi s/C)$. However, there was no requirement for which function should be $\cos(2n\pi s/C)$ and which one should be $\sin(2n\pi s/C)$. Similarly, $\Phi_n^u(s)$ can be chosen as either $\cos(2n\pi s/C)$ or $\sin(2n\pi s/C)$. However, identical functions for $\Phi_n^u(s)$ and $\Phi_n^w(s)$ lead to lower fundamental frequencies than identical functions for $\Phi_n^v(s)$ and $\Phi_n^w(s)$, independent of whether a cosine or a sine function is considered. In other words, there are four forms for $\Phi_n^u(s)$, $\Phi_n^v(s)$, and $\Phi_n^w(s)$ which satisfy the boundary conditions, as illustrated in Table 3- 1. In Table 3- 1 only the cells outlined with bold lines refer to the combination of functions which lead to the fundamental frequencies. Therefore, once $\Phi_n^w(s)$ is decided, $\Phi_n^u(s)$ and $\Phi_n^v(s)$ are determined. Consequently, it can be concluded that for a circular cylinder the proper use of a cosine function or a sine function for $\Phi_n^w(s)$ will produce the same fundamental frequency. The difference is that the normal displacement of the vibration mode shape as a function of circumferential coordinate is shifted a specific amount in the circumferential direction when a sine function is used for $\Phi_n^w(s)$ relative to when a cosine function is used. Since for a circular cylinder the geometry and material properties are axisymmetric, this is of no consequence and the fundamental frequency computed using a sine function for $\Phi_n^w(s)$ is the same as when using a cosine function.

Table 3- 1 Natural frequency characteristics for different Rayleigh-Ritz forms

	$\Phi_n^v(s) = \sin\left(\frac{2n\pi s}{C}\right)$ $\Phi_n^w(s) = \cos\left(\frac{2n\pi s}{C}\right)$	$\Phi_n^v(s) = -\cos\left(\frac{2n\pi s}{C}\right)$ $\Phi_n^w(\mathrm{s}) = \sin\left(\frac{2n\pi s}{C}\right)$
$\Phi_n^u(s) = \cos\left(\frac{2n\pi s}{C}\right)$	Fundamental frequency	Higher natural frequency
$\Phi_n^u(s) = \sin\left(\frac{2n\pi s}{C}\right)$	Higher natural frequency	Fundamental frequency

On the other hand, because for noncircular cylinders the cylinder geometry is not axisymmetric, using a cosine function for $\Phi_n^w(s)$ rather than a sine function actually represents a different vibration mode shape for the normal displacement. Table 3- 2 illustrates schematically the normal displacement vibration mode shapes for circular and noncircular cross sections with cosine and sine functions for $\Phi_n^w(s)$ for $n = 5$. To be noted is the fact that for the circular cylinder the amplitudes of the peaks in normal displacement are independent of circumferential location. However, because of the variation of cylinder stiffness with circumferential location due to the variation of radius of curvature with circumferential location, for a noncircular cylinder the amplitudes of the peaks are not expected to be independent of circumferential location, being larger where the radius of curvature is larger.

For the noncircular cylinder, vibrating so the maximum normal displacement amplitude coincides with the location of maximum radius of curvature is different than vibrating such that the maximum normal displacement amplitude coincides with a location where the radius of curvature is not the maximum. It is not clear from the onset which situation results in the fundamental frequency, i.e., the lowest frequency of the two analyses. Both cases must be examined, i.e., both the cosine-based predictions and the sine-based predictions must be considered for determining the fundamental frequency. It is clear from the onset, however, that the amplitude of the vibration mode will be greatest near the location of maximum radius of curvature. This is the basis for introducing the concept of a so-called shape factor for the

functions representing the normal displacement when adapting the Rayleigh-Ritz approach for circular cylinders to noncircular cylinders. Specifically, the shape factor is defined as $R(s)/R_0$, and is employed to modulate variation of normal displacement $w°$ with the circumferential location. Recall, R_0 is the radius of a circular cylinder of the same circumference as the noncircular cylinder and it is introduced simply so the shape factor is nondimensional. The radius of the noncircular cylinder as a function of arc-length, $R(s)$, can be computed using Eq. 1-6 and Eq. 1- 7. For a circular cylinder $R(s)$ is a constant, so the magnitude of the peaks in the normal displacement is not modulated.

Table 3- 2 Normal displacement vibration mode shape for circular and noncircular cylinders

$\Phi_n^w(s)$	Circular cylindrical shells	Noncircular cylindrical shells
$\cos\left(\frac{10\pi s}{C}\right)$	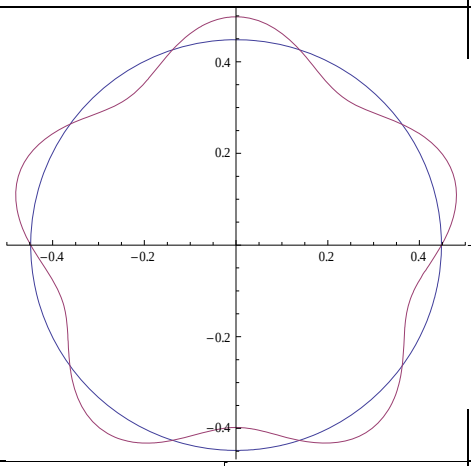	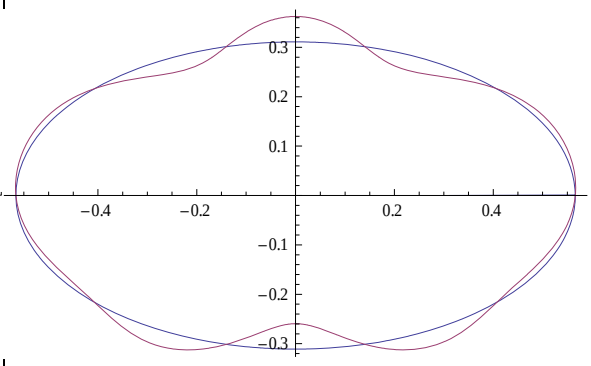
$\sin\left(\frac{10\pi s}{C}\right)$	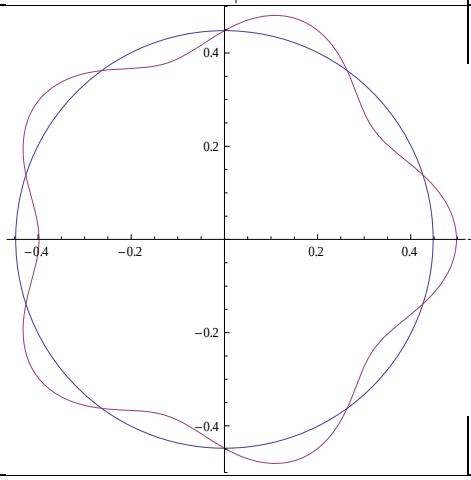	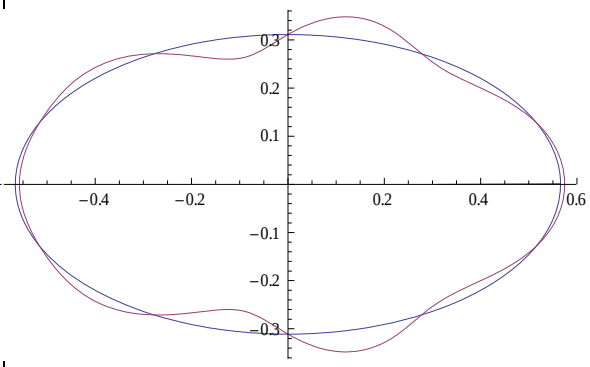

The shape factor is independent of the length of the circumference and depends only on the aspect ratio *b*/*a*, or alternatively, the eccentricity *e*. Though Eq. 1- 6 and Eq. 1- 7 can be used to compute the shape factor, $R(s)/R_0$, since the inverse of $s(\xi)$ in Eq. 1- 7 is not easily developed, a Fourier cosine series expansion of the shape factor is used instead for the elliptical cross sections. In terms of Fourier cosine series, $R(s)/R_0$ is expressed as

$$\frac{R(s)}{R_0} = A_0 + A_2\cos\frac{4\pi s}{C} + A_4\cos\frac{8\pi s}{C} + A_6\cos\frac{12\pi s}{C} + \cdots \qquad \text{Eq. 3- 45}$$

where

$$A_n = \frac{\int_0^C R(\xi)\cos\left(\frac{2n\pi s(\xi)}{C}\right)\mathrm{d}s(\xi)}{R_0\int_0^C \cos^2\left(\frac{2n\pi s(\xi)}{C}\right)\mathrm{d}s(\xi)} \qquad \text{Eq. 3- 46}$$

Considering Eq. 1- 6, Eq. 1- 7, and the relation

$$\mathrm{d}s(\xi) = \sqrt{\mathrm{dY}^2 + \mathrm{dZ}^2} = \sqrt{a^2\cos^2\xi + b^2\sin^2\xi}\,\mathrm{d}\xi \qquad \text{Eq. 3- 47}$$

the coefficients of Fourier cosine series for the shape factor are found. To determine how many terms should be used, a comparison for the four cylinder cross-sectional aspect ratios considered in the present study is shown in Fig. 3- 1. In Fig. 3- 1 the horizontal axis is *s*/*C* and the vertical axis is the shape factor $R(s)/R_0$. The black lines refer to the exact radius of curvature vs. *s*/*C*. The approximate radius of curvatures with different number of terms in the Fourier series are plotted in orange using one term, i.e., only using A_0, in green using two terms, in red using three terms, and in blue using four terms. From Fig. 3- 1 it can be concluded that for low values of eccentricity two terms are sufficient, as in Fig. 3- 1b. In Fig. 3- 1d as the eccentricity increases, four terms provide a good approximation. It is important to mention that since the Rayleigh-Ritz technique is an approximate approach, the use of the Fourier series to represent the shape function need only result in a good approximation to stay within the spirit of the technique rather having to be highly accurate. Accordingly, the four-term Fourier cosine series is employed in the next section for the development of estimates of the natural frequencies for noncircular cylinders.

$$\frac{R(s)}{R_0} = A_0 + A_2\cos\frac{4\pi s}{C} + A_4\cos\frac{8\pi s}{C} + A_6\cos\frac{12\pi s}{C} \qquad \text{Eq. 3- 48}$$

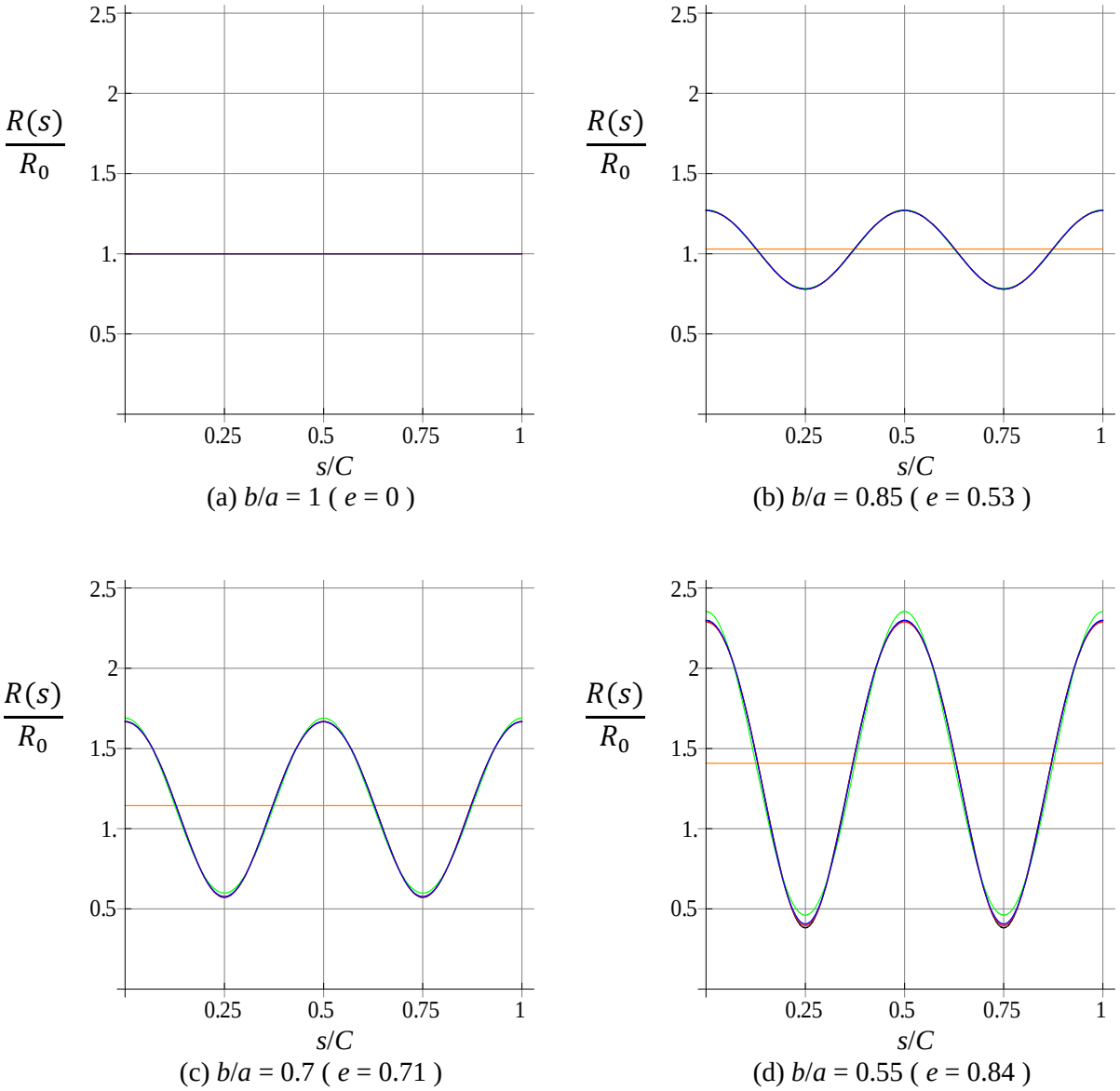

(a) b/a = 1 (e = 0) (b) b/a = 0.85 (e = 0.53)

(c) b/a = 0.7 (e = 0.71) (d) b/a = 0.55 (e = 0.84)

Fig. 3- 1 Effect of number of terms in Fourier series on shape factors for different aspect ratios

3.3 Natural Frequency Equation for Elliptical Cylinders

There are two subsections to follow: simply-supported cylinders are addressed in the first subsection, while clamped support cylinders are addressed in the second. As mentioned in the last section, for noncircular cylinders using a cosine function for representing the circumferential variation of the normal displacement, i.e., the function $\Phi_n^w(s)$, as opposed to using a sine

function results in solving physically different problems. Therefore, in each subsection to follow equations for natural frequencies with consideration of inertia in the axial, circumferential, and normal directions are developed using both the cosine and sine functions for $\Phi_n^w(s)$. A simplified version of the natural frequency equation will be developed by ignoring inertia in both axial and circumferential direction, but retaining the inertia terms associated with the normal displacement. In the development the function $\Phi_n^w(s)$ used will be the product of the shape factor $R(s)/R_0$ and a sine or cosine function of $2n\pi s/C$. That is, as mentioned, the shape factor will modulate the sine or cosine functions. Accordingly, the derivatives with respect to s for noncircular cylinders lead to more complicated expressions than those for circular cylinders, specifically for terms such as $\partial^2 w^o(x,s)/\partial s^2$. Therefore, to derive natural frequency equations which are further simplified, derivatives $\mathrm{d}R(s)/\mathrm{d}s$ and $\mathrm{d}^2R(s)/\mathrm{d}s^2$ will be ignored. Finally, a third stage of simplification leads to what is referred to here as Lo's approximation for the fundamental frequency of elliptical cylinders.

3.3.1 Simply-Supported Cylinders

The assumed forms for the spatial dependence of the displacements for the application of the Rayleigh-Ritz technique for noncircular simply-supported cylinders are taken to be:

$$u^\circ = \sum_{m=0}^{\infty}\sum_{n=0}^{\infty} \mathrm{U}_{mn}\cos\left(\frac{m\pi x}{L}\right)\Phi_n^0(s) \qquad \text{Eq. 3- 49}$$

$$v^\circ = \sum_{m=0}^{\infty}\sum_{n=0}^{\infty} \mathrm{V}_{mn}\sin\left(\frac{m\pi x}{L}\right)\Phi_n^1(s) \qquad \text{Eq. 3- 50}$$

$$w^\circ = \sum_{m=0}^{\infty}\sum_{n=0}^{\infty} \mathrm{W}_{mn}\sin\left(\frac{m\pi x}{L}\right)\Phi_n^2(s) \qquad \text{Eq. 3- 51}$$

where for the cosine-based normal displacement

$$\Phi_n^0(s) = \cos\left(\frac{2n\pi s}{C}\right)$$

$$\Phi_n^1(s) = -\frac{C}{2n\pi}\frac{\mathrm{d}\Phi_n^0(s)}{\mathrm{d}s} = \sin\left(\frac{2n\pi s}{C}\right) \qquad \text{Eq. 3- 52}$$

$$\Phi_n^2(s) = \frac{R(s)}{R_0}\Phi_n^0(s) = \frac{R(s)}{R_0}\cos\left(\frac{2n\pi s}{C}\right)$$

and for the sine-based normal displacement

$$\Phi_n^0(s) = \sin\left(\frac{2n\pi s}{C}\right)$$

$$\Phi_n^1(s) = -\frac{C}{2n\pi}\frac{\mathrm{d}\Phi_n^0(s)}{\mathrm{d}s} = -\cos\left(\frac{2n\pi s}{C}\right) \qquad \text{Eq. 3- 53}$$

$$\Phi_n^2(s) = \frac{R(s)}{R_0}\Phi_n^0(s) = \frac{R(s)}{R_0}\sin\left(\frac{2n\pi s}{C}\right)$$

Then Eq. 3- 50 and Eq. 3- 51 can be rewritten as

$$v^\circ = -\sum_{m=0}^{\infty}\sum_{n=0}^{\infty} \mathrm{V}_{mn}\frac{C}{2n\pi}\sin\left(\frac{m\pi x}{L}\right)\frac{\mathrm{d}\Phi_n^0(s)}{\mathrm{d}s} \qquad \text{Eq. 3- 54}$$

$$w^\circ = \sum_{m=0}^{\infty}\sum_{n=0}^{\infty} \mathrm{W}_{mn}\frac{R(s)}{R_0}\sin\left(\frac{m\pi x}{L}\right)\Phi_n^0(s) \qquad \text{Eq. 3- 55}$$

Considering m = 0 case, the corresponding natural frequency equation for elliptical cylinders is exactly the same as that for circular cylinders. That is the situation because only Eq. 3- 55 contains the shape factor, and for the m = 0 case Eq. 3- 55 is zero so the shape factor is not involved, thereby causing the natural frequency equations for the m = 0 case for circular and elliptical cylinders to be the same. Considering m > 0, by substituting Eq. 3- 49, Eq. 3- 54, and Eq. 3- 55 into Eq. 2- 38, the reference surface strains become

$$\varepsilon_x{}^\circ = -\sum_{m=1}^{\infty}\sum_{n=0}^{\infty} \mathrm{U}_{mn}\frac{m\pi}{L}\sin\left(\frac{m\pi x}{L}\right)\Phi_n^0(s)$$

$$\varepsilon_s{}^\circ = \sum_{m=1}^{\infty}\sum_{n=0}^{\infty} \frac{\mathrm{W}_{mn}}{R_0}\sin\left(\frac{m\pi x}{L}\right)\Phi_n^0(s) - \sum_{m=1}^{\infty}\sum_{n=0}^{\infty} \mathrm{V}_{mn}\frac{C}{2n\pi}\sin\left(\frac{m\pi x}{L}\right)\frac{\mathrm{d}^2\Phi_n^0(s)}{\mathrm{d}s^2} \qquad \text{Eq. 3- 56}$$

$$\gamma_{xs}{}^\circ = \sum_{m=1}^{\infty}\sum_{n=0}^{\infty} \left(\mathrm{U}_{mn} - \mathrm{V}_{mn}\frac{mC}{2nL}\right)\cos\left(\frac{m\pi x}{L}\right)\frac{\mathrm{d}\Phi_n^0(s)}{\mathrm{d}s}$$

and the reference curvatures become

$$\kappa_x{}^\circ = \sum_{m=1}^{\infty}\sum_{n=0}^{\infty} \mathrm{W}_{mn}\left(\frac{m\pi}{L}\right)^2\sin\left(\frac{m\pi x}{L}\right)\Phi_n^2(s)$$

$$\kappa_s{}^\circ = -\sum_{m=1}^{\infty}\sum_{n=0}^{\infty} \mathrm{W}_{mn}\sin\left(\frac{m\pi x}{L}\right)\frac{\mathrm{d}^2\Phi_n^2(s)}{\mathrm{d}s^2} \qquad \text{Eq. 3- 57}$$

$$\kappa_{xs}{}^{\circ} = -2\sum_{m=1}^{\infty}\sum_{n=0}^{\infty} \mathrm{W}_{mn}\left(\frac{m\pi}{L}\right)\cos\left(\frac{m\pi x}{L}\right)\frac{\mathrm{d}\Phi_n^2(s)}{\mathrm{d}s}$$

The total potential energy then becomes

$$\begin{aligned}\Pi = \frac{LC}{8}\Bigg(&\mathrm{A}_{11}\left(\mathrm{U}_{mn}\frac{m\pi}{L}\right)^2 - 2\mathrm{A}_{12}\left(\mathrm{U}_{mn}\frac{m\pi}{L}\right)\left(\mathrm{V}_{mn}\frac{2n\pi}{C}+\frac{\mathrm{W}_{mn}}{R_0}\right)\\ &+\mathrm{A}_{22}\left(\mathrm{V}_{mn}\frac{2n\pi}{C}+\frac{\mathrm{W}_{mn}}{R_0}\right)^2 + \mathrm{A}_{66}\left(\mathrm{V}_{mn}\frac{m\pi}{L}-\mathrm{U}_{mn}\frac{2n\pi}{C}\right)^2\\ &+\mathrm{D}_{11}{\mathrm{W}_{mn}}^2\left(\frac{m\pi}{L}\right)^4\mathrm{S}_{1n} + 2\mathrm{D}_{12}\,{\mathrm{W}_{mn}}^2\left(\frac{m\pi}{L}\right)^2\left(\frac{2n\pi}{C}\right)^2\mathrm{S}_{2n}\\ &+\mathrm{D}_{22}{\mathrm{W}_{mn}}^2\left(\frac{2n\pi}{C}\right)^4\mathrm{S}_{3n} + 4\mathrm{D}_{66}{\mathrm{W}_{mn}}^2\left(\frac{m\pi}{L}\right)^2\left(\frac{2n\pi}{C}\right)^2\mathrm{S}_{4n}\Bigg)\end{aligned} \qquad \text{Eq. 3- 58}$$

where

$$\begin{aligned}\mathrm{S}_{1n} &= \frac{\int_0^C \Phi_n^2(s)^2\,\mathrm{d}s}{\frac{C}{2}}\\ \mathrm{S}_{2n} &= \frac{-\int_0^C\left(\Phi_n^2(s)\frac{\mathrm{d}^2\Phi_n^2(s)}{\mathrm{d}s^2}\right)\mathrm{d}s}{\left(\frac{2n\pi}{C}\right)^2\frac{C}{2}}\\ \mathrm{S}_{3n} &= \frac{\int_0^C\left(\frac{\mathrm{d}^2\Phi_n^2(s)}{\mathrm{d}s^2}\right)^2\mathrm{d}s}{\left(\frac{2n\pi}{C}\right)^4\frac{C}{2}}\\ \mathrm{S}_{4n} &= \frac{\int_0^C\left(\frac{\mathrm{d}\Phi_n^2(s)}{\mathrm{d}s}\right)^2\mathrm{d}s}{\left(\frac{2n\pi}{C}\right)^2\frac{C}{2}}\end{aligned} \qquad \text{Eq. 3- 59}$$

Notice that for circular cylinders S_{1n}, S_{2n}, S_{3n}, and S_{4n} are unity. The kinetic energy is

$$\mathrm{K} = \frac{LC}{8}\rho H\omega_{mn}{}^2\left({\mathrm{U}_{mn}}^2 + {\mathrm{V}_{mn}}^2 + {\mathrm{W}_{mn}}^2\mathrm{S}_{1n}\right) \qquad \text{Eq. 3- 60}$$

The matrix-form natural frequency equation is written as before (Eq. 3- 12) as

$$\begin{bmatrix}\mathrm{T}_{11}-\rho H\omega_{mn}{}^2 & \mathrm{T}_{12} & \mathrm{T}_{13}\\ \mathrm{T}_{12} & \mathrm{T}_{22}-\rho H\omega_{mn}{}^2 & \mathrm{T}_{23}\\ \mathrm{T}_{13} & \mathrm{T}_{23} & \mathrm{T}_{33}-\rho H\omega_{mn}{}^2\mathrm{S}_{1n}\end{bmatrix}\begin{Bmatrix}\mathrm{U}_{mn}\\ \mathrm{V}_{mn}\\ \mathrm{W}_{mn}\end{Bmatrix} = \begin{Bmatrix}0\\0\\0\end{Bmatrix} \qquad \text{Eq. 3- 61}$$

where

$$\mathrm{T}_{11} = \mathrm{A}_{11}\left(\frac{m\pi}{L}\right)^2 + \mathrm{A}_{66}\left(\frac{2n\pi}{C}\right)^2$$

$$\mathrm{T}_{12} = -(\mathrm{A}_{12} + \mathrm{A}_{66})\left(\frac{m\pi}{L}\right)\left(\frac{2n\pi}{C}\right)$$

$$\mathrm{T}_{13} = -\mathrm{A}_{12}\frac{1}{R_0}\left(\frac{m\pi}{L}\right) \qquad \text{Eq. 3- 62}$$

$$\mathrm{T}_{22} = \mathrm{A}_{66}\left(\frac{m\pi}{L}\right)^2 + \mathrm{A}_{22}\left(\frac{2n\pi}{C}\right)^2$$

$$\mathrm{T}_{23} = \mathrm{A}_{22}\frac{1}{R_0}\left(\frac{2n\pi}{C}\right)$$

and

$$\mathrm{T}_{33} = \mathrm{T}_{33}^{\mathrm{A}} + \mathrm{T}_{33}^{\mathrm{D}} \qquad \text{Eq. 3- 63}$$

where

$$\mathrm{T}_{33}^{\mathrm{A}} = \mathrm{A}_{22}\left(\frac{1}{R_0}\right)^2 \qquad \text{Eq. 3- 64}$$

$$\mathrm{T}_{33}^{\mathrm{D}} = \mathrm{D}_{11}\left(\frac{m\pi}{L}\right)^4 \mathrm{S}_{1n} + 2\mathrm{D}_{12}\left(\frac{m\pi}{L}\right)^2\left(\frac{2n\pi}{C}\right)^2 \mathrm{S}_{2n} + \mathrm{D}_{22}\left(\frac{2n\pi}{C}\right)^4 \mathrm{S}_{3n} + 4\mathrm{D}_{66}\left(\frac{m\pi}{L}\right)^2\left(\frac{2n\pi}{C}\right)^2 \mathrm{S}_{4n} \qquad \text{Eq. 3- 65}$$

Except for the $\mathrm{T}_{33}^{\mathrm{D}}$ term, all other T terms are the same as those in the natural frequency equation for circular cylinders. The equation for natural frequency is expressed as a sixth degree polynomial in ω_{mn} as

$$\left(\rho H {\omega_{mn}}^2\right)^3 - P_4^s\left(\rho H {\omega_{mn}}^2\right)^2 + P_2^s\left(\rho H {\omega_{mn}}^2\right) - P_0^s = 0 \qquad \text{Eq. 3- 66}$$

where

$$P_4^s = \left(\mathrm{T}_{11} + \mathrm{T}_{22} + \frac{\mathrm{T}_{33}}{\mathrm{S}_{1n}}\right)$$

$$P_2^s = \left(\mathrm{T}_{11}\mathrm{T}_{22} - {\mathrm{T}_{12}}^2 + \frac{\mathrm{T}_{22}\mathrm{T}_{33} + \mathrm{T}_{33}\mathrm{T}_{11} - {\mathrm{T}_{23}}^2 - {\mathrm{T}_{13}}^2}{\mathrm{S}_{1n}}\right) \qquad \text{Eq. 3- 67}$$

$$P_0^s = \frac{\left(\mathrm{T}_{11}\mathrm{T}_{22}\mathrm{T}_{33} + 2\mathrm{T}_{12}\mathrm{T}_{23}\mathrm{T}_{13} - \mathrm{T}_{33}{\mathrm{T}_{12}}^2 - \mathrm{T}_{11}{\mathrm{T}_{23}}^2 - \mathrm{T}_{22}{\mathrm{T}_{13}}^2\right)}{\mathrm{S}_{1n}}$$

The lowest root, from which the fundamental frequency is derived, is given as

$$\rho H\omega_{mn}{}^2 = \frac{P_4^s}{3} - \frac{1}{3}\sqrt[3]{\frac{\mathrm{RT} + \sqrt{\mathrm{RT}^2 - 4\left(P_4^{s\,2} - 3P_2^s\right)^3}}{2}} - \frac{1}{3}\sqrt[3]{\frac{\mathrm{RT} - \sqrt{\mathrm{RT}^2 - 4\left(P_4^{s\,2} - 3P_2^s\right)^3}}{2}} \qquad \text{Eq. 3- 68}$$

where

$$\mathrm{RT} = -2P_4^{s\,3} + 9P_4^s P_2^s - 27P_0^s \qquad \text{Eq. 3- 69}$$

Equation 3- 68 is the natural frequency equation for noncircular simply-supported cylindrical shells with consideration of axial, circumferential, and radial inertia effects. A simplified equation for natural frequency can be derived by ignoring the inertia terms in axial and circumferential directions in Eq. 3- 61. That equation has the form

$$\begin{bmatrix} \mathrm{T}_{11} & \mathrm{T}_{12} & \mathrm{T}_{13} \\ \mathrm{T}_{12} & \mathrm{T}_{22} & \mathrm{T}_{23} \\ \mathrm{T}_{13} & \mathrm{T}_{23} & \mathrm{T}_{33} - \rho H\omega_{mn}{}^2\mathrm{S}_{1n} \end{bmatrix} \begin{Bmatrix} \mathrm{U}_{mn} \\ \mathrm{V}_{mn} \\ \mathrm{W}_{mn} \end{Bmatrix} = \begin{Bmatrix} 0 \\ 0 \\ 0 \end{Bmatrix} \qquad \text{Eq. 3- 70}$$

The simplified natural frequency equation is given by the less complex form as

$$\rho H\omega_{mn}{}^2 = \mathrm{D}_{11}\left(\frac{m\pi}{L}\right)^4 + 2\mathrm{D}_{12}\left(\frac{m\pi}{L}\right)^2\left(\frac{2n\pi}{C}\right)^2\frac{\mathrm{S}_{2n}}{\mathrm{S}_{1n}} + \mathrm{D}_{22}\left(\frac{2n\pi}{C}\right)^4\frac{\mathrm{S}_{3n}}{\mathrm{S}_{1n}} + 4\mathrm{D}_{66}\left(\frac{m\pi}{L}\right)^2\left(\frac{2n\pi}{C}\right)^2\frac{\mathrm{S}_{4n}}{\mathrm{S}_{1n}} + \frac{\mathrm{A}_{66}}{R_0{}^2}\left(\frac{m\pi}{L}\right)^4\frac{\mathrm{A}_{11}\mathrm{A}_{22} - \mathrm{A}_{12}{}^2}{\mathrm{T}_{11}\mathrm{T}_{22} - \mathrm{T}_{12}{}^2}\frac{1}{\mathrm{S}_{1n}} \qquad \text{Eq. 3- 71}$$

When $\mathrm{d}R(s)/\mathrm{d}s$ and $\mathrm{d}^2R(s)/\mathrm{d}s^2$ are ignored, the parameters $\mathrm{S}_{1n}, \mathrm{S}_{2n}$, and S_{3n} all have the same value and S_{4n} is very close to that value when *n* is greater than two. Therefore, the cosine-based natural frequency equation for noncircular cylinders can be further simplified by equating all four parameters of these parameters. The result becomes

$$\rho H\omega_{mn}{}^2 = \mathrm{D}_{11}\left(\frac{m\pi}{L}\right)^4 + (2\mathrm{D}_{12} + 4\mathrm{D}_{66})\left(\frac{m\pi}{L}\right)^2\left(\frac{2n\pi}{C}\right)^2 + \mathrm{D}_{22}\left(\frac{2n\pi}{C}\right)^4 + \mathrm{A}_{66}\left(\frac{m\pi}{L}\right)^4\frac{\mathrm{A}_{11}\mathrm{A}_{22} - \mathrm{A}_{12}{}^2}{\mathrm{T}_{11}\mathrm{T}_{22} - \mathrm{T}_{12}{}^2}\frac{C}{2\int_0^C R^2(s)\cos^2\frac{2n\pi s}{C}\,\mathrm{d}s} \qquad \text{Eq. 3- 72}$$

and the sine-based equation becomes

$$\rho H {\omega_{mn}}^2 = \mathrm{D}_{11}\left(\frac{m\pi}{L}\right)^4 + (2\mathrm{D}_{12} + 4\mathrm{D}_{66})\left(\frac{m\pi}{L}\right)^2\left(\frac{2n\pi}{C}\right)^2 + \mathrm{D}_{22}\left(\frac{2n\pi}{C}\right)^4 + \mathrm{A}_{66}\left(\frac{m\pi}{L}\right)^4 \frac{\mathrm{A}_{11}\mathrm{A}_{22} - {\mathrm{A}_{12}}^2}{\mathrm{T}_{11}\mathrm{T}_{22} - {\mathrm{T}_{12}}^2} \frac{C}{2\int_0^C R^2(s)\sin^2\frac{2n\pi s}{C}\,\mathrm{d}s} \quad \text{Eq. 3- 73}$$

In order to distinguish among the various equations above, Eq. 3- 71 is subsequently called the *first simplified equation* and Eq. 3- 72 and Eq. 3- 73 are called the *second simplified equations*. It can be observed that an approximation to Eq. 3- 72 and Eq. 3- 73, without consideration of whether using cosine-based or sine-based normal displacements, can be written as

$$\rho H {\omega_{mn}}^2 = \mathrm{D}_{11}\left(\frac{m\pi}{L}\right)^4 + (2\mathrm{D}_{12} + 4\mathrm{D}_{66})\left(\frac{m\pi}{L}\right)^2\left(\frac{2n\pi}{C}\right)^2 + \mathrm{D}_{22}\left(\frac{2n\pi}{C}\right)^4 + \frac{\mathrm{A}_{66}}{R_0 R_{\max}}\left(\frac{m\pi}{L}\right)^4 \frac{\mathrm{A}_{11}\mathrm{A}_{22} - {\mathrm{A}_{12}}^2}{\mathrm{T}_{11}\mathrm{T}_{22} - {\mathrm{T}_{12}}^2} \quad \text{Eq. 3- 74}$$

Equation 3- 74 is subsequently called *Lo's approximate equation*.

3.3.2 Clamped Support Cylinders

The Rayleigh-Ritz form of the assumed displacements for clamped support cylinders are:

$$u^\circ = \sum_{m=0}^{\infty}\sum_{n=0}^{\infty} \mathrm{U}_{mn} X_m^1(x)\Phi_n^0(s) \quad \text{Eq. 3- 75}$$

$$v^\circ = \sum_{m=0}^{\infty}\sum_{n=0}^{\infty} \mathrm{V}_{mn}\, X_m^0(x)\Phi_n^1(s) \quad \text{Eq. 3- 76}$$

$$w^\circ = \sum_{m=0}^{\infty}\sum_{n=0}^{\infty} \mathrm{W}_{mn} X_m^0(x)\Phi_n^2(s) \quad \text{Eq. 3- 77}$$

where $X_m^1(x)$ and $X_m^0(x)$ are defined in Section 3.1.2 and $\Phi_n^0(s)$, $\Phi_n^1(s)$, and $\Phi_n^2(s)$ are defined in Section 3.3.1. Equation 3- 76 and Eq. 3- 77 can be rewritten as

$$v^\circ = -\sum_{m=0}^{\infty}\sum_{n=0}^{\infty} \mathrm{V}_{mn}\frac{C}{2n\pi} X_m^0(x)\frac{\mathrm{d}\Phi_n^0(s)}{\mathrm{d}s} \quad \text{Eq. 3- 78}$$

$$w^\circ = \sum_{m=0}^{\infty}\sum_{n=0}^{\infty} \mathrm{W}_{mn}\frac{R(s)}{R_0} X_m^0(x)\Phi_n^0(s) \quad \text{Eq. 3- 79}$$

As mentioned in Section 3.1.2, the $m = 0$ case will lead to trivial solutions. Considering $m > 0$ case, substituting Eq. 3- 75, Eq. 3- 78, and Eq. 3- 79 into Eq. 2- 38, the reference surface strains become

$$\begin{aligned}
\varepsilon_x{}^\circ &= \sum_{m=1}^{\infty}\sum_{n=0}^{\infty} \mathrm{U}_{mn} X_m^2(x)\Phi_n^0(s) \\
\varepsilon_s{}^\circ &= \sum_{m=1}^{\infty}\sum_{n=0}^{\infty} \left(\frac{\mathrm{W}_{mn}}{R_0} + \mathrm{V}_{mn}\frac{2n\pi}{C}\right) X_m^0(x)\Phi_n^0(s) \\
\gamma_{xs}{}^\circ &= \sum_{m=1}^{\infty}\sum_{n=0}^{\infty} \left(\mathrm{U}_{mn} - \mathrm{V}_{mn}\frac{C}{2n\pi}\right) X_m^1(x)\frac{\mathrm{d}\Phi_n^0(s)}{\mathrm{d}s}
\end{aligned} \qquad \text{Eq. 3- 80}$$

and the reference curvatures become

$$\begin{aligned}
\kappa_x{}^\circ &= -\sum_{m=1}^{\infty}\sum_{n=0}^{\infty} \mathrm{W}_{mn} X_m^2(x)\Phi_n^2(s) \\
\kappa_s{}^\circ &= -\sum_{m=1}^{\infty}\sum_{n=0}^{\infty} \mathrm{W}_{mn} X_m^0(x)\frac{\mathrm{d}^2\Phi_n^2(s)}{\mathrm{d}s^2} \\
\kappa_{xs}{}^\circ &= -2\sum_{m=1}^{\infty}\sum_{n=0}^{\infty} \mathrm{W}_{mn} X_m^1(x)\frac{\mathrm{d}\Phi_n^2(s)}{\mathrm{d}s}
\end{aligned} \qquad \text{Eq. 3- 81}$$

The total potential energy becomes

$$\begin{aligned}
\Pi = \frac{C}{4}\Big(&\mathrm{A}_{11}{\mathrm{U}_{mn}}^2\mathrm{I}_{1m} + 2\mathrm{A}_{12}\mathrm{U}_{mn}\mathrm{I}_{2m}\left(\mathrm{V}_{mn}\frac{2n\pi}{C} + \frac{\mathrm{W}_{mn}}{R_0}\right) \\
&+\mathrm{A}_{22}\mathrm{I}_{3m}\left(\mathrm{V}_{mn}\frac{2n\pi}{C} + \frac{\mathrm{W}_{mn}}{R_0}\right)^2 + \mathrm{A}_{66}\mathrm{I}_{4m}\left(\mathrm{V}_{mn} - \mathrm{U}_{mn}\frac{2n\pi}{C}\right)^2 \\
&+\mathrm{D}_{11}{\mathrm{W}_{mn}}^2\mathrm{I}_{1m}\mathrm{S}_{1n} - 2\mathrm{D}_{12}\,{\mathrm{W}_{mn}}^2\mathrm{I}_{2m}\left(\frac{2n\pi}{C}\right)^2\mathrm{S}_{2n} \\
&+\mathrm{D}_{22}{\mathrm{W}_{mn}}^2\mathrm{I}_{3m}\left(\frac{2n\pi}{C}\right)^4\mathrm{S}_{3n} + 4\mathrm{D}_{66}{\mathrm{W}_{mn}}^2\mathrm{I}_{4m}\left(\frac{2n\pi}{C}\right)^2\mathrm{S}_{4n}\Big)
\end{aligned} \qquad \text{Eq. 3- 82}$$

where I_{1m}, I_{2m}, I_{3m}, and I_{4m} are those defined in 3.1.2, whereas S_{1n}, S_{2n}, S_{3n}, and S_{4n} are those defined in 3.3.1. The kinetic energy is

$$\mathrm{K} = \frac{C}{4}\rho H\omega_{mn}{}^2\left({\mathrm{U}_{mn}}^2\,\mathrm{I}_{4m} + {\mathrm{V}_{mn}}^2\,\mathrm{I}_{3m} + {\mathrm{W}_{mn}}^2\,\mathrm{I}_{3m}\mathrm{S}_{1n}\right) \qquad \text{Eq. 3- 83}$$

Substituting the potential and kinetic energies into Eq. 3- 11, the matrix form of the natural frequency equation becomes

$$\begin{bmatrix} \mathrm{T_{11}}' - \mathrm{I_{4m}}\rho H{\omega_{mn}}^2 & \mathrm{T_{12}}' & \mathrm{T_{13}}' \\ \mathrm{T_{12}}' & \mathrm{T_{22}}' - \mathrm{I_{3m}}\rho H{\omega_{mn}}^2 & \mathrm{T_{23}}' \\ \mathrm{T_{13}}' & \mathrm{T_{23}}' & \mathrm{T_{33}}' - \mathrm{I_{3m}}\rho H{\omega_{mn}}^2 \mathrm{S_{1n}} \end{bmatrix} \begin{Bmatrix} \mathrm{U}_{mn} \\ \mathrm{V}_{mn} \\ \mathrm{W}_{mn} \end{Bmatrix} = \begin{Bmatrix} 0 \\ 0 \\ 0 \end{Bmatrix} \quad \text{Eq. 3- 84}$$

where

$$\mathrm{T_{11}}' = \mathrm{A_{11}I_{1m}} + \mathrm{A_{66}I_{4m}}\left(\frac{2n\pi}{C}\right)^2$$

$$\mathrm{T_{12}}' = (\mathrm{A_{12}I_{2m}} - \mathrm{A_{66}I_{4m}})\left(\frac{2n\pi}{C}\right)$$

$$\mathrm{T_{13}}' = \frac{\mathrm{A_{12}I_{2m}}}{R_0} \quad \text{Eq. 3- 85}$$

$$\mathrm{T'_{22}} = \mathrm{A_{66}I_{4m}} + \mathrm{A_{22}I_{3m}}\left(\frac{2n\pi}{C}\right)^2$$

$$\mathrm{T_{23}}' = \frac{\mathrm{A_{22}I_{3m}}}{R_0}\left(\frac{2n\pi}{C}\right)$$

and

$$\mathrm{T_{33}}' = \mathrm{T_{33}^{A}}' + \mathrm{T_{33}^{D}}', \quad \text{Eq. 3- 86}$$

where

$$\mathrm{T_{33}^{A}}' = \mathrm{A_{22}I_{3m}}\left(\frac{1}{R_0}\right)^2 \quad \text{Eq. 3- 87}$$

$$\mathrm{T_{33}^{D}}' = \mathrm{D_{11}I_{1m}S_{1n}} - 2\mathrm{D_{12}I_{2m}S_{2n}}\left(\frac{2n\pi}{C}\right)^2 + \mathrm{D_{22}I_{3m}S_{3n}}\left(\frac{2n\pi}{C}\right)^4 + 4\mathrm{D_{66}I_{4m}S_{4n}}\left(\frac{2n\pi}{C}\right)^2 \quad \text{Eq. 3- 88}$$

As with the simple support case, the equation for natural frequency is presented as a sixth degree polynomial in ω_{mn} as

$$\left(\rho H{\omega_{mn}}^2\right)^3 - P_4^f\left(\rho H{\omega_{mn}}^2\right)^2 + P_2^f\left(\rho H{\omega_{mn}}^2\right) - P_0^f = 0 \quad \text{Eq. 3- 89}$$

where

$$P_4^f = \left(\frac{\mathrm{T_{11}}'}{\mathrm{I_{4m}}} + \frac{\mathrm{T_{22}}'}{\mathrm{I_{3m}}} + \frac{\mathrm{T_{33}}'}{\mathrm{I_{3m}S_{1n}}}\right)$$

$$P_2^f = \left(\frac{\mathrm{T_{11}}'\mathrm{T_{22}}' - \mathrm{T_{12}}'^2}{\mathrm{I_{3m}I_{4m}}} + \frac{\mathrm{T_{22}}'\mathrm{T_{33}}' - \mathrm{T_{23}}'^2 - \mathrm{T_{13}}'^2}{{\mathrm{I_{3m}}^2}\mathrm{S_{1n}}} + \frac{\mathrm{T_{33}}'\mathrm{T_{11}}'}{\mathrm{I_{3m}I_{4m}S_{1n}}}\right) \quad \text{Eq. 3- 90}$$

$$P_0^f = \frac{\mathrm{T_{11}}'\mathrm{T_{22}}'\mathrm{T_{33}}' + 2\mathrm{T_{12}}'\mathrm{T_{23}}'\mathrm{T_{13}}' - \mathrm{T_{33}}'\mathrm{T_{12}}'^2 - \mathrm{T_{11}}'\mathrm{T_{23}}'^2 - \mathrm{T_{22}}'\mathrm{T_{13}}'^2}{\mathrm{I_{3m}}^2\,\mathrm{I_{4m}}\mathrm{S_{1n}}}$$

Again, the lowest root, from which the fundamental frequency is derived, is given as

$$\rho H\omega_{mn}{}^2 = \frac{P_4^f}{3} - \frac{1}{3}\sqrt[3]{\frac{\mathrm{RT} + \sqrt{\mathrm{RT}^2 - 4\left(P_4^{f\,2} - 3P_2^f\right)^3}}{2}} - \frac{1}{3}\sqrt[3]{\frac{\mathrm{RT} - \sqrt{\mathrm{RT}^2 - 4\left(P_4^{f\,2} - 3P_2^f\right)^3}}{2}} \qquad \text{Eq. 3- 91}$$

where

$$\mathrm{RT} = -2P_4^{f\,3} + 9P_4^f P_2^f - 27P_0^f \qquad \text{Eq. 3- 92}$$

As with the simple support case, a simplified equation based on ignoring inertia effects in axial and circumferential directions is derivable from the matrix form as

$$\begin{bmatrix} \mathrm{T_{11}}' & \mathrm{T_{12}}' & \mathrm{T_{13}}' \\ \mathrm{T_{12}}' & \mathrm{T_{22}}' & \mathrm{T_{23}}' \\ \mathrm{T_{13}}' & \mathrm{T_{23}}' & \mathrm{T_{33}}' - \mathrm{I_{3m}}\rho H\omega_{mn}{}^2\mathrm{S_{1n}} \end{bmatrix} \begin{Bmatrix} \mathrm{U}_{mn} \\ \mathrm{V}_{mn} \\ \mathrm{W}_{mn} \end{Bmatrix} = \begin{Bmatrix} 0 \\ 0 \\ 0 \end{Bmatrix} \qquad \text{Eq. 3- 93}$$

The corresponding equation is

$$\rho H\omega_{mn}{}^2\mathrm{I_{3m}} = \mathrm{D_{11}I_{1m}} - 2\mathrm{D_{12}I_{2m}}\frac{\mathrm{S_{2n}}}{\mathrm{S_{1n}}}\left(\frac{2n\pi}{C}\right)^2 + \mathrm{D_{22}I_{3m}}\frac{\mathrm{S_{3n}}}{\mathrm{S_{1n}}}\left(\frac{2n\pi}{C}\right)^4 + 4\mathrm{D_{66}I_{4m}}\frac{\mathrm{S_{4n}}}{\mathrm{S_{1n}}}\left(\frac{2n\pi}{C}\right)^2 + \frac{\mathrm{A_{66}I_{4m}}}{{R_0}^2}\frac{\mathrm{A_{11}I_{1m}A_{22}I_{3m}} - (\mathrm{A_{12}I_{2m}})^2}{\mathrm{T_{11}}'\,\mathrm{T_{22}}' - \mathrm{T_{12}}'^2}\frac{1}{\mathrm{S_{1n}}} \qquad \text{Eq. 3- 94}$$

Again, when $\mathrm{d}R(s)/\mathrm{d}s$ and $\mathrm{d}^2R(s)/\mathrm{d}s^2$ are ignored, $\mathrm{S_{1n}}$, $\mathrm{S_{2n}}$, and $\mathrm{S_{3n}}$ are the same and $\mathrm{S_{4n}}$ is very close in value to those parameters when *n* is greater than two. Therefore, the further simplified cosine-based natural frequency equation for noncircular cylinders is

$$\rho H\omega_{mn}{}^2\mathrm{I_{3m}} = \mathrm{D_{11}I_{1m}} - (2\mathrm{D_{12}I_{2m}} - 4\mathrm{D_{66}I_{4m}})\left(\frac{2n\pi}{C}\right)^2 + \mathrm{D_{22}I_{3m}}\left(\frac{2n\pi}{C}\right)^4 + \mathrm{A_{66}I_{4m}}\frac{\mathrm{A_{11}I_{1m}A_{22}I_{3m}} - (\mathrm{A_{12}I_{2m}})^2}{\mathrm{T_{11}}'\,\mathrm{T_{22}}' - \mathrm{T_{12}}'^2}\frac{C}{2\int_0^C R^2(s)\cos^2\frac{2n\pi s}{C}\,\mathrm{d}s} \qquad \text{Eq. 3- 95}$$

and the further simplified sine-based equation is

$$\rho H\omega_{mn}{}^2\mathrm{I}_{3m} = \mathrm{D}_{11}\mathrm{I}_{1m} - (2\mathrm{D}_{12}\mathrm{I}_{2m} - 4\mathrm{D}_{66}\mathrm{I}_{4m})\left(\frac{2n\pi}{C}\right)^2 + \mathrm{D}_{22}\mathrm{I}_{3m}\left(\frac{2n\pi}{C}\right)^4 + \mathrm{A}_{66}\mathrm{I}_{4m}\frac{\mathrm{A}_{11}\mathrm{I}_{1m}\mathrm{A}_{22}\mathrm{I}_{3m} - (\mathrm{A}_{12}\mathrm{I}_{2m})^2}{\mathrm{T}_{11}{}'\,\mathrm{T}_{22}{}' - \mathrm{T}_{12}{}'^2}\frac{C}{2\int_0^C R^2(s)\sin^2\frac{2n\pi s}{C}\,\mathrm{d}s} \quad \text{Eq. 3- 96}$$

Again it can be observed that an approximate equation without considering cosine-based or sine-based normal displacements is obtained as

$$\rho H\omega_{mn}{}^2\mathrm{I}_{3m} = \mathrm{D}_{11}\mathrm{I}_{1m} - (2\mathrm{D}_{12}\mathrm{I}_{2m} - 4\mathrm{D}_{66}\mathrm{I}_{4m})\left(\frac{2n\pi}{C}\right)^2 + \mathrm{D}_{22}\mathrm{I}_{3m}\left(\frac{2n\pi}{C}\right)^4 + \frac{\mathrm{A}_{66}\mathrm{I}_{4m}}{R_0 R_{\max}}\frac{\mathrm{A}_{11}\mathrm{I}_{1m}\mathrm{A}_{22}\mathrm{I}_{3m} - (\mathrm{A}_{12}\mathrm{I}_{2m})^2}{\mathrm{T}_{11}{}'\,\mathrm{T}_{22}{}' - \mathrm{T}_{12}{}'^2} \quad \text{Eq. 3- 97}$$

As named for simply-supported cylinders, Eq. 3- 94 is also called the *first simplified equation* whereas Eq. 3- 95 and Eq. 3- 96 are called the *second simplified equations*. Equation 3- 97 is called *Lo's approximate equation*.

In the next chapter numerical results from the application of the frequency equations derived in this chapter for elliptical and, for comparison, circular cylinders are presented. In addition to providing a comparison of the predicted frequencies from the developed equations with finite element results, the influences of problem parameters on fundamental frequencies will be illustrated.

Chapter 4 Numerical Results

Recall from Ch. 1, in particular Section 1.3, the two overarching objectives of this study are to determine the general roles of cylinder geometry and material properties on the fundamental frequency of elliptical cylinders, and to determine if varying layer fiber angles with circumferential position can be used to control any detrimental effects of a noncircular geometry as regards the fundamental frequency. In this chapter the former issues will be considered. In addition, the accuracy of the formulations developed in the previous chapter will be evaluated by comparing selected results from the developed formulations with finite-element calculations. Then, further results from the developed formulations will be used to illustrate the sensitivity of the fundamental frequency of elliptical cylinders to geometric and material properties, and to compare and contrast the characteristic of the fundamental frequency behavior of circular and elliptical cylinders. Details of the finite-element calculations, based on the commercial code Abaqus, are given in Appendix A.

4.1 Geometric and Material Properties Considered

To study the influence of geometry on the fundamental frequency of noncircular cylinders, four aspect ratios, b/a, a range of length-to-circumference ratios, L/C, and so-called large and small cylinders are investigated. Large cylinders have a circumference four times that of the small cylinders, but the wall thickness of the large cylinder is only twice that of the small cylinders. In terms of the equivalent circular cylinder, the ratios of the radius R_0 to the thickness of the cylinder wall H are $R_0/H = 200$ and 100, respectively. The reason for considering large and small cylinders is that small-scale cylinders might be most appropriate for any initial experiments related to the vibration characteristics of noncircular composite cylinders, but the large-scale is closer to physical applications. That the ratio L/C instead of the usual ratio L/R is used as one measure of cylinder geometry is a reflection of investigating noncircular cylinders. It is possible that ratios such as L/R_{max} or L/R_{min} could be used as a measure of cylinder geometry, but R_{max} and R_{min} are functions of cross-sectional aspect ratio. For investigating the influence of aspect ratio, it is of value to maintain consistency of circumference or consistency of cross-sectional area. Here consistency of circumference is used. Therefore, using the ratio L/C seems a natural and investigating cylinders

for a range of values of L/C means investigating the influence of cylinder length on fundamental frequency.

For the initial discussions in this chapter the value of L/C will range from 0.3 to 1.0. Considering that for a circular cylinder $L/C = L/\pi D$, where D is the diameter of the cylinder, with L/C ranging from 0.3 to 1.0, L/D will range from about 1, a short cylinder, to about 3, which could be an impractically long cylinder. However, this range will be used to compare results from the developed formulations with finite-element calculations. Later discussions will focus on the three discrete values of L/C = 0.3, 0.5, and 0.7, corresponding approximately to values of L/D of 1, 1.5, and 2, a reasonable range for a monocoque cylinder.

To investigate the influence of material properties within the context of fiber-reinforced materials, two lamination sequences are used for each value of R_0/H. It must be understood that the value of H is not completely arbitrary, as H must be an integer number of layer thicknesses in dimension. Here for the 'small' cylinders the wall is taken to be eight layers thick, so $H=8h$, where h is the thickness of one layer. For 'large' cylinders the wall is taken to be 16 layers thick, so $H=16h$. Subsection 4.1.1 describes the details for large cylinders and subsection 4.1.2 describes the details for small cylinders.

4.1.1 Geometry of Large Cylinders

The thickness h assumed here for one layer of fiber-reinforced composite material is 0.1400 mm. Based on that number and considering that the large cylindrical shells have 16-layer walls, the thickness H for the large cylinders is 2.24 mm. In particular, the 16-layer balanced symmetric lamination sequences $[\pm\vartheta/0/90]_{2S}$ and $[\pm\vartheta]_{4S}$ for the cylinder walls are studied. The $\pm\vartheta$ layers provide a mechanism for controlling the relative levels of axial and circumferential stiffness. In determining whether varying fiber angle with circumferential location has any advantages, it is the angle of these $\pm\vartheta$ layers that in the next chapter will be assumed to vary with circumferential location. The second lamination sequence provides even more leverage in controlling the relative levels of axial and circumferential stiffness, but in the limits of ϑ, 0° and 90°, result in a cylinder with all fibers in the axial direction or all fibers in the circumferential direction, situations which are not practical. All large cylinders have the same circumference, and since radius of the

equivalent large circular cylinder, R_0, is 200 times the thickness, that is, 0.448 m, the circumference, $C = 2\pi R_0$, of all large cylinders is 2.81m. Aspect ratios b/a = 1.00, 0.85, 0.70, 0.55 are considered, the first value, of course, representing the equivalent circular cylinder, the second a mild elliptical cross section, and the last an extreme elliptical cross section. Detailed descriptions of the geometry of the large cylinders are given in Tables 4- 1 and 4- 2.

Table 4- 1 Major and minor radii of large cylinders[1]

	Major Radius, a (m)	Minor Radius, b (m)
b/a =1.00 (e = 0)	0.448 (R_0)	0.448 (R_0)
b/a =0.85 (e = 0.53)	0.484	0.411
b/a =0.70 (e = 0.71)	0.523	0.366
b/a =0.55 (e = 0.84)	0.566	0.311

1 - h = 0.1400 mm, H = 2.24 mm, $C = 2\pi R_0$ = 2.82 m

Table 4- 2 Lengths and length ratios of large cylinders[1]

	L=0.3C (0.844m)	L=0.5C (1.407m)	L=0.7C (1.970m)
b/a =1.00 (e = 0)	a/L=0.531 b/L=0.531	a/L=0.318 b/L=0.318	a/L=0.227 b/L=0.227
b/a =0.85 (e = 0.53)	a/L=0.573 b/L=0.487	a/L=0.344 b/L=0.292	a/L=0.246 b/L=0.209
b/a =0.70 (e = 0.71)	a/L=0.620 b/L=0.434	a/L=0.372 b/L=0.260	a/L=0.265 b/L=0.1858
b/a =0.55 (e = 0.84)	a/L=0.671 b/L=0.369	a/L=0.402 b/L=0.221	a/L=0.287 b/L=0.1580

1 - h = 0.1400 mm, H = 2.24 mm, $C = 2\pi R_0$ = 2.82 m

4.1.2 Geometry of Small Cylinders

Considering the same layer thickness, the thickness of the 8-layer walls of the small cylinders is 1.120 mm. For these thinner walls the balanced symmetric laminate sequences $[\pm\vartheta/0/90]_S$ and $[\pm\vartheta]_{2S}$ are studied. These are analogues of the two lamination sequences for the thicker-walled large cylinders. As the radius of the small equivalent circular cylinders is 100 times their thickness, $R_0 = 0.1120$ m and the corresponding circumference is 0.704 m. Like the large cylinders, aspect ratios 1.00, 0.85, 0.70, and 0.55 are studied. The major and minor radii for the small cylinders are listed in Table 4- 3 and other geometric data are in Table 4- 4.

Table 4- 3 Major and minor radii of small cylinders[1]

	Major Radius, a (m)	Minor Radius, b (m)
b/a =1.00 (e = 0)	0.1120	0.1120
b/a =0.85 (e = 0.53)	0.1209	0.1028
b/a =0.70 (e = 0.71)	0.1307	0.0915
b/a =0.55 (e = 0.84)	0.1415	0.0778

1 - h = 0.1400 mm, H = 1.120 mm, $C = 2\pi R_0 = 0.704$ m

Table 4- 4 Length and length ratios of small cylinders[1]

	L=0.3C (0.211m)	L=0.5C (0.352m)	L=0.7C (0.493m)
b/a =1.00 (e = 0)	a/L=0.531 b/L=0.531	a/L=0.318 b/L=0.318	a/L=0.227 b/L=0.227
b/a =0.85 (e = 0.53)	a/L=0.573 b/L=0.487	a/L=0.344 b/L=0.292	a/L=0.246 b/L=0.209
b/a =0.70 (e = 0.71)	a/L=0.620 b/L=0.434	a/L=0.372 b/L=0.260	a/L=0.265 b/L=0.1858
b/a =0.55 (e = 0.84)	a/L=0.671 b/L=0.369	a/L=0.402 b/L=0.221	a/L=0.287 b/L=0.1580

1 - h = 0.1400 mm, H = 1.120 mm, $C = 2\pi R_0 = 0.704$ m

4.1.3 Material Properties

The fiber-reinforced composite material is assumed to be a medium-modulus graphite-epoxy material. The engineering properties are listed in Table 4- 5[1]

Table 4- 5 Material properties of graphite-polymer composite

Property	Number (unit)
E_1	130.0 (GPa)
E_2	9.70 (GPa)
G_{12}	5.00 (GPa)
G_{13}	5.00 (GPa)
G_{23}	3.64 (GPa)
ν_{12}	0.3
ρ	1661 (kg/m^3)

4.2 Comparison with Finite-Element Calculations

In the figures to follow, the relationships between the fundamental frequency of elliptical cylinders and cylinder geometry and wall fiber angle are illustrated by way of a series of plots. Circular cylinders are considered as a special case of elliptical cylinders.

On the plots are the results calculated by the various non-simplified and simplified equations and results calculated by the Abaqus finite-element model, which is based on shell elements. The figures to follow serve two purposes. First, the accuracy of the developed formulations can be evaluated by direct comparison with more refined finite-element calculations. Second, the dependencies of the fundamental frequency on important geometric and material parameters of the cylinders are illustrated and are discussed. On all plots the fundamental frequency is on the vertical axis, and L/C or ϑ is on the horizontal axis. On all plots in this section the fundamental frequency is normalized by the fundamental frequency for a so-called baseline cylinder as

computed by the Abaqus, with mesh 336×170 in the circumferential and lengthwise directions, respectively, and is denoted here as ω_0. The baseline cylinder is circular, simply-supported, has a quasi-isotropic lay-up, and L/C = 0.5, which for the circular case translates into L/D of approximately 1.5. The baseline geometries, lamination sequences, and fundamental frequencies for the large and small cylinders are shown in Table 4- 6.

Table 4- 6 Data for baseline cylinders

	Large cylinder	Small cylinder
$R_0=a=b$, m (D_0, m) [C, m]	0.448 (0.896) [2.81]	0.1120 (0.224) [0.704]
L, m	1.407	0.352
Lamination sequences	$[\pm 45/0/90]_{2S}$	$[\pm 45/0/90]_{S}$
Boundary conditions	Simple supports	Simple supports
Fundamental frequency, ω_0 (rad/s)	630	3490

4.2.1 Circular Cylinders

In Fig. 4- 1 the variations of the normalized fundamental frequencies of large simply-supported circular cylinders with L/C are illustrated. Since all large cylinders have the same circumference, each sub-figure essentially illustrates frequency variation with cylinder length. Three lamination sequences for each of the two laminate families are considered, $[\pm 15/0/90]_{2S}$, $[\pm 45/0/90]_{2S}$, and $[\pm 75/0/90]_{2S}$ from the $[\pm\vartheta/0/90]_{2S}$ family, and $[\pm 15]_{4S}$, $[\pm 45]_{4S}$, and $[\pm 75]_{4S}$ from the $[\pm\vartheta]_{4S}$ family. The notation symbol ϑ is used for fiber orientation in the specified layer. These three choices of fiber angle ϑ result in what could be considered axially-stiff construction (ϑ = 15º), circumferentially-stiff construction (ϑ = 75º), and construction with equal stiffness in the axial and circumferential directions (ϑ = 45º). With the $[\pm\vartheta/0/90]_{2S}$ family the stiffness

effects in the two directions are tempered somewhat relative to the $[\pm\vartheta]_{4S}$ family by the presence of the 0 and 90º layers. For $m > 0$, results from the developed formulation for circular cylinders with no simplifications, Eq. 3- 19, with the single simplification, i.e., ignoring axial and circumferential inertia, Eq. 3- 22, and from the finite-element calculations are shown. As mentioned, for the $m = 0$ case the lowest frequencies based on Eq. 3- 7 are significantly higher than those for $m > 0$. Since only the fundamental frequency is of interest, the results from Eq. 3-7 are not shown here. The case of circular cylinders can be considered simply a necessary check case, as nothing new will be learned because, as mentioned in the literature review, circular cylinders have been investigated in a number of previous studies. However, the circular cylinder, besides serving as a legitimate check case, provides an opportunity to discuss the vibration response of cylinders in the context of the figure format used here. Regarding the axial wave number, for all cylinders investigated in this study the axial wave number of the fundamental mode was $m = 1$.

A quick look at Fig. 4- 1 reveals that for these cases the developed formulations predict very much the same frequency magnitudes and trends with cylinder length and fiber angle ϑ as the finite-element analysis, lending some credibility to the developed formulation, at least for circular cylinders. The developed formulation with no simplification predicts slightly higher frequencies and the simplification predicts even slightly higher frequencies, but always within 10% of the case with no simplifications. The circumferential wave number predictions, n, from the developed formulations agree well with the finite element calculations. The largest discrepancy between the developed analysis and the finite element calculations occurs for the case with $\vartheta = 75º$ and for quite long cylinders. Overall, the agreement among calculations is very good, both frequency and wave number predictions. It can also be observed that the frequencies for the $[\pm\vartheta]_{4S}$ family are lower than the frequencies for the $[\pm\vartheta/0/90]_{2S}$ family. The lack of any fibers directly in the axial and circumferential directions is responsible for this characteristic. Surprisingly, it can be concluded that for both laminate families the fiber angle ϑ does not appear to have a large influence on the magnitude of the predicted frequencies. That is, the magnitude of frequency vs. L/C for the $[\pm15/0/90]_{2S}$, $[\pm45/0/90]_{2S}$, and $[\pm75/0/90]_{2S}$ cases are very much the same, and the relations for the $[\pm15]_{4S}$, $[\pm45]_{4S}$, and $[\pm75]_{4S}$ cases are also very much the same. There is variation in the prediction of the wave numbers as fiber angle ϑ varies for these two families. For example, from Figs. 4-1a, b, and c, for the $[\pm15/0/90]_{2S}$ cylinder with $L/C = 0.5$ the

value of n = 6 is predicted, while for the $[\pm 45/0/90]_{2S}$ cylinder with L/C = 0.5 the value of n = 5 is predicted, and for the $[\pm 75/0/90]_{2S}$ cylinder with L/C = 0.5 the value of n = 4 is predicted, while at that value of L/C the fundamental frequencies for these three cases are quite close to each other. This n = 6, 5, 4 behavior is also true for the $[\pm 15]_{4S}$, $[\pm 45]_{4S}$, and $[\pm 75]_{4S}$ cases in Figs. 4- 1d, e, f. Stated differently, while frequency magnitude is relatively insensitive to fiber angle, the range of L/C for which a particular value of n is predicted is quite sensitive to fiber angle. In fact, that there is a variation of n with L/C is responsible for the piecewise smooth character of the frequency vs. L/C relation. That is, a particular value of n is predicted over a limited range of L/C, then over an adjacent range another value of n is predicted, and so on with other ranges of L/C, leading to the scalloped character of the relation, which is more evident with the simplified relationship represented by the thin unbroken multicolored line than the broken lines used for the non-simplified relation. The insensitivity of frequency magnitude to fiber angle will be further discussed in a later section.

A comment is in order regarding Fig. 4- 1. As stated, the frequencies in the figures have been normalized by the frequency of the baseline cylinder, a large circular cylinder with a quasi-isotropic cylinder wall, lamination $[\pm 45/0/90]_{2S}$, and with L/C = 0.5 (see Table 4- 6). That is why the open circular symbol in Fig. 4- 1b for L/C = 0.5 coincides *exactly* with $\omega/\omega_0 = 1$. Had the normalization scheme consisted of normalizing the frequencies computed from the finite-element analysis by the frequency of the baseline cylinder as computed from the finite-element analysis, but normalizing the frequencies computed from the developed formulation by the frequency of the baseline cylinder as computed from the developed formulation, then in Fig. 4- 1b the results for the developed formulation with no simplification for the case L/C = 0.5 would also coincide exactly with $\omega/\omega_0 = 1$. Though it could be argued that this approach could be taken here, as primary interest is with the trends of the frequency with variations in material and geometric properties, this approach is not taken because there is interest in the accuracy of the developed formulation in an absolute sense. If that approach were taken, however, the results from the developed formulation would all be shifted downward slightly and for the $[\pm 45/0/90]_{2S}$ case the results from the developed formulation and the finite element results would very nearly coincide for all values of L/C. These comments apply to all the figures to follow.

In Fig. 4- 2 the normalized fundamental frequencies of large circular clamped support cylinders are illustrated in a format similar to Fig. 4 -1. When comparing the results in Fig. 4- 2 with the results in Fig. 4- 1, the increased frequency due to the less compliant clamped supports is evident. The increase of frequency due to boundary conditions ranges from about 25% to about 70%, the larger number being associated with the longer cylinders. Overall, except for the $[\pm 45]_{4S}$ case, Fig. 4- 2e, the developed formulation agrees well with the finite-element calculations, both in frequency magnitude, trends with geometric and material parameters, and wave number, though not quite as well as for the simply supported cases of Fig. 4- 1. The results from the simplified formulation, Eq. 3- 44, and results from the formulation with no simplification, Eq. 3- 41, agree with each other to the same degree as for the simply supported cylinders of Fig. 4- 1. For the $[\pm 45]_{4S}$ case the error between the developed formulation and the finite-element results is in the range from about 15% at $L/C = 0.3$ to about 25% at $L/C = 1.0$. Again, considering the wide range of fiber angle variation, from 15 to 75°, there is minimal sensitivity of the frequency magnitude to fiber angle, though the range of L/C for which a particular value of n is predicted is influenced by fiber angle. The possible source of the discrepancy for the $[\pm 45]_{4S}$ case will be discussed in Ch. 6, along with other possible sources of error.

In Fig. 4- 3 the focus is again on simply-supported cylinders, but for the case of small cylinders. The format of the six sub-figures is the same as that for the past two figures. For small cylinders, however, there are some differences as compared to the figures for the large simply-supported cylinders. For low values of L/C there are differences between the non-simplified predictions of the developed formulation, Eq. 3- 19, and the predictions of the finite-element model. This difference is particularly acute for the $[\pm 45]_{2S}$ cylinder, and to some degree for the $[\pm 75]_{2S}$ and $[\pm 45/0/90]_S$ cylinders. For other situations in the figures, the differences are generally less than 10%. Interestingly, the simplified formulation, Eq. 3- 22, compares quite well over the range of laminates and lengths considered. Figures 4- 3a, b, and c provide further evidence of how the wave number n is influenced by L/C and fiber angle ϑ. In Fig. 4- 3a, for the $[\pm 15/0/90]_S$ cylinder, $n = 4$, 5, and 6 are part of the picture, $n = 6$ being associated with the shorter cylinders. For the $[\pm 75/0/90]_S$ cylinders, at least according to the developed formulation, $n = 3$ has emerged, $n = 4$ remains in the picture, but $n = 5$ and 6 are no longer involved. Note that for $L/C = 0.3$ for the $[\pm 75/0/90]_S$ cylinder the Abaqus predicts an n of 5, while the developed formulations predict

an n of 4. These slight differences over limited ranges of L/C have occurred for particular cases throughout this study.

In Fig. 4- 4 the normalized fundamental frequencies of small circular clamped support cylinders with the six different lamination sequences are shown. Of the circular cylinders considered in this study, the largest differences between the developed formulation and the finite-element model are exhibited with the small clamped support cylinders. Like the large clamped support $[\pm 45]_{4S}$ cylinder, the developed formulation predicts noticeable higher frequencies, as compared to the other five cases, for the small clamped support cylinders. For a value of $L/C = 0.3$ the difference for the non-simplified calculation is much larger than the 15% difference at that value of $L/C = 0.3$ for the large clamped support cylinder. For the lower values of L/C the simplified developed formulation is more accurate, the accuracy comparable to that for the large clamped support cylinder.

To summarize at this point, it can be stated that overall, the developed formulations, both non-simplified and simplified, predict the frequencies and values of n as a function of L/C with reasonable accuracy. As observed, cylinder length has a strong influence on the fundamental frequency, but fiber angle does not have a significant influence. On the other hand, the fiber angle does influence the value of the circumferential wave number n.

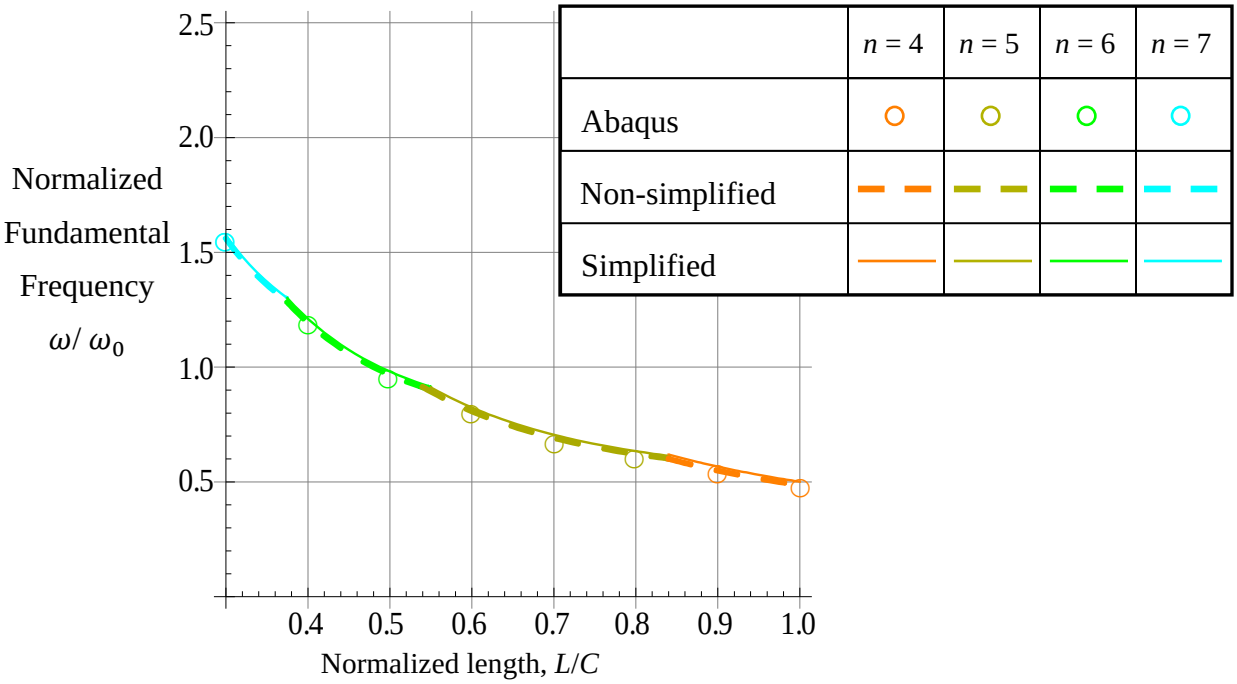

(a) Lamination sequences $[\pm 15/0/90]_{2S}$

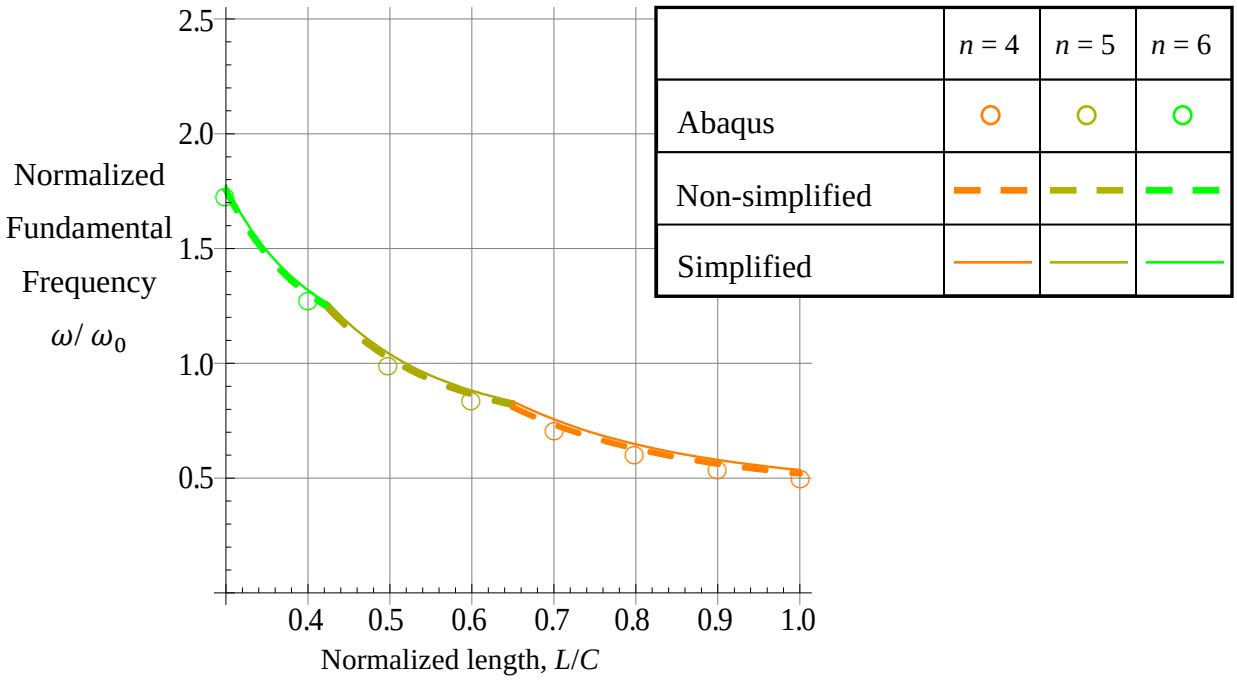

(b) Lamination sequences $[\pm 45/0/90]_{2S}$

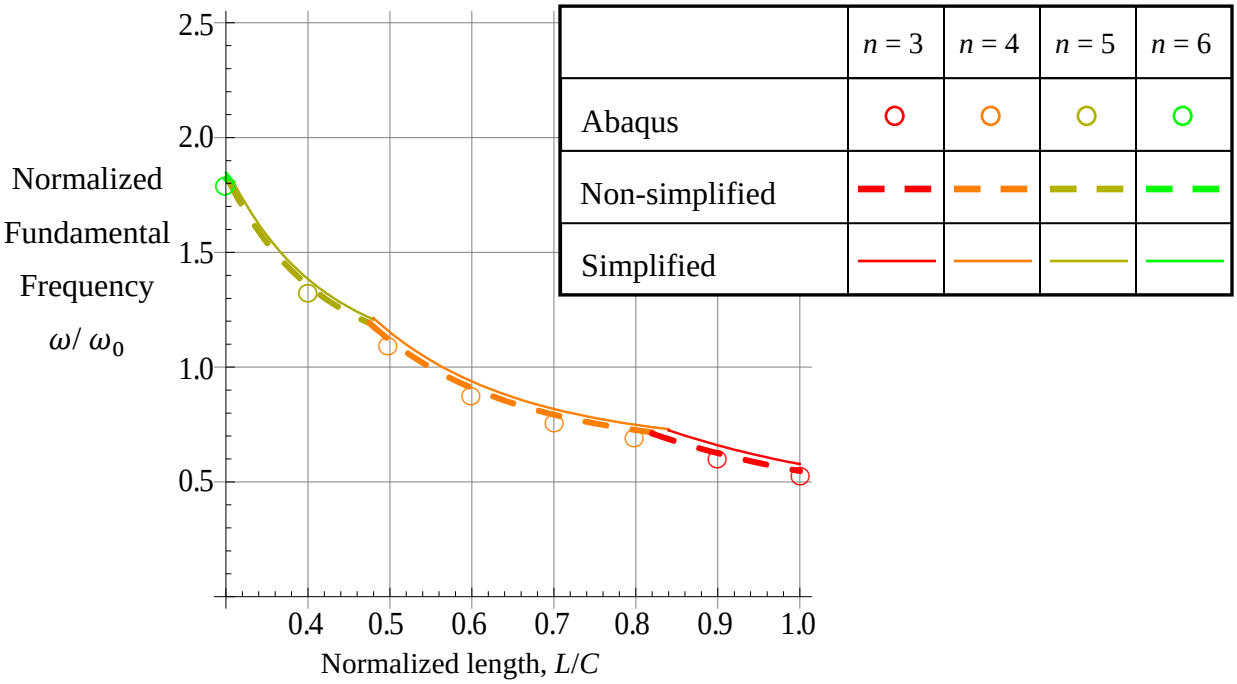

(c) Lamination sequences $[\pm 75/0/90]_{2S}$

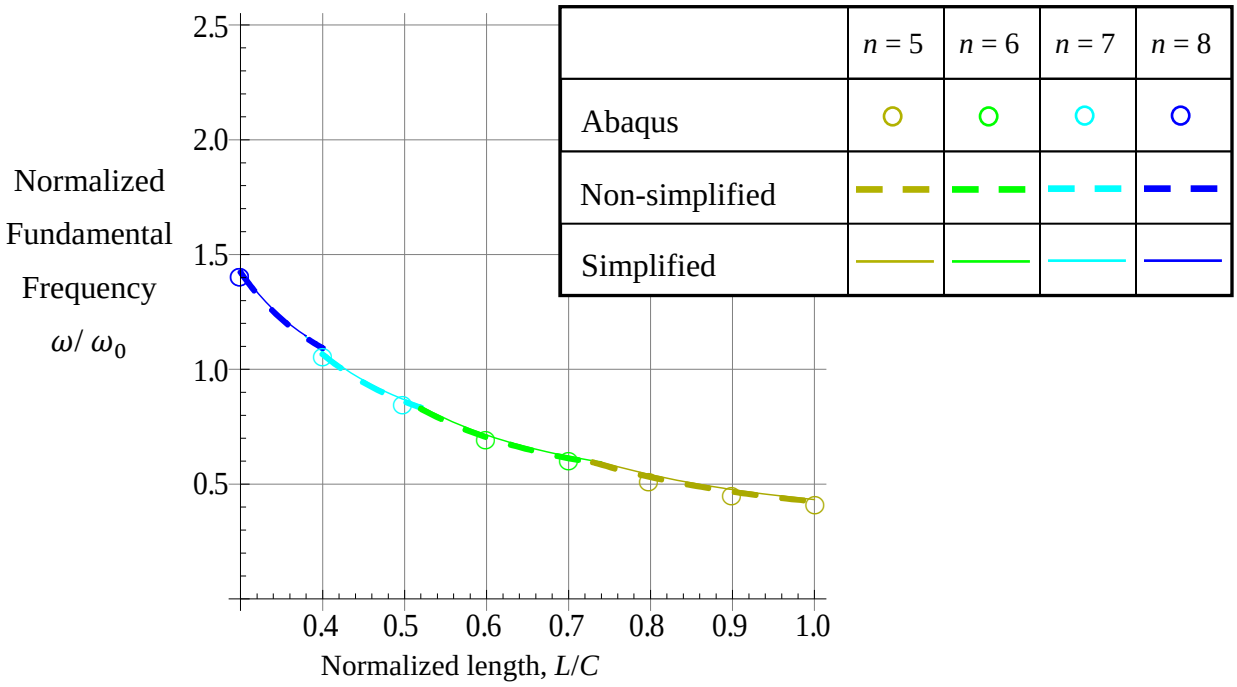

(d) Lamination sequences $[\pm 15]_{4S}$

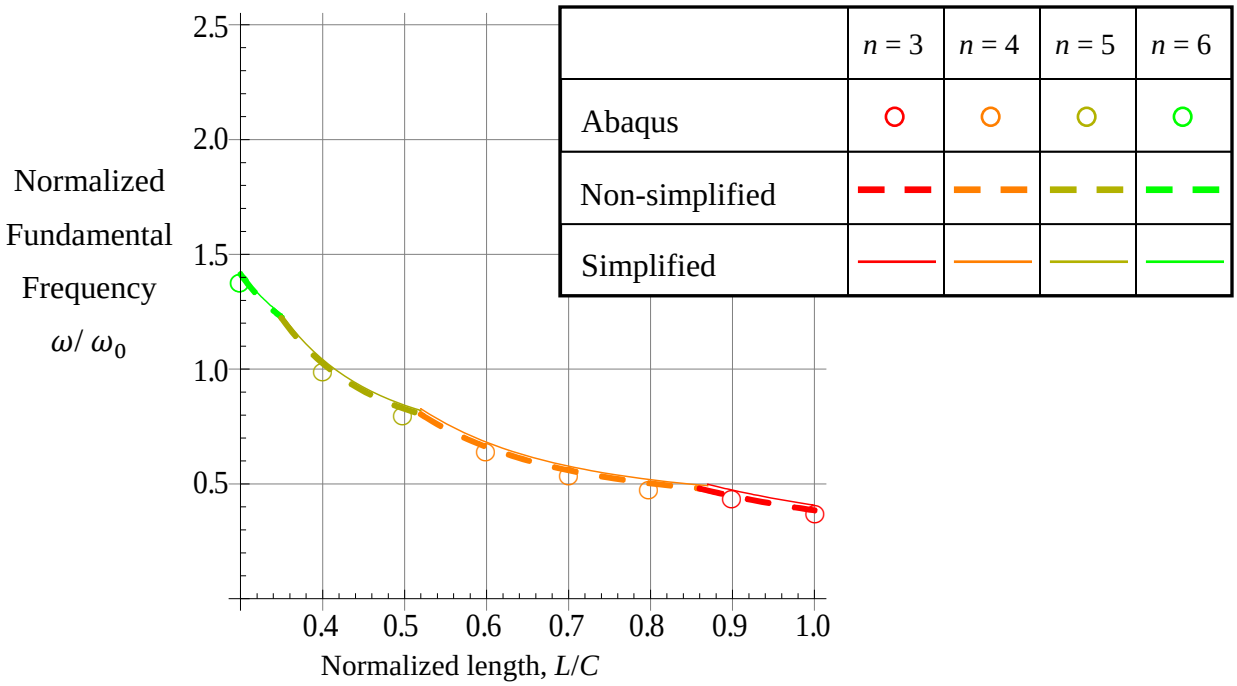

(e) Lamination sequences $[\pm 45]_{4S}$

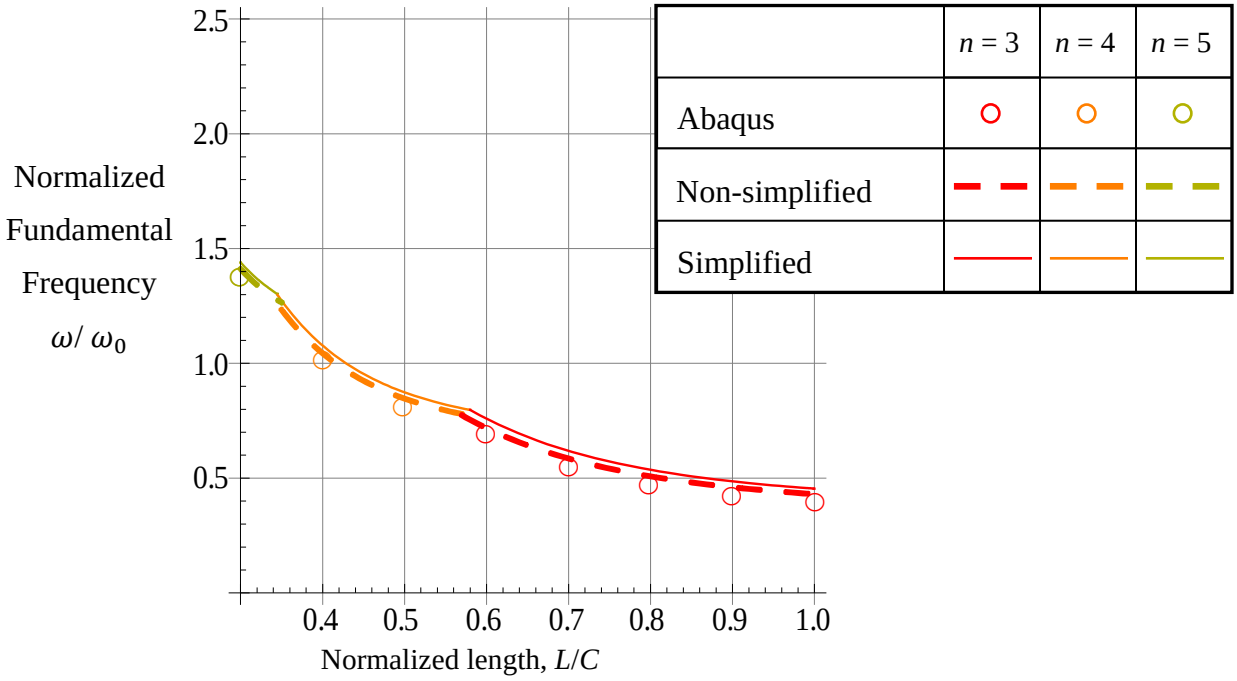

(f) Lamination sequences $[\pm 75]_{4S}$

Fig. 4- 1 Normalized fundamental frequency of large circular cylinders, simple supports

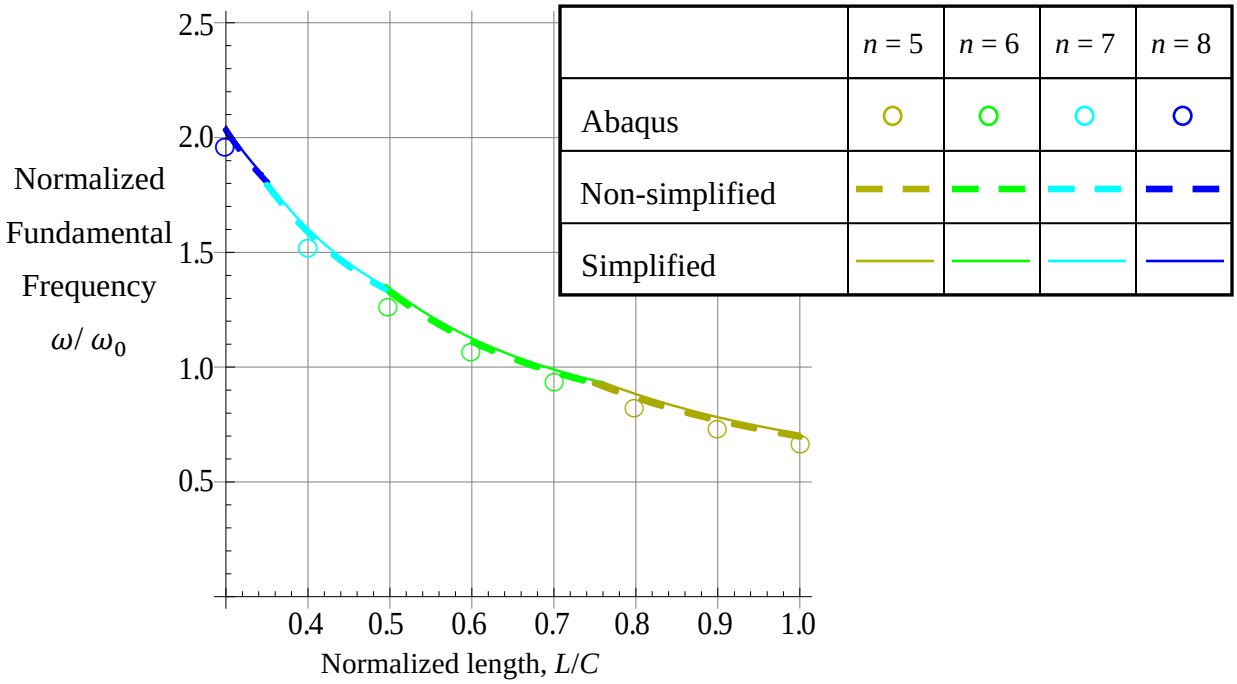

(a) Lamination sequences $[\pm 15/0/90]_{2S}$

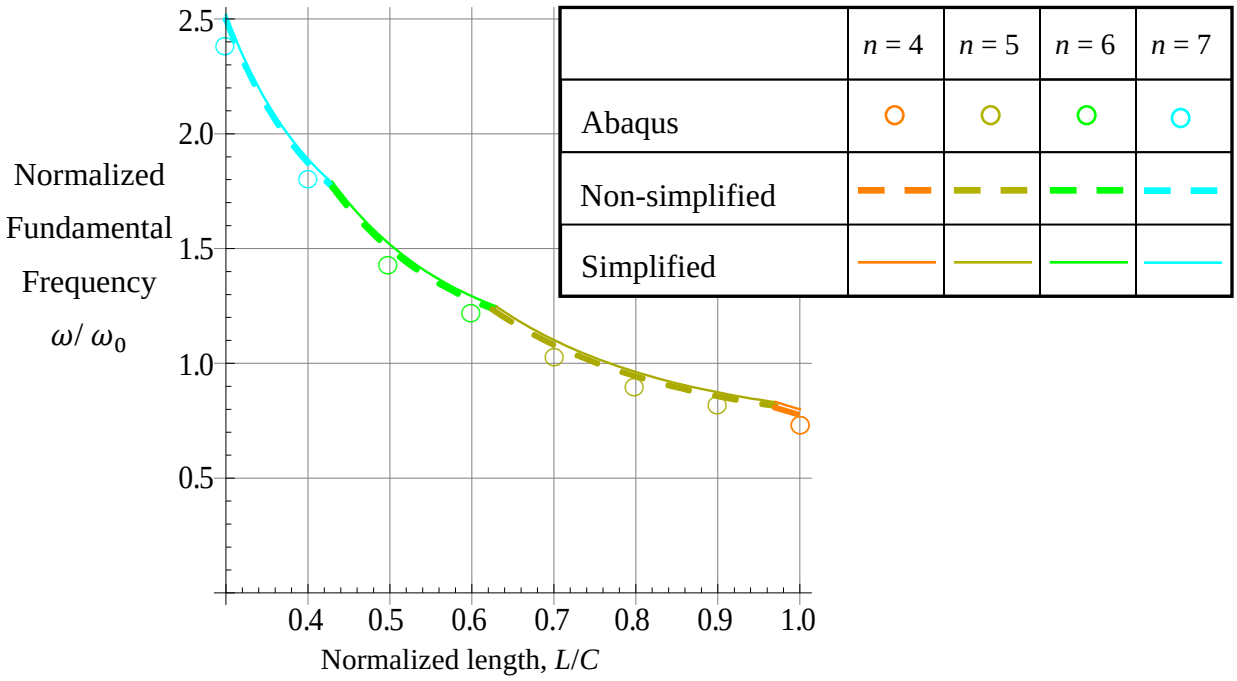

(b) Lamination sequences $[\pm 45/0/90]_{2S}$

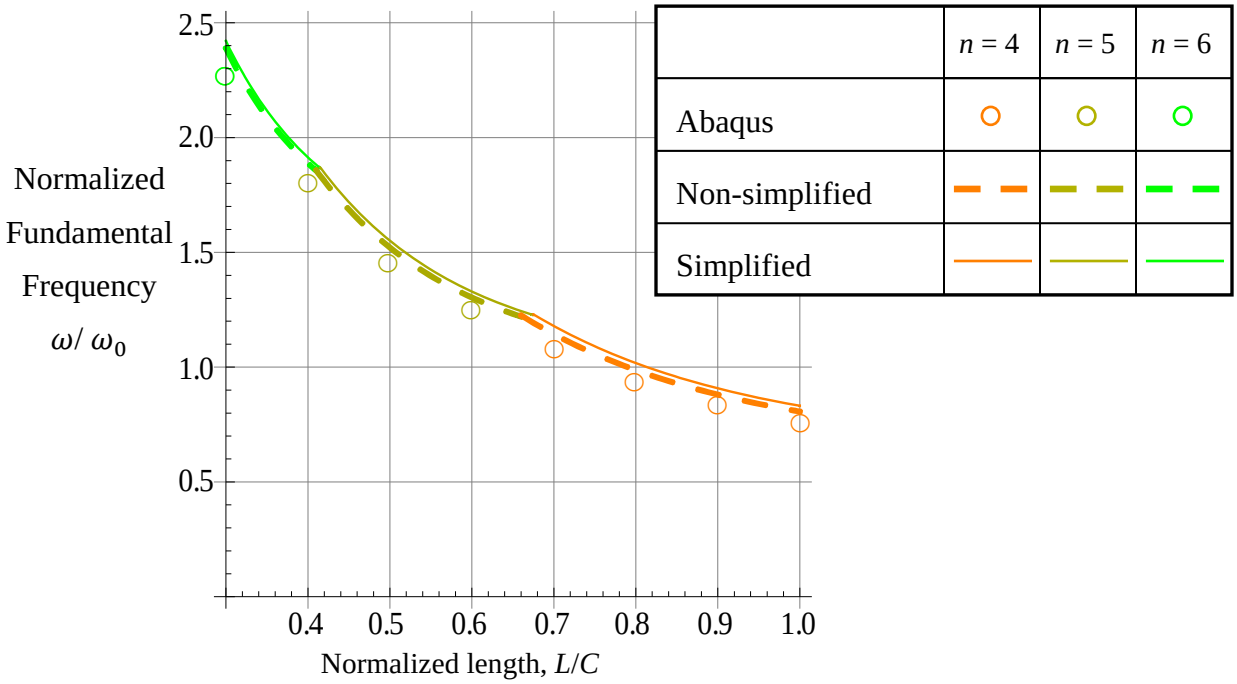

(c) Lamination sequences $[\pm 75/0/90]_{2S}$

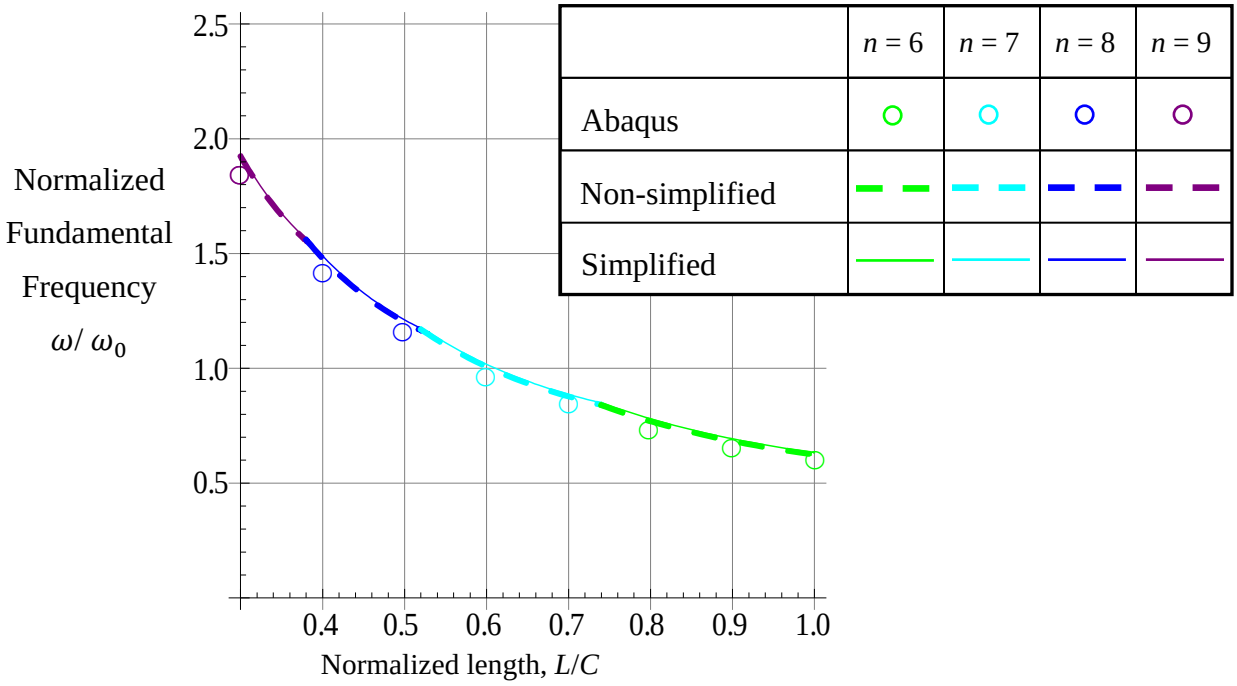

(d) Lamination sequences $[\pm 15]_{4S}$

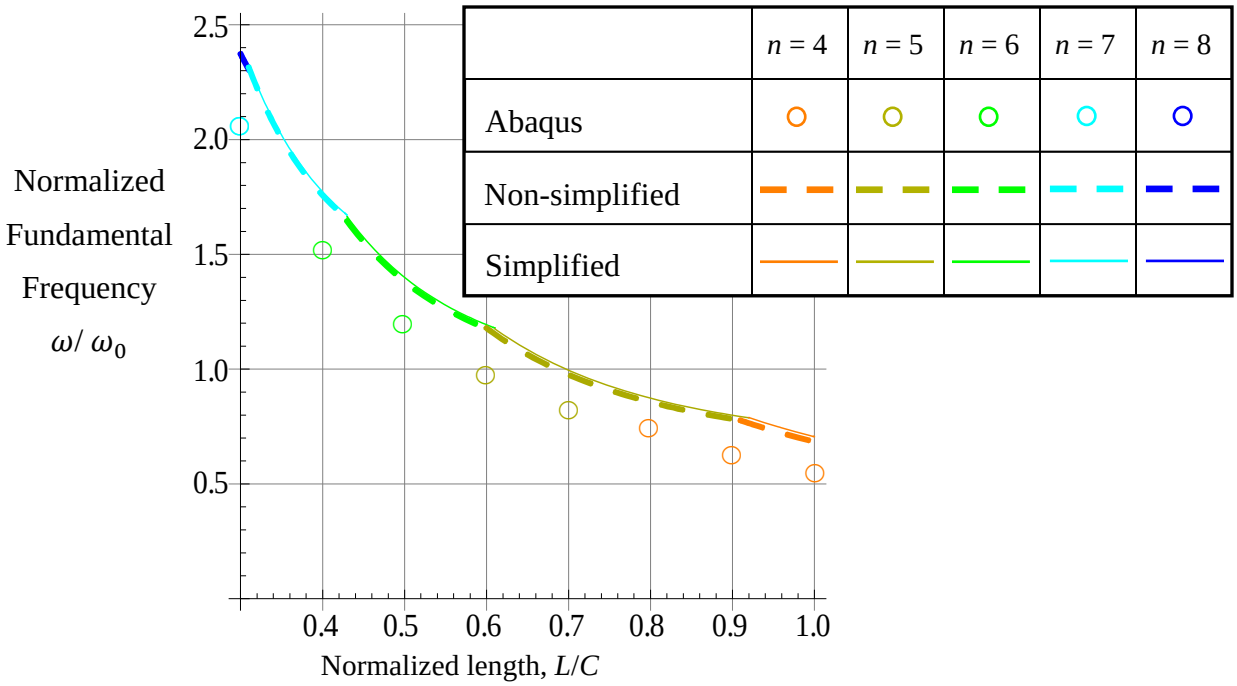

(e) Lamination sequences $[\pm 45]_{4S}$

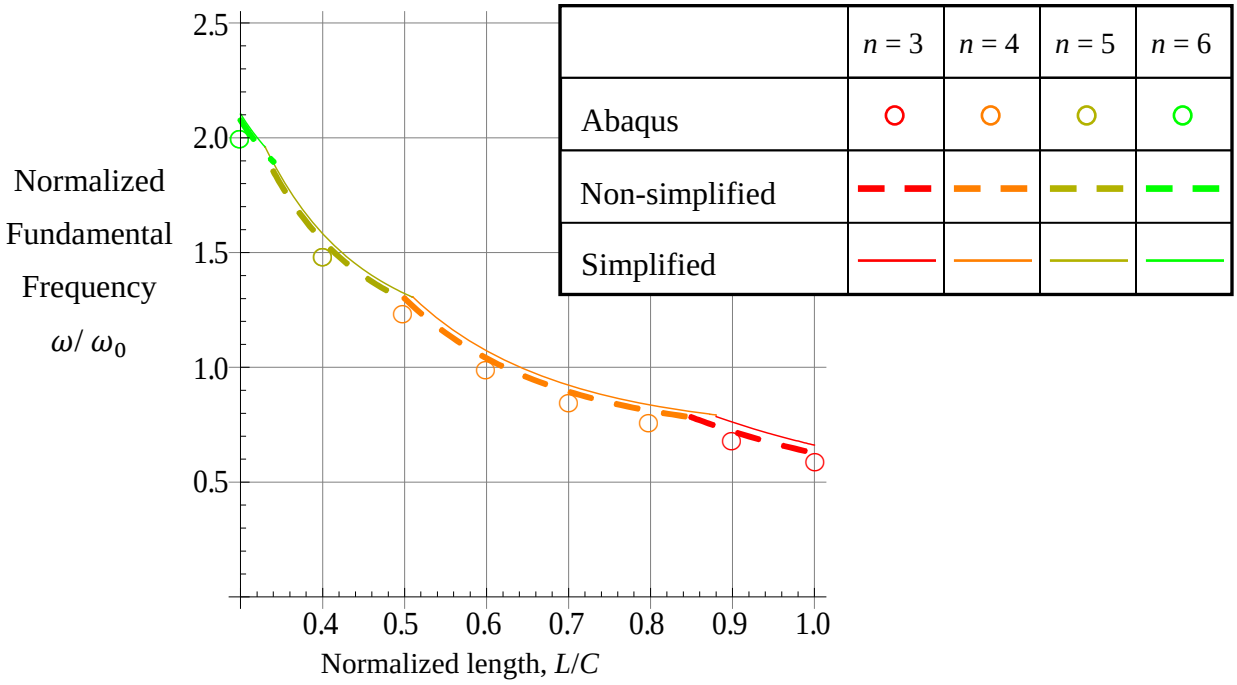

(f) Lamination sequences $[\pm 75]_{4S}$

Fig. 4- 2 Normalized fundamental frequency of large circular cylinders, clamped supports

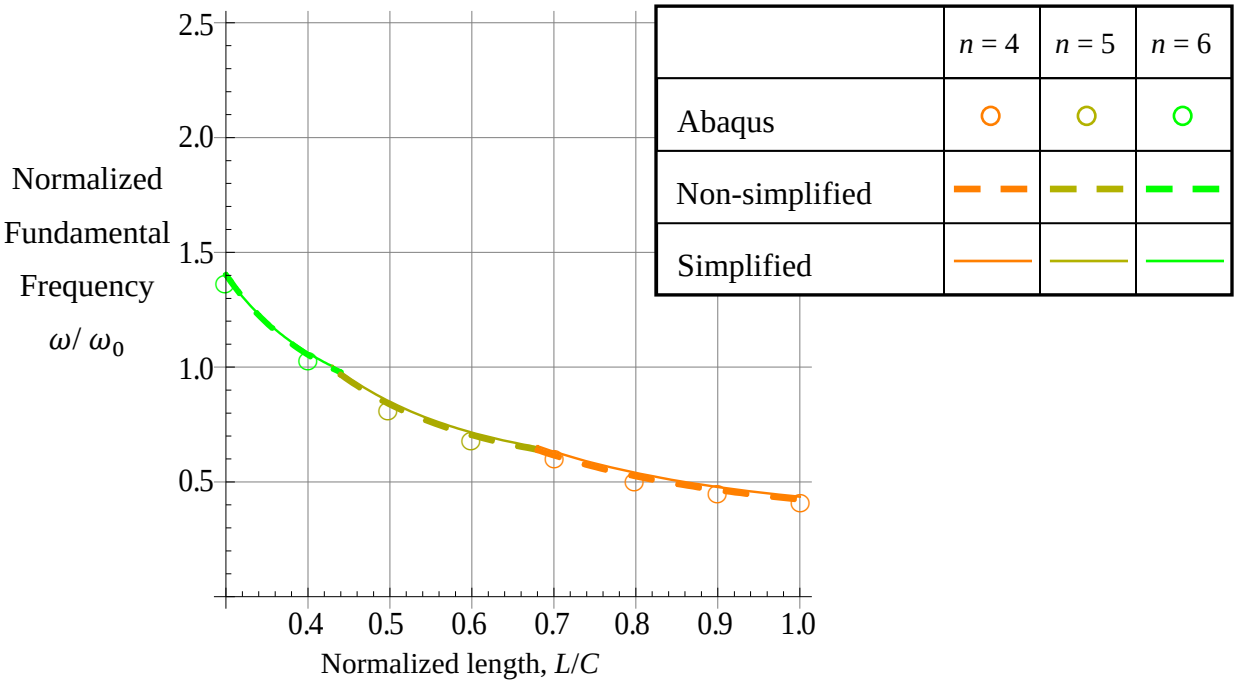

(a) Lamination sequences $[\pm 15/0/90]_S$

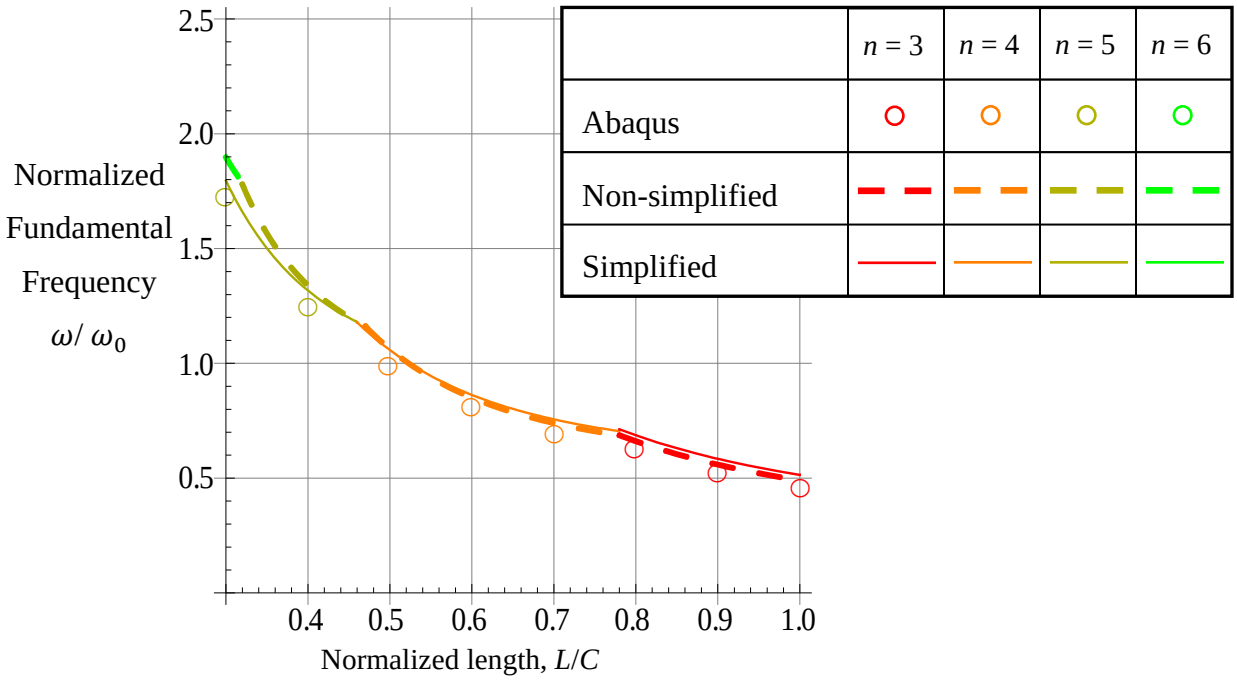

(b) Lamination sequences $[\pm 45/0/90]_S$

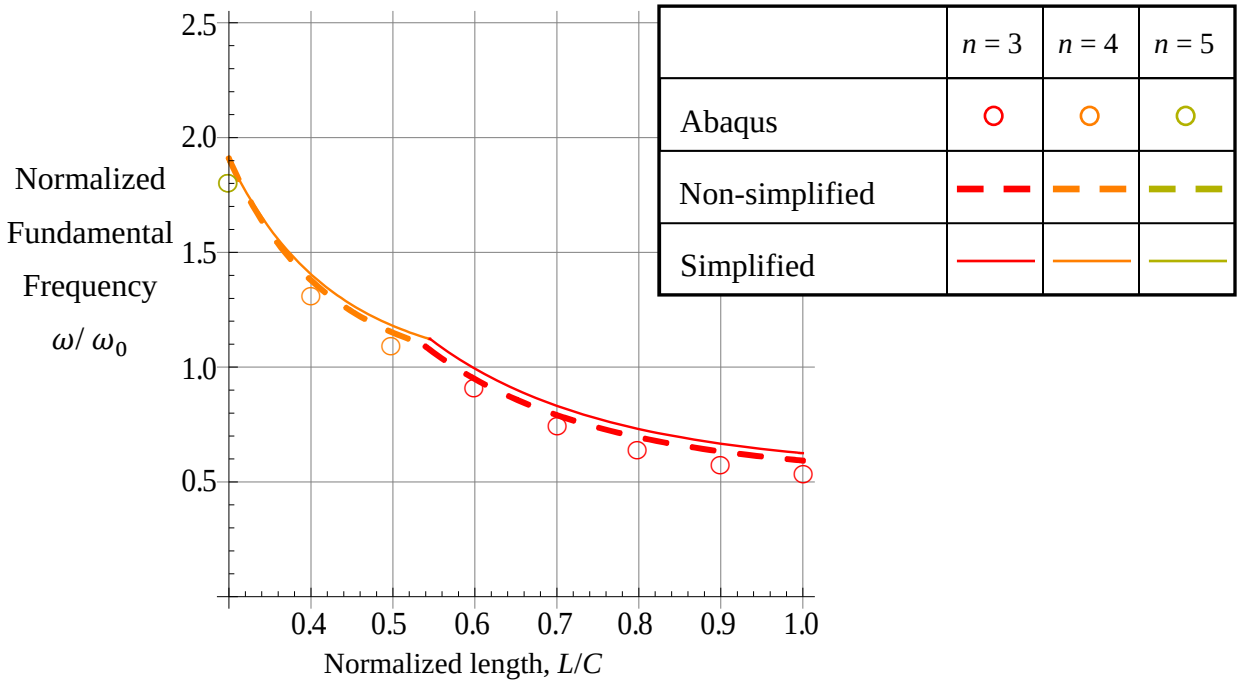

(c) Lamination sequences $[\pm 75/0/90]_S$

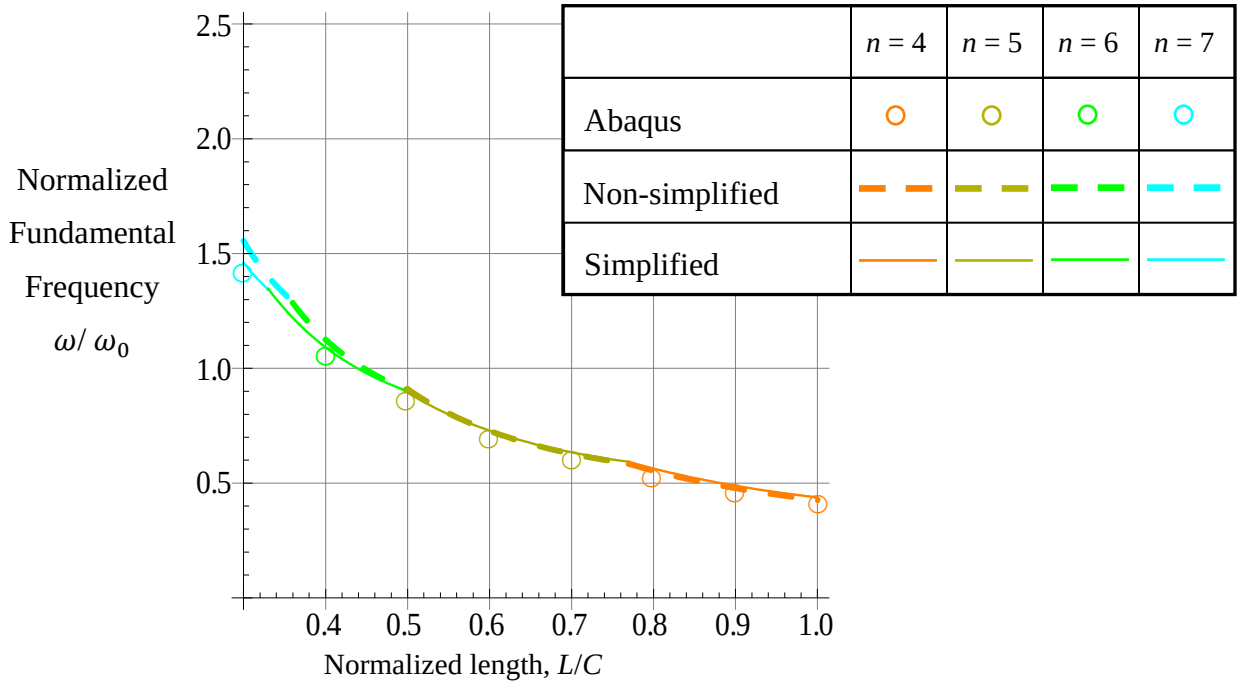

(d) Lamination sequences $[\pm 15]_{2S}$

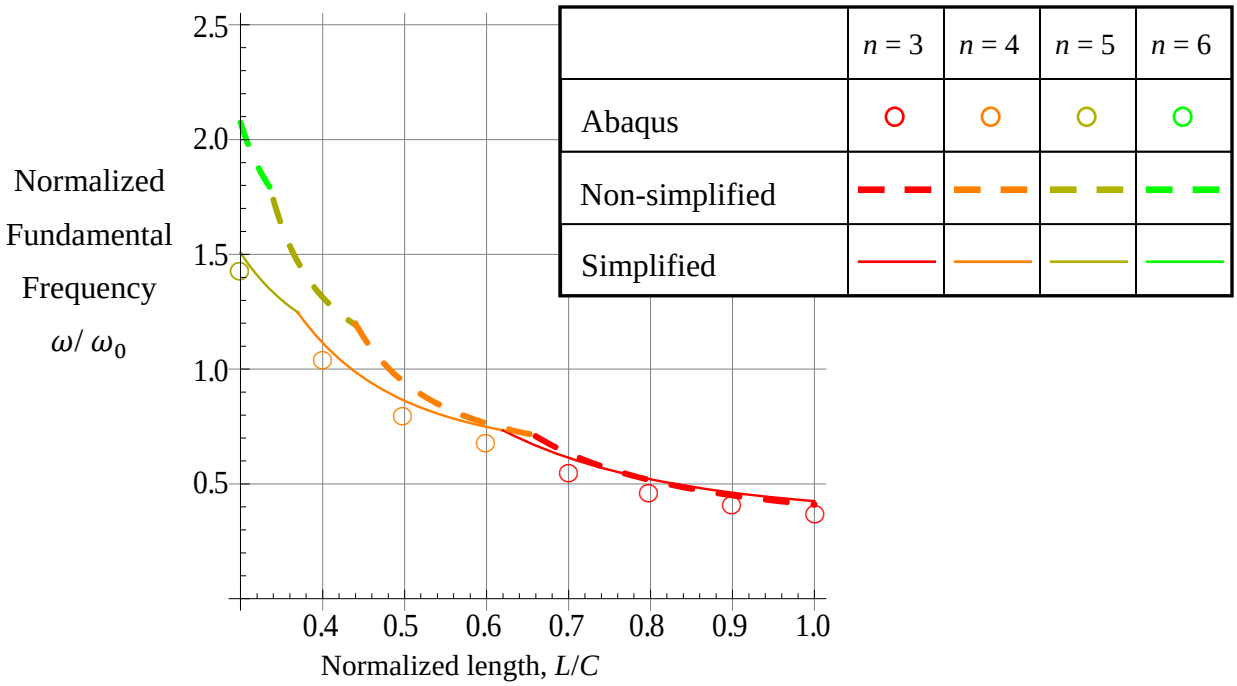

(e) Lamination sequences $[\pm 45]_{2S}$

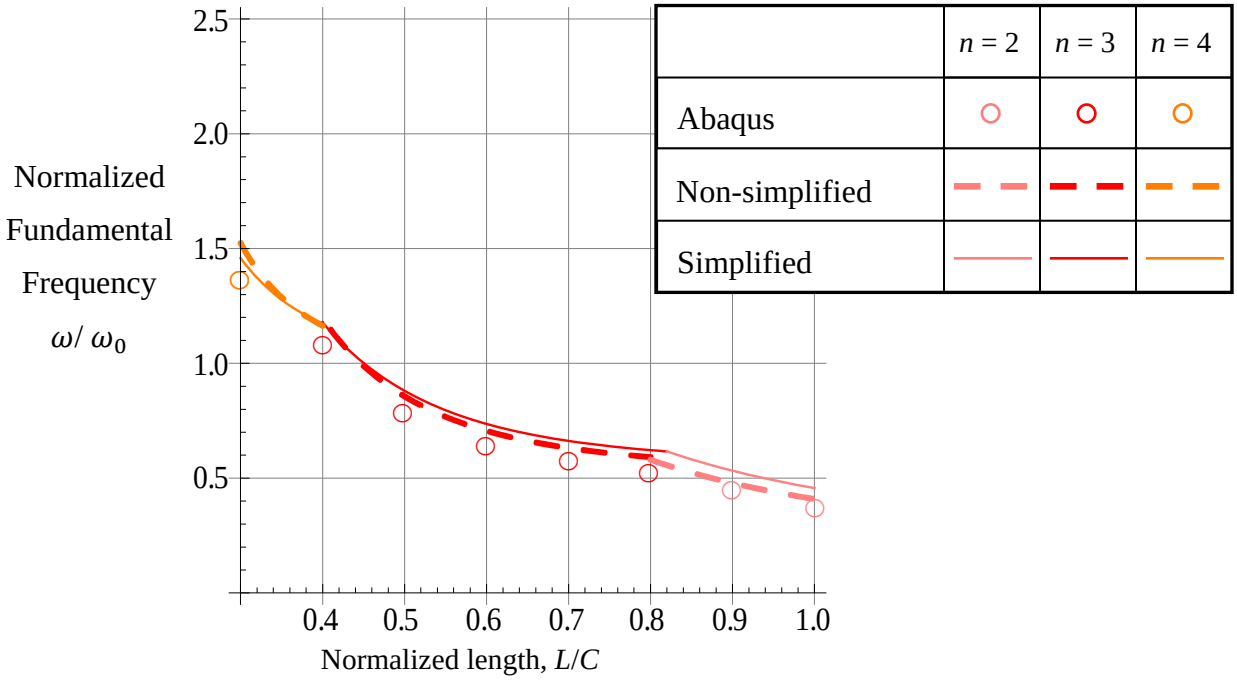

(f) Lamination sequences $[\pm 75]_{2S}$

Fig. 4- 3 Normalized fundamental frequency of small circular cylinders, simple supports

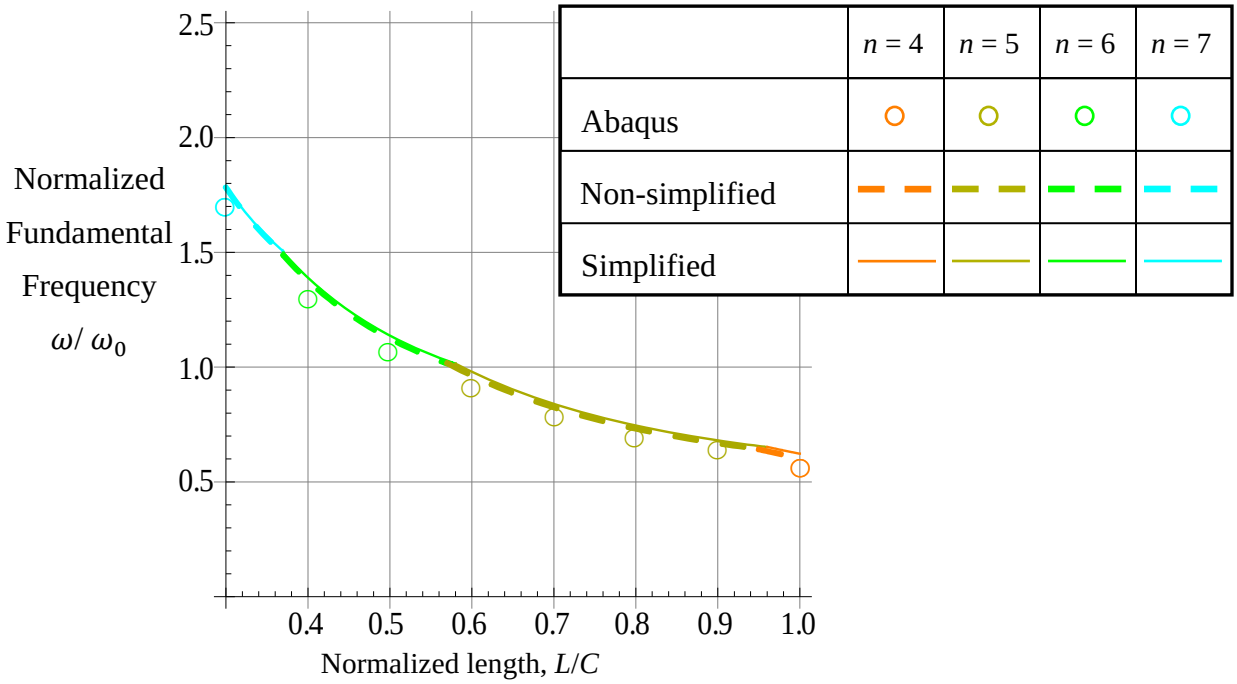

(a) Lamination sequences $[\pm 15/0/90]_S$

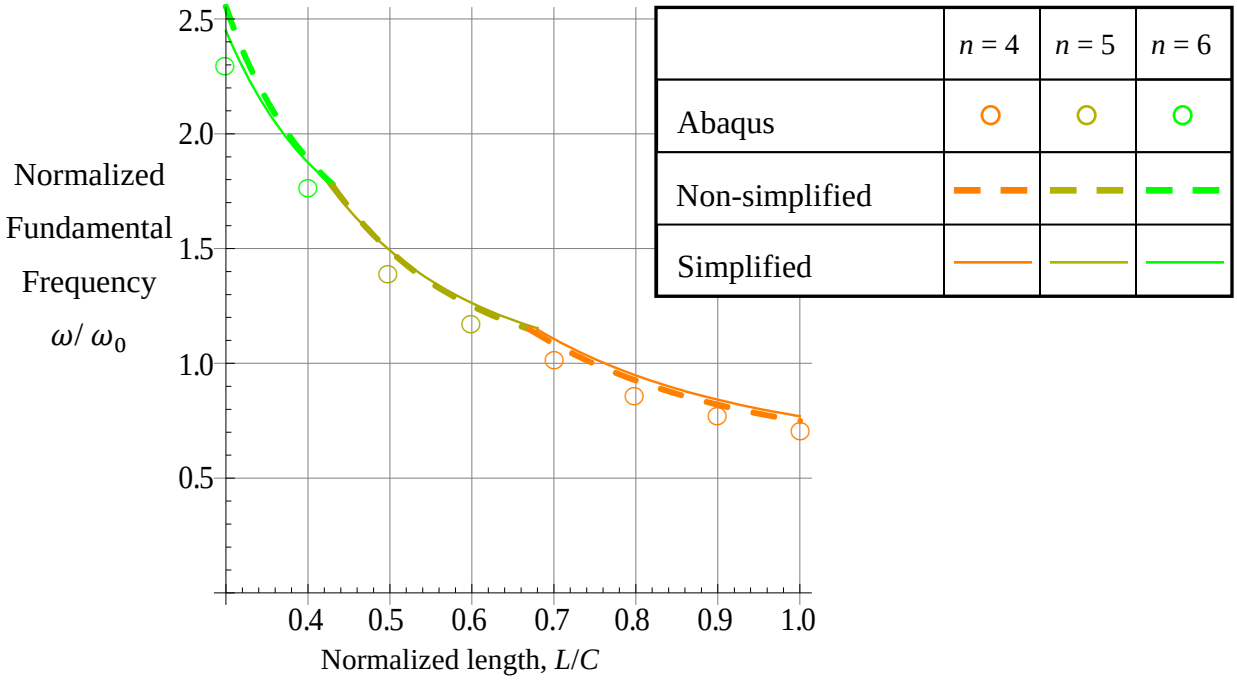

(b) Lamination sequences $[\pm 45/0/90]_S$

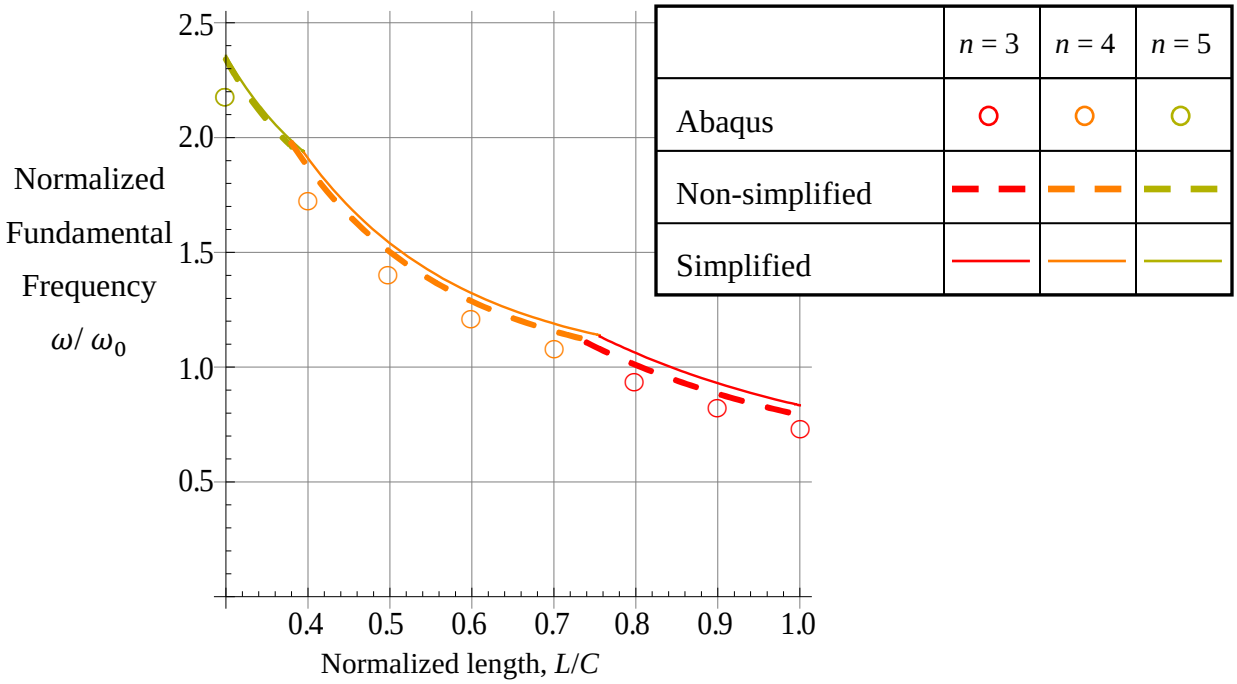

(c) Lamination sequences $[\pm 75/0/90]_S$

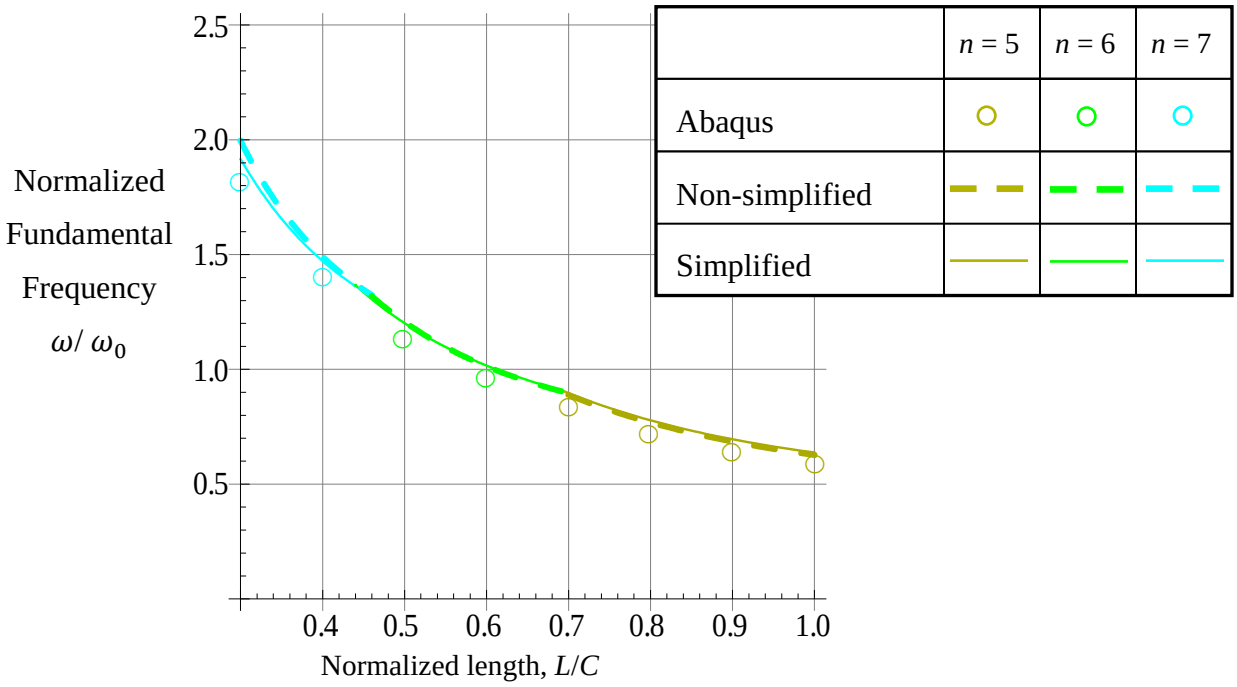

(d) Lamination sequences $[\pm 15]_{2S}$

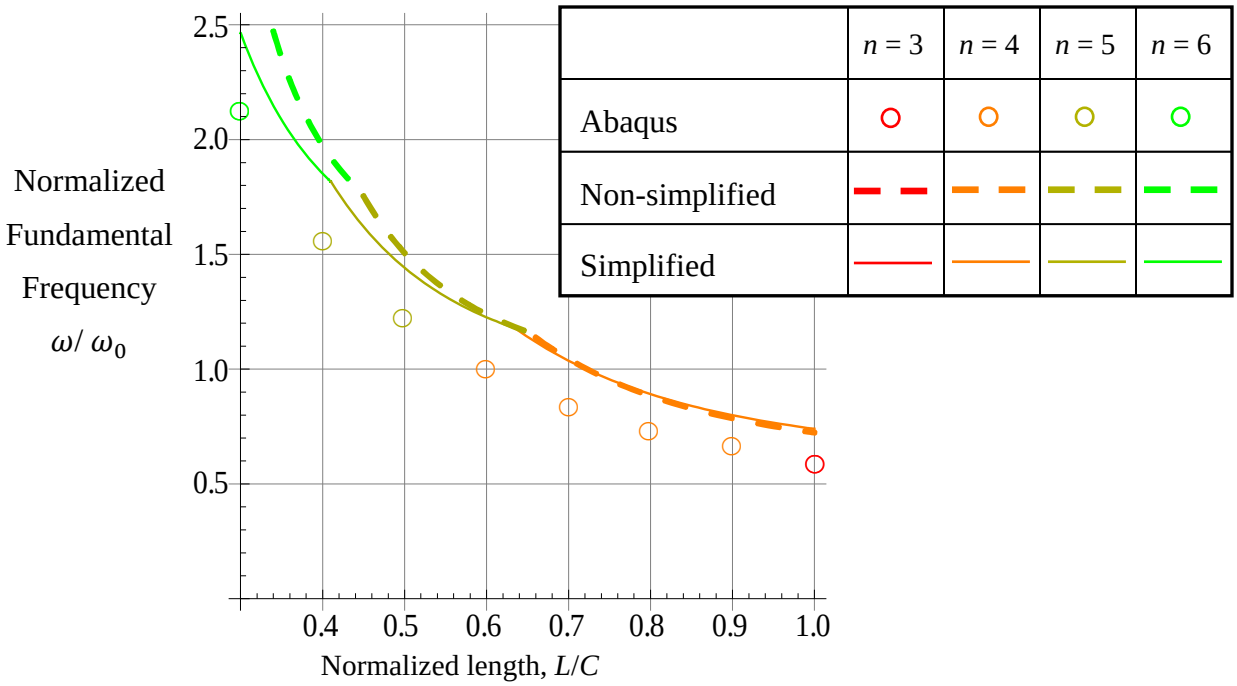

(e) Lamination sequences $[\pm 45]_{2S}$

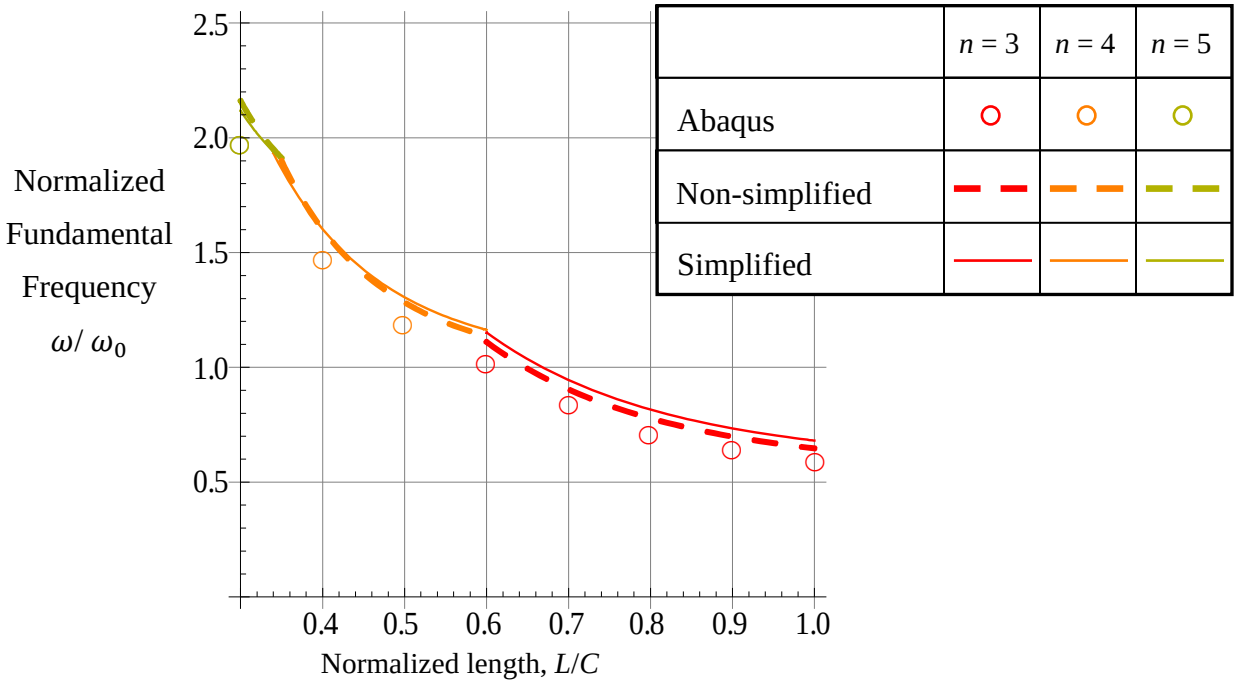

(f) Lamination sequences $[\pm 75]_{2S}$

Fig. 4- 4 Normalized fundamental frequency of small circular cylinders, clamped supports

4.2.2 Elliptical Cylinders and Comparisons with Circular Cylinders

Attention now turns to elliptical cylinders, in particular the dependency of the fundamental frequency on cylinder length and fiber angle in the two laminate families, and importantly, the accuracy of the developed formulation with no simplifications, the various levels of simplification, and Lo's approximation, when compared to finite-element calculations. Only results for an aspect ratio $b/a = 0.55$ ($e = 0.84$) are discussed at this point because this is the most severe elliptical geometry considered in this study and is believed to present the greatest challenge to the developed formulation, and exhibit the largest differences compared to circular cylinders.

The figures to follow can be considered to be in three groups. The first group consists of Figs. 4- 5 through 4- 8. These figures are analogs to the previous four figures, but for the elliptical geometry, illustrating the fundamental frequencies for large and small simply-supported and clamped support cylinders with three laminates each from the two laminate families and L/C ranging from 0.3 to 1.0. The calculations from the developed formulations have been computed using the cosine-based functional form for $\Phi_n^w(s)$, as was discussed in relation to Tables 3- 1 and 3- 2.

The second group of figures consists of Figs. 4- 9 and 4- 10. To illustrate the influence on the fundamental frequency of the elliptical geometry, in these two figures the difference between frequencies for circular and elliptical cylinders with $b/a = 0.55$ ($e = 0.84$) and with like values of L/C, R_0/H, lamination arrangement, and boundary conditions are illustrated.

The third group of figures consists of Figs. 4- 11 through 4- 14. Recall that the cosine-based and sine-based development in Ch. 3 led to different equations from which to predict the fundamental frequencies. And, as mentioned, for circular cylinders the cosine- and sine-based formulations lead to the same results. For noncircular cylinders, that is not the case. Table 3- 1 illustrated this point, and as mentioned in the discussion related to Tables 3- 1 and 3- 2, both a cosine-base analysis and a sine-based analysis must be considered. For results such as illustrated in Figs. 4- 5 through 4- 8, a parallel series of figures must be constructed and then compared case-by-case with Figs. 4- 5 through 4- 8 to determine what differences there may be, for what

conditions they occur, what features are different, etc. That is not the approach taken here. For the range of elliptical cylinders considered in this study, the difference between the cosine-based analysis and the sine-based analysis generally could not be resolved within the resolution of the figures. There were some situations where the difference could be detected, and it is important to point those conditions out. Therefore, the second group of figures focuses on the differences by illustrating the difference in predicted frequencies between the sine-based and cosine-based analyses, expressed as a percentage, in the same format as Figs. 4- 1 through 4- 4, but with the percent difference on the vertical axis.

Fundamental Frequencies of Elliptical Cylinders

In Fig. 4- 5 the variations of the normalized fundamental frequencies of large simply-supported elliptical cylinders with *L/C* are illustrated. A quick look at Fig. 4- 5 reveals that for these cases the non-simplified formulation, the two levels of simplified formulations, and Lo's approximation, Eq. 3- 68, Eq. 3- 71, Eq. 3- 72, and Eq. 3- 74, respectively, agree quite well with the calculations from the finite-element model. All predictions of the developed formulations are higher than those of the finite-element model. Though it is difficult to detect, in Fig. 4- 5 the various formulations from a low fundamental frequency prediction to a high frequency prediction are, in order, 2nd simplification, Lo's approximation, non-simplified formulation, and 1st simplification. These formulations are within 10% of each other and that is also the difference between the finite-element predictions and those of the 2nd simplification. The predicted value of the circumferential wave number *n* is also quite accurate. Where there is a difference between the predictions of the developed formulation and the finite-element model as regards *n*, the value of *n* in the developed formulation is always less by one over a limited range of *L*/*C*. As mentioned, in all cases $m = 1$.

In Fig. 4- 6 the fundamental frequencies of large elliptical cylinders with clamped supports are illustrated in the familiar format. Equation 3- 91, Eq. 3- 94, Eq. 3- 95, and Eq. 3- 97 from the developed formulation are used. The comments regarding the accuracy of the predictions of the various developed formulations relative to each other and relative to the finite-element predictions are the same as for the simply-supported elliptical cylinders. Though the error between the most accurate prediction of the developed formulation and the finite-element model

for the clamped support cylinder is greater than that for the simply supported case, except for the $[\pm 45]_{4S}$ laminate, it does not exceed 15% as compared to 10% for the simply supported case.

For the small simply supported elliptical cylinders, Fig. 4- 7, for some cases the predictions of non-simplified formulation and the 1st simplification cluster together and the predictions of the 2nd simplification and Lo's approximation form another cluster, these two clusters being separated slightly for particular laminates. This was somewhat the case with the large simply supported elliptical cylinders, but it is more so for the small simply supported cylinders. The cluster with the non-simplified formulation and the 1st simplification always predict higher fundamental frequencies than the other cluster. Unlike the situation for the larger simply supported elliptical cylinder in Fig. 4- 5, for the small simply supported cylinders the 1st simplification does not always predict frequencies higher than the non-simplified formulation. Additional, regarding the 2nd cluster and unlike the situation for the larger simply supported cylinders, the predictions of Lo's approximation are not always higher than the predictions of the 2nd simplification. For the $[\pm 45]_{2S}$ laminate, which has stood out as being a somewhat different case, Lo's approximation and the 2nd simplification, the second cluster, agree quite well with the finite-element predictions.

Finally, for the small clamped support elliptical cylinders, in Fig. 4- 8, the two clusters are again obvious and no one developed formulation predicts the fundamental frequencies well for all laminates and the full range of L/C, as has been the case with other cylinder sizes and support conditions. The difference between the finite-element predictions and the predictions of the 2nd simplification and Lo's approximation for $[\pm 45]_{2S}$ laminate is about 15% for short cylinders and 20% for the long cylinders.

Regarding the prediction of the circumferential wave number n: There is some disagreement between the predictions of the developed formulation and the finite element results as to the value of L/C where the wave number changes. However, overall for the elliptical cylinders the prediction of the circumferential wave number by the developed formulation is in agreement with the finite-element prediction.

In summary, as with the circular cylinders, the cosine-based developed formulation, particularly the 2nd simplification and Lo's approximation, generally does a reasonably accurate job of predicting the fundamental frequency of cylinders with the most extreme eccentricity of all the cylinders considered in this study. Lo's approximation, for example, would be very good for design and trade-off studies.

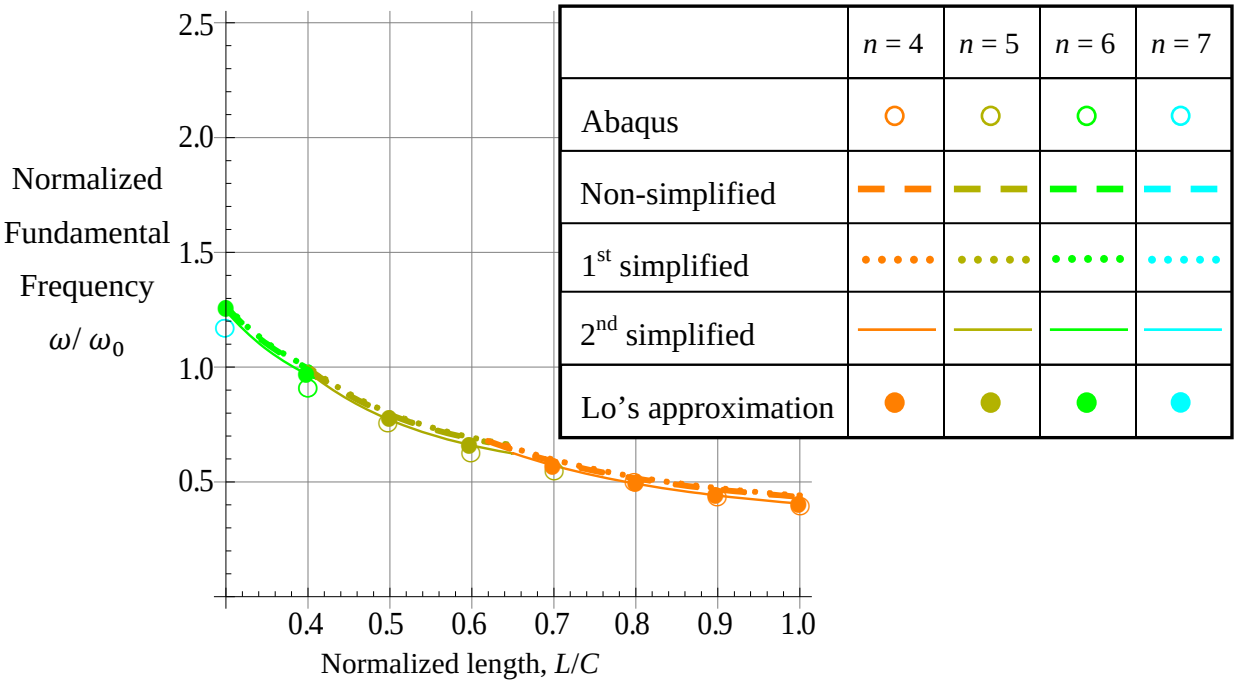

(a) Lamination sequences $[\pm 15/0/90]_{2S}$

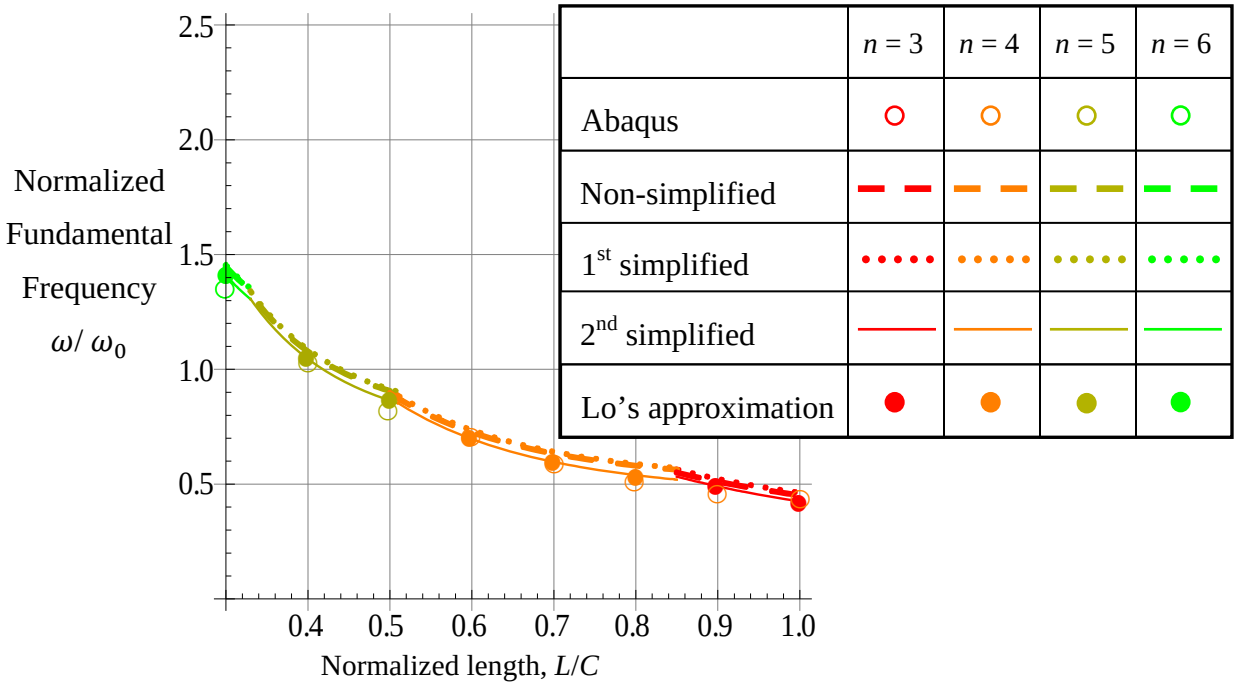

(b) Lamination sequences $[\pm 45/0/90]_{2S}$

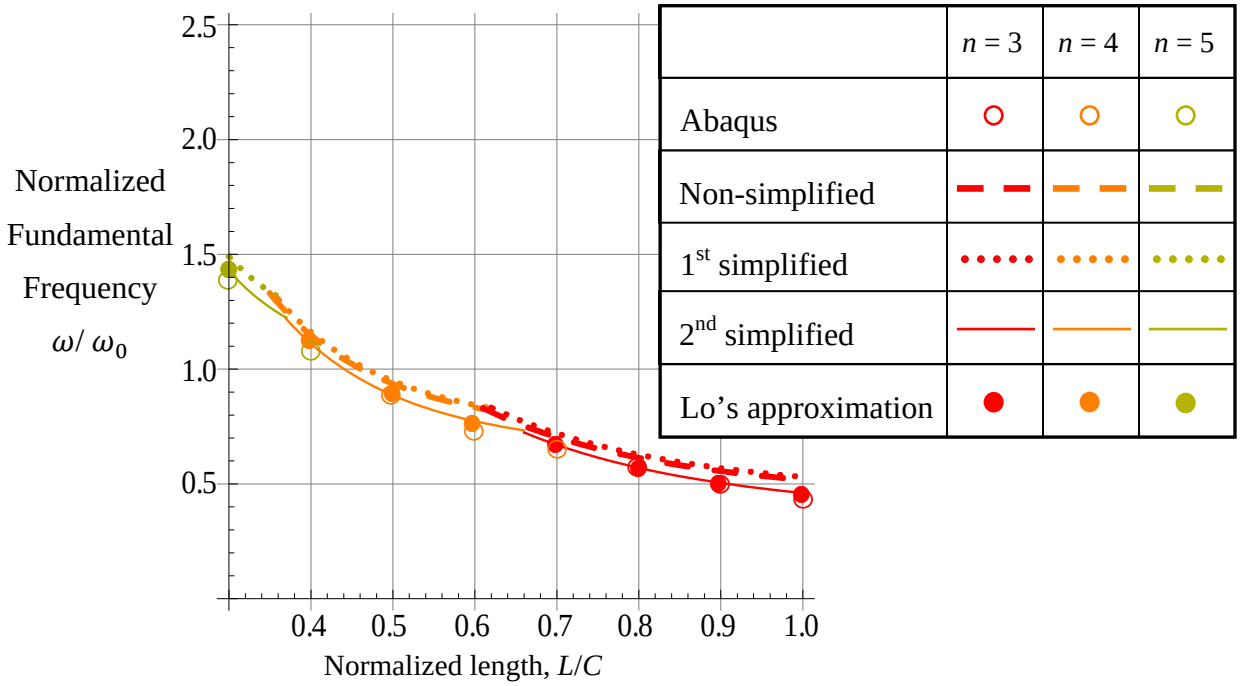

(c) Lamination sequences $[\pm 75/0/90]_{2S}$

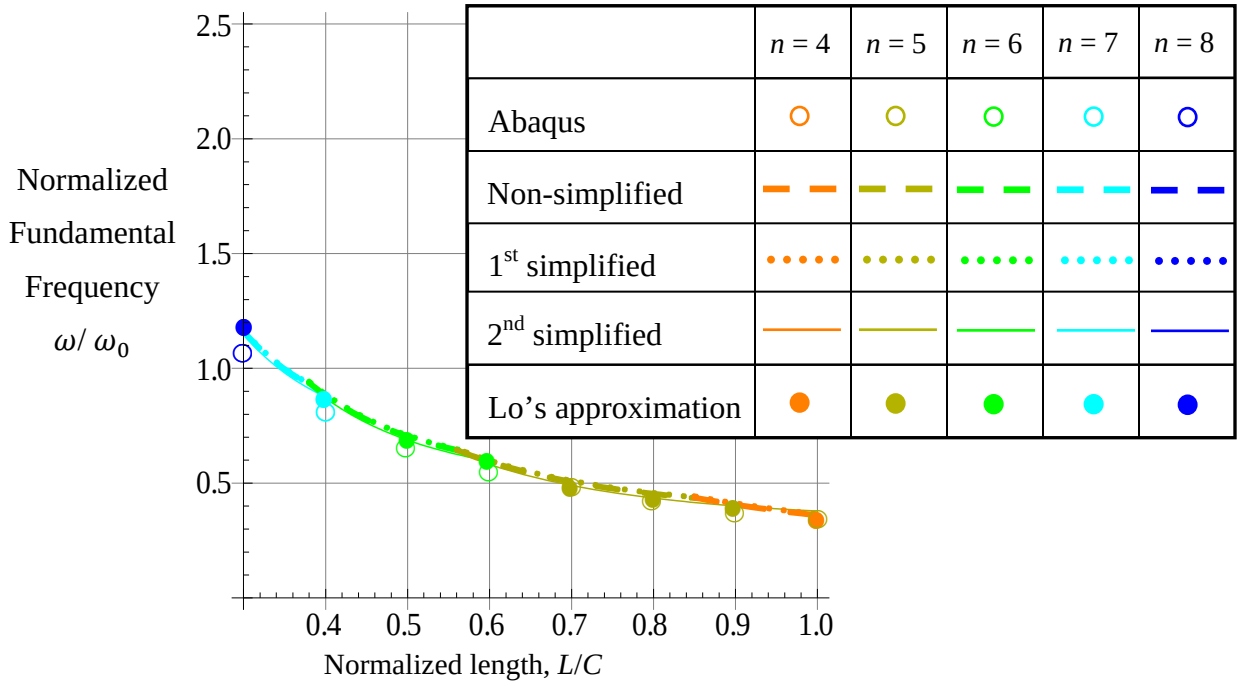

(d) Lamination sequences $[\pm 15]_{4S}$

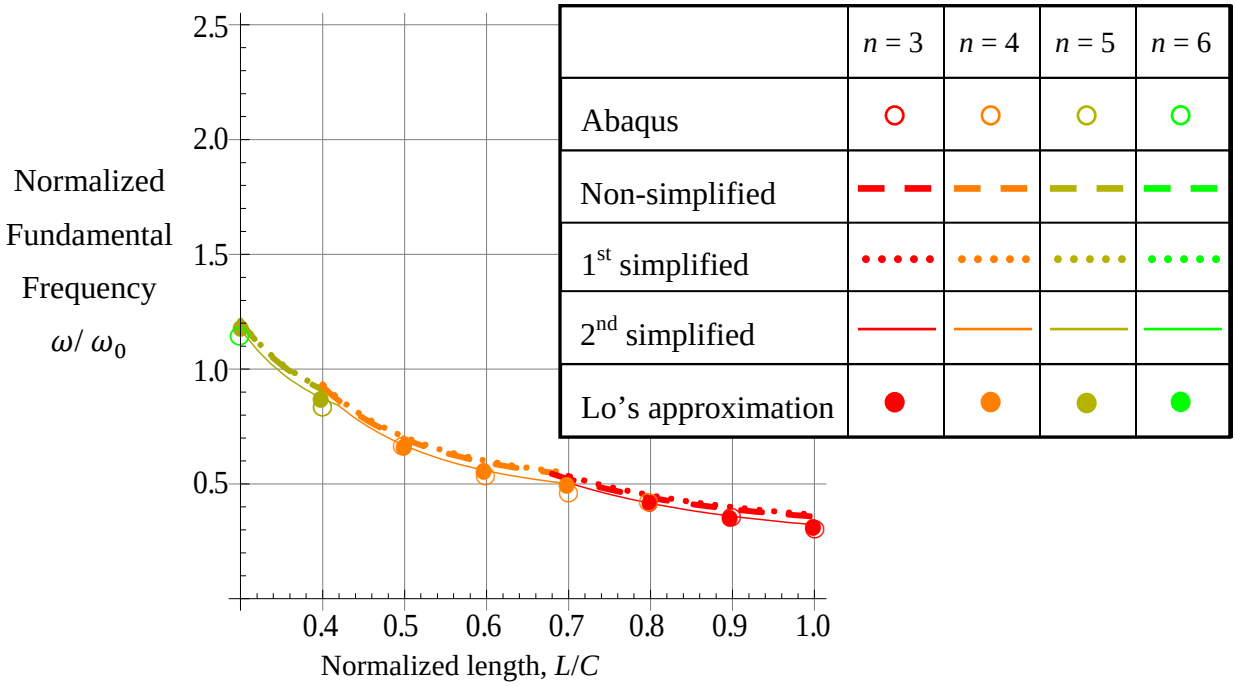

(e) Lamination sequences $[\pm 45]_{4S}$

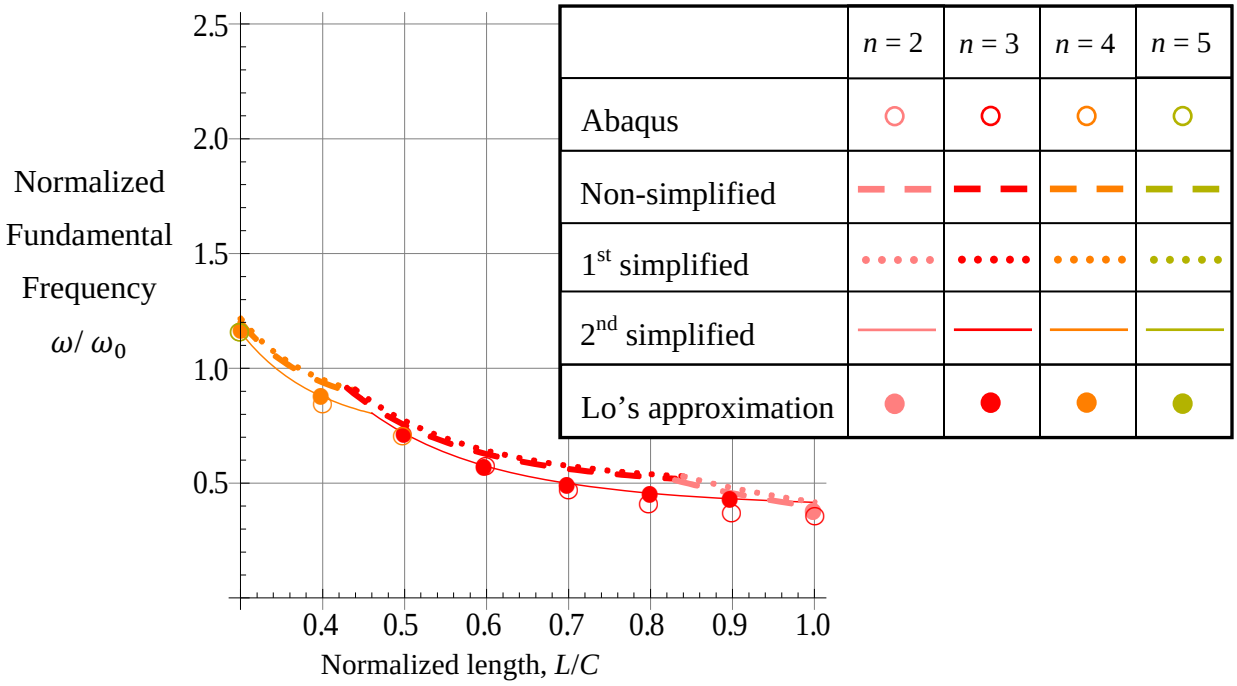

(f) Lamination sequences $[\pm 75]_{4S}$

Fig. 4- 5 Normalized fundamental frequency of large elliptical cylinders, $b/a = 0.55$ ($e = 0.84$), simple supports, cosine-based

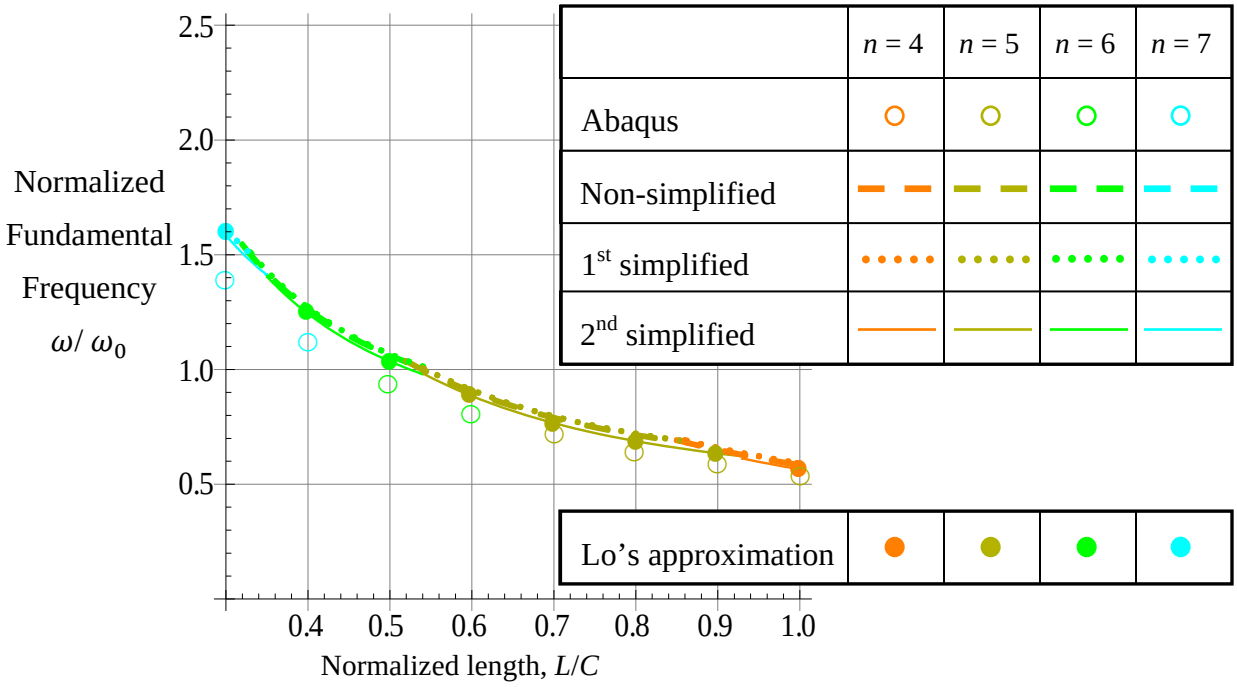

(a) Lamination sequences $[\pm 15/0/90]_{2S}$

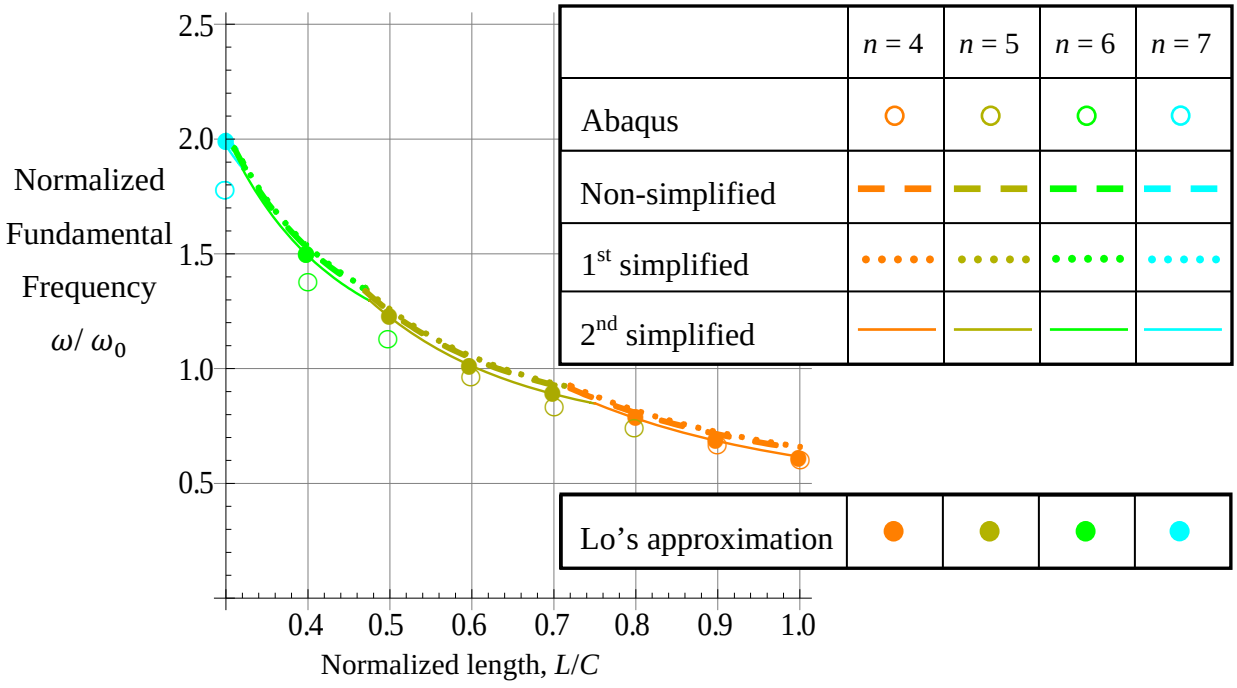

(b) Lamination sequences $[\pm 45/0/90]_{2S}$

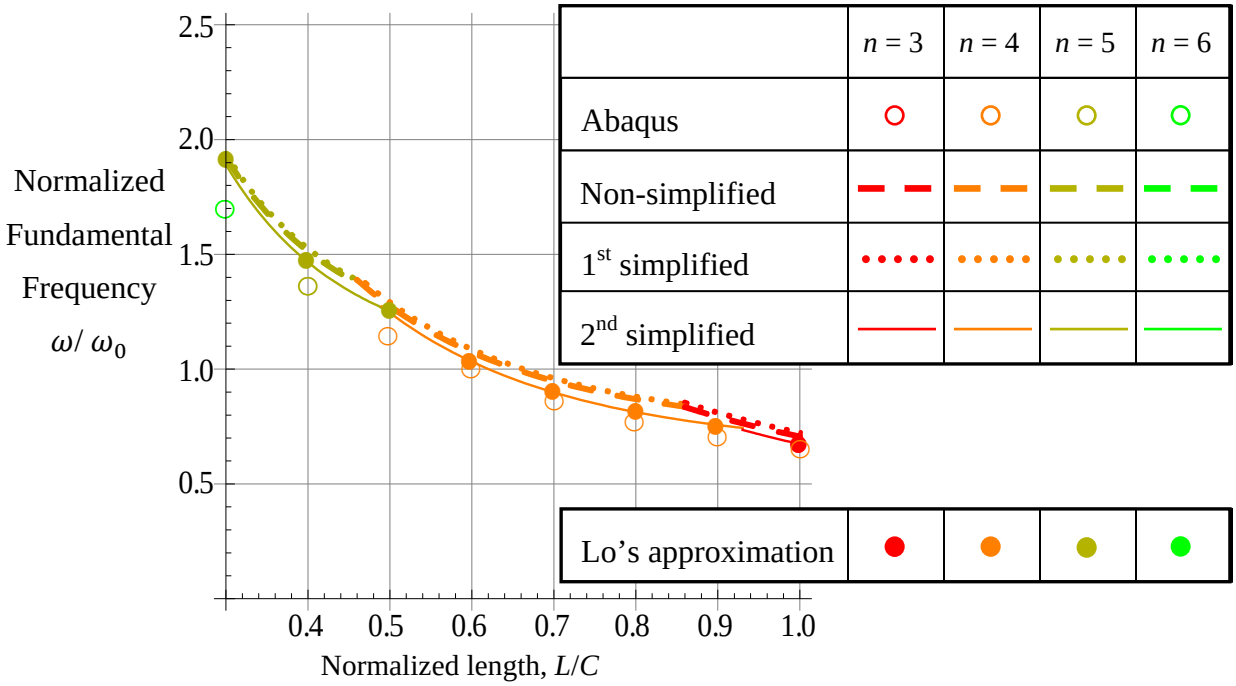

(c) Lamination sequences $[\pm 75/0/90]_{2S}$

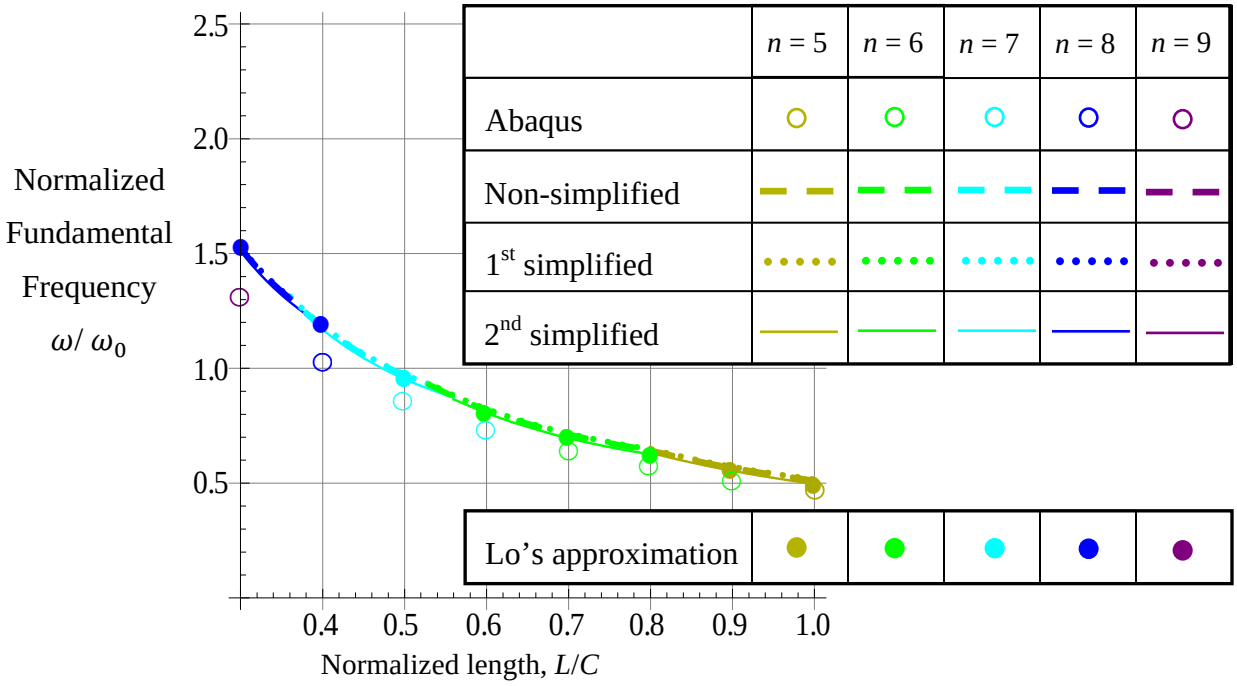

(d) Lamination sequences $[\pm 15]_{4S}$

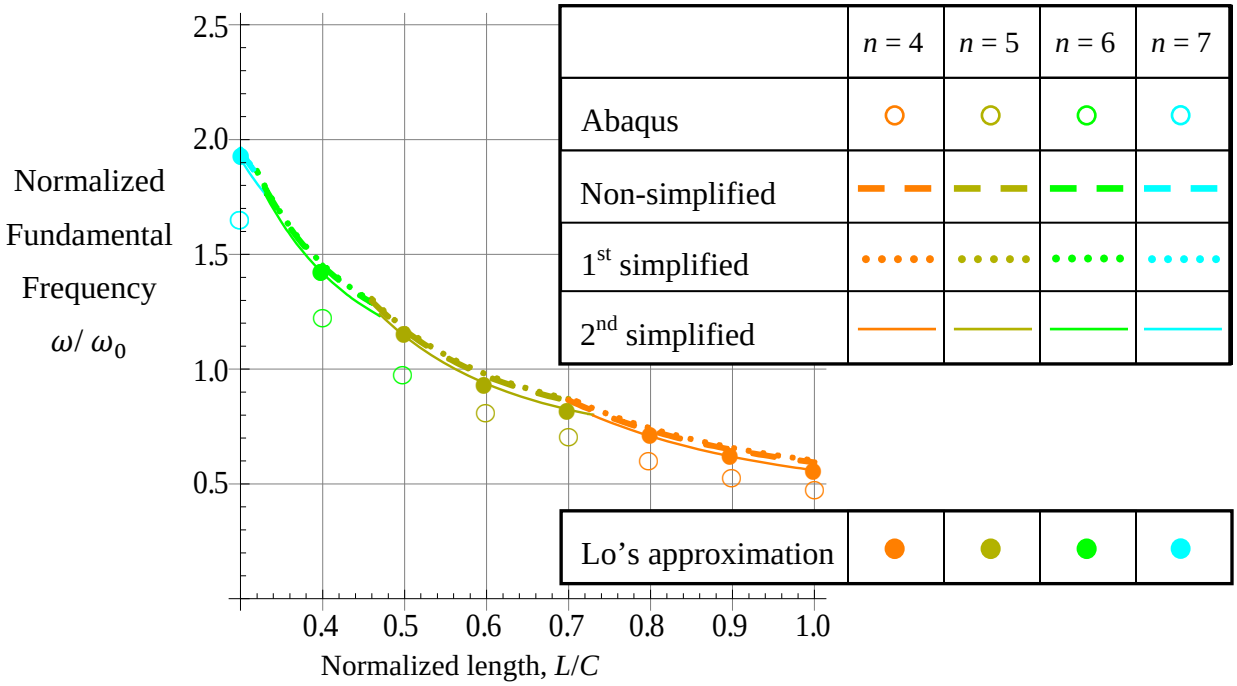

(e) Lamination sequences $[\pm 45]_{4S}$

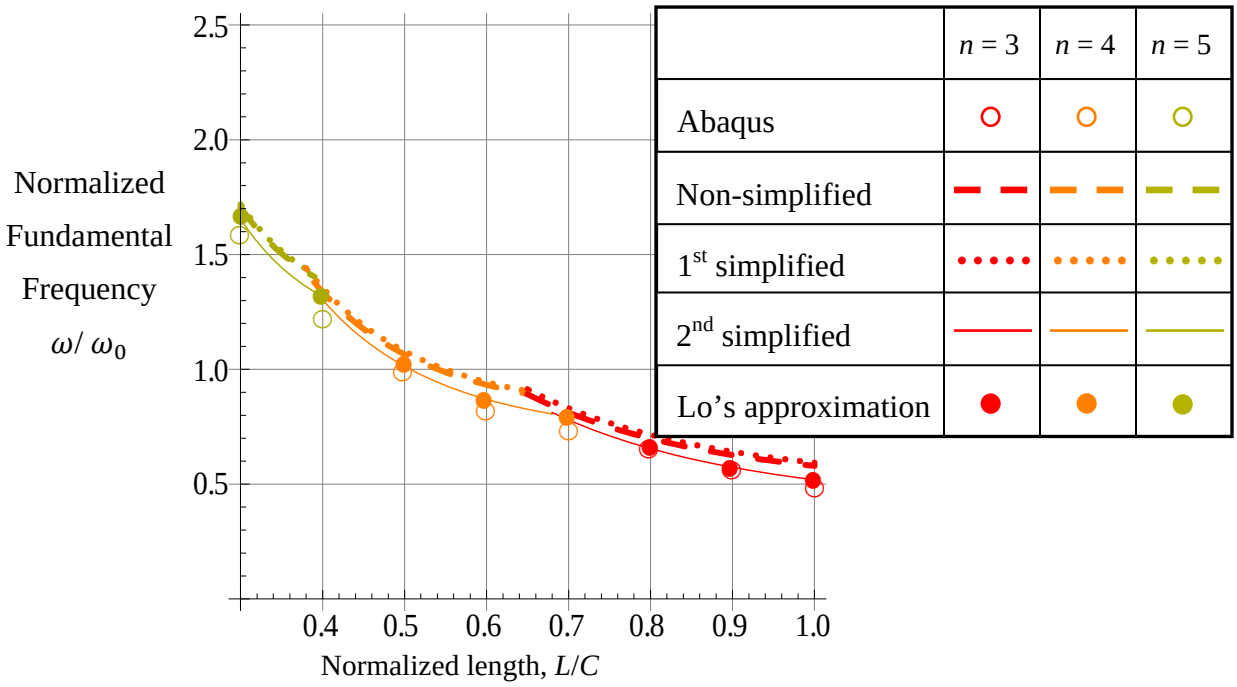

(f) Lamination sequences $[\pm 75]_{4S}$

Fig. 4- 6 Normalized fundamental frequency of large elliptical cylinders, b/a = 0.55 (e = 0.84), clamped supports, cosine based

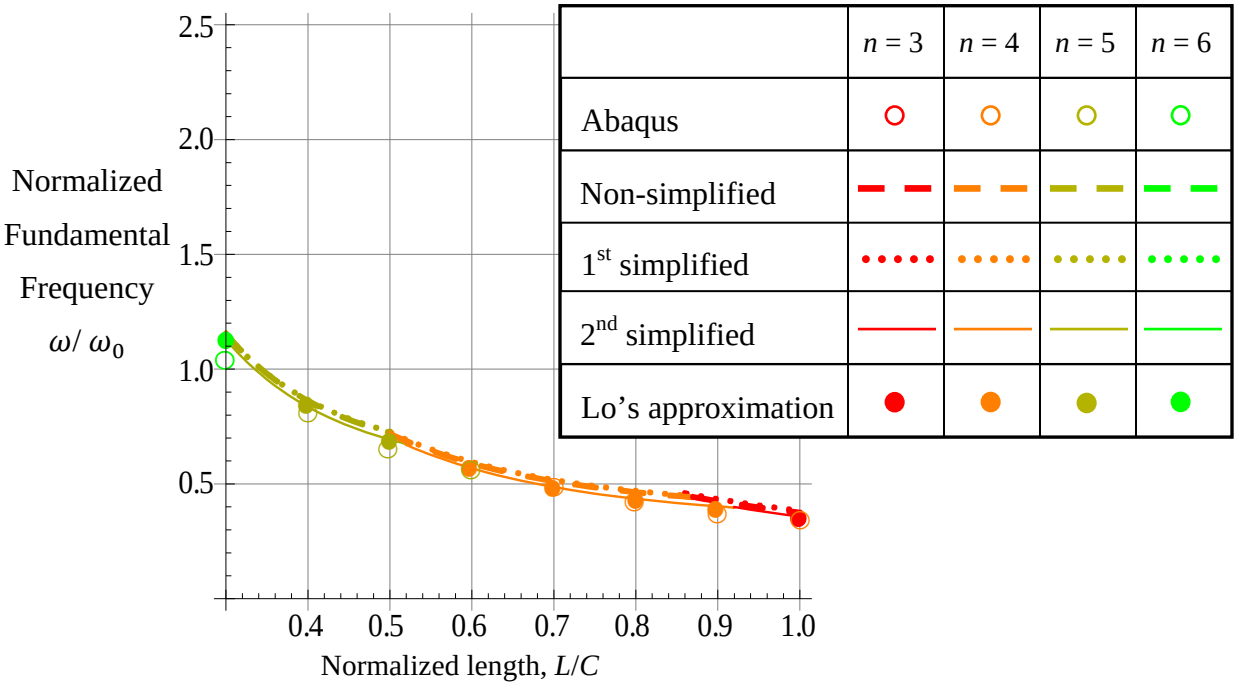

(a) Lamination sequences $[\pm 15/0/90]_S$

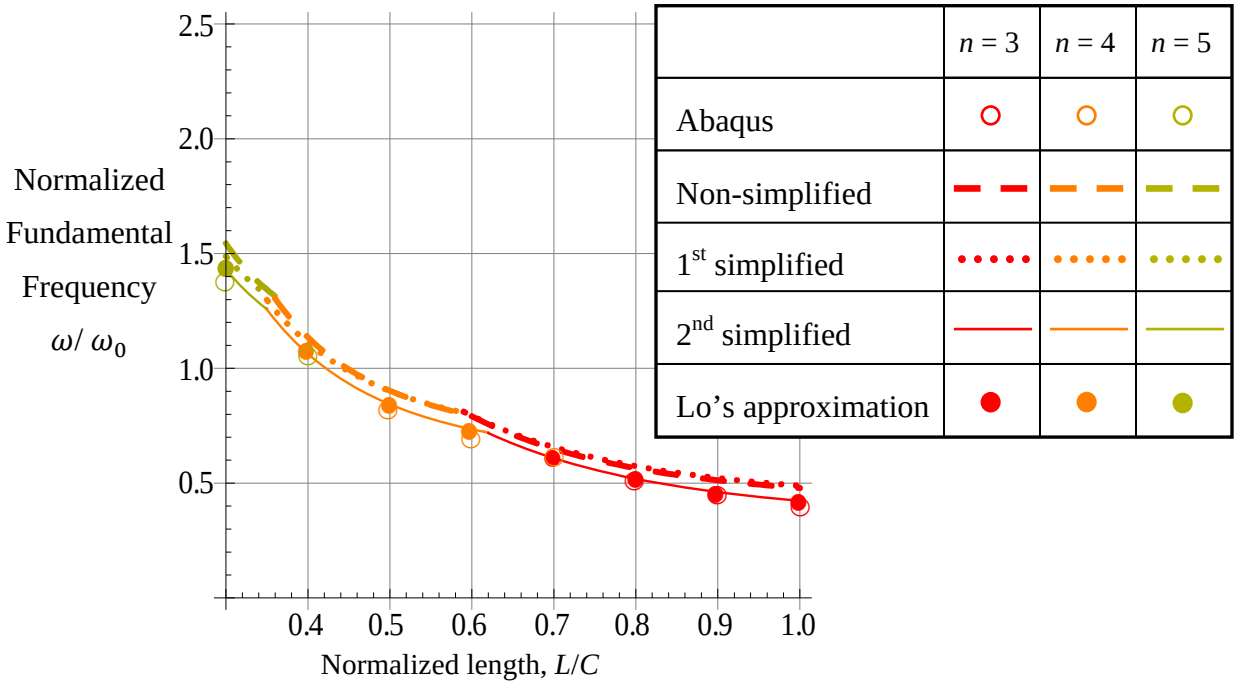

(b) Lamination sequences $[\pm 45/0/90]_S$

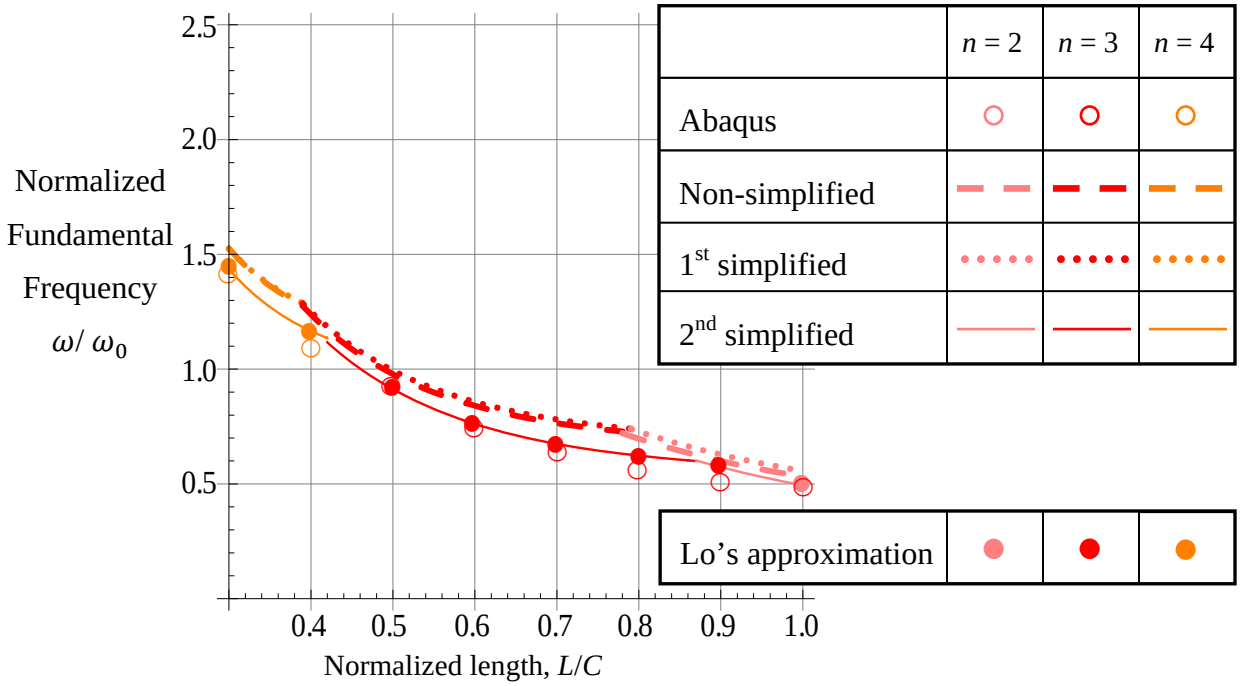

(c) Lamination sequences $[\pm 75/0/90]_S$

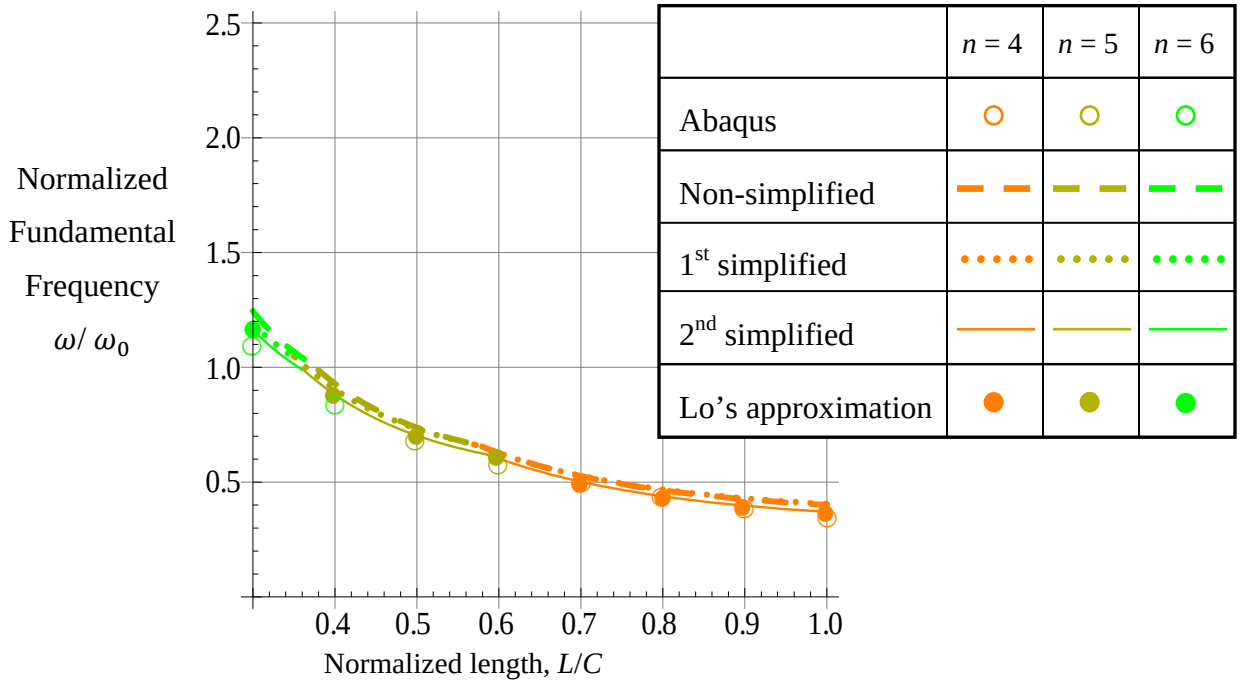

(d) Lamination sequences $[\pm 15]_{2S}$

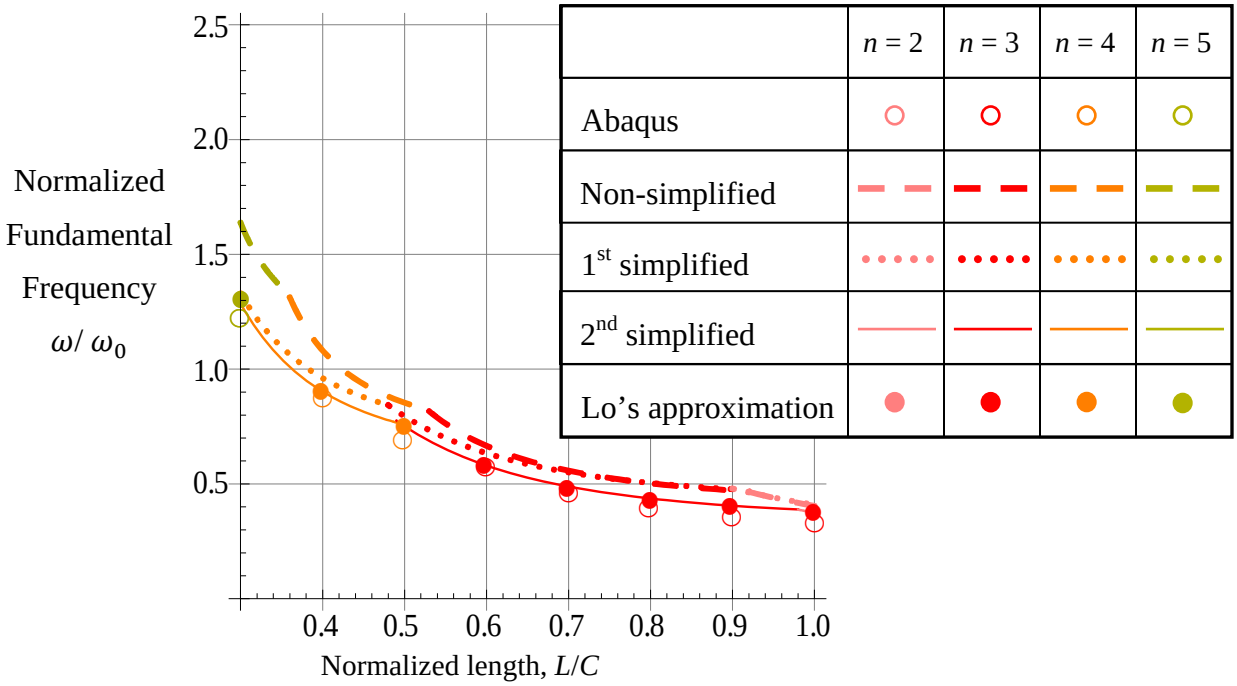

(e) Lamination sequences $[\pm 45]_{2S}$

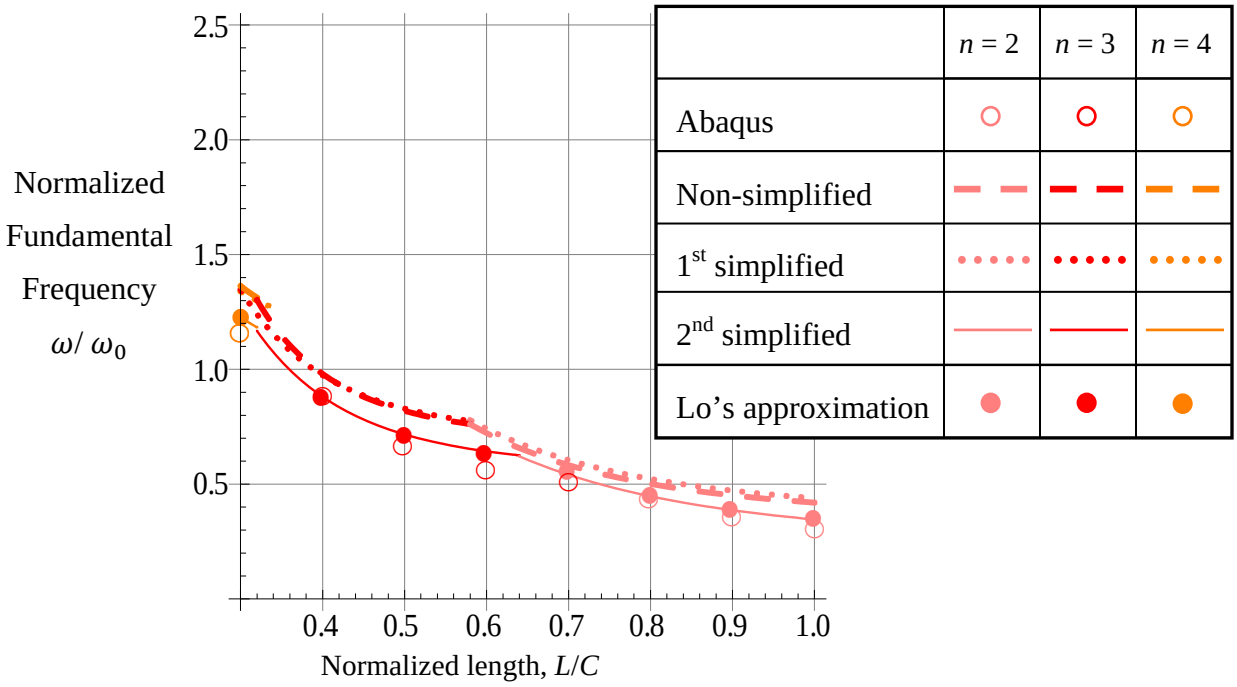

(f) Lamination sequences $[\pm 75]_{2S}$

Fig. 4- 7 Normalized fundamental frequency of small elliptical cylinders, b/a = 0.55 (e = 0.84), simple supports, cosine-based

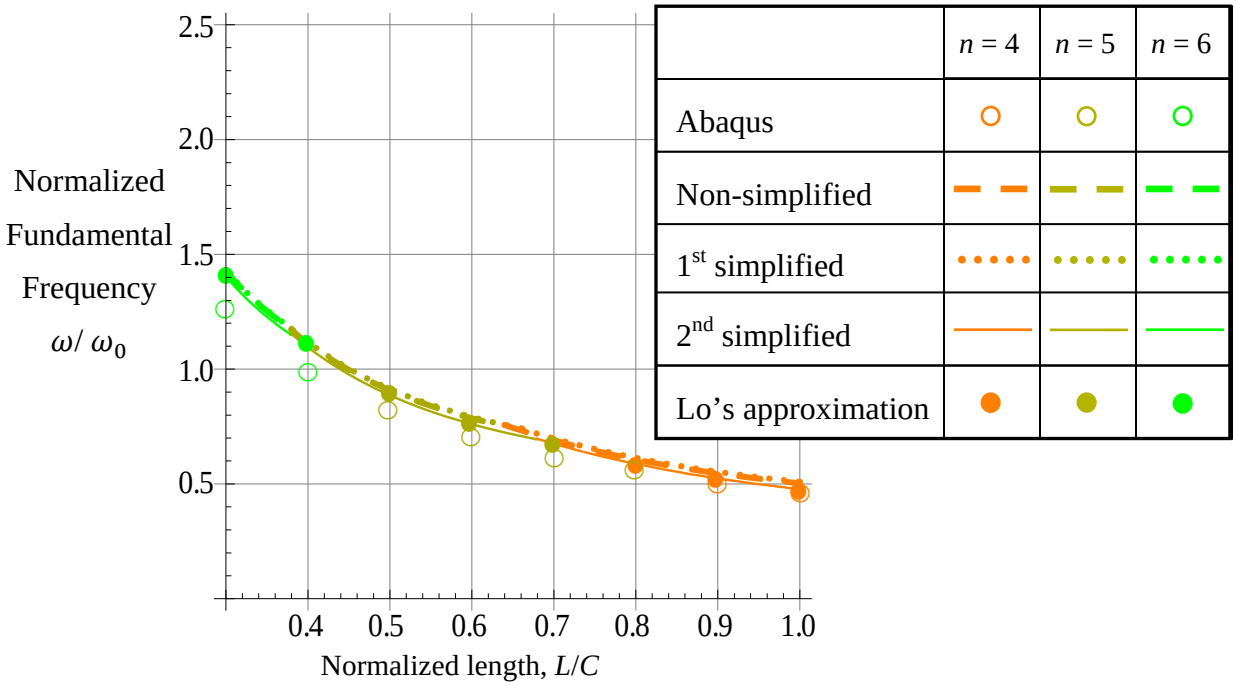

(a) Lamination sequences $[\pm 15/0/90]_S$

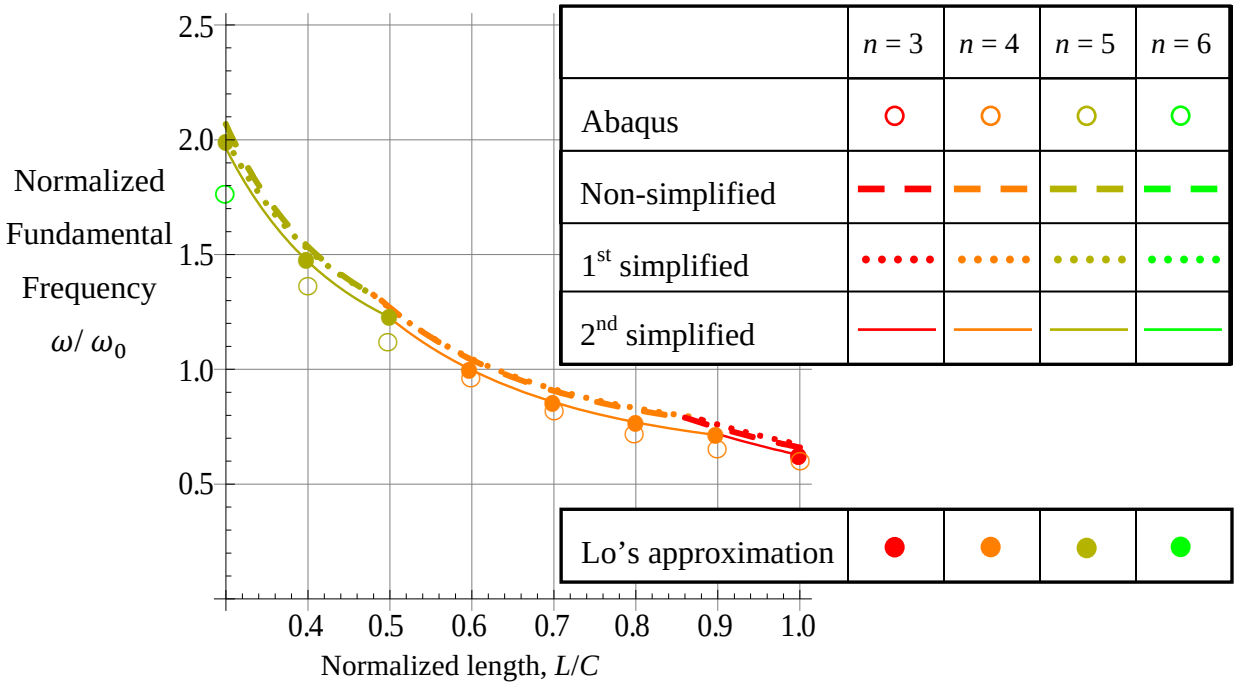

(b) Lamination sequences $[\pm 45/0/90]_S$

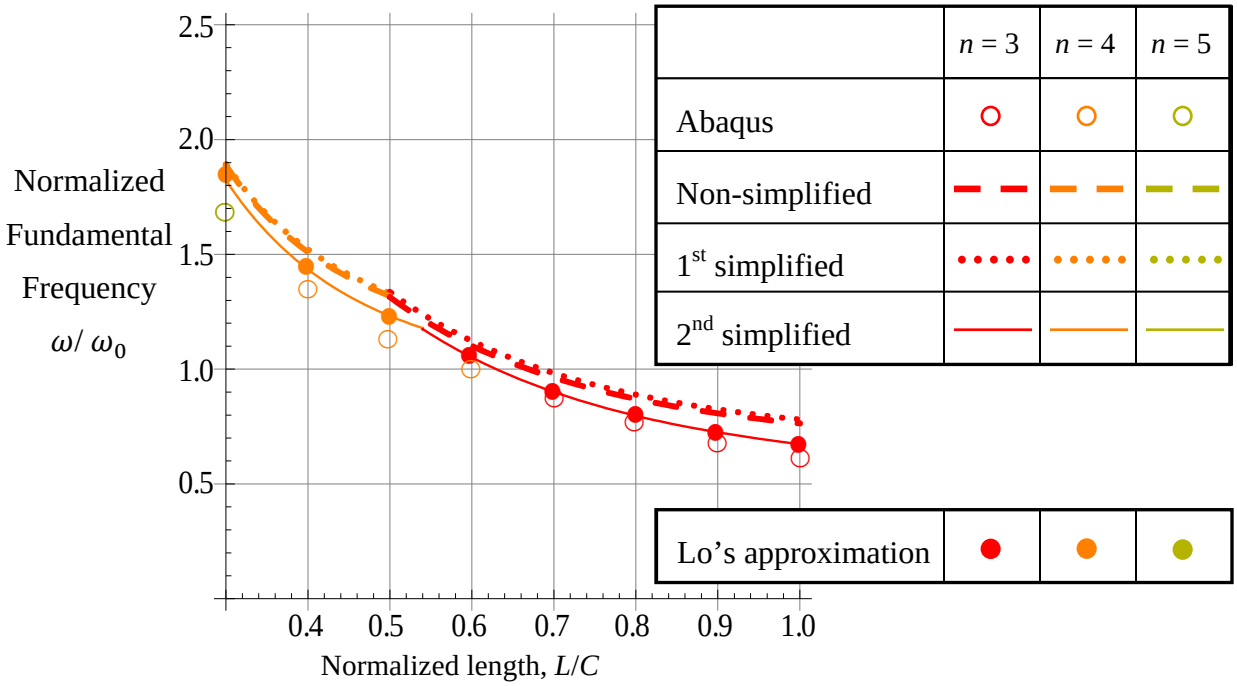

(c) Lamination sequences $[\pm 75/0/90]_S$

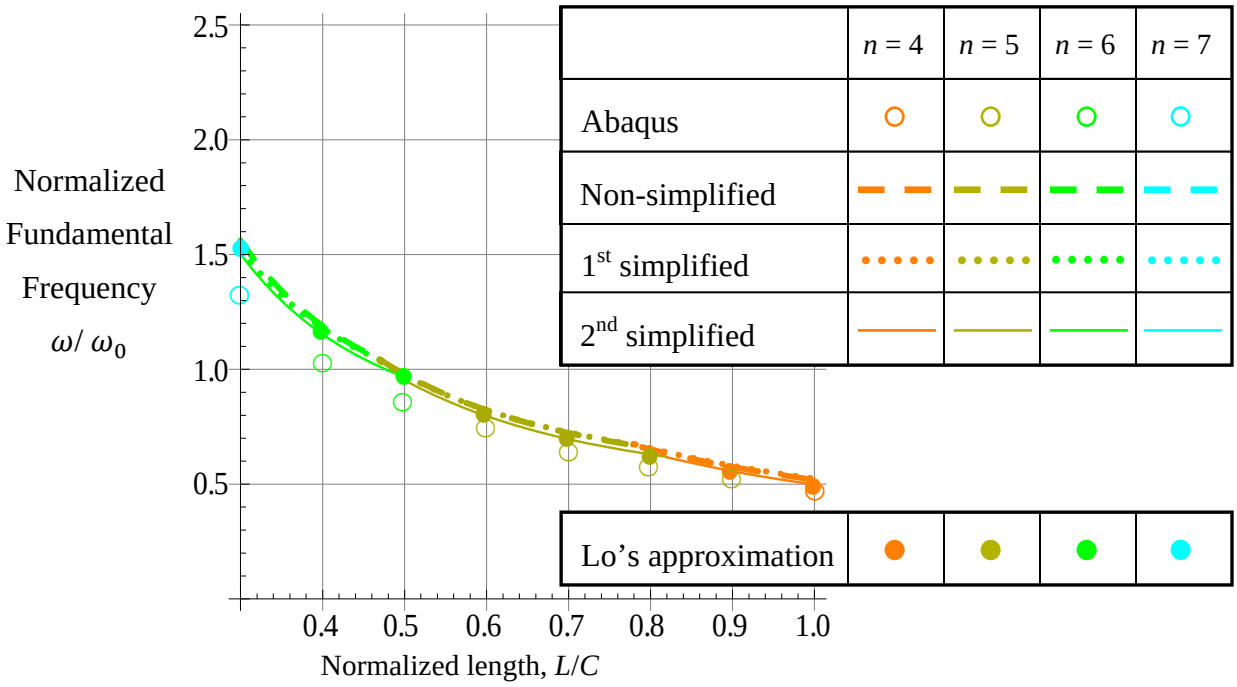

(d) Lamination sequences $[\pm 15]_{2S}$

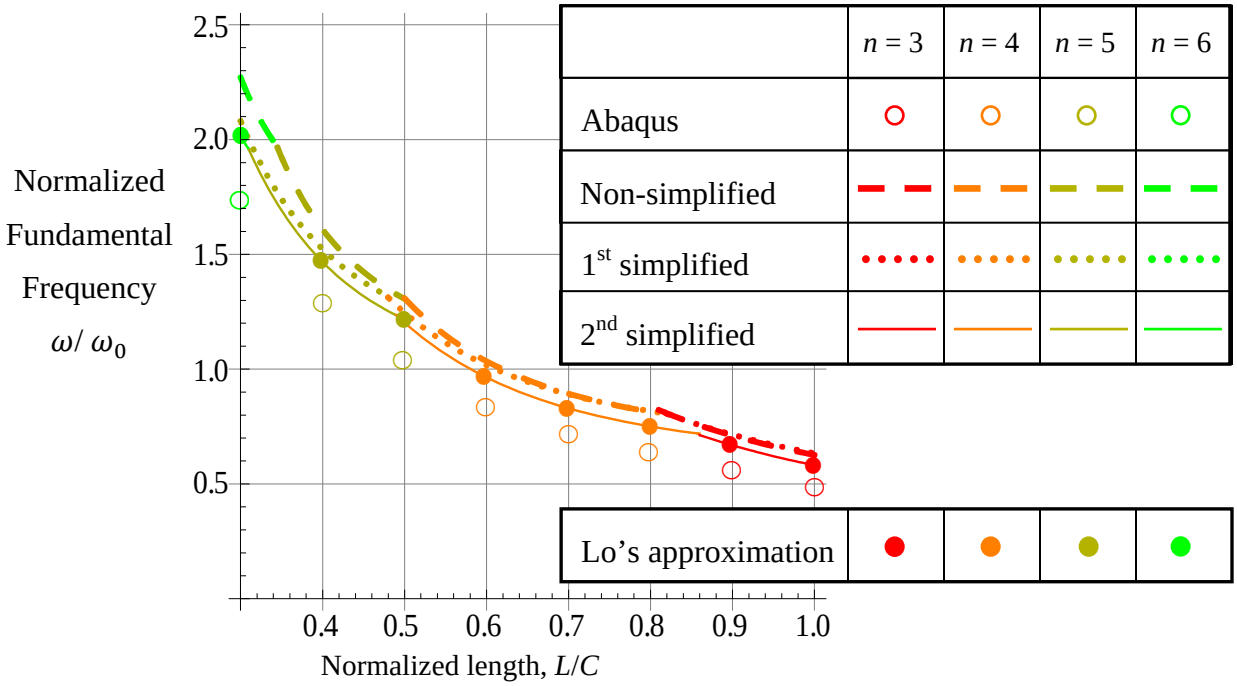

(e) Lamination sequences $[\pm 45]_{2S}$

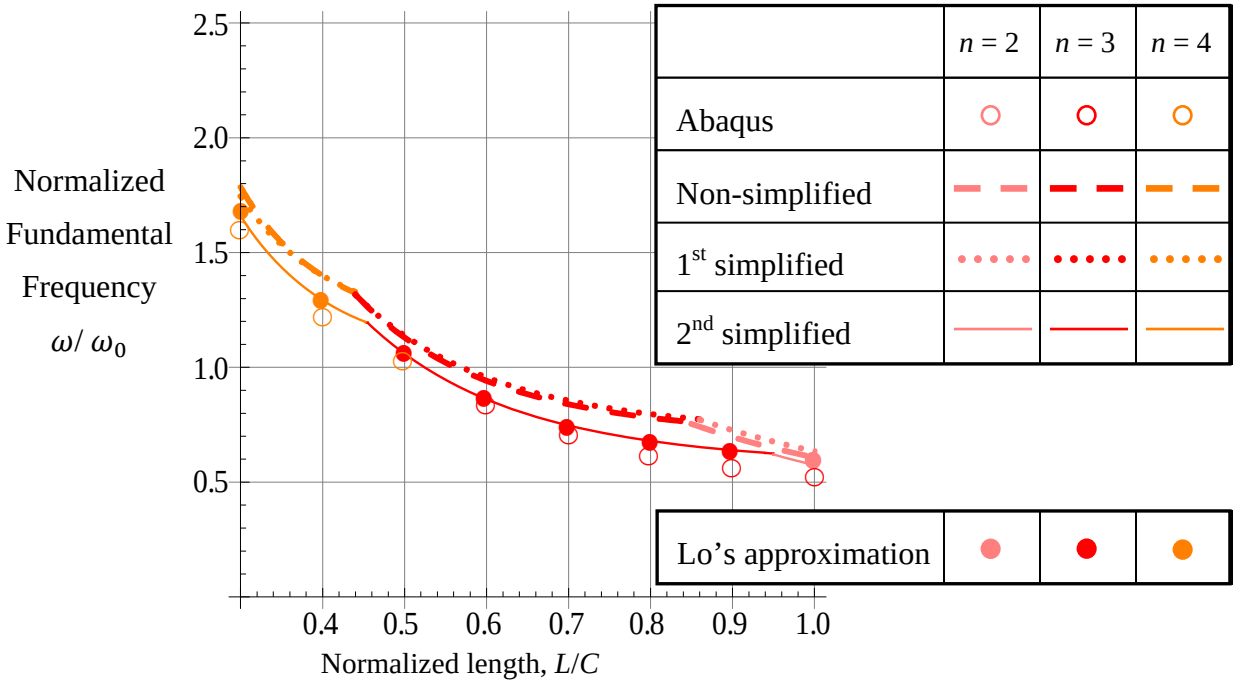

(f) Lamination sequences $[\pm 75]_{2S}$

Fig. 4- 8 Normalized fundamental frequency of small elliptical cylinders, b/a = 0.55 (e = 0.84), clamped supports, cosine-based

Effect of Elliptical Geometry on Frequency

While Figs. 4- 1 through 4- 4 and 4- 5 through 4- 8 have been used to provide an indication of the accuracy and utility of the predictive capability by comparing the predictions of various simplified and approximate formulas with finite-element predictions, these two groups of figures can also be used to illustrate the effect of a noncircular geometry on the fundamental frequency. By comparing results from similar cylinder sizes, values of R_0/H, lamination arrangement, and boundary conditions, e.g., Fig. 4- 1a with Fig. 4- 5a, it is clear that the fundamental frequency of an elliptical cylinder is less than the fundamental frequency of a circular cylinder of the same circumference, length, value of R_0/H, lamination arrangement, and with the same boundary conditions. How much less, as might be expected, depends on the particulars of those parameters, so it is not easy to cite a number that covers all situations. However, there are some trends. To provide a better evaluation of the decrease in the fundamental frequency due to the noncircular geometry, the percentage decrease in fundamental frequency due to eccentricity is plotted in Figs. 4- 9 and 4- 10 for the two groups of figures, Fig. 4- 9 for the large simply supported and clamped cylinders, and Fig. 4- 10 for the small simply supported and clamped cylinders. The percent plotted is defined by

$$\frac{\left(\omega_{ellipse} - \omega_{circle}\right)}{\omega_{circle}} \times 100\% \qquad \text{Eq. 4- 1}$$

and only the calculations from the finite element analyses are shown to keep the figures less cluttered. The percent differences for the $[\pm\vartheta/0/90]_{2S}$ and $[\pm\vartheta/0/90]_S$ laminate families are represented by solid symbols and the percent differences for the $[\pm\vartheta]_{4S}$ and $[\pm\vartheta]_{2S}$ laminate families are represented by open symbols. Considering all cases in Figs. 4- 9 and 4- 10, it is clear that the percent difference decreases with increasing L/C. For the $[\pm\vartheta]_{4S}$ and $[\pm\vartheta]_{2S}$ laminate families, the cylinders with the ±15° layers (open triangles) generally experience the largest decrease in fundamental frequency (upwards of a 30% decrease for small L/C), while the families with the ±75° layers (open circles) or the ±45° layers (open diamonds) exhibit the smallest decrease (as low as 10% for large L/C). For the $[\pm\vartheta/0/90]_{2S}$ and $[\pm\vartheta/0/90]_S$ laminate families, the cylinders with the ±15° layers (solid triangles) also experience the largest decrease (also upwards of a 30% decrease for low L/C). Again, for the $[\pm\vartheta/0/90]_{2S}$ and $[\pm\vartheta/0/90]_S$ laminate families the cylinders with the ±75° layers (solid circles) or the ±45° layers (solid diamonds) exhibit the smallest decrease (again as low as 10% for large L/C). Given the range of

fiber orientations among the two laminate families, from ±15° to the ±75°, the range of decrease in the fundamental frequencies for this extreme ellipse is interesting, and it can be concluded that fiber angle has a strong influence on the decrease.

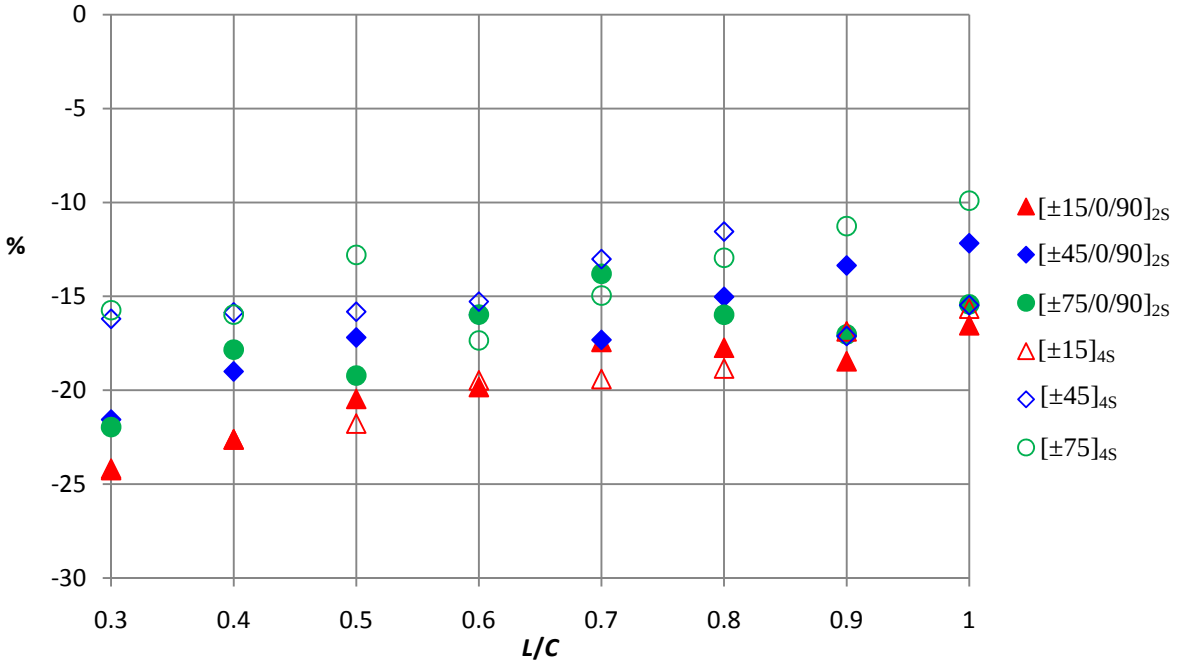

(a) with simple supports

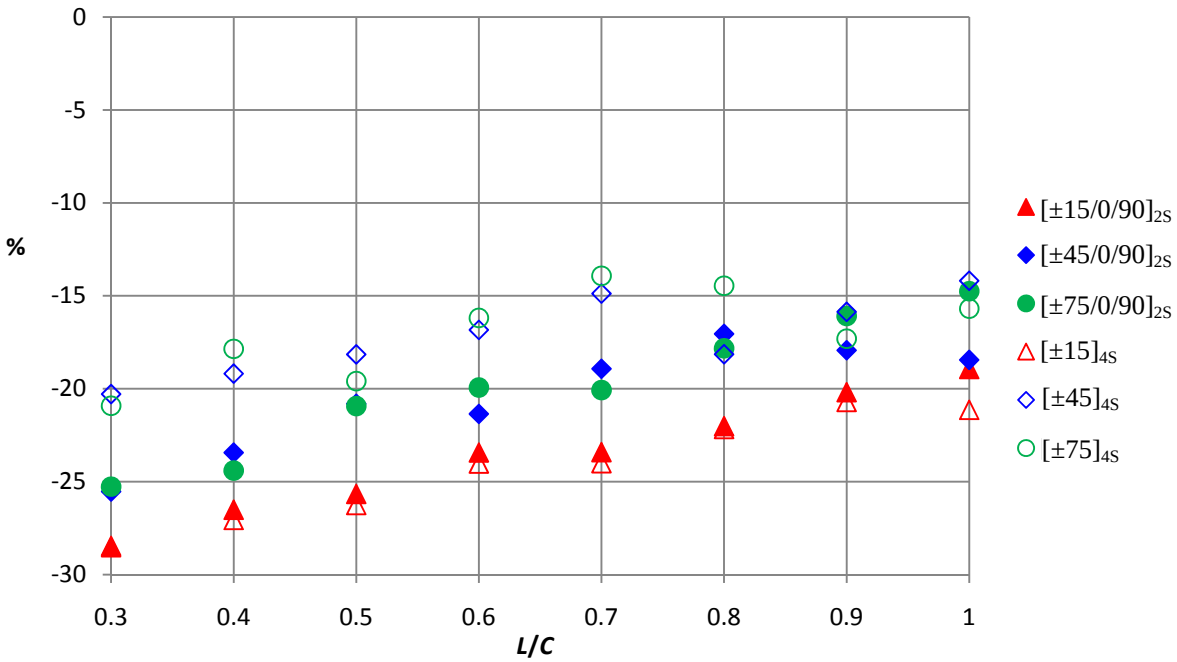

(b)with clamped supports

Fig. 4- 9 Percentage difference of cross-sectional effect for large cylinders upon their fundamental frequency

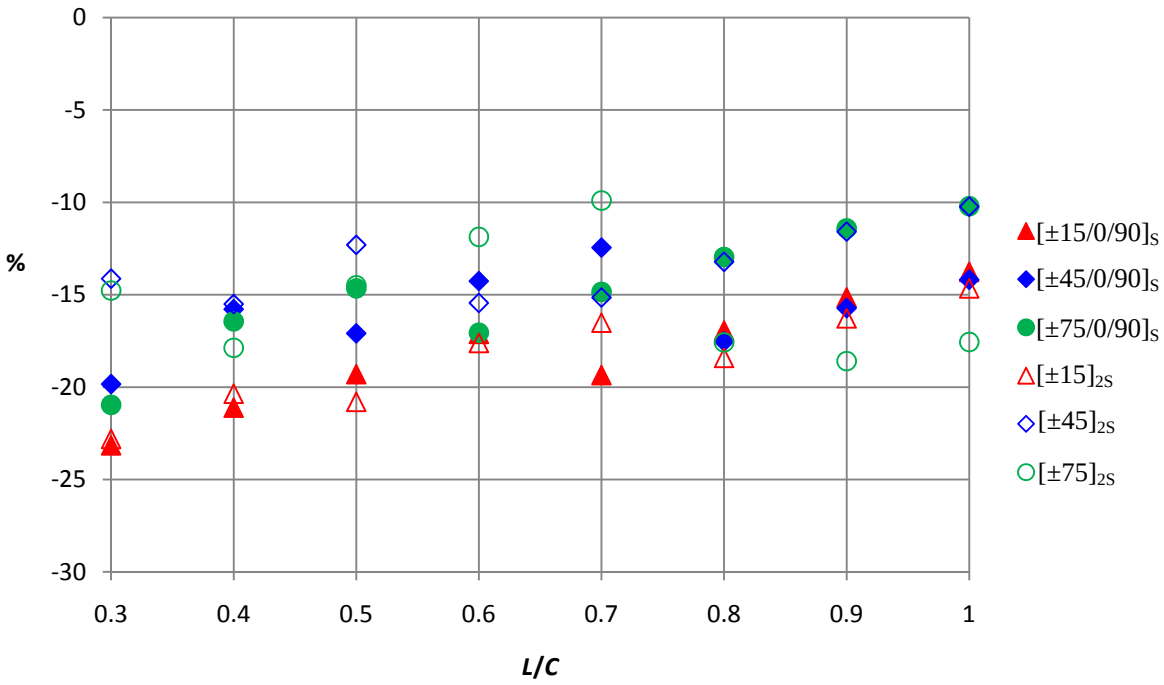

(a) with simple supports

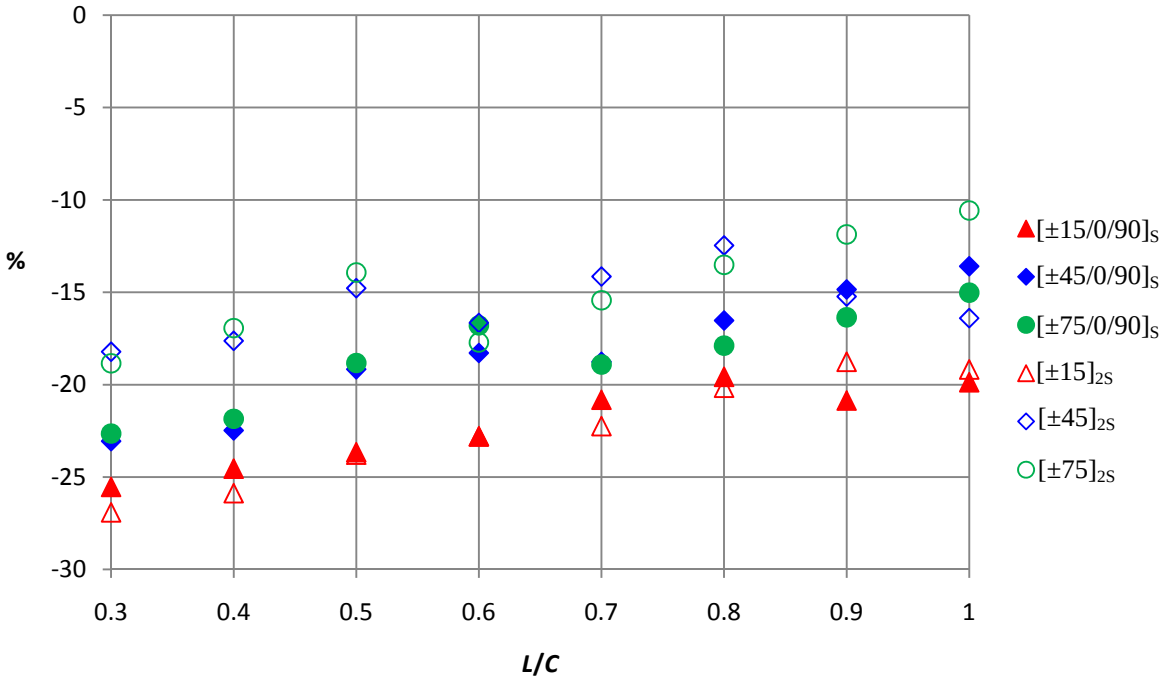

(b)with clamped supports

Fig. 4- 10 Percentage difference of cross-sectional effect for small cylinders upon their fundamental frequency

Differences between Cosine-Based and Sine-Based Calculations

As mentioned previously, the differences in the predictions of the sine-based calculations and the cosine-based calculations are illustrated in Figs. 4- 11 through 4- 14 in the same format as Figs. 4- 5 through 4- 8 except the vertical axes are now given by

$$\frac{(\omega_{cosine\ based} - \omega_{sine\ based})}{\omega_{cosine\ based}} \times 100\% \qquad \text{Eq. 4- 2}$$

A quick glance at Figs. 4- 11 through 4- 14 reveals that for 19 of the 24 cases considered (cylinder sizes large and small; boundary conditions simply-supported and clamped support; wall properties with two lamination sequences and three fiber angles), the difference in the fundamental frequency predicted by the cosine-based and sine-based formulations is less that 1% and for certain combinations of parameters, well less than 1%. For those cylinder sizes, boundary conditions, and wall laminates for which the difference is less than 1% for the entire range of L/C, e.g., all the cases in Figs. 4- 12a-f, the difference is essentially zero for short cylinders, slightly negative for intermediate length cylinders, and positive or negative for long cylinders. For those five cases for which the difference is greater that 1%, for some values of geometric and material parameters the difference is negative and in the range 6-8%. Interestingly, these cases all involve long cylinders and a lamination sequence involving a 75° fiber angle in four of the five cases and a 45° fiber angle in the other case. Specifically, these are the cases of Fig. 4- 11f (large simply supported cylinder with wall laminate $[\pm 75]_{4S}$), Fig. 4- 13c (small simply supported cylinder with wall laminate $[\pm 75/0/90]_{S}$), Fig. 4- 13e (small simply supported cylinder with wall laminate $[\pm 45]_{2S}$) , Fig. 4- 13f (small simply supported cylinder with wall laminate $[\pm 75]_{2S}$), and Fig. 4- 14f (small clamped support cylinder with wall laminate $[\pm 75]_{2S}$). Interestingly, these cases correspond to cases where the value of n is 2. To expand on this point: the deformation characteristics of the elliptical cross section for $n = 2$ are illustrated in Fig. 4- 15. The cosine- and sine-based deformations are illustrated in Fig. 4- 15a and Fig.4- 15b, respectively. Consider the change of normal displacement in the quarter of circumference from $s = 0$ to $s = C/4$ (top to right side). For the cosine-based cross section the normal displacement varies from a maximum to zero and then to a minimum, whereas for sine-based cross section the normal displacement varies from zero to a maximum and then to zero again. These different characteristics cause cosine- and sine-based values for S_{1n} for $n = 2$ in Eq. 3- 59 to be quite different, leading to the 6-8% difference in the predicted fundamental frequencies discussed above. However, as seen, the effect decreases with increasing the circumferential mode n.

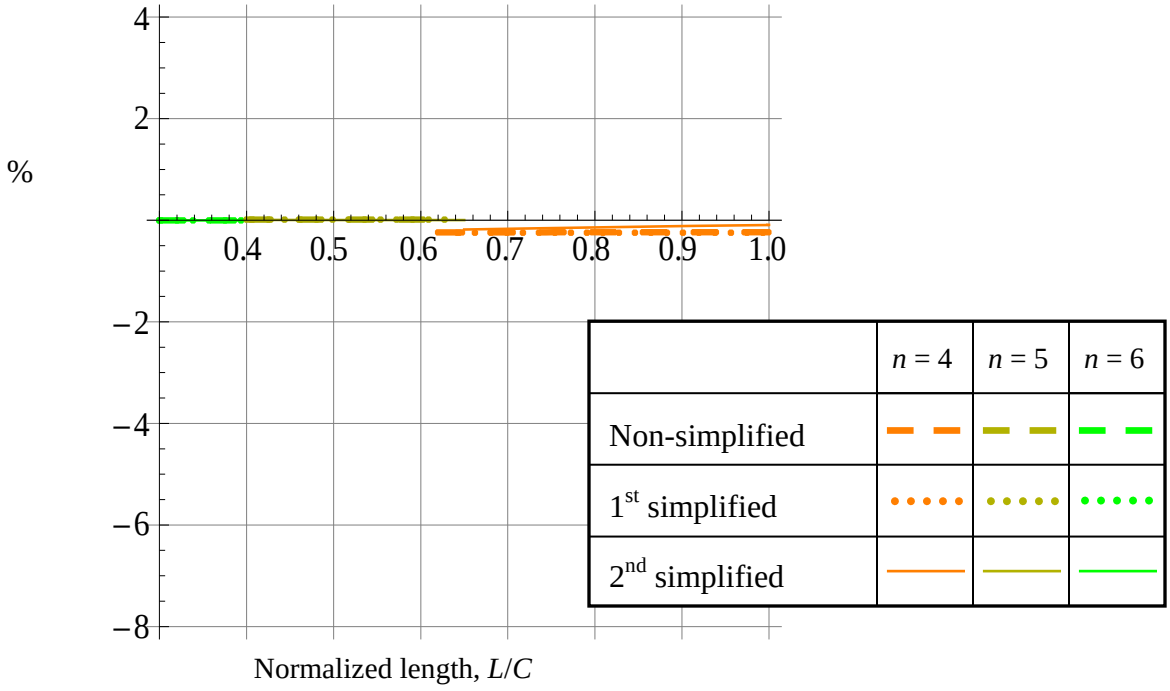

(a) Lamination sequences $[\pm 15/0/90]_{2S}$

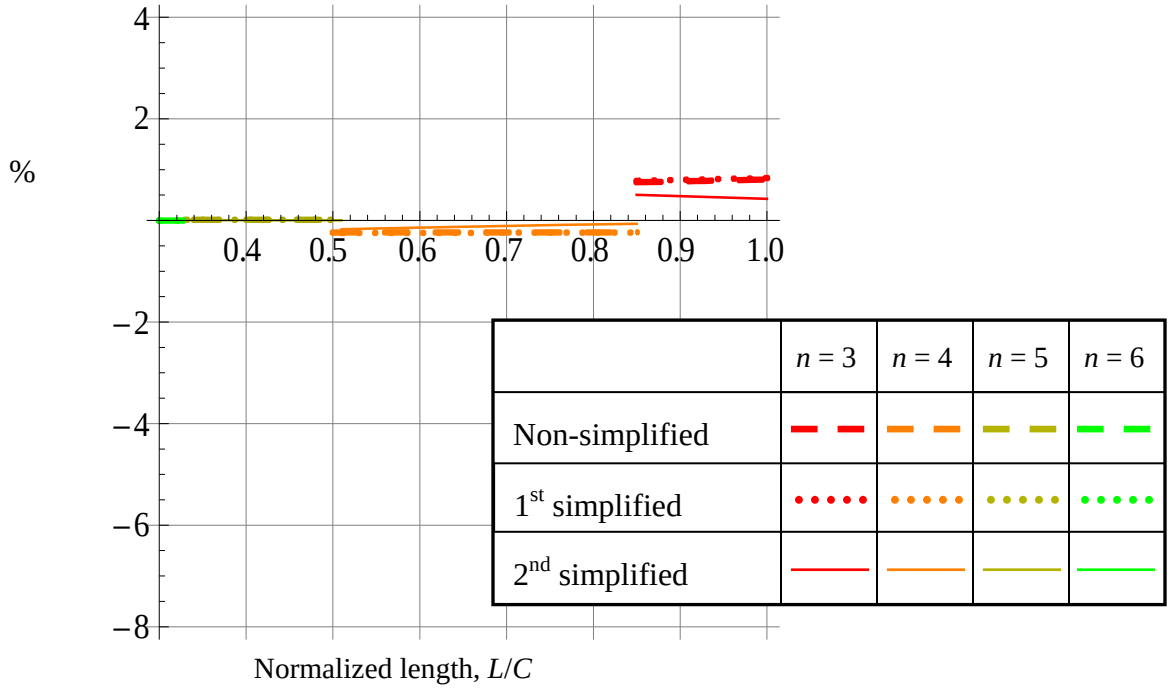

(b) Lamination sequences $[\pm 45/0/90]_{2S}$

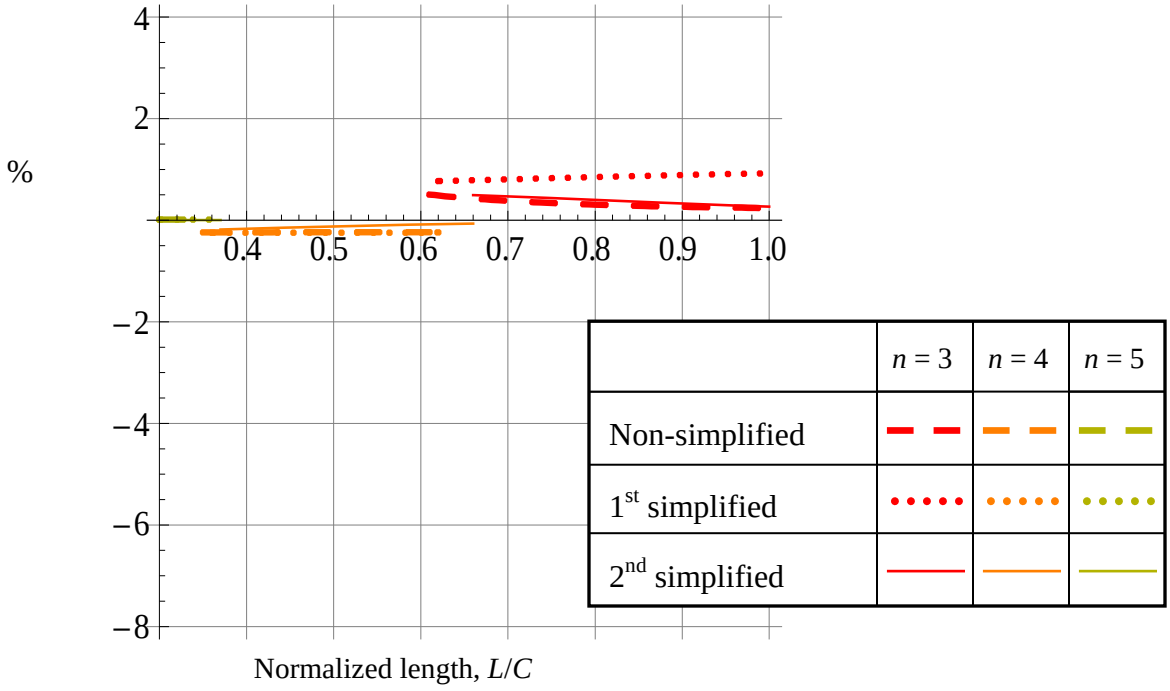

(c) Lamination sequences $[\pm 75/0/90]_{2S}$

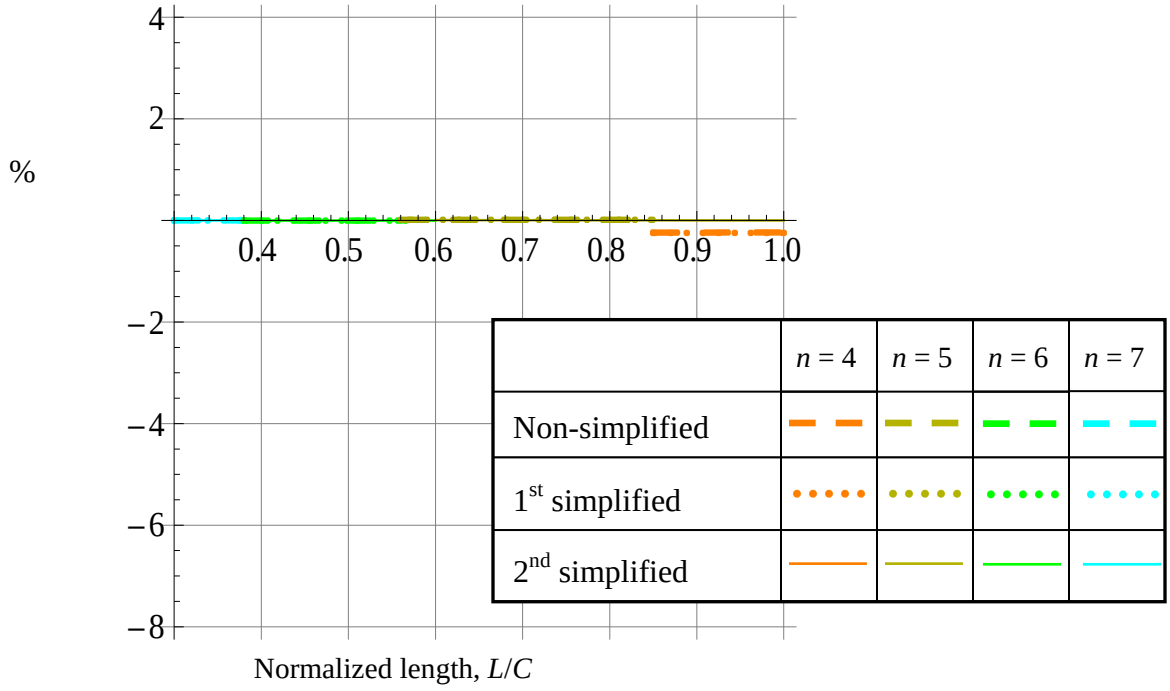

(d) Lamination sequences $[\pm 15]_{4S}$

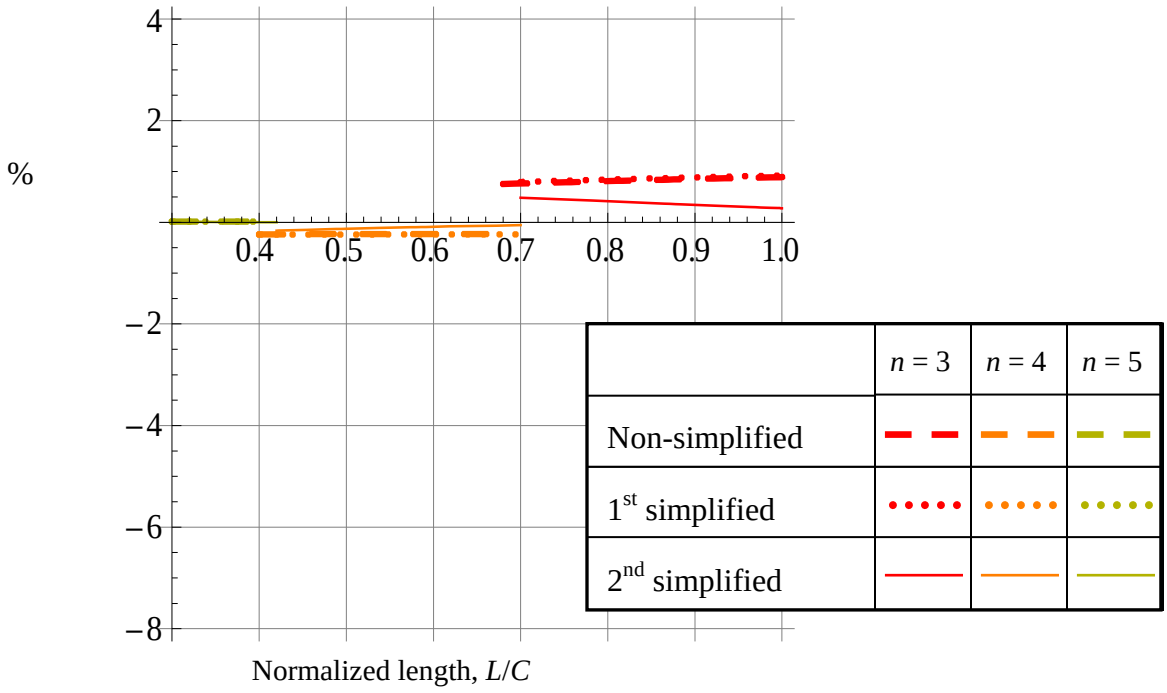

(e) Lamination sequences $[\pm 45]_{4S}$

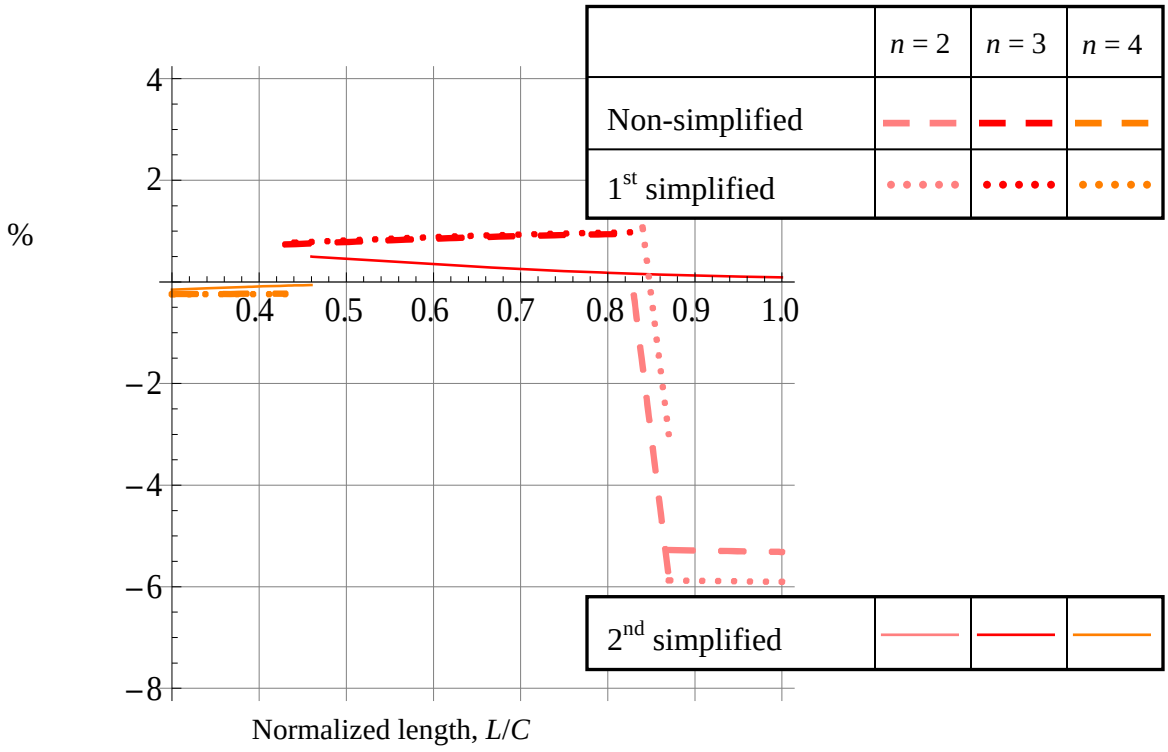

(f) Lamination sequences $[\pm 75]_{4S}$

Fig. 4- 11 Percentage difference between cosine- and sine-based large elliptical cylinders (b/a = 0.55, e = 0.84) with simple supports

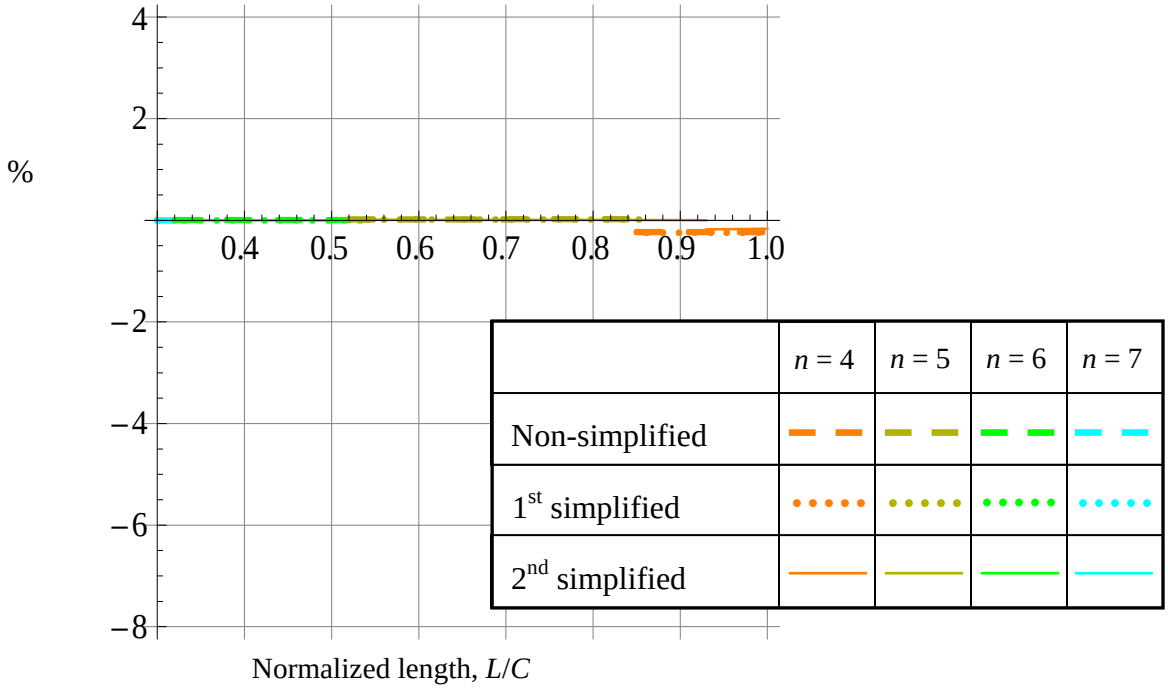

(a) Lamination sequences $[\pm 15/0/90]_{2S}$

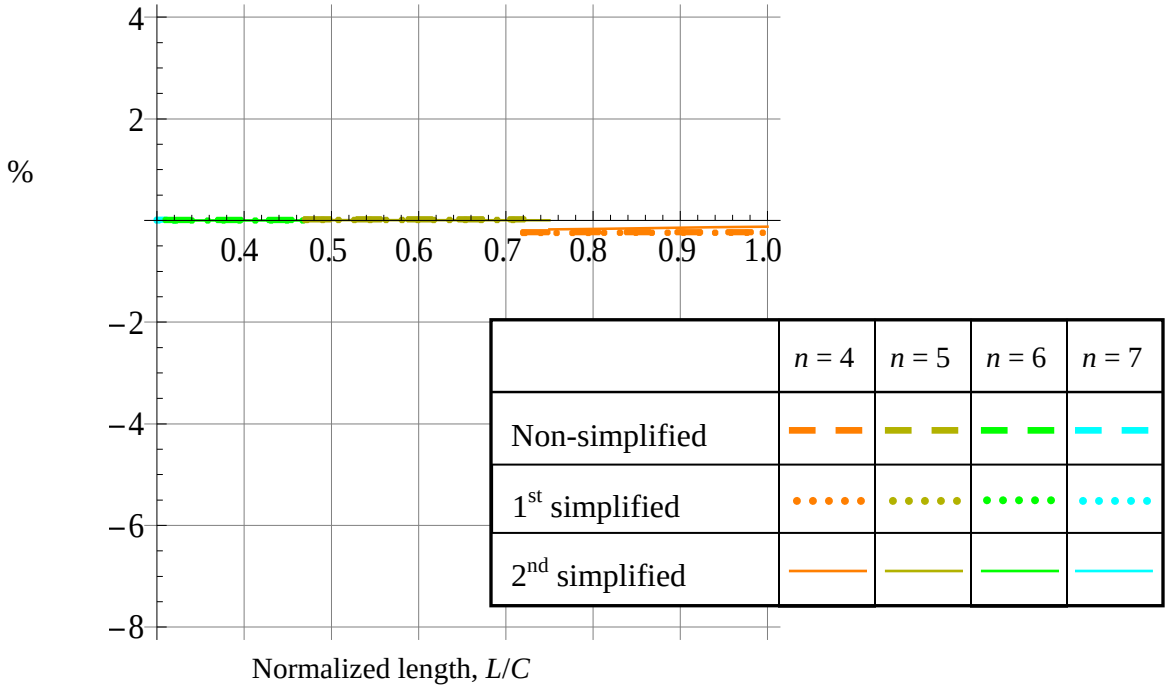

(b) Lamination sequences $[\pm 45/0/90]_{2S}$

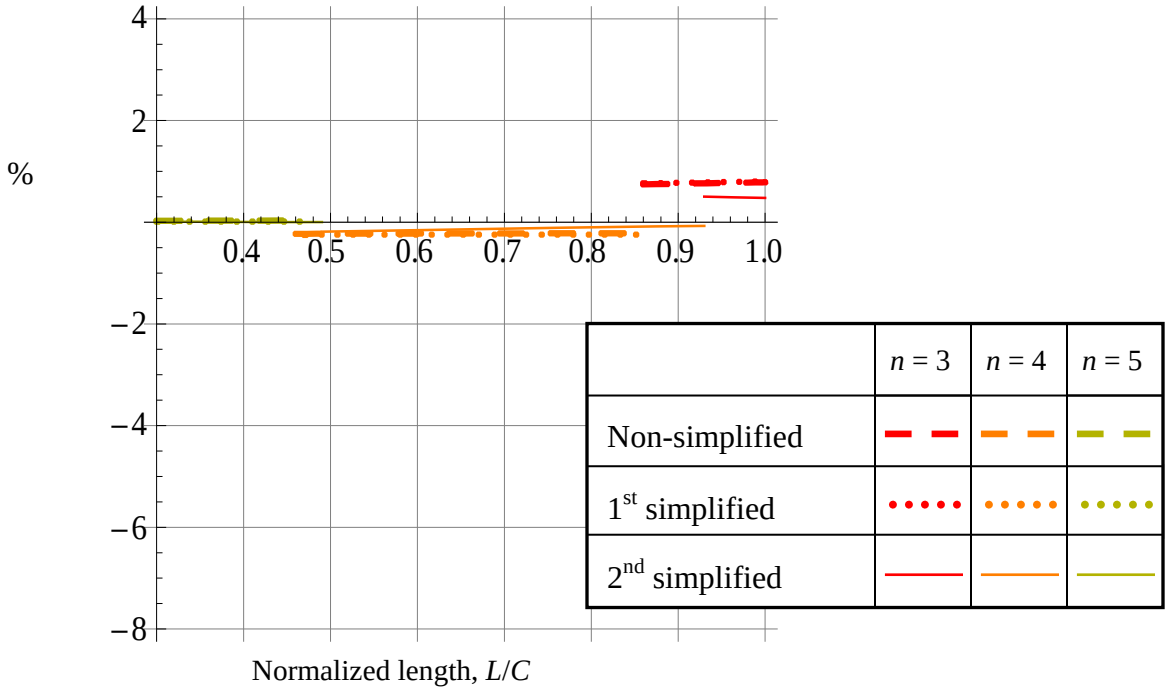

(c) Lamination sequences $[\pm 75/0/90]_{2S}$

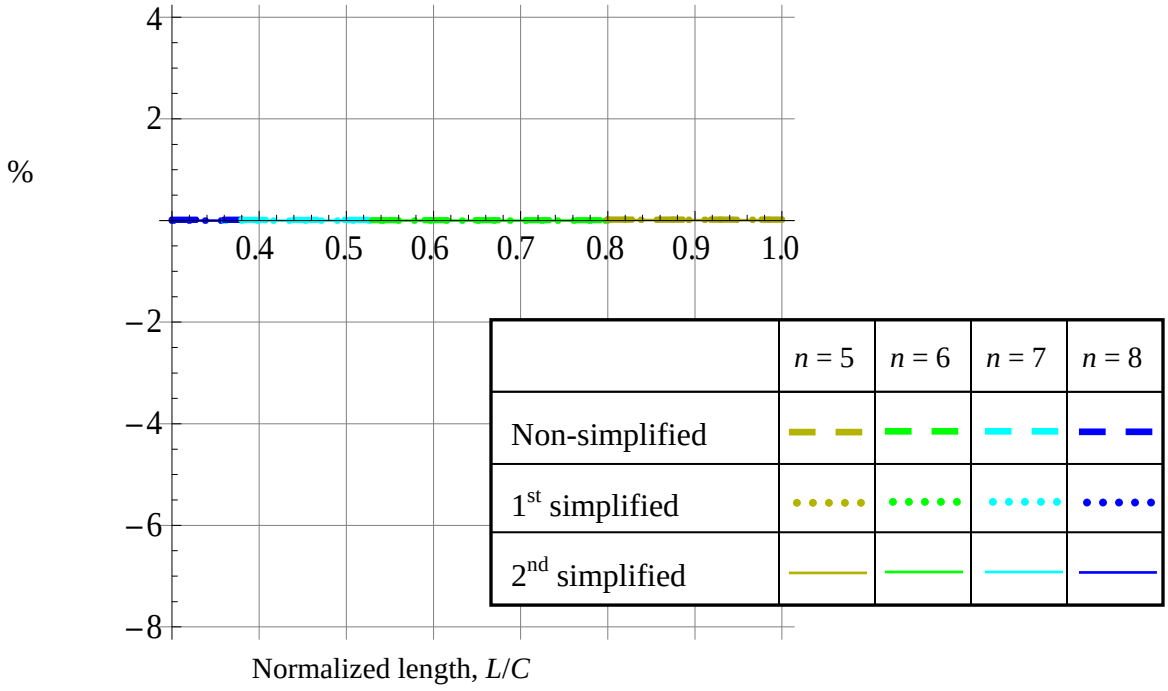

(d) Lamination sequences $[\pm 15]_{4S}$

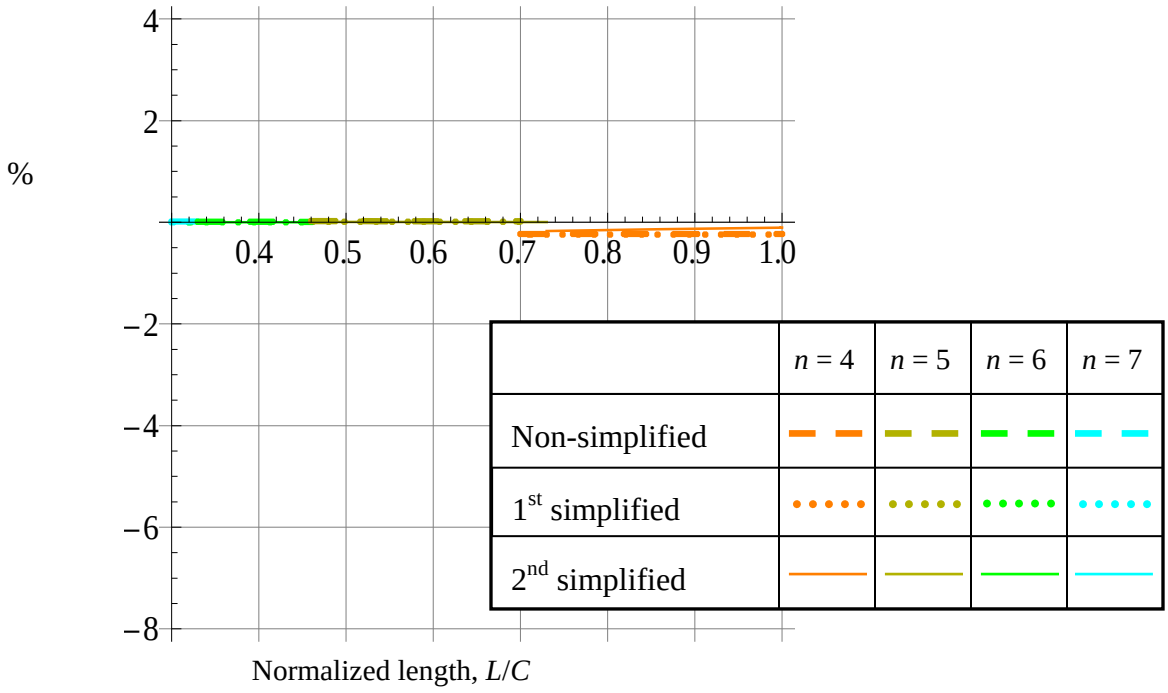

(e) Lamination sequences $[\pm 45]_{4S}$

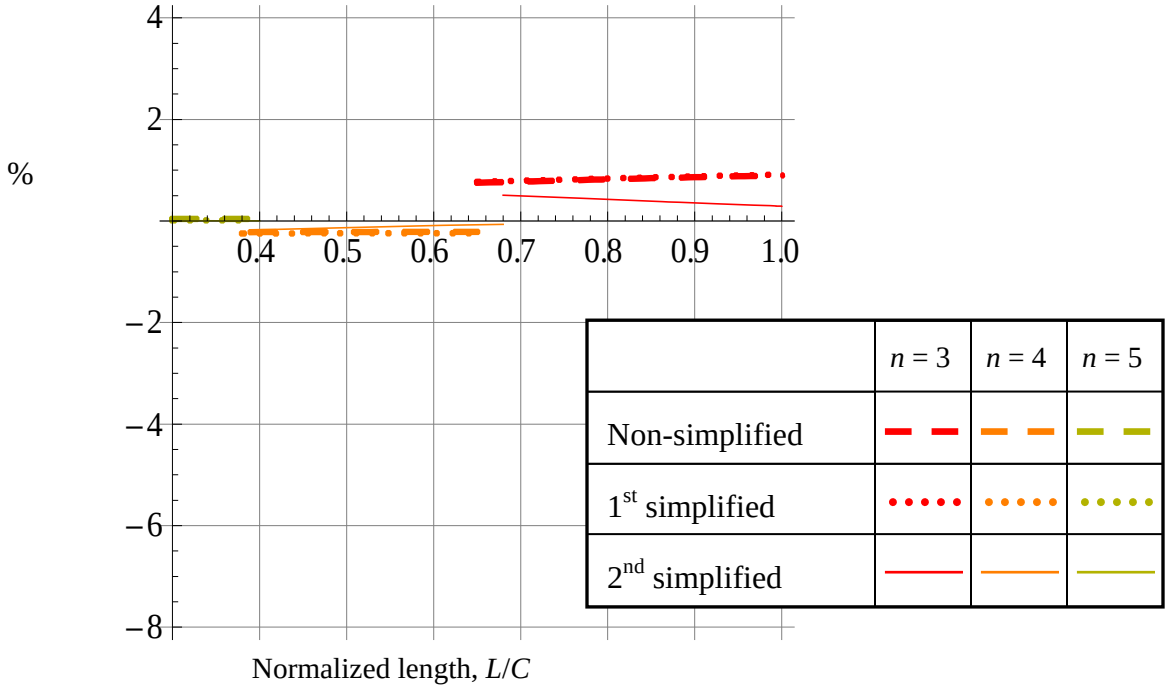

(f) Lamination sequences $[\pm 75]_{4S}$

Fig. 4- 12 Percentage difference between cosine- and sine-based large elliptical cylinders (b/a = 0.55, e = 0.84) with clamped supports

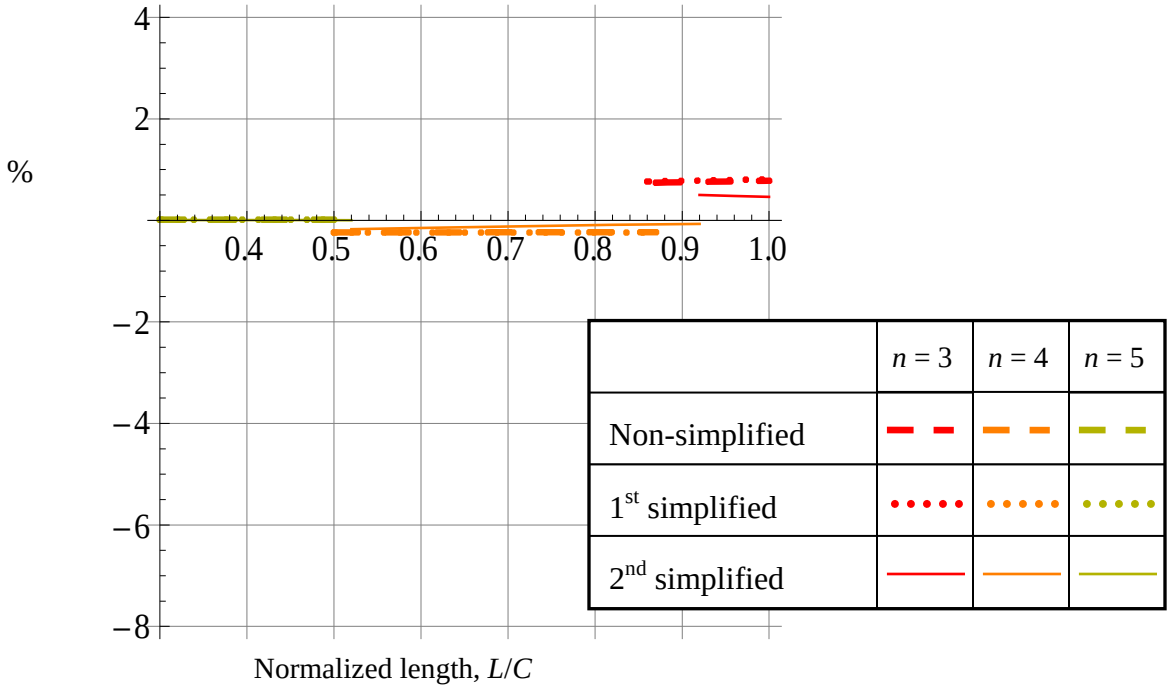

(a) Lamination sequences $[\pm 15/0/90]_S$

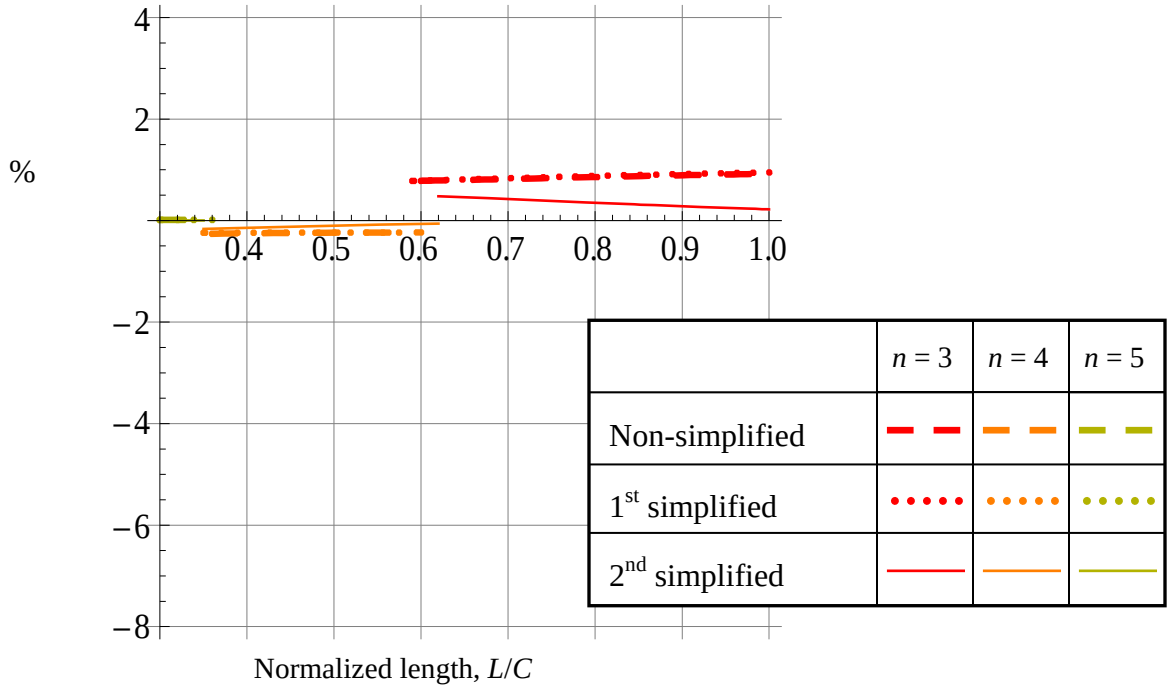

(b) Lamination sequences $[\pm 45/0/90]_S$

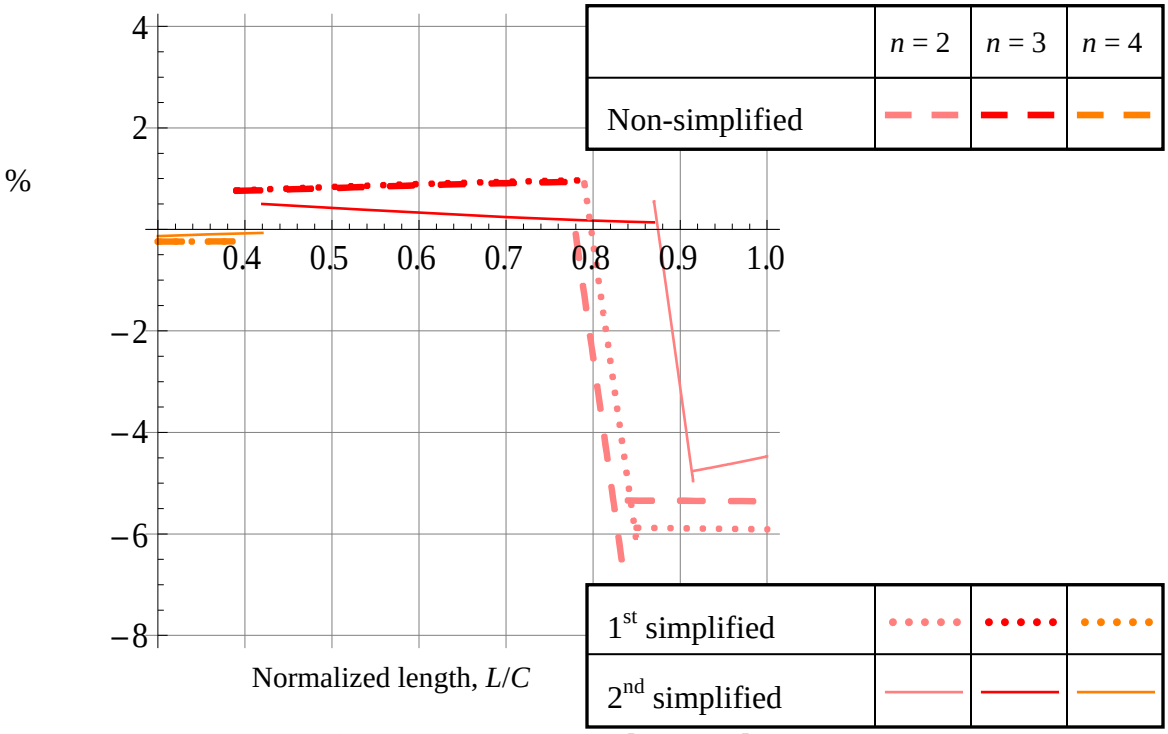

(c) Lamination sequences $[\pm 75/0/90]_S$

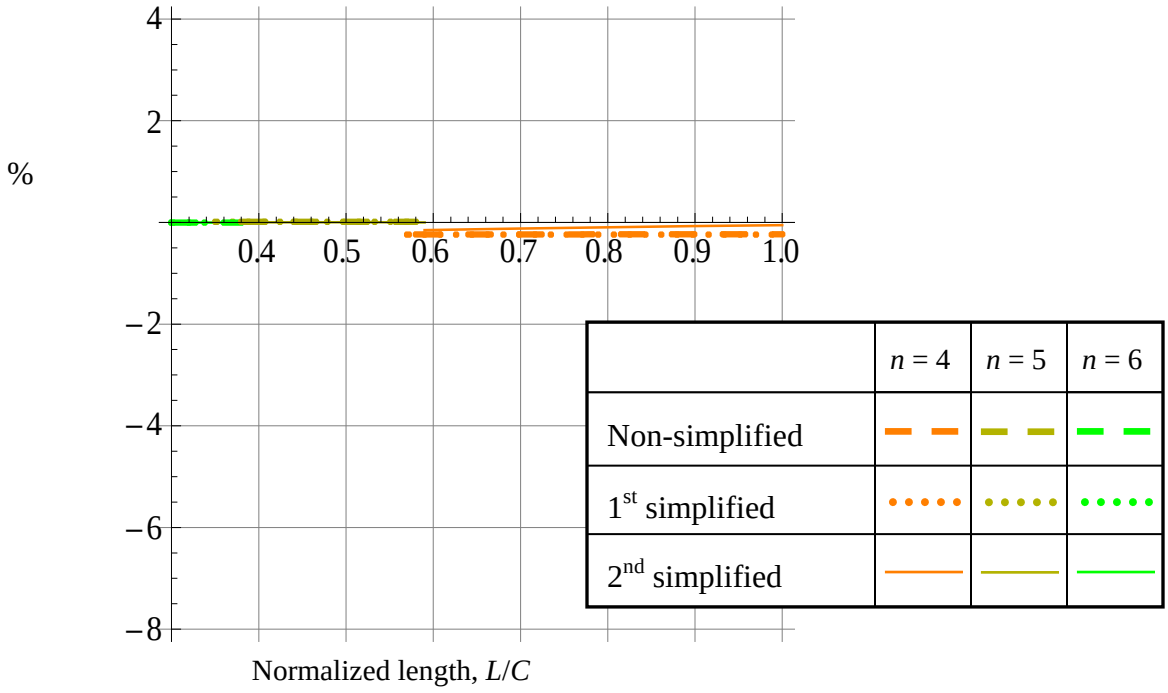

(d) Lamination sequences $[\pm 15]_{2S}$

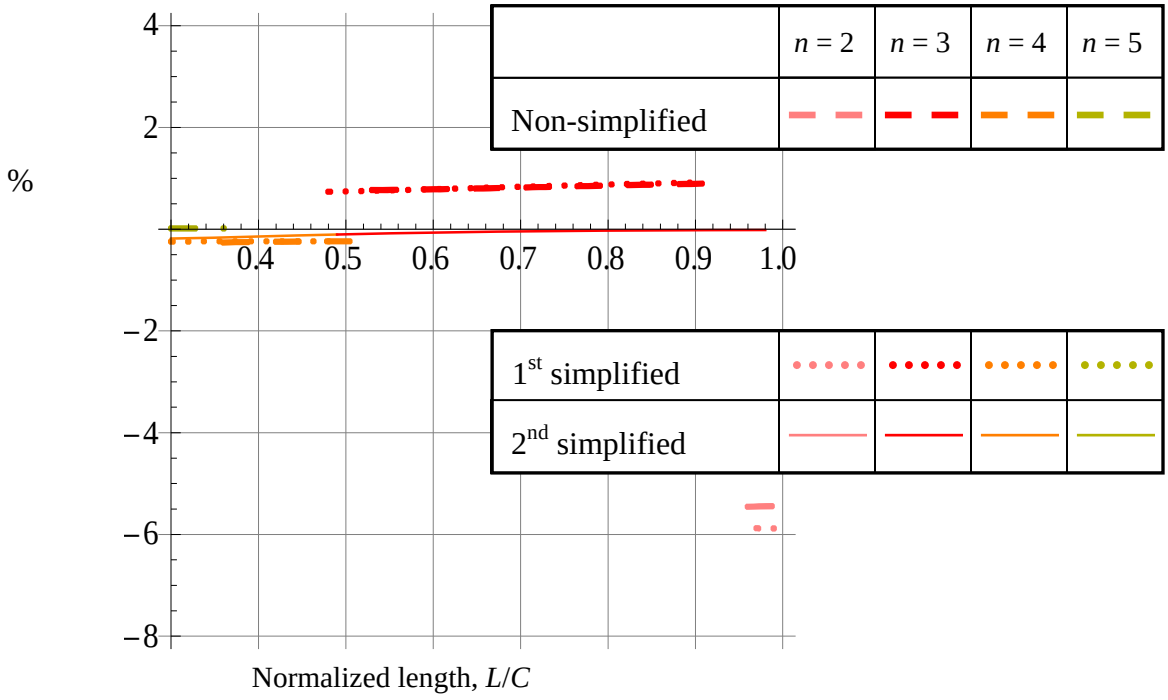

(e) Lamination sequences $[\pm 45]_{2S}$

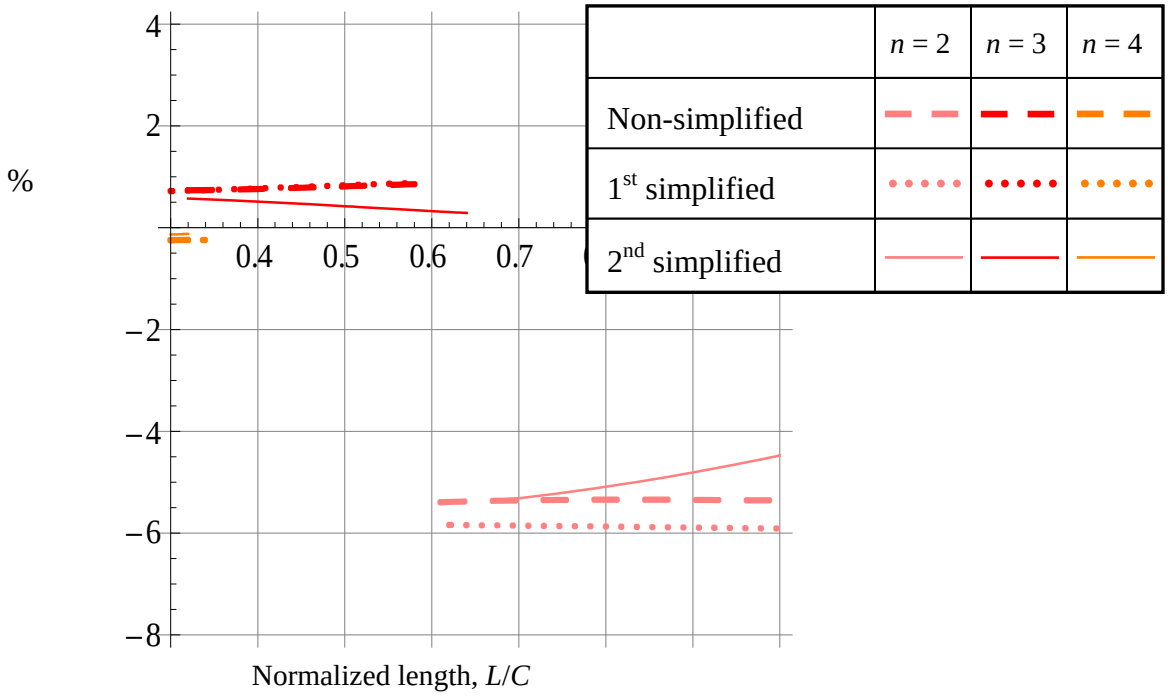

(f) Lamination sequences $[\pm 75]_{2S}$

Fig. 4- 13 Percentage difference between cosine- and sine-based small elliptical cylinders (b/a = 0.55, e = 0.84) with simple supports

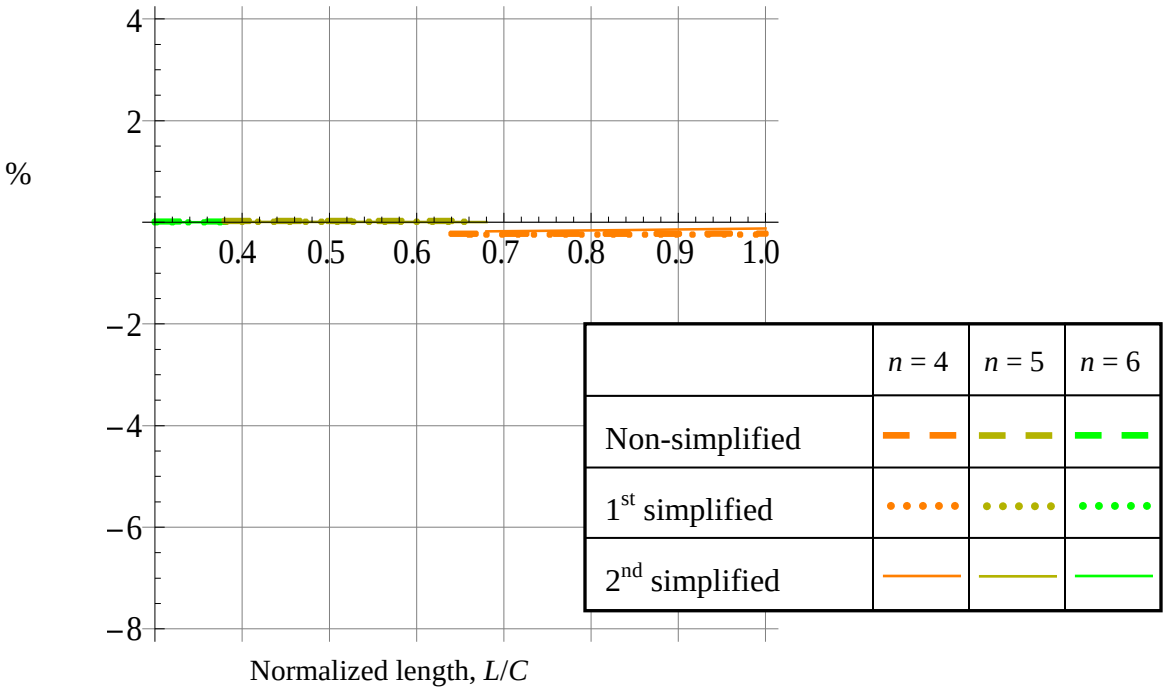

(a) Lamination sequences $[\pm 15/0/90]_S$

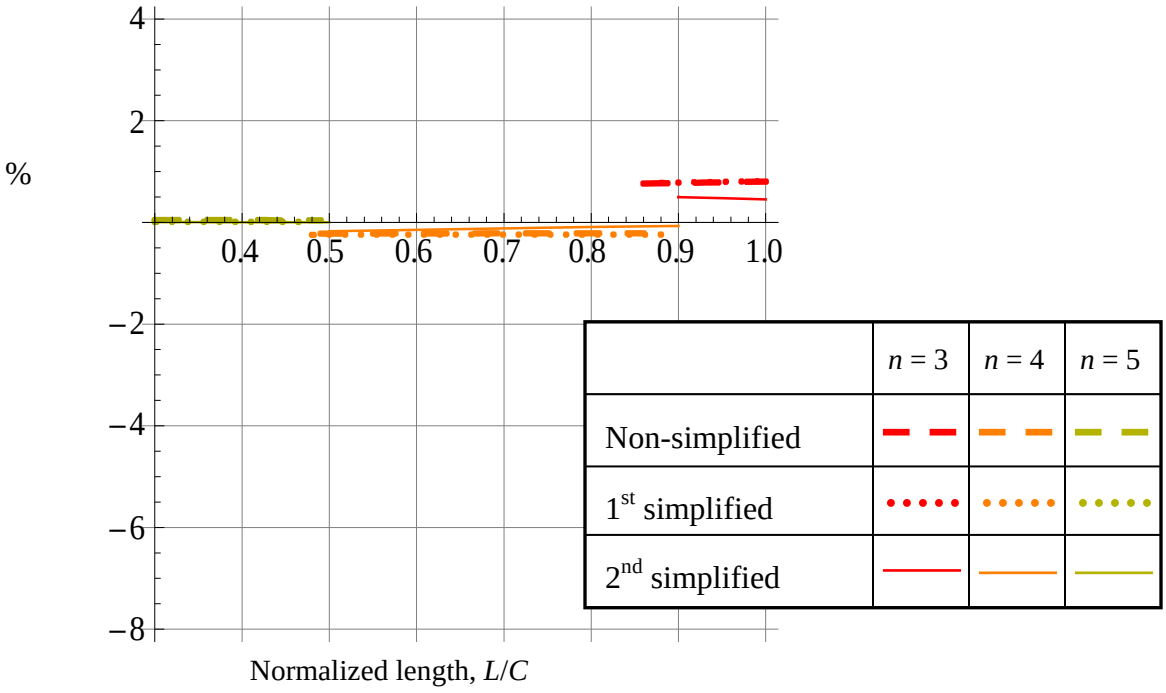

(b) Lamination sequences $[\pm 45/0/90]_S$

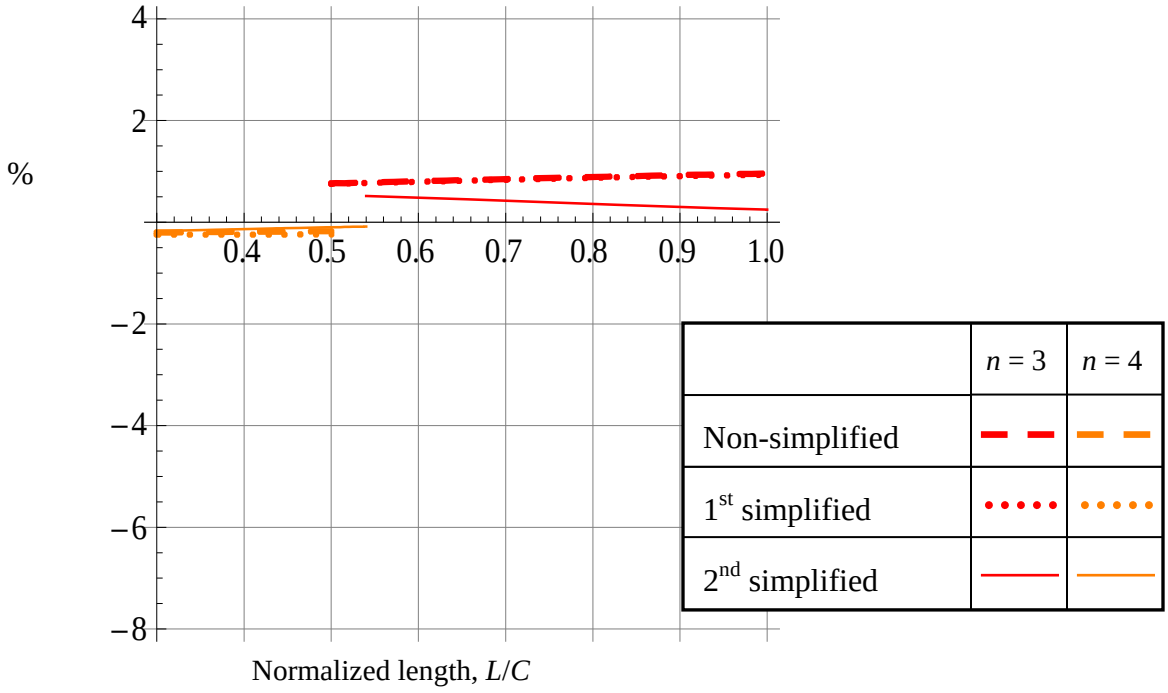

(c) Lamination sequences $[\pm 75/0/90]_S$

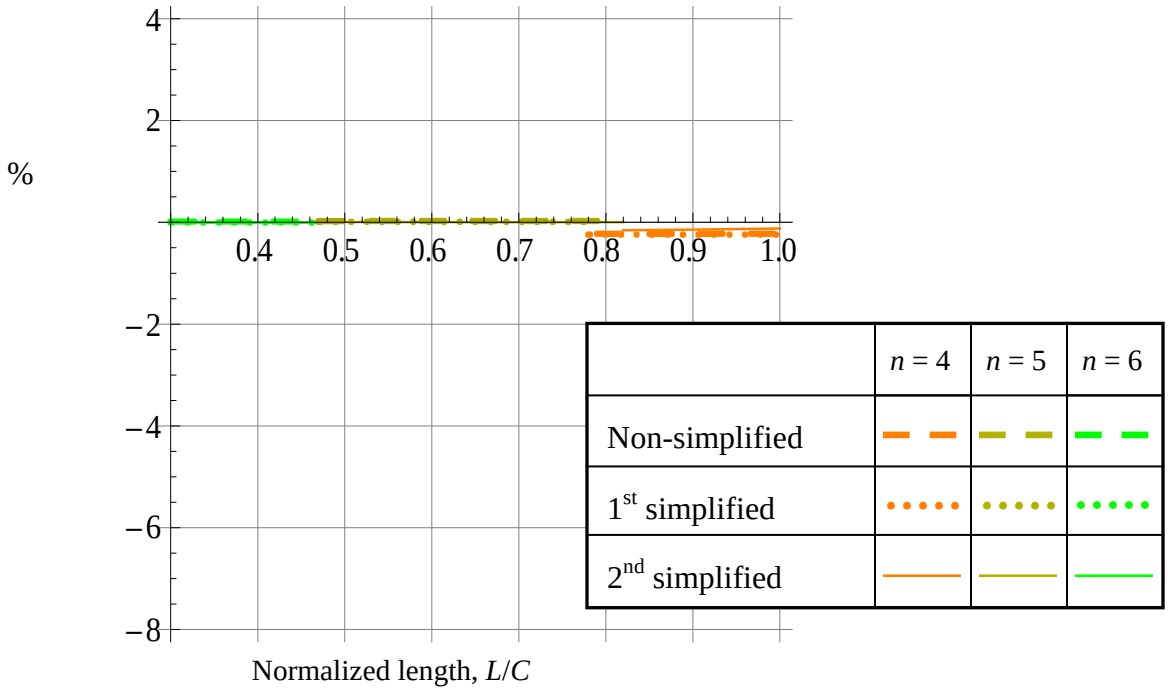

(d) Lamination sequences $[\pm 15]_{2S}$

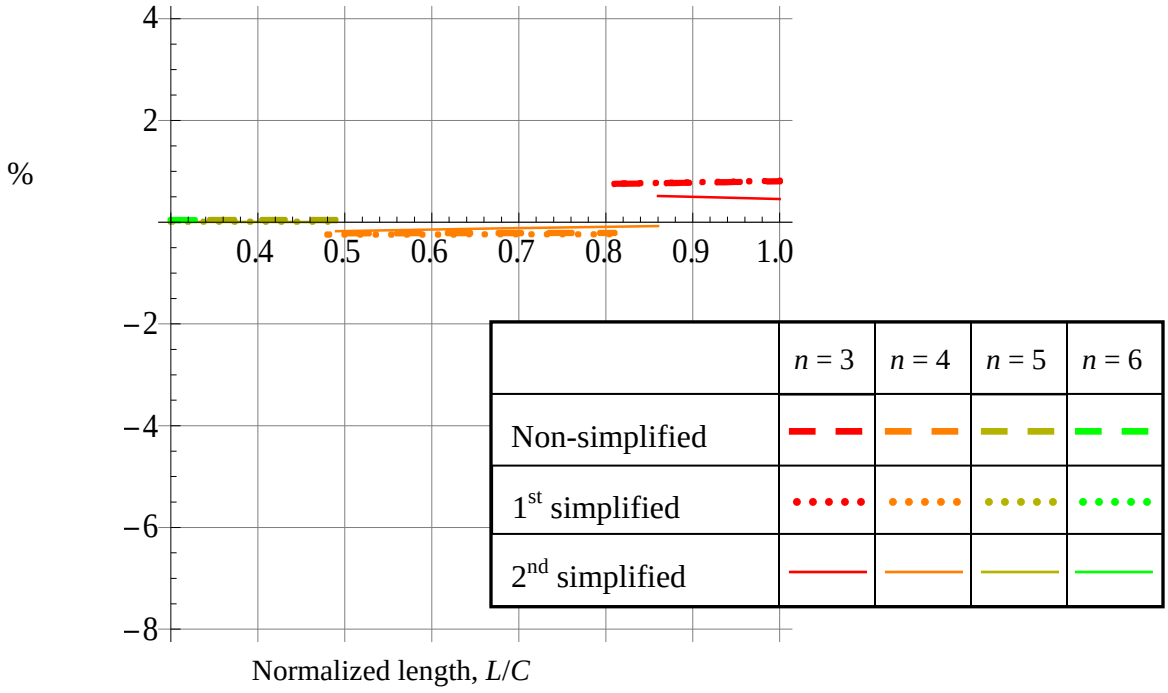

(e) Lamination sequences $[\pm 45]_{2S}$

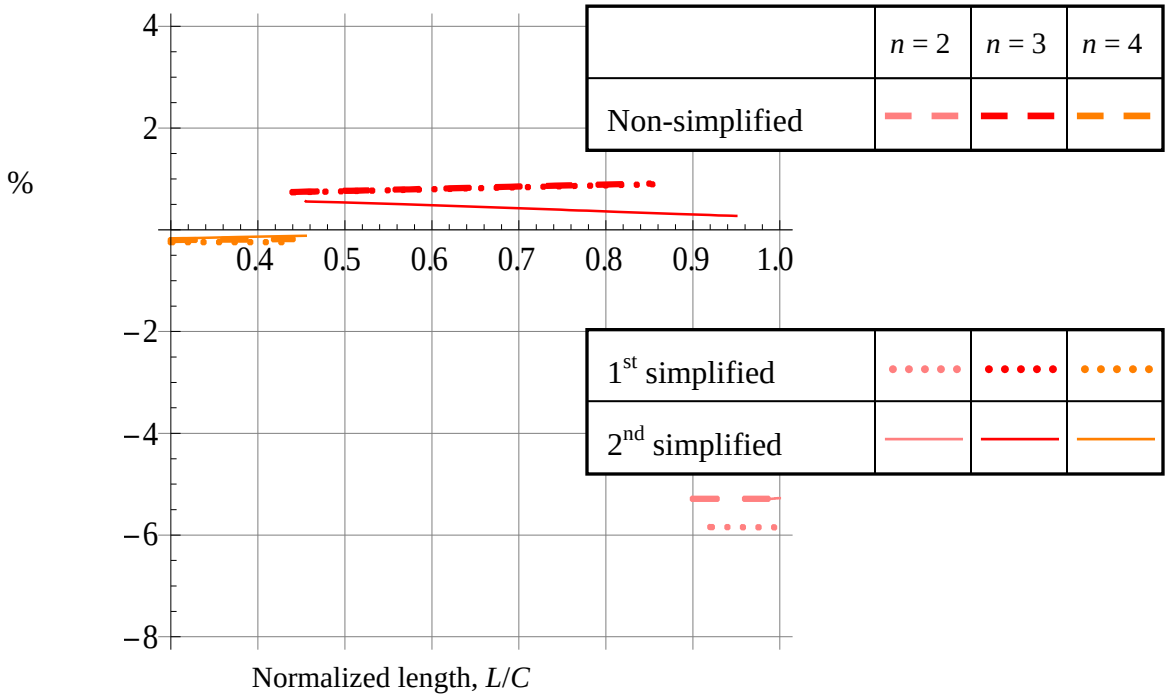

(f) Lamination sequences $[\pm 75]_{2S}$

Fig. 4-14 Percentage difference between cosine- and sine-based small elliptical cylinders (b/a = 0.55, e = 0.84) with clamped supports

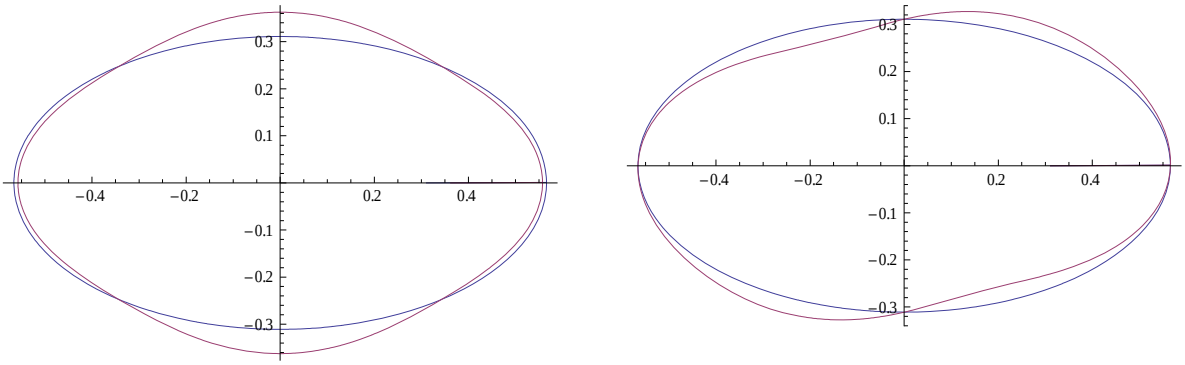

(a) Cosine-based (b) Sine-based

Fig. 4- 15 Elliptical cross-sectional shape for $n = 2$, $b/a = 0.55$ ($e = 0.84$)

In summary, by combining the findings Fig 4- 5 through 4- 10 with the findings of Figs. 4- 11 through 4- 14 it can be stated that either a cosine-based or a sine-based formulation can be used with reasonable accuracy for determining the characteristics of the fundamental frequency of elliptical cylinders. In particular, using Lo's approximation, which is equally as valid for the sine-based formulation as for the cosine-based formulation, would be a very convenient tool for conducting parameter studies regarding cylinder geometry and wall laminate properties. Though it has not been shown explicitly, the developed formulation works well for aspect ratios between 1.00 and 0.55, circular cylinders and the most extreme ellipse studied here, respectively. The fundamental frequencies for the sine-based calculations are provided in Appendix B.

4.3 Results for Other Aspect Ratios and Fiber Angles

As the developed formulation has been shown to be reasonable accurate when compared to calculations from the finite-element model, it is of value to use the formulation to explore the characteristics of the fundamental frequency as a function of other fiber angles and other cross sectional aspect ratios. To that end, the figures to follow explore a range of values for both of these parameters. As the case of $L/C = 1$ represents a cylinder that could be considered impractically long, the values of L/C considered are 0.3, 0.5, and 0.7. For the case of circular cylinders the values of L/D would be approximately 1, 1.5, and 2. For this study of the effects of fiber angles and cross-sectional geometry using the developed formulation, the frequencies are

normalized by the fundamental frequencies of the two baseline cylinders as computed by the developed formulation. The normalizing frequencies are listed in Table 4- 7.

Table 4.7 Data for baseline cylinders

	Large cylinder	Small cylinder
$R_0=a=b$, m (D_0, m) [C, m]	0.448 (0.896) [2.81]	0.1120 (0.224) [0.704]
L, m	1.407	0.352
Lamination sequences	$[\pm 45/0/90]_{2S}$	$[\pm 45/0/90]_{S}$
Boundary conditions	Simple supports	Simple supports
Fundamental frequency, ω_0 (rad/s)	655	3690

Based on Lo's approximate equation, in Fig. 4- 16 the normalized fundamental frequencies of the large simply supported cylinders for different aspect ratios, b/a, and different normalized lengths, L/C, are shown. From Table 4- 7 the normalization factor is 655 rad/s. The horizontal axis is the fiber orientation ϑ. In Fig. 4-16a the lamination sequence is $[\pm\vartheta/0/90]_{2S}$ whereas in Fig. 4- 16b the lamination sequence is $[\pm\vartheta]_{4S}$. The results show that the fundamental frequencies change somewhat more while varying ϑ in just eight layers of the $[\pm\vartheta/0/90]_{2S}$ laminate rather than in all sixteen layers in the $[\pm\vartheta]_{4S}$ laminate. In either case the fundamental frequency is not significantly sensitive to the fiber angle. That will be discussed more shortly. For the $[\pm\vartheta/0/90]_{2S}$ laminate the highest fundamental frequencies occur for fiber angle ϑ in the range 45-90°, depending on the value of other parameters. As was seen earlier, the fundamental frequency decreases with decreasing aspect ratio. As expected, the decrease for aspect ratio 0.55 relative to the circular case is greatest of the three noncircular cross sections studied and was quantified earlier. The baseline case for the large cylinders is indicated with a solid symbol in Figs. 4- 16a-b

at $\vartheta = 45°$, $\omega/\omega_0 = 1$. For the $[\pm\vartheta]_{4S}$ laminate it is difficult to conclude from the figures which angle or range of angles leads to the highest fundamental frequency.

In Fig. 4- 17 the normalized fundamental frequencies of the large clamped support cylinders are illustrated. In general, for lamination sequence $[\pm\vartheta/0/90]_{2S}$ the highest fundamental frequencies again occur for cylinders with ϑ in the range 50-75°, while for lamination sequence $[\pm\vartheta]_{4S}$ the highest fundamental frequencies occur in the range $\vartheta = 45\text{-}50°$. For these clamped cylinders the fundamental frequency changes more with ϑ for the $[\pm\vartheta]_{4S}$ laminates than for the $[\pm\vartheta/0/90]_{2S}$ laminates.

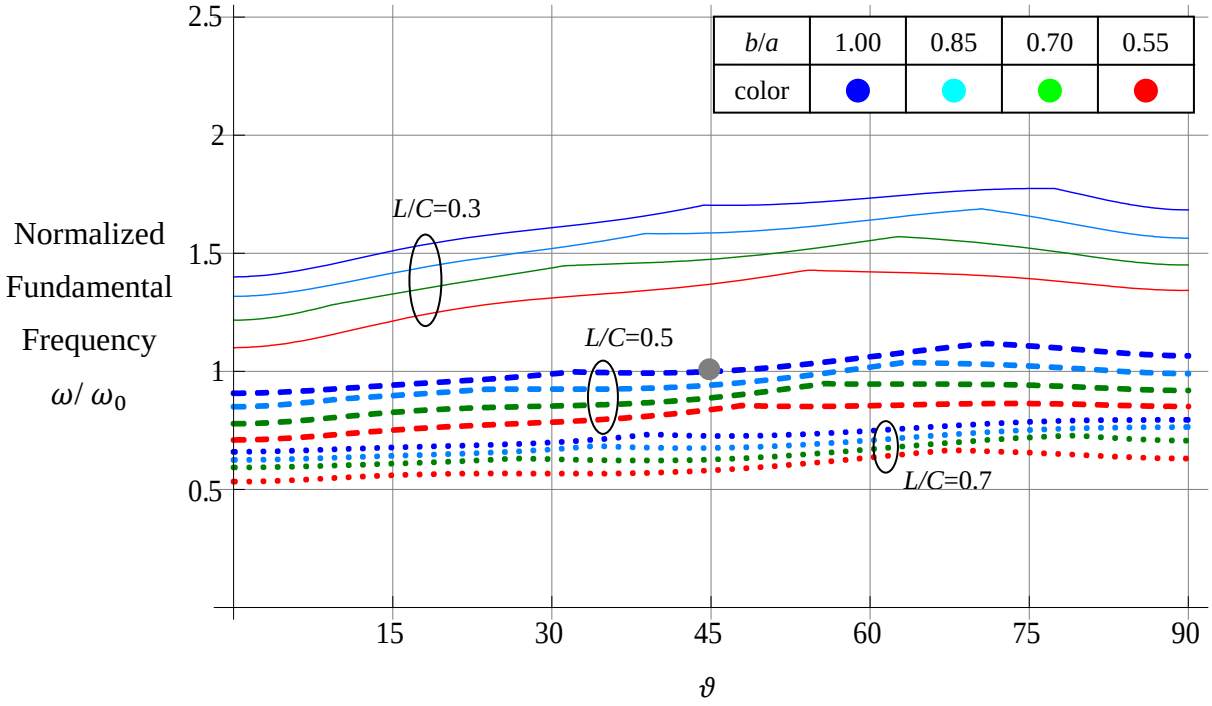

(a) Lamination sequences $[\pm\vartheta/0/90]_{2S}$

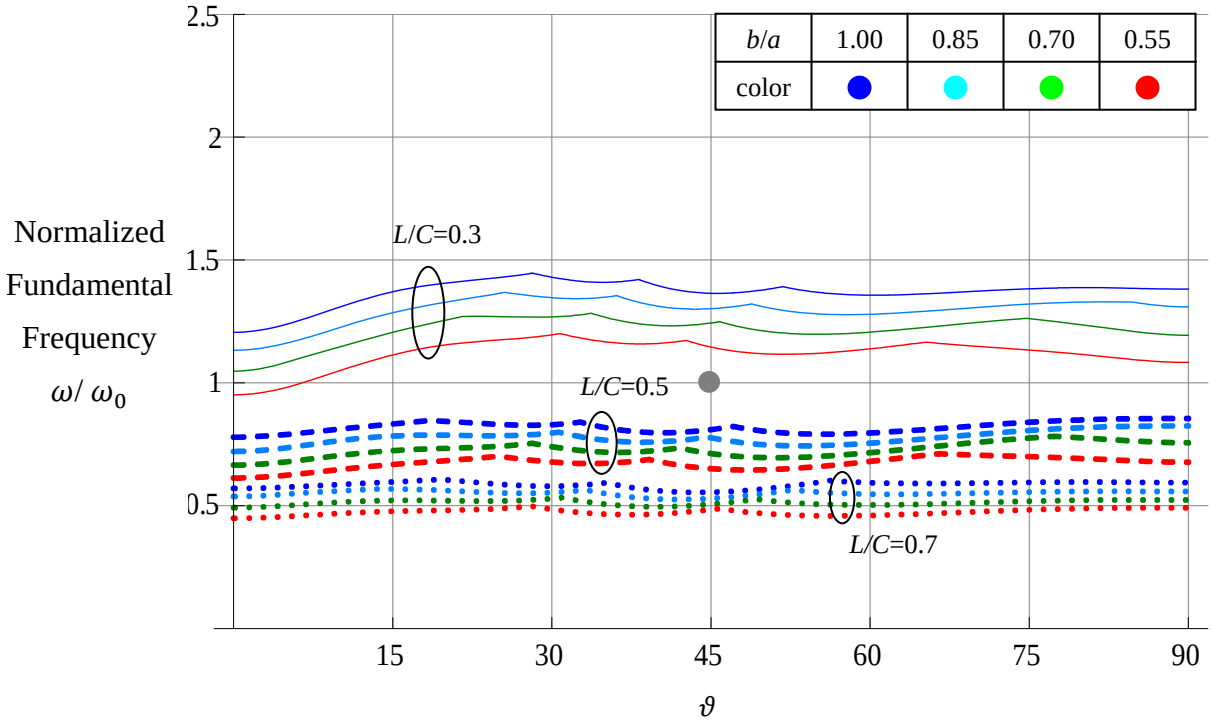

(b) Lamination sequences $[\pm\vartheta]_{4S}$

Fig. 4- 16 Normalized fundamental frequency of large elliptical cylinders, simple supports

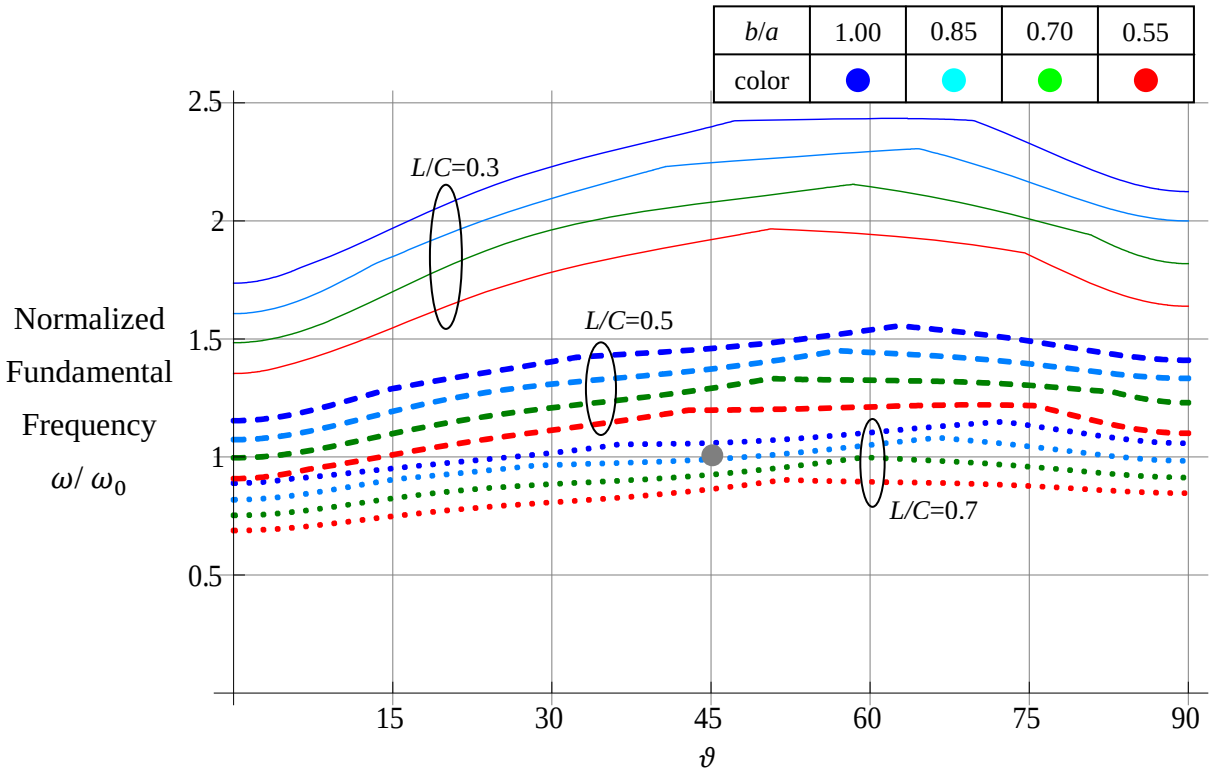

(a) Lamination sequences $[\pm\vartheta/0/90]_{2S}$

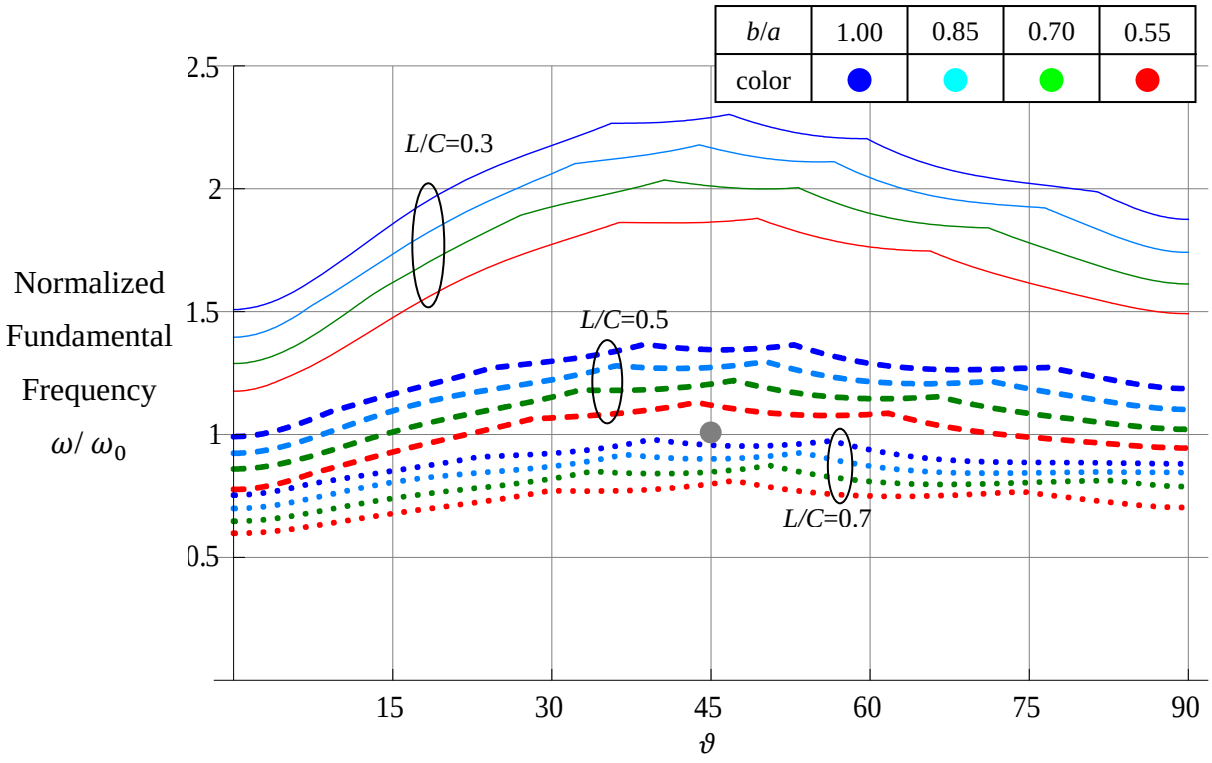

(b) Lamination sequences $[\pm\vartheta]_{4S}$

Fig. 4- 17 Normalized fundamental frequency of large elliptical cylinders, clamped supports

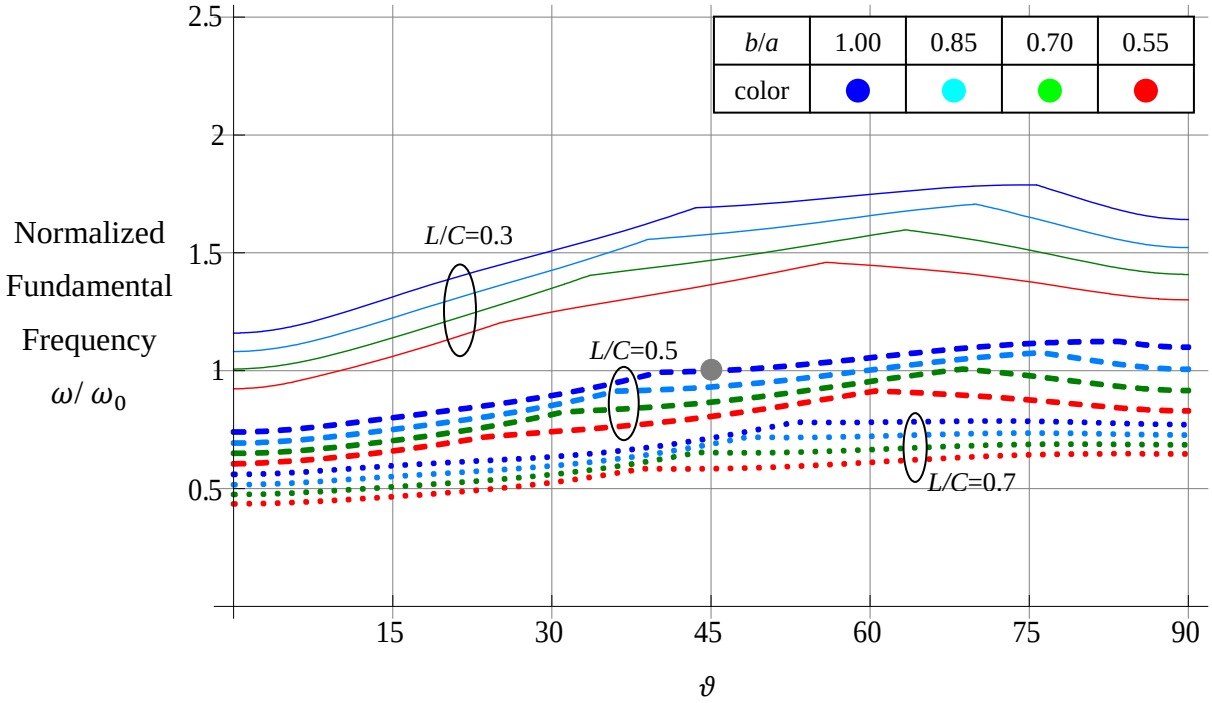

(a) Lamination sequences $[\pm\vartheta/0/90]_S$

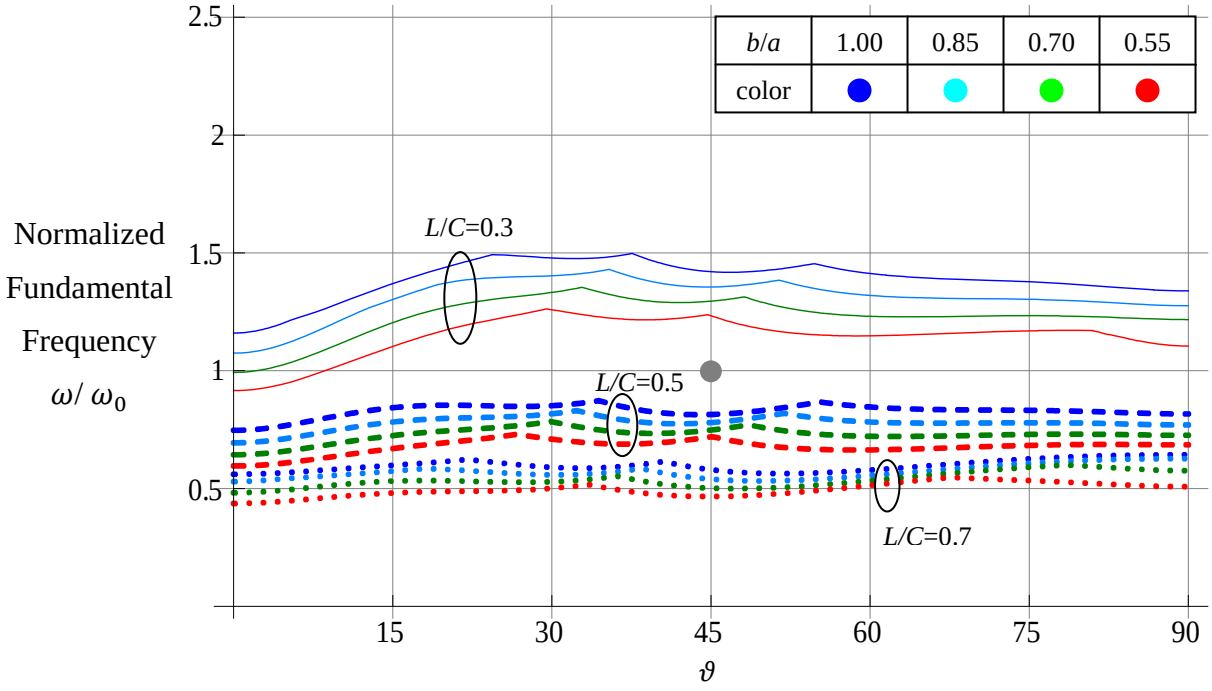

(b) Lamination sequences $[\pm\vartheta]_{2S}$

Fig. 4- 18 Normalized fundamental frequency of small elliptical cylinder, simple supports

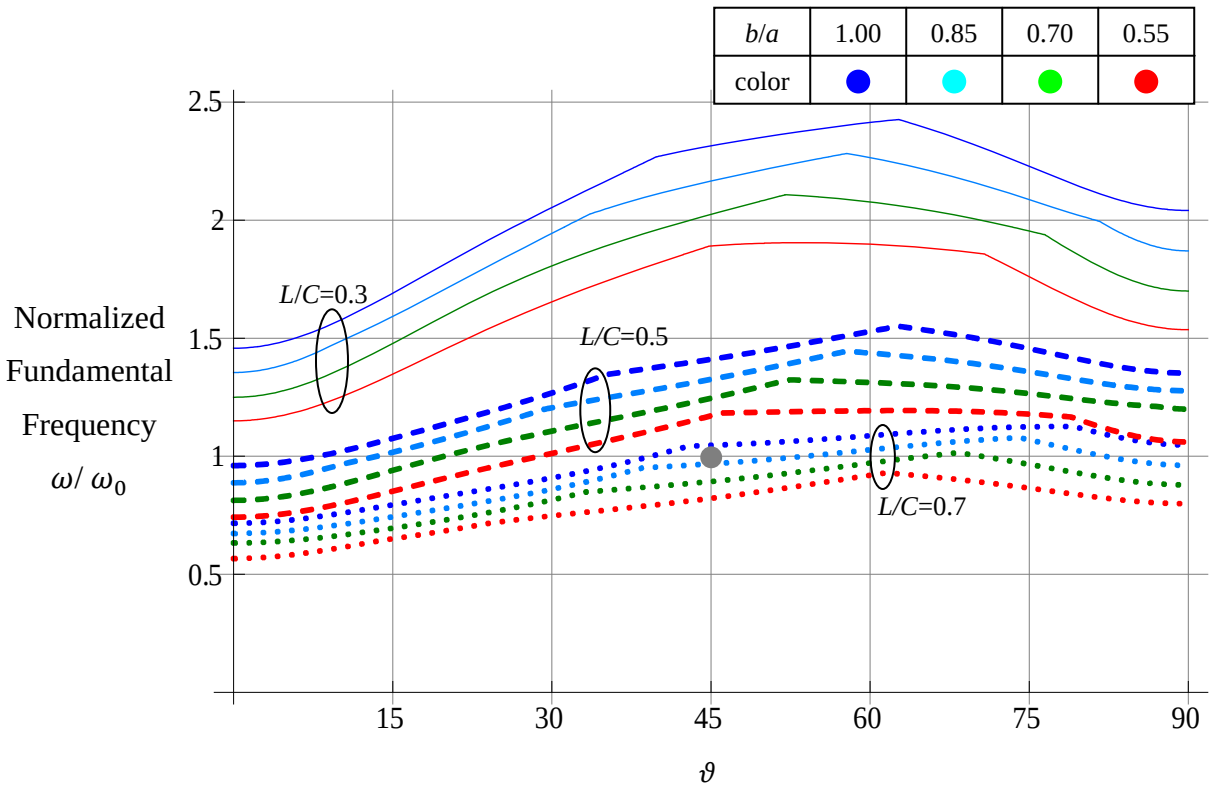

(a) Lamination sequences $[\pm\vartheta/0/90]_S$

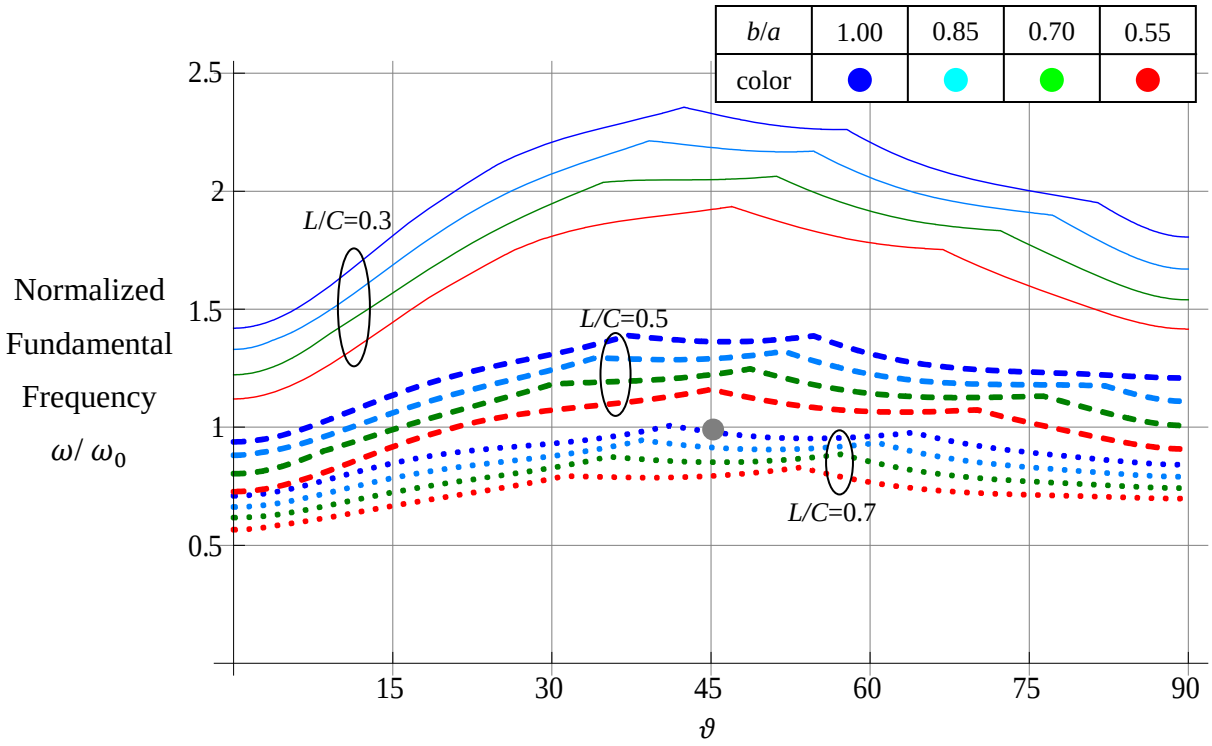

(b) Lamination sequences $[\pm\vartheta]_{2S}$

Fig. 4- 19 Normalized fundamental frequency of small elliptical cylinders, clamped supports

In Fig. 4- 18 the normalized fundamental frequencies of the small simply-supported cylinders are shown. The values of the normalized fundamental frequencies are divided by 3690 rad/s and that baseline case is identified with a solid circle in the figure. The results show that the fundamental frequencies vary more with ϑ in the four layers of the $[\pm\vartheta/0/90]_S$ laminate than with the eight layers of the $[\pm\vartheta]_{2S}$ laminate, as was the case for the large simply-supported cylinders in Figs. 4- 16. For the $[\pm\vartheta/0/90]_S$ laminate the highest fundamental frequencies occur for the range ϑ = 50-85°, while for the $[\pm\vartheta]_{2S}$ laminate it could be argued that the highest fundamental frequencies occur near ϑ = 30°, which for L/C = 0.3, 0.5, and 0.7 and a mildly elliptical cross section ϑ closer to 90° results in the highest fundamental frequency.

In Fig. 4- 19 the normalized fundamental frequencies of the small clamped support cylinders are shown. In general, for the $[\pm\vartheta/0/90]_S$ laminate the highest fundamental frequencies cluster around ϑ = 60-75°, while for the $[\pm\vartheta]_{2S}$ laminate the highest fundamental frequencies cluster around ϑ = 45°.

Before closing this chapter, it is important to consider the seemingly insensitive behavior of the fundamental frequencies for broad variations in fiber angle, as has been observed for a number of cases throughout the discussions in this chapter. Considering large simply supported cylinders with lamination sequences $[\pm\vartheta]_{4S}$, as in Fig. 4- 16b, with a aspect ratio b/a = 0.55 and length L/C = 0.5, details of the frequencies with varied circumferential wave number n are shown in Fig. 4- 20. As seen, for small fiber angles the wave number n = 6 is associated with the fundamental frequency. The frequency associated with that wave number increases quickly as the fiber angle increases. However, at a fiber angle of about 25° the frequency corresponding to wave number n = 5 is lower than the frequency corresponding to wave number n = 6. As the fiber angle continues to increase, the frequency associated with n = 5 again increases quickly, and at a fiber angle of approximately 39° the frequency associated with wave number n = 4 is lower, and so forth. Considering the locus of lowest frequencies, i.e., the fundamental frequency, it is basically insensitive to fiber angle. What is sensitive to fiber angle is the circumferential wave number, and significantly so. As the fiber angle increases, the number of circumferential waves decreases. This number of circumferential waves seems to be correlated with circumferential stiffness, as dictated by fiber angle. Circumferential stiffness increases with increasing fiber angle, so developing short wavelength curvatures in the circumferential direction

for fiber angles near 90° would seem to be more difficult than for fiber angles closer to 0°. This appears to be the case, as the circumferential wavelength decreases with increasing fiber angle.

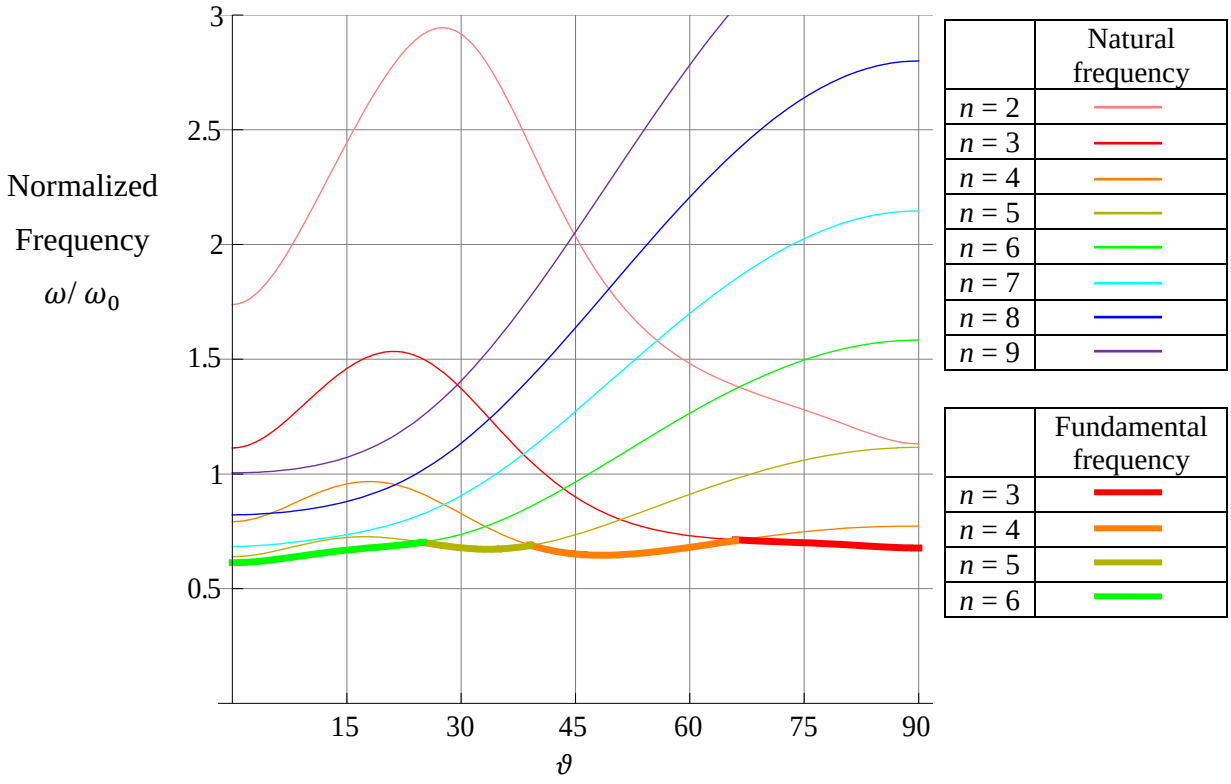

Fig. 4- 20 Normalized fundamental frequency of large elliptical cylinders, lamination sequences $[\pm\vartheta]_{4S}$, b/a = 0.55, L/C = 0.5, various circumferential wave numbers n, simple supports, based on Lo's approximation

While Fig. 4- 20 is based on Lo's approximation, Fig. 4- 21 is based on the second simplification. There is slight difference between the results based on Lo's approximation and the 2nd simplification. For example, the junction of the fundamental frequency with n =4 and n = 5 is around ϑ= 39° based on Lo's approximation, whereas the junction of the fundamental frequency with n =4 and n = 5 is around ϑ= 37° based on the 2nd simplification. However, both approximations refer to the same conclusion and explain the insensitive behavior. From Fig. 4-

21 it can also be seen that the difference of the fundamental frequency based on the cosine-based and sine-based assumed functions for n larger than 3 can hardly be distinguished while those for n = 2 can be observed. The differences between the cosine-based and sine-based analyses were considered in detail earlier.

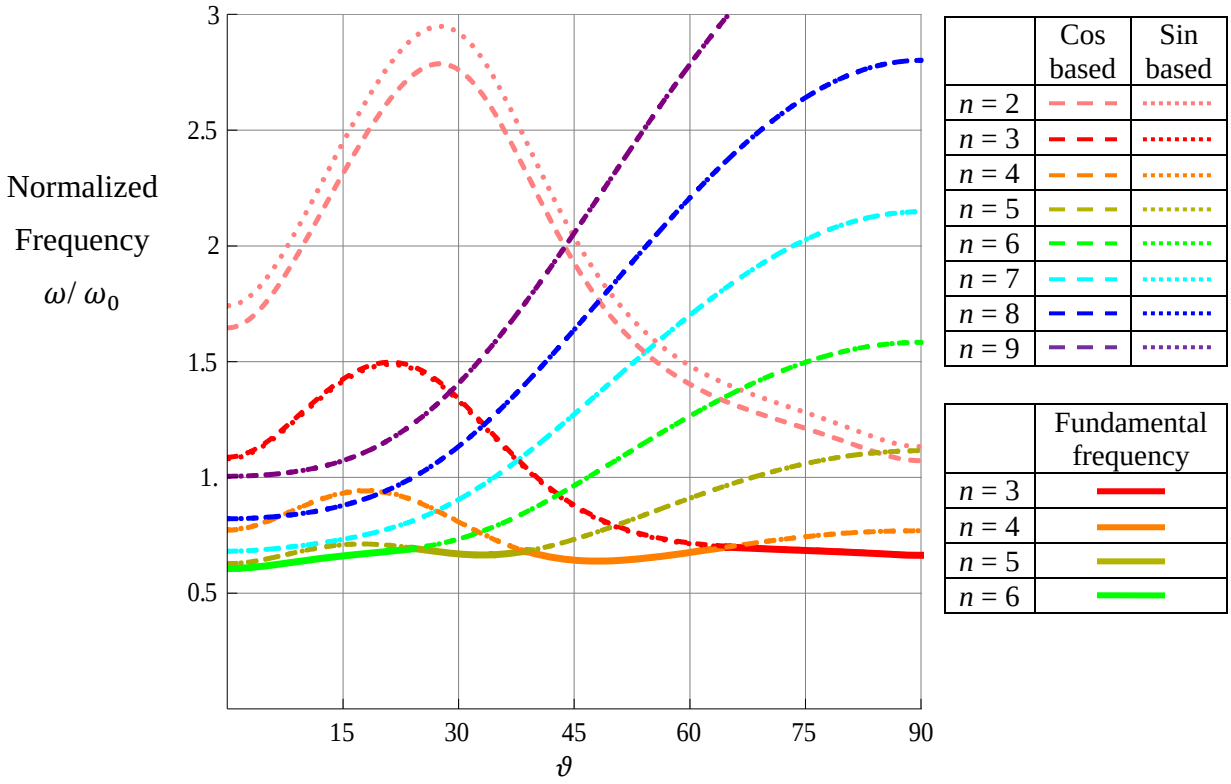

Fig. 4- 21 Normalized fundamental frequency of large elliptical cylinders, lamination sequences $[\pm\vartheta]_{4S}$, b/a = 0.55, L/C = 0.5, various circumferential wave numbers n, simple supports, based on the second simplification

Attention now turns to the other objective of this research, namely, the influence of circumferentially varying fiber angle on the fundamental frequencies of elliptical cylinders.

Chapter 5 Varying Fiber Orientation with Circumferential Location

The role of lamination sequence, fiber angle, cylinder size, and cross-sectional geometry on the fundamental frequency of composite cylinders constructed of layers with fiber orientations that do not change with circumferential location, which in this chapter will be referred to as constant fiber orientation, has been discussed in previous chapters. As mentioned, it has been shown that allowing the fiber orientation to vary with circumferential location can substantially improve axial buckling of an elliptical cylinder relative to, for example, a quasi-isotropic baseline case [1]. Additionally, the so-called one-spatial-coordinate fiber angle tailoring technique can increase the buckling of flat composite panels [60], and the so-called two-spatial-coordinate tailoring technique can increase the fundamental frequency [61] and the buckling load [62] of flat composite panels. Since there is evidence in the results of the previous chapters that the fundamental frequency is somewhat insensitive to fiber orientation, particularly for simply-supported cylinders, it is of value to determine if the fundamental frequency of an elliptical cylinder suffers from any detrimental effects if the fiber orientation is varied with circumferential location to provide particular structural advantages, such as increasing buckling load. Likewise, it is important to know if there is there any gain as regards fundamental frequency for the case of varying the fiber angle with circumferential location.

To investigate the impact of varying the fiber orientation with circumferential location, here a so-called linear approach to varying fiber orientation with circumferential location is employed. In particular, the description of fiber angle variation with circumferential location used herein is given in Eq. 5- 1, where θ_1 is the fiber orientation at $s = C/4$ and $s = 3C/4$, the more curved portions of the cylinder cross section, and θ_2 is the fiber orientation at $s = 0$ and $s = C/2$, the flatter portions of the cylinder cross section (see Figs. 1- 2 and 1- 3 for the definition of s.)

$$\begin{aligned} \vartheta &= \frac{4(\theta_1 - \theta_2)s}{C} + \theta_2, && 0 \le s < \frac{C}{4} \\ \vartheta &= \frac{4(-\theta_1 + \theta_2)s}{C} - \theta_2 + 2\theta_1, && \frac{C}{4} \le s < \frac{C}{2} \\ \vartheta &= \frac{4(\theta_1 - \theta_2)s}{C} + 3\theta_2 - 2\theta_1, && \frac{C}{2} \le s < \frac{3C}{4} \end{aligned} \qquad \text{Eq. 5- 1}$$

$$\vartheta = \frac{4(-\theta_1 + \theta_2)s}{C} - 3\theta_2 + 4\theta_1, \quad \frac{3C}{4} \leq s < C$$

The piecewise linear forms of Eq. 5- 1 are dictated by the fact that there must be a double symmetry to the fiber angle variation around the circumference. A schematic of the fibers in one of the layers of a cylinder with a constant fiber orientation of 75°, as studied in the former chapters, is illustrated in Fig. 5- 1a. The fiber orientation in one of the layers of a cylinder with varying fiber orientation, in particular with $\theta_1 = 15°$ and $\theta_2 = 75°$, is shown in Fig. 5- 1b.

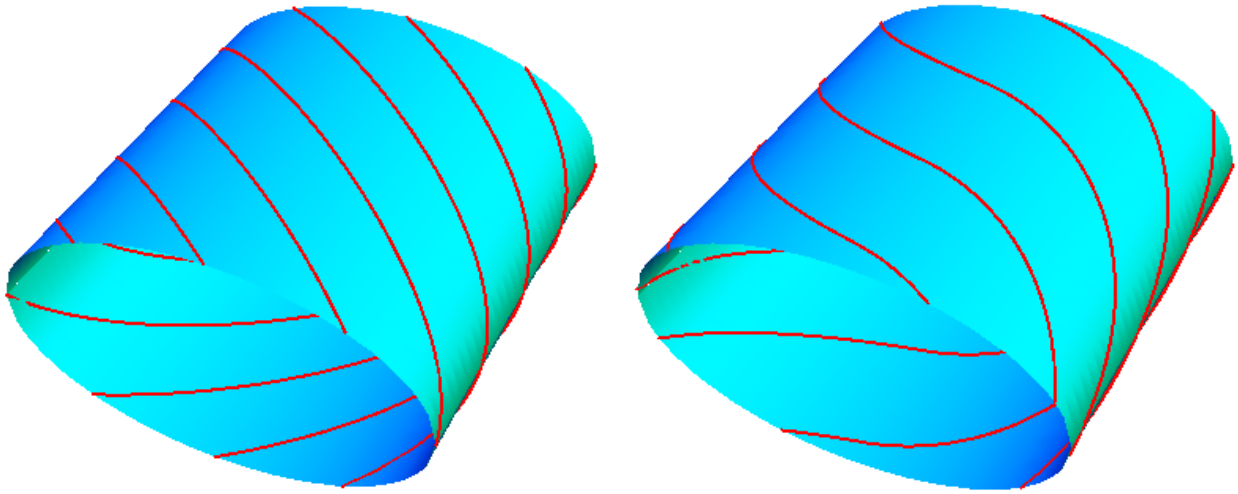

(a) $\vartheta = 45°$ (b) $\theta_1 = 15°$ and $\theta_2 = 75°$

Fig. 5- 1 Illustration of layer fiber direction within cylinders

To further illustrate the constant and variable fiber angle concepts, in Fig. 5- 2a and b the layers are unrolled into a planar sheet.

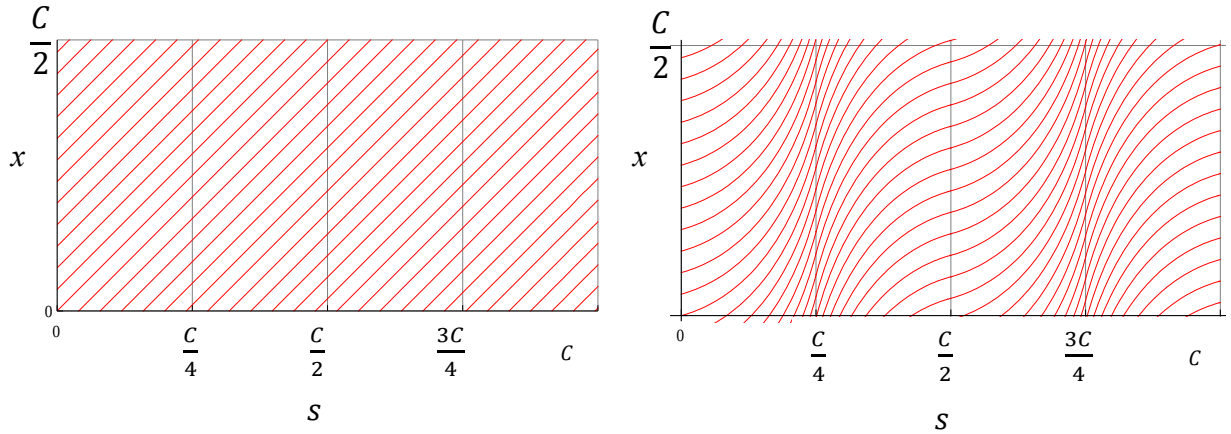

(a) $\vartheta = 45°$ (b) $\theta_1 = 15°$ and $\theta_2 = 75°$

Fig. 5- 2 Unrolled cylinders with varying fiber orientation

With varying fiber orientation combined with several lamination sequences, cylinder size, boundary conditions, and cross-sectional geometry, the number of parameters to investigate is large. For that reason, the study of the influence of varying fiber orientation will be restricted to just a few combinations of parameters, mainly to determine the extent of the influence of variable fiber orientation on the fundamental frequency. The parameters considered are listed in Tables 5- 1 and 5- 2.

Table 5- 1 Cylinder parameters considered

Aspect ratio (b/a)	1, 0.55
Length-to-circumference ratio(L/C)	0.5
Cylinder size (C)	Large 2.82 m Small 0.704 m
Laminates	Large $[\pm\vartheta/0/90]_{2S}$, $[\pm\vartheta]_{4S}$ Small $[\pm\vartheta/0/90]_{S}$, $[\pm\vartheta]_{2S}$
Boundary conditions	simple supports

Table 5- 2 Range of θ_1 and θ_2 Considered

θ_1	15, 45, 75°
θ_2	15, 45, 75°

A Rayleigh-Ritz formulation will be developed to obtain a closed-form expression for the fundamental frequency for the variable fiber angle cylinders. A finite element model will also be used to compute results and compare with the closed-form expression. To develop an expression for the fundamental frequency of cylinders with linearly varying fiber orientation, the invariant properties of a composite layer are used. These are introduced in the next section, and the fundamental frequency equations are developed in the section following that.

5.1 Invariant Properties of an Orthotropic Lamina

By rewriting Eq. 2- 46 in terms of invariant properties [63], in any layer with fiber orientation θ the transformed reduced stiffnesses can be expressed as

$$\begin{aligned}
\overline{Q}_{11} &= \Lambda_1 + \Lambda_2\cos 2\theta + \Lambda_3\cos 4\theta \\
\overline{Q}_{12} &= \Lambda_4 - \Lambda_3\cos 4\theta \\
\overline{Q}_{22} &= \Lambda_1 - \Lambda_2\cos 2\theta + \Lambda_3\cos 4\theta \\
\overline{Q}_{16} &= \tfrac{1}{2}\Lambda_2\sin 2\theta + \Lambda_3\sin 4\theta \\
\overline{Q}_{26} &= \tfrac{1}{2}\Lambda_2\sin 2\theta - \Lambda_3\sin 4\theta \\
\overline{Q}_{66} &= \Lambda_5 - \Lambda_3\cos 4\theta
\end{aligned} \qquad \text{Eq. 5- 2}$$

where

$$\begin{aligned}
\Lambda_1 &= \frac{3Q_{11} + 3Q_{22} + 2Q_{12} + 4Q_{66}}{8} \\
\Lambda_2 &= \frac{Q_{11} - Q_{22}}{2} \\
\Lambda_3 &= \frac{Q_{11} + Q_{22} - 2Q_{12} - 4Q_{66}}{8} \\
\Lambda_4 &= \frac{Q_{11} + Q_{22} + 6Q_{12} - 4Q_{66}}{8} \\
\Lambda_5 &= \frac{Q_{11} + Q_{22} - 2Q_{12} + 4Q_{66}}{8}
\end{aligned} \qquad \text{Eq. 5- 3}$$

In the matrix form, the transformed reduced stiffnesses become

$$\begin{bmatrix} \overline{\mathrm{Q}}_{11} & \overline{\mathrm{Q}}_{12} & \overline{\mathrm{Q}}_{16} \\ \overline{\mathrm{Q}}_{12} & \overline{\mathrm{Q}}_{22} & \overline{\mathrm{Q}}_{26} \\ \overline{\mathrm{Q}}_{16} & \overline{\mathrm{Q}}_{26} & \overline{\mathrm{Q}}_{66} \end{bmatrix} = \overline{\boldsymbol{\Lambda}}_0 + \overline{\boldsymbol{\Lambda}}_1 \cos 2\theta + \overline{\boldsymbol{\Lambda}}_2 \cos 4\theta + \overline{\boldsymbol{\Lambda}}_3 \sin 2\theta + \overline{\boldsymbol{\Lambda}}_4 \sin 4\theta \qquad \text{Eq. 5- 4}$$

where

$$\overline{\boldsymbol{\Lambda}}_0 = \begin{bmatrix} \Lambda_1 & \Lambda_4 & 0 \\ \Lambda_4 & \Lambda_1 & 0 \\ 0 & 0 & \Lambda_5 \end{bmatrix}$$

$$\overline{\boldsymbol{\Lambda}}_1 = \begin{bmatrix} \Lambda_2 & 0 & 0 \\ 0 & -\Lambda_2 & 0 \\ 0 & 0 & 0 \end{bmatrix}$$

$$\overline{\boldsymbol{\Lambda}}_2 = \begin{bmatrix} \Lambda_3 & -\Lambda_3 & 0 \\ -\Lambda_3 & \Lambda_3 & 0 \\ 0 & 0 & -\Lambda_3 \end{bmatrix} \qquad \text{Eq. 5- 5}$$

$$\overline{\boldsymbol{\Lambda}}_3 = \begin{bmatrix} 0 & 0 & \Lambda_2/2 \\ 0 & 0 & \Lambda_2/2 \\ \Lambda_2/2 & \Lambda_2/2 & 0 \end{bmatrix}$$

$$\overline{\boldsymbol{\Lambda}}_4 = \begin{bmatrix} 0 & 0 & \Lambda_3 \\ 0 & 0 & -\Lambda_3 \\ \Lambda_3 & -\Lambda_3 & 0 \end{bmatrix}$$

The expression for the potential energy per unit area of cylinder reference surface is

$$\begin{aligned} \overline{\Pi} \; = & \int_{-H/2}^{H/2} \overline{\mathrm{Q}}_{11} \, \mathrm{d}z \; {\varepsilon_x}^{\circ 2} + 2 \int_{-H/2}^{H/2} \overline{\mathrm{Q}}_{12} \, \mathrm{d}z \; {\varepsilon_x}^{\circ} {\varepsilon_s}^{\circ} + \int_{-H/2}^{H/2} \overline{\mathrm{Q}}_{22} \, \mathrm{d}z \; {\varepsilon_s}^{\circ 2} \\ & + 2 \int_{-H/2}^{H/2} \overline{\mathrm{Q}}_{16} \, \mathrm{d}z \; {\varepsilon_x}^{\circ} {\gamma_{xs}}^{\circ} + 2 \int_{-H/2}^{H/2} \overline{\mathrm{Q}}_{26} \, \mathrm{d}z \; {\gamma_{xs}}^{\circ} {\varepsilon_s}^{\circ} + \int_{-H/2}^{H/2} \overline{\mathrm{Q}}_{66} \, \mathrm{d}z \; {\gamma_{xs}}^{\circ 2} \\ & + 2 \int_{-H/2}^{H/2} \overline{\mathrm{Q}}_{11} \, z\mathrm{d}z \;\; {\varepsilon_x}^{\circ} {\kappa_x}^{\circ} + 2 \int_{-H/2}^{H/2} \overline{\mathrm{Q}}_{12} \, z\mathrm{d}z \; {\varepsilon_s}^{\circ} {\kappa_x}^{\circ} + 2 \int_{-H/2}^{H/2} \overline{\mathrm{Q}}_{12} \, z\mathrm{d}z \; {\varepsilon_x}^{\circ} {\kappa_s}^{\circ} \\ & + 2 \int_{-H/2}^{H/2} \overline{\mathrm{Q}}_{22} \, z\mathrm{d}z \;\; {\varepsilon_s}^{\circ} {\kappa_s}^{\circ} + 2 \int_{-H/2}^{H/2} \overline{\mathrm{Q}}_{16} \, z\mathrm{d}z \; {\varepsilon_x}^{\circ} {\kappa_{xs}}^{\circ} + 2 \int_{-H/2}^{H/2} \overline{\mathrm{Q}}_{16} \, z\mathrm{d}z \; {\gamma_{xs}}^{\circ} {\kappa_x}^{\circ} \\ & + 2 \int_{-H/2}^{H/2} \overline{\mathrm{Q}}_{26} \, z\mathrm{d}z \;\; {\varepsilon_s}^{\circ} {\kappa_{xs}}^{\circ} + 2 \int_{-H/2}^{H/2} \overline{\mathrm{Q}}_{26} \, z\mathrm{d}z \; {\gamma_{xs}}^{\circ} {\kappa_s}^{\circ} + 2 \int_{-H/2}^{H/2} \overline{\mathrm{Q}}_{66} \, z\mathrm{d}z \; {\gamma_{xs}}^{\circ} {\kappa_{xs}}^{\circ} \\ & + \int_{-H/2}^{H/2} \overline{\mathrm{Q}}_{11} z^2 \, \mathrm{d}z \; {\kappa_x}^{\circ 2} + 2 \int_{-H/2}^{H/2} \overline{\mathrm{Q}}_{12} z^2 \, \mathrm{d}z \; {\kappa_x}^{\circ} {\kappa_s}^{\circ} + \int_{-H/2}^{H/2} \overline{\mathrm{Q}}_{22} z^2 \, \mathrm{d}z \; {\kappa_s}^{\circ 2} \\ & + 2 \int_{-H/2}^{H/2} \overline{\mathrm{Q}}_{16} z^2 \, \mathrm{d}z \; {\kappa_x}^{\circ} {\kappa_{xs}}^{\circ} + 2 \int_{-H/2}^{H/2} \overline{\mathrm{Q}}_{26} z^2 \, \mathrm{d}z \; {\kappa_s}^{\circ} {\kappa_{xs}}^{\circ} + \int_{-H/2}^{H/2} \overline{\mathrm{Q}}_{66} z^2 \, \mathrm{d}z \; {\kappa_{xs}}^{\circ 2} \end{aligned} \qquad \text{Eq. 5- 6}$$

The potential energy for the entire cylinder, Π, is

$$\Pi = \frac{1}{2}\int_0^C \int_0^L \overline{\Pi}\ \mathrm{d}x\mathrm{d}s \qquad \text{Eq. 5- 7}$$

For symmetric lamination sequences, $\overline{\Pi}$ can be rewritten as the matrix form

$$\overline{\Pi} = \langle \varepsilon_x{}^\circ \quad \varepsilon_s{}^\circ \quad \gamma_{xs}{}^\circ \rangle \bar{A} \begin{Bmatrix} \varepsilon_x{}^\circ \\ \varepsilon_s{}^\circ \\ \gamma_{xs}{}^\circ \end{Bmatrix} + \langle \kappa_x{}^\circ \quad \kappa_s{}^\circ \quad \kappa_{xs}{}^\circ \rangle \overline{D} \begin{Bmatrix} \kappa_x{}^\circ \\ \kappa_s{}^\circ \\ \kappa_{xs}{}^\circ \end{Bmatrix} \qquad \text{Eq. 5- 8}$$

where

$$\begin{aligned} \bar{A} &= H\overline{\mathbf{\Lambda}}_0 + \alpha_1\overline{\mathbf{\Lambda}}_1 + \alpha_2\overline{\mathbf{\Lambda}}_2 + \alpha_3\overline{\mathbf{\Lambda}}_3 + \alpha_4\overline{\mathbf{\Lambda}}_4 \\ \overline{D} &= \frac{H^3}{12}\overline{\mathbf{\Lambda}}_0 + \beta_1\overline{\mathbf{\Lambda}}_1 + \beta_2\overline{\mathbf{\Lambda}}_2 + \beta_3\overline{\mathbf{\Lambda}}_3 + \beta_4\overline{\mathbf{\Lambda}}_4 \end{aligned} \qquad \text{Eq. 5- 9}$$

and

$$\begin{aligned} \alpha_1 &= \int_{-H/2}^{H/2} \cos 2\theta \mathrm{d}z \\ \alpha_2 &= \int_{-H/2}^{H/2} \cos 4\theta \mathrm{d}z \\ \alpha_3 &= \int_{-H/2}^{H/2} \sin 2\theta \mathrm{d}z \\ \alpha_4 &= \int_{-H/2}^{H/2} \sin 4\theta \mathrm{d}z \\ \beta_1 &= \int_{-H/2}^{H/2} z^2 \cos 2\theta \mathrm{d}z \\ \beta_2 &= \int_{-H/2}^{H/2} z^2 \cos 4\theta \mathrm{d}z \\ \beta_3 &= \int_{-H/2}^{H/2} z^2 \sin 2\theta \mathrm{d}z \\ \beta_4 &= \int_{-H/2}^{H/2} z^2 \sin 4\theta \mathrm{d}z \end{aligned} \qquad \text{Eq. 5- 10}$$

By substituting the four different lamination sequences being studied (see Table 5- 1) into Eq. 5- 10, α_1, α_2, α_3, α_4, β_1, β_2, β_3, and β_4 can be found and are given in Table 5- 3. The

parameters α_3 and α_4 are zero because the lamination sequences are balanced. The parameters $\bar{A}$ and $\bar{D}$ are rewritten to separate the effects of fiber angle ϑ as below.

$$\bar{A} = (H\overline{\mathbf{\Lambda}}_0 + \alpha_1^c\overline{\mathbf{\Lambda}}_1 + \alpha_2^c\overline{\mathbf{\Lambda}}_2) + (\alpha_1^t\overline{\mathbf{\Lambda}}_1\cos 2\vartheta + \alpha_2^t\overline{\mathbf{\Lambda}}_2\cos 4\vartheta) \quad \text{Eq. 5- 11}$$

$$\bar{D} = \left(\frac{H^3}{12}\overline{\mathbf{\Lambda}}_0 + \beta_1^c\overline{\mathbf{\Lambda}}_1 + \beta_2^c\overline{\mathbf{\Lambda}}_2 + \beta_3^c\overline{\mathbf{\Lambda}}_3 + \beta_4^c\overline{\mathbf{\Lambda}}_4\right) + (\beta_1^t\overline{\mathbf{\Lambda}}_1\cos 2\vartheta + \beta_2^t\overline{\mathbf{\Lambda}}_2\cos 4\vartheta + \beta_3^t\overline{\mathbf{\Lambda}}_3\sin 2\vartheta + \beta_4^t\overline{\mathbf{\Lambda}}_4\sin 4\vartheta) \quad \text{Eq. 5- 12}$$

Table 5- 3 Coefficients of invariant properties for different lamination sequences

	$[\pm\vartheta/0/90]_{2S}$	$[\pm\vartheta]_{4S}$	$[\pm\vartheta/0/90]_{S}$	$[\pm\vartheta]_{2S}$
$\alpha_1 = \alpha_1^t\cos 2\vartheta + \alpha_1^c$ (α_1^t, α_1^c)	$\left(\frac{H}{2}, 0\right)$	$(H, 0)$	$\left(\frac{H}{2}, 0\right)$	$(H, 0)$
$\alpha_2 = \alpha_2^t\cos 4\vartheta + \alpha_2^c$ (α_2^t, α_2^c)	$\left(\frac{H}{2}, \frac{H}{2}\right)$	$(H, 0)$	$\left(\frac{H}{2}, \frac{H}{2}\right)$	$(H, 0)$
α_3	0	0	0	0
α_4	0	0	0	0
$\beta_1 = \beta_1^t\cos 2\vartheta + \beta_1^c$ (β_1^t, β_1^c)	$\left(\frac{11H^3}{192}, \frac{3H^3}{512}\right)$	$\left(\frac{H^3}{12}, 0\right)$	$\left(\frac{7H^3}{96}, \frac{H^3}{128}\right)$	$\left(\frac{H^3}{12}, 0\right)$
$\beta_2 = \beta_2^t\cos 4\vartheta + \beta_2^c$ (β_2^t, β_2^c)	$\left(\frac{11H^3}{192}, \frac{5H^3}{192}\right)$	$\left(\frac{H^3}{12}, 0\right)$	$\left(\frac{7H^3}{96}, \frac{H^3}{96}\right)$	$\left(\frac{H^3}{12}, 0\right)$
$\beta_3 = \beta_3^t\sin 2\vartheta + \beta_3^c$ (β_3^t, β_3^c)	$\left(\frac{5H^3}{512}, 0\right)$	$\left(\frac{H^3}{64}, 0\right)$	$\left(\frac{3H^3}{128}, 0\right)$	$\left(\frac{H^3}{32}, 0\right)$
$\beta_4 = \beta_4^t\sin 4\vartheta + \beta_4^c$ (β_4^t, β_4^c)	$\left(\frac{5H^3}{512}, 0\right)$	$\left(\frac{H^3}{64}, 0\right)$	$\left(\frac{3H^3}{128}, 0\right)$	$\left(\frac{H^3}{32}, 0\right)$

5.2 Development of Rayleigh-Ritz Analysis

As discussed in the previous chapters, for the cylinders with constant fiber orientation the *m* = 0 case represents frequencies higher than the fundamental frequencies. It is expected this would be the case for variable fiber angle cylinders. Therefore, only the *m* > 0 case will be considered here.

The assumed forms for the applying the Rayleigh-Ritz technique to Hamilton's principle are as they were for the cylinders with constant fiber orientation, namely,

$$u^\circ = \sum_{m=1}^{\infty}\sum_{n=1}^{\infty} \mathrm{U}_{mn} X_m^1(x)\Phi_n^0(s)$$

$$v^\circ = \sum_{m=1}^{\infty}\sum_{n=1}^{\infty} \mathrm{V}_{mn}\, X_m^0(x)\Phi_n^1(s) \qquad \text{Eq. 5- 13}$$

$$w^\circ = \sum_{m=1}^{\infty}\sum_{n=1}^{\infty} \mathrm{W}_{mn} X_m^0(x)\Phi_n^2(s)$$

where $X_m^1(x)$ and $X_m^0(x)$ are $\frac{L}{m\pi}\cos\frac{m\pi x}{L}$ and $\sin\frac{m\pi x}{L}$, respectively, for simple supports. The functions $\Phi_n^0(s)$, $\Phi_n^1(s)$, and $\Phi_n^2(s)$ are as defined in Section 3.3.1. The reference surface strains become

$$\varepsilon_x{}^\circ = \sum_{m=1}^{\infty}\sum_{n=1}^{\infty} \mathrm{U}_{mn} X_m^2(x)\Phi_n^0(s)$$

$$\varepsilon_s{}^\circ = \sum_{m=1}^{\infty}\sum_{n=1}^{\infty} \left(\frac{\mathrm{W}_{mn}}{R_0} + \mathrm{V}_{mn}\frac{2n\pi}{C}\right) X_m^0(x)\Phi_n^0(s) \qquad \text{Eq. 5- 14}$$

$$\gamma_{xs}{}^\circ = \sum_{m=1}^{\infty}\sum_{n=1}^{\infty} \left(-\mathrm{U}_{mn}\frac{2n\pi}{C} + \mathrm{V}_{mn}\right) X_m^1(x)\Phi_n^1(s)$$

where Eq. 3- 28 and Eq. 3- 30 are used, and the reference curvatures become

$$\kappa_x{}^\circ = -\sum_{m=1}^{\infty}\sum_{n=1}^{\infty} \mathrm{W}_{mn} X_m^2(x)\Phi_n^2(s)$$

$$\kappa_s{}^\circ = -\sum_{m=1}^{\infty}\sum_{n=1}^{\infty} \mathrm{W}_{mn} X_m^0(x) \frac{\mathrm{d}^2 \Phi_n^2(s)}{\mathrm{d}s^2} \qquad \text{Eq. 5- 15}$$

$$\kappa_{xs}{}^\circ = -2\sum_{m=1}^{\infty}\sum_{n=1}^{\infty} \mathrm{W}_{mn} X_m^1(x) \frac{\mathrm{d}\Phi_n^2(s)}{\mathrm{d}s}$$

Rewriting $\varepsilon_x{}^\circ$, $\varepsilon_s{}^\circ$, $\gamma_{xs}{}^\circ$, $\kappa_x{}^\circ$, $\kappa_s{}^\circ$, and $\kappa_{xs}{}^\circ$ in matrix form in term of U_{mn}, V_{mn}, and W_{mn}

$$\begin{Bmatrix} \varepsilon_x{}^\circ \\ \varepsilon_s{}^\circ \\ \gamma_{xs}{}^\circ \end{Bmatrix} = \mathbb{S} \begin{Bmatrix} \mathrm{U}_{mn} \\ \mathrm{V}_{mn} \\ \mathrm{W}_{mn} \end{Bmatrix} \qquad \text{Eq. 5- 16}$$

$$\begin{Bmatrix} \kappa_x{}^\circ \\ \kappa_s{}^\circ \\ \kappa_{xs}{}^\circ \end{Bmatrix} = -\mathbb{K} \begin{Bmatrix} \mathrm{U}_{mn} \\ \mathrm{V}_{mn} \\ \mathrm{W}_{mn} \end{Bmatrix} \qquad \text{Eq. 5- 17}$$

where

$$\mathbb{S} = \begin{bmatrix} X_m^2(x)\Phi_n^0(s) & 0 & 0 \\ 0 & X_m^0(x)\Phi_n^0(s)\dfrac{2n\pi}{C} & \dfrac{X_m^0(x)\Phi_n^0(s)}{R_0} \\ -X_m^1(x)\Phi_n^1(s)\dfrac{2n\pi}{C} & X_m^1(x)\Phi_n^1(s) & 0 \end{bmatrix} \qquad \text{Eq. 5- 18}$$

$$\mathbb{K} = \begin{bmatrix} 0 & 0 & X_m^2(x)\Phi_n^2(s) \\ 0 & 0 & X_m^0(x)\dfrac{\mathrm{d}^2\Phi_n^2(s)}{\mathrm{d}s^2} \\ 0 & 0 & 2X_m^1(x)\dfrac{\mathrm{d}\Phi_n^2(s)}{\mathrm{d}s} \end{bmatrix} \qquad \text{Eq. 5- 19}$$

As developed in Chapter 3, the kinetic energy is

$$\mathrm{K} = \frac{C}{4}\rho H \omega_{mn}{}^2 \left(\mathrm{U}_{mn}{}^2\, \mathrm{I}_{4m} + \mathrm{V}_{mn}{}^2\, \mathrm{I}_{3m} + \mathrm{W}_{mn}{}^2\, \mathrm{I}_{3m}\mathrm{S}_{1n}\right) \qquad \text{Eq. 5- 20}$$

and total potential energy becomes

$$\Pi = \frac{1}{2}\langle \mathrm{U}_{mn} \quad \mathrm{V}_{mn} \quad \mathrm{W}_{mn} \rangle \mathbb{M} \begin{Bmatrix} \mathrm{U}_{mn} \\ \mathrm{V}_{mn} \\ \mathrm{W}_{mn} \end{Bmatrix} \qquad \text{Eq. 5- 21}$$

where

$$\mathbb{M} = \frac{C}{2}\begin{bmatrix} \mathrm{T}_{11} & \mathrm{T}_{12} & \mathrm{T}_{13} \\ \mathrm{T}_{12} & \mathrm{T}_{22} & \mathrm{T}_{23} \\ \mathrm{T}_{13} & \mathrm{T}_{23} & \mathrm{T}_{33} \end{bmatrix} = \int_0^L \int_0^C (\mathbb{S}^T \bar{A}\, \mathbb{S} + \mathbb{K}^T \bar{D}\, \mathbb{K})\, \mathrm{d}s\mathrm{d}x \qquad \text{Eq. 5- 22}$$

The elements of the T matrix can be written as

$$T_{11} = I_{1m}A_{11}' + \left(\frac{2n\pi}{C}\right)^2 I_{4m}A_{66}'$$

$$T_{12} = \left(\frac{2n\pi}{C}\right) I_{2m}A_{12}' - \left(\frac{2n\pi}{C}\right) I_{4m}A_{66}'$$

$$T_{13} = \frac{2\pi}{C} I_{2m}A_{12}' \qquad \text{Eq. 5- 23}$$

$$T_{22} = I_{4m}A_{66}' + \left(\frac{2n\pi}{C}\right)^2 I_{3m}A_{22}'$$

$$T_{23} = \frac{4n\pi^2}{C^2} I_{3m}A_{22}'$$

$$T_{33} = T_{33}^{A} + T_{33}^{D}$$

where

$$T_{33}^{A} = \frac{4\pi^2}{C^2} I_{3m}A_{22}' \qquad \text{Eq. 5- 24}$$

$$T_{33}^{D} = I_{1m}D_{11}' - 2\left(\frac{2n\pi}{C}\right)^2 I_{2m}D_{12}' + \left(\frac{2n\pi}{C}\right)^4 I_{3m}D_{22}'$$

$$+4\left(\frac{2n\pi}{C}\right)^2 I_{4m}D_{66}' \qquad \text{Eq. 5- 25}$$

and

$$A_{11}' = H\Lambda_1 + \alpha_1^c\Lambda_2 + \alpha_2^c\Lambda_3 + \alpha_1^t\Lambda_2 S_{5n} + \alpha_2^t\Lambda_3 S_{6n}$$

$$A_{12}' = H\Lambda_4 - \alpha_2^c\Lambda_3 - \alpha_2^t\Lambda_3 S_{6n}$$

$$A_{22}' = H\Lambda_1 - \alpha_1^c\Lambda_2 + \alpha_2^c\Lambda_3 - \alpha_1^t\Lambda_2 S_{5n} + \alpha_2^t\Lambda_3 S_{6n}$$

$$A_{66}' = H\Lambda_5 - \alpha_2^c\Lambda_3 - \alpha_2^t\Lambda_3 S_{7n} \qquad \text{Eq. 5- 26}$$

$$D_{11}' = \left(\frac{H^3}{12}\Lambda_1 + \beta_1^c\Lambda_2 + \beta_2^c\Lambda_3\right) S_{1n} + \beta_1^t\Lambda_2 S_{8n} + \beta_2^t\Lambda_3 S_{9n}$$

$$\mathrm{D}_{12}{}' = \left(\frac{H^3}{12}\Lambda_4 - \beta_2^c\Lambda_3\right)\mathrm{S}_{2n} - \beta_2^t\Lambda_3\mathrm{S}_{10n}$$

$$\mathrm{D}_{22}{}' = \left(\frac{H^3}{12}\Lambda_1 - \beta_1^c\Lambda_2 + \beta_2^c\Lambda_3\right)\mathrm{S}_{3n} - \beta_1^t\Lambda_2\mathrm{S}_{11n} + \beta_2^t\Lambda_3\mathrm{S}_{12n}$$

$$\mathrm{D}_{66}' = \left(\frac{H^3}{12}\Lambda_5 - \beta_2^c\Lambda_3\right)\mathrm{S}_{4n} - \beta_2^t\Lambda_3\mathrm{S}_{13n}$$

and

$$\mathrm{S}_{5n} = \frac{2}{C}\int_0^C \Phi_n^0(s)^2\cos 2\theta\,\mathrm{d}s$$

$$\mathrm{S}_{6n} = \frac{2}{C}\int_0^C \Phi_n^0(s)^2\cos 4\theta\,\mathrm{d}s$$

$$\mathrm{S}_{7n} = \frac{2}{C}\int_0^C \Phi_n^1(s)^2\cos 4\theta\,\mathrm{d}s$$

$$\mathrm{S}_{8n} = \frac{2}{C}\int_0^C \Phi_n^2(s)^2\cos 2\theta\,\mathrm{d}s$$

$$\mathrm{S}_{9n} = \frac{2}{C}\int_0^C \Phi_n^2(s)^2\cos 4\theta\,\mathrm{d}s \qquad \text{Eq. 5- 27}$$

$$\mathrm{S}_{10n} = -\frac{2}{C}\left(\frac{C}{2n\pi}\right)^2\int_0^C \Phi_n^2(s)\frac{\mathrm{d}^2\Phi_n^2(s)}{\mathrm{d}s^2}\cos 4\theta\,\mathrm{d}s$$

$$\mathrm{S}_{11n} = \frac{2}{C}\left(\frac{C}{2n\pi}\right)^4\int_0^C \left(\frac{\mathrm{d}^2\Phi_n^2(s)}{\mathrm{d}s^2}\right)^2\cos 2\theta\,\mathrm{d}s$$

$$\mathrm{S}_{12n} = \frac{2}{C}\left(\frac{C}{2n\pi}\right)^4\int_0^C \left(\frac{\mathrm{d}^2\Phi_n^2(s)}{\mathrm{d}s^2}\right)^2\cos 4\theta\,\mathrm{d}s$$

$$\mathrm{S}_{13n} = \frac{2}{C}\left(\frac{C}{2n\pi}\right)^2\int_0^C \left(\frac{\mathrm{d}\Phi_n^2(s)}{\mathrm{d}s}\right)^2\cos 4\theta\,\mathrm{d}s$$

Substituting Eq. 5- 20 and Eq. 5- 21 into Eq. 3- 11, a matrix form of simultaneous equations becomes

$$\begin{bmatrix} \mathrm{T}_{11} - \rho H\omega_{mn}^2\mathrm{I}_{4m} & \mathrm{T}_{12} & \mathrm{T}_{13} \\ \mathrm{T}_{12} & \mathrm{T}_{22} - \rho H\omega_{mn}^2\mathrm{I}_{3m} & \mathrm{T}_{23} \\ \mathrm{T}_{13} & \mathrm{T}_{23} & \mathrm{T}_{33} - \rho H\omega_{mn}^2\mathrm{I}_{3m}\mathrm{S}_{1n} \end{bmatrix}\begin{Bmatrix} \mathrm{U}_{mn} \\ \mathrm{V}_{mn} \\ \mathrm{W}_{mn} \end{Bmatrix} = \begin{Bmatrix} 0 \\ 0 \\ 0 \end{Bmatrix} \qquad \text{Eq. 5- 28}$$

Equating the determinant of Eq. 5- 28 to zero, the natural frequency equation can be written as

$$\left(\rho H {\omega_{mn}}^2\right)^3 - P_4\ \left(\rho H {\omega_{mn}}^2\right)^2 + P_2\ \left(\rho H {\omega_{mn}}^2\right) - P_0\ = 0 \qquad \text{Eq. 5- 29}$$

where

$$P_4\ = \left(\frac{\mathrm{T}_{11}}{\mathrm{I}_{4m}} + \frac{\mathrm{T}_{22}}{\mathrm{I}_{3m}} + \frac{\mathrm{T}_{33}}{\mathrm{I}_{3m}\mathrm{S}_{1n}}\right)$$

$$P_2\ = \left(\frac{\mathrm{T}_{11}\mathrm{T}_{22} - {\mathrm{T}_{12}}^2}{\mathrm{I}_{3m}\mathrm{I}_{4m}} + \frac{\mathrm{T}_{22}\mathrm{T}_{33} - {\mathrm{T}_{23}}^2 - {\mathrm{T}_{13}}^2}{{\mathrm{I}_{3m}}^2\mathrm{S}_{1n}} + \frac{\mathrm{T}_{33}\mathrm{T}_{11}}{\mathrm{I}_{3m}\mathrm{I}_{4m}\mathrm{S}_{1n}}\right) \qquad \text{Eq. 5- 30}$$

$$P_0\ = \frac{\mathrm{T}_{11}\mathrm{T}_{22}\mathrm{T}_{33} + 2\mathrm{T}_{12}\mathrm{T}_{23}\mathrm{T}_{13} - \mathrm{T}_{33}{\mathrm{T}_{12}}^2 - \mathrm{T}_{11}{\mathrm{T}_{23}}^2 - \mathrm{T}_{22}{\mathrm{T}_{13}}^2}{{\mathrm{I}_{3m}}^2\ \mathrm{I}_{4m}\mathrm{S}_{1n}}$$

The lowest root, from which the fundamental frequency is derived, is given as

$$\rho H {\omega_{mn}}^2 = \frac{P_4}{3} - \frac{1}{3}\sqrt[3]{\frac{\mathrm{RT} + \sqrt{\mathrm{RT}^2 - 4\left(P_4^2 - 3P_2\ \right)^3}}{2}} - \frac{1}{3}\sqrt[3]{\frac{\mathrm{RT} - \sqrt{\mathrm{RT}^2 - 4\left(P_4^2 - 3P_2\ \right)^3}}{2}} \qquad \text{Eq. 5- 31}$$

where

$$\mathrm{RT} = -2P_4^3 + 9P_4\ P_2\ - 27P_0 \qquad \text{Eq. 5- 32}$$

As in Ch. 3, a simplified equation based on ignoring inertia effects in axial and circumferential directions is derivable from the matrix form from Eq. 5- 28 as

$$\begin{bmatrix} \mathrm{T}_{11} & \mathrm{T}_{12} & \mathrm{T}_{13} \\ \mathrm{T}_{12} & \mathrm{T}_{22} & \mathrm{T}_{23} \\ \mathrm{T}_{13} & \mathrm{T}_{23} & \mathrm{T}_{33} - \mathrm{I}_{3m}\rho H {\omega_{mn}}^2\mathrm{S}_{1n} \end{bmatrix} \begin{Bmatrix} \mathrm{U}_{mn} \\ \mathrm{V}_{mn} \\ \mathrm{W}_{mn} \end{Bmatrix} = \begin{Bmatrix} 0 \\ 0 \\ 0 \end{Bmatrix} \qquad \text{Eq. 5- 33}$$

The corresponding frequency equation is

$$\rho H {\omega_{mn}}^2 \mathrm{I}_{3m}\mathrm{S}_{1n} = \mathrm{T}_{33} + \frac{2\mathrm{T}_{12}\mathrm{T}_{13}\mathrm{T}_{23} - \mathrm{T}_{11}{\mathrm{T}_{23}}^2 - \mathrm{T}_{22}{\mathrm{T}_{13}}^2}{\mathrm{T}_{11}\mathrm{T}_{22} - {\mathrm{T}_{12}}^2} \qquad \text{Eq. 5- 34}$$

In Eq. 5- 34 T_{33} is a very large positive number and the collection of terms to the right of the plus sign results in another number of large magnitude, but with a negative sign. When considering with different values of θ_1 and θ_2 the calculation error due to the effective subtraction of these large numbers is an issue. As the first simplified equation, then, for variable fiber angle cylinders, $\mathrm{T}_{33}^{\mathrm{A}}$ (Eq. 5- 24) can combine with the negative term, resulting in the *first simplified equation* based on Eq. 5- 34 for variable fiber angle noncircular cylinders that can be written as

$$\rho H \omega_{mn}{}^2 \mathrm{I}_{3m} \mathrm{S}_{1n} = \mathrm{T}_{33}^{\mathrm{D}} + \frac{\mathrm{A}_{66}{}' \mathrm{I}_{4m}}{R_0{}^2} \frac{\mathrm{A}_{11}{}' \mathrm{I}_{1m} \mathrm{A}_{22}{}' \mathrm{I}_{3m} - (\mathrm{A}_{12}{}' \mathrm{I}_{2m})^2}{\mathrm{T}_{11}\, \mathrm{T}_{22} - \mathrm{T}_{12}{}^2} \qquad \text{Eq. 5- 35}$$

Again, when $\mathrm{d}R(s)/\mathrm{d}s$ and $\mathrm{d}^2R(s)/\mathrm{d}s^2$ are ignored, $\mathrm{S}_{1n}, \mathrm{S}_{2n}$, and S_{3n} are the same and S_{4n} is very close in value to those parameters when *n* is greater than two. Similarly, S_{11n} is considered to be close to S_{8n}. On the other hand, $\mathrm{S}_{10n}, \mathrm{S}_{12n}$, and S_{13n} are considered to be close to S_{9n}. Moreover, the value of I_{2m} is the same as $-\mathrm{I}_{4m}$. Therefore, the *second simplified equation* for variable fiber angle noncircular cylinders is

$$\rho H \omega_{mn}{}^2 \mathrm{I}_{3m} = \mathrm{T}_{33}^{\mathrm{DR}} + \frac{\mathrm{A}_{66}{}' \mathrm{I}_{4m}}{R_0{}^2\, \mathrm{S}_{1n}} \frac{\mathrm{A}_{11}{}' \mathrm{I}_{1m} \mathrm{A}_{22}{}' \mathrm{I}_{3m} - (\mathrm{A}_{12}{}' \mathrm{I}_{2m})^2}{\mathrm{T}_{11}\, \mathrm{T}_{22} - \mathrm{T}_{12}{}^2} \qquad \text{Eq. 5- 36}$$

where

$$\begin{aligned} \mathrm{T}_{33}^{\mathrm{DR}} = {} & \mathrm{I}_{1m}\left(\frac{H^3}{12}\Lambda_1 + \beta_1^c \Lambda_2 + \beta_2^c \Lambda_3\right) + \mathrm{I}_{3m}\left(\frac{2n\pi}{C}\right)^4 \left(\frac{H^3}{12}\Lambda_1 - \beta_1^c \Lambda_2 + \beta_2^c \Lambda_3\right) \\ & + \mathrm{I}_{4m}\left(\frac{2n\pi}{C}\right)^2 \left(\frac{H^3}{6}\Lambda_1 + \frac{H^3}{3}\Lambda_5 - 6\beta_2^c \Lambda_3\right) + \left(\mathrm{I}_{1m} - \mathrm{I}_{3m}\left(\frac{2n\pi}{C}\right)^4\right)\beta_2^t \Lambda_3 \frac{\mathrm{S}_{8n}}{\mathrm{S}_{1n}} \\ & + \left(\mathrm{I}_{1m} + \mathrm{I}_{3m}\left(\frac{2n\pi}{C}\right)^4 - 6\mathrm{I}_{4m}\left(\frac{2n\pi}{C}\right)^2\right)\beta_2^t \Lambda_3 \frac{\mathrm{S}_{9n}}{\mathrm{S}_{1n}} \end{aligned} \qquad \text{Eq. 5- 37}$$

Again considering $\mathrm{S}_{1n} \approx R_{\max}/R_0$ as applied in Ch. 3, *Lo's approximate equation* for variable fiber angle noncircular cylinders is obtained as

$$\rho H \omega_{mn}{}^2 \mathrm{I}_{3m} = \mathrm{T}_{33}^{\mathrm{DR}} + \frac{\mathrm{A}_{66}{}' \mathrm{I}_{4m}}{R_0 R_{\max}} \frac{\mathrm{A}_{11}{}' \mathrm{I}_{1m} \mathrm{A}_{22}{}' \mathrm{I}_{3m} - (\mathrm{A}_{12}{}' \mathrm{I}_{4m})^2}{\mathrm{T}_{11}\, \mathrm{T}_{22} - \mathrm{T}_{12}{}^2} \qquad \text{Eq. 5- 38}$$

Remark Lo's approximate equation for variable fiber angle cylinders (Eq. 5- 38) is not close-form expression though Eq. 3- 74 is a close-form equation for simply-supported cylinders.

5.3 Numerical Results

As with the constant fiber angle cylinder in Ch. 4, comparison of the various simplified equations for variable fiber angle cylinders will be discussed here. The fundamental frequencies will be normalized by the fundamental frequencies of the two baseline circular cases as computed by the finite element model, namely the large circular cylinder with lamination sequence the $[\pm 45/0/90]_{2S}$ and the small circular cylinder with lamination sequence $[\pm 45/0/90]_{S}$. Those frequencies, from Table 4- 6, are 3490 rad/s and 630 rad/s for the large and small simply-supported cylinders, respectively.

The normalized fundamental frequencies of large circular cylinders with linearly varying fiber angle ϑ are shown in Fig. 5- 3. For circular cylinders, the first simplified equation, the second simplified equation, and Lo's approximate equation all refer to the same equation, namely the simplified equation here. The format of each sub-figure in Fig. 5- 3, and each sub-figure in figures to follow, is to illustrate the fundamental frequency on the vertical axis as a function of θ_1 on the horizontal axis, where θ_1 = 15, 45, and 75°, and with θ_2 held constant at 15, 45, or 75°. With $\theta_1 = \theta_2$ the fibers have a constant orientation and the results from Ch. 5 are reproduced. The cylinder with θ_1 = 45° and θ_2 = 45° and lamination sequence $[\pm\vartheta/0/90]_{2S}$ is the baseline case for the large cylinders and has a normalized frequency of unity.

In Fig. 5- 3, the developed equations, including non-simplified and simplified equations, have close predictions. The fundamental frequency from the non-simplified equation is about 2% lower than that from the simplified equation, but the prediction of Abaqus is always the lowest. In Fig. 5- 3a is shown the results of lamination sequences $[\pm\vartheta/0/90]_{2S}$ where θ_2 = 15° and θ_1 = 15, 45, and 75°, respectively. The maximum difference between the results from the simplified equation and from Abaqus occurs at θ_2 = 15° and θ_1 = 75° with around 8% disagreement. In Fig. 5- 3b is shown the results of lamination sequences $[\pm\vartheta/0/90]_{2S}$ where θ_2 = 45° and θ_1 = 15, 45, and 75°, respectively, and the maximum difference occurs at θ_2 = 45° and θ_1 = 75° where the difference is less than 6%. In Fig. 5- 3c is shown the results of lamination sequences $[\pm\vartheta/0/90]_{2S}$ where θ_2 = 75° and θ_1 = 15, 45, and 75°, respectively, However, because of the circular geometry and linear variation of fiber orientation, there is nothing new to discuss in this figure, as the varying fiber angle with θ_1 = 75°, θ_2 = 15° and θ_1 = 15°, θ_2 = 75° are exactly the same

problem, as are the cases $\theta_1 = 45°$, $\theta_2 = 75°$ and $\theta_1 = 75°$, $\theta_2 = 45°$. This will not be true for the elliptical geometry, but it does serve as double check on Figs. 5- 3a and 5- 3b and the results for the constant fibers in Fig. 4- 1c. Based on the results from either the developed equations or from Abaqus, and considering each sub-figure, it can be said that varying the fiber angle in a linear fashion with circumferential location does not result in more than a 10% increase or decrease of the fundamental frequency relative to the constant fiber angle cylinder for that sub-figure, i.e., the $\theta_1 = \theta_2$ case. However, the fundamental frequency does increase as θ_2 increases from 15 to 75°. Also, the fundamental frequency gradually increases as θ_1 increases from 15 to 75°. Based on Figs. 5- 3a, b, c, since the difference of the result for each specified laminate case from the non-simplified equation, simplified equation, and Abaqus is less than 10%, it can be said that the developed equations and Abaqus have good agreement with the fundamental frequencies for laminate $[\pm\vartheta/0/90]_{2S}$ circular cylinders.

Although the $[\pm\vartheta/0/90]_{2S}$ family displays good agreement between the developed equations and the results from Abaqus, the $[\pm\vartheta]_{4S}$ family exhibits some notable disagreements in specified cases. The disagreement will be discussed in the next chapter. In Fig. 5- 3d is shown the results of lamination sequences $[\pm\theta]_{4S}$ where $\theta_2 = 15°$ and $\theta_1 = 15$, 45, and 75°, respectively. For $\theta_2 = 15°$, $\theta_1 = 45°$ the difference between the simplified equation and Abaqus reaches about 9%, and for $\theta_2 = 15°$, $\theta_1 = 75°$ the difference between the simplified equation and Abaqus is 25%, a serious discrepancy. In Fig. 5- 3e is shown the results of lamination sequences $[\pm\vartheta]_{4S}$ where $\theta_2 = 45°$ and $\theta_1 = 15$, 45, and 75°, respectively, and the maximum difference occurs at $\theta_2 = 45°$ and $\theta_1 = 75°$ where the maximum difference is about 12%. In Fig. 5- 3f is shown the results of lamination sequences $[\pm\vartheta]_{4S}$ where $\theta_2 = 75°$ and $\theta_1 = 15$, 45, and 75°, respectively. Again, there is nothing new to discuss in this figure. If the $\theta_2 = 15°$, $\theta_1 = 75°$ case (and it complementary case $\theta_2 = 75°$, $\theta_1 = 15°$) of the $[\pm\vartheta]_{4S}$ laminate family could be ignored, it could be asserted that the simplified equation agrees reasonably well with the Abaqus calculations. Considering only the predictions from Abaqus, it can again be stated that varying the fiber angle in a linear fashion with circumferential location for the $[\pm\vartheta]_{4S}$ lamination sequence does not result in more than a 10% increase or decrease of the fundamental frequency relative to the constant fiber angle cylinder for that sub-figure, i.e., the $\theta_1 = \theta_2$ case. Interestingly, considering the results from Abaqus, the fundamental frequency decreases as θ_2 increases from 15 to 75° and it also decreases as θ_1 increases from 15 to 75°, trends opposite the $[\pm\vartheta/0/90]_{2S}$ cylinders of Figs. 5- 3a,

b, c. Overall, in terms of the fundamental frequency improvement, as predicted by the non-simplified equation, the simplified equation, and Abaqus, the large circular cylinder with the straight fiber laminate $[\pm 75/0/90]_{2S}$ has the highest fundamental frequency. The lowest fundamental frequency occurs for the cylinders with laminate $[\pm 45]_{4S}$, based on the simplified equation, and for the linearly varying fiber case with $\theta_2 = 75°$, $\theta_1 = 45°$ (and its complementary case $\theta_2 = 45°$, $\theta_1 = 75°$), based on the results of Abaqus. In all cases the fundamental frequency predicted by Abaqus is less than the fundamental frequency predicted by the simplified equation. This is consistent with previous findings.

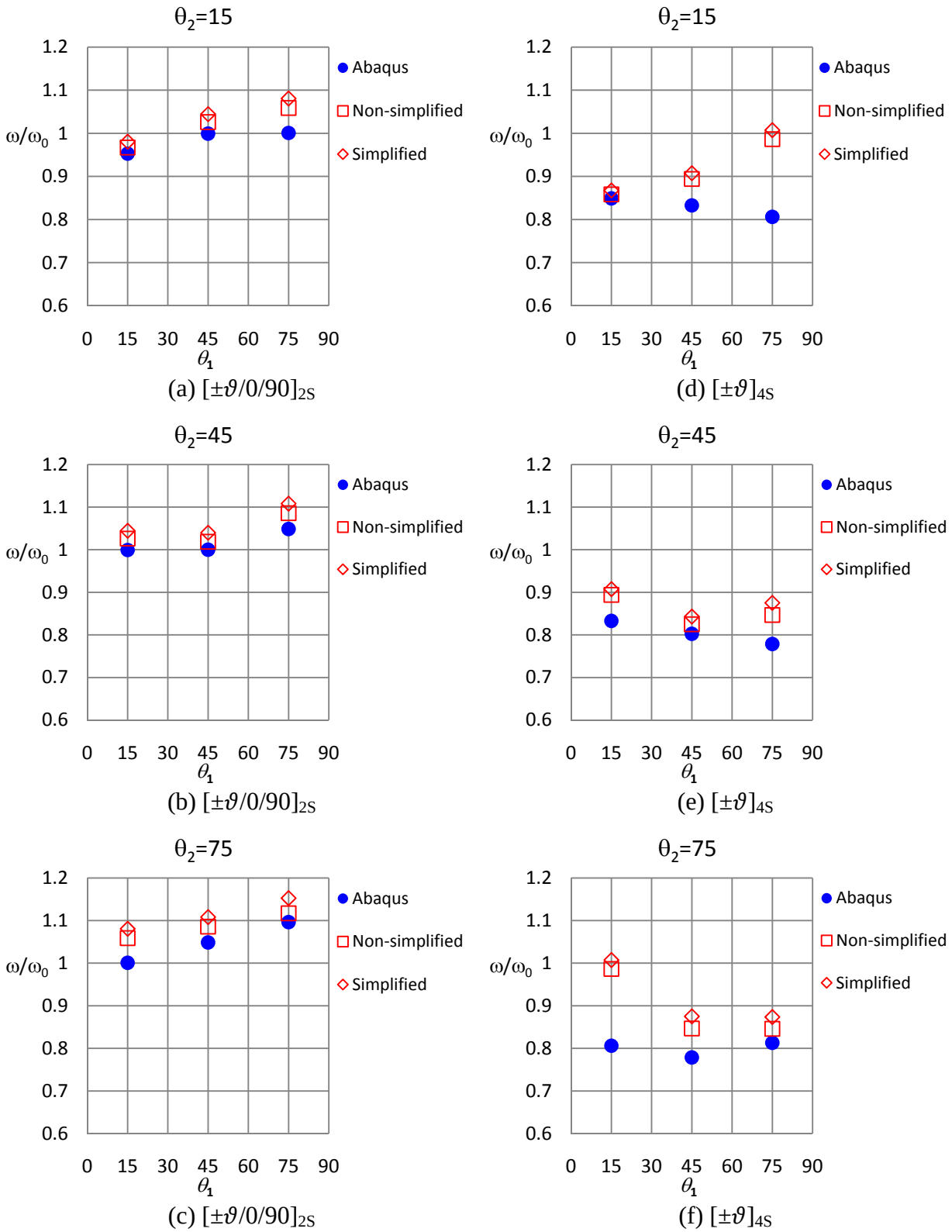

(a) $[\pm\vartheta/0/90]_{2S}$ (d) $[\pm\vartheta]_{4S}$

(b) $[\pm\vartheta/0/90]_{2S}$ (e) $[\pm\vartheta]_{4S}$

(c) $[\pm\vartheta/0/90]_{2S}$ (f) $[\pm\vartheta]_{4S}$

Fig. 5- 3 Normalized fundamental frequency of large circular cylinders with linearly varying fiber angle

In Fig. 5- 4 the normalized fundamental frequencies of large elliptical cylinders with b/a = 0.55 and with varying fiber angle ϑ are shown in the same format as Fig. 5- 3. The results from Abaqus, the non-simplified equation, the first simplified equation, the second simplified equation, and Lo's approximation are presented. In terms of developed equations, the developed equations have good agreement with each other and, in detail, the prediction of the non-simplified equation is close but a little lower than the prediction of the first simplified equation; the result from the second simplified equation is close but a little lower than Lo's approximation. Compared with the results from Abaqus, in most cases the fundamental frequencies from the developed equations are close but a little higher than those from Abaqus, and in few cases the fundamental frequencies from the second simplified equation are close but a little lower than those from Abaqus. That implies for the elliptical cylinders with b/a = 0.55, among all the developed equations, the results from the second simplified equation can be seen as closest to the results from Abaqus.

In terms of the $[\pm\vartheta/0/90]_{2S}$ laminate, the fundamental frequencies for lamination sequences with $\theta_2 = 15°$ and $\theta_1 = 15, 45, 75°$, $\theta_2 = 45°$ and $\theta_1 = 15, 45, 75°$, and $\theta_2 = 75°$ and $\theta_1 = 15, 45, 75°$ are presented in Fig. 5- 4a, Fig. 5- 4b, and Fig. 5- 4c, respectively. In Figs. 5- 4a to c the maximum difference between the results from the second simplified equation and Abaqus is less than 10% and the maximum difference occurs for the case of $\theta_2 = 75°$, $\theta_1 = 15°$. Unlike the $\theta_2 = 75°$, $\theta_1 = 15°$, case, the difference for the $\theta_2 = 15°$, $\theta_1 = 75°$, is less than 1%. Surprisingly, as was observed for the large circular cylinders in Fig. 5- 3, varying the fiber angle in a linear fashion with circumferential location does not result in more than a 10% increase or decrease of the fundamental frequency relative to the constant fiber angle cylinder for that sub-figure, i.e., the $\theta_1 = \theta_2$ case. In fact, any trends of increasing or decreasing fundamental frequency with increasing θ_1 or increasing θ_2 are weak for the large elliptical $[\pm\vartheta/0/90]_{2S}$ cylinders as compared to the trends for the large circular $[\pm\vartheta/0/90]_{2S}$ cylinders of Figs. 5- 3a, b, c. For the $[\pm\vartheta]_{4S}$ laminates, the fundamental frequencies for lamination sequences with $\theta_2 = 15°$ and $\theta_1 = 15, 45, 75°$, $\theta_2 = 45°$ and $\theta_1 = 15, 45, 75°$, and $\theta_2 = 75°$ and $\theta_1 = 15, 45, 75°$ are presented in Fig. 5- 4d, Fig. 5- 4e, and Fig. 5- 4f, respectively. In Figs. 5- 4d, e, f the maximum difference between the results from the second simplified equation and Abaqus reaches almost 26% and that maximum difference occurs for $\theta_2 = 75°$ and $\theta_1 = 15°$. For the $\theta_2 = 45°$, $\theta_1 = 15°$ and $\theta_2 = 75°$, $\theta_1 = 45°$ cases the differences are also as high as 13% and 14%, respectively. Surprisingly, the difference

for $\theta_2 = 15°$ and $\theta_1 = 75°$ is only about 5%, lower than the case $\theta_2 = 75°$ and $\theta_1 = 15°$. But, as mentioned, with the noncircular geometry these cases are not complements of one another. The highest fundamental frequency occurs with a varying fiber angle laminate $[\pm\vartheta/0/90]_{2S}$ with $\theta_2 = 75°$, $\theta_1 = 15°$ and $\theta_2 = 75°$, $\theta_1 = 45°$ based on the developed equation and on Abaqus, respectively. For the $[\pm\vartheta]_{4S}$ laminate the lowest fundamental frequency occurs for the constant fiber angle with $\vartheta = 45°$ or $\vartheta = 15°$, based on the developed equation or Abaqus, respectively. Considering just the Abaqus results, there is a weak dependence on the value θ_1 or θ_2.

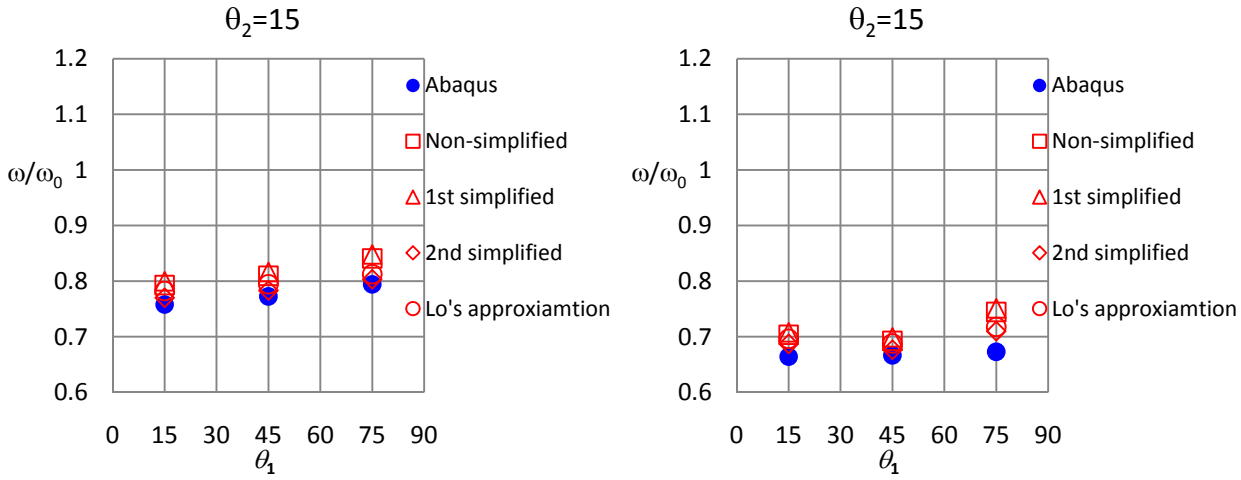

(a) $[\pm\vartheta/0/90]_{2S}$

(d) $[\pm\vartheta]_{4S}$

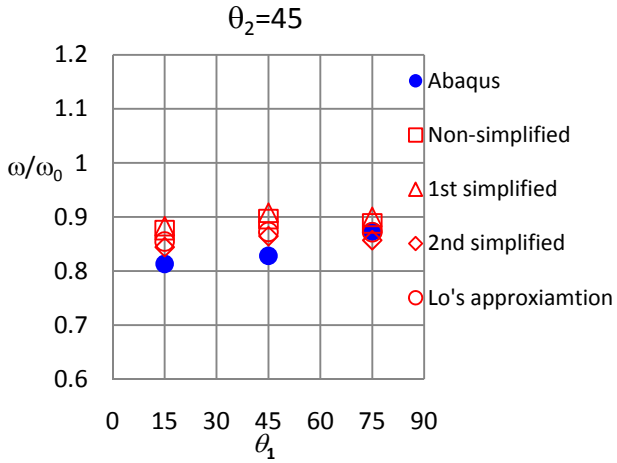

(b) $[\pm\vartheta/0/90]_{2S}$

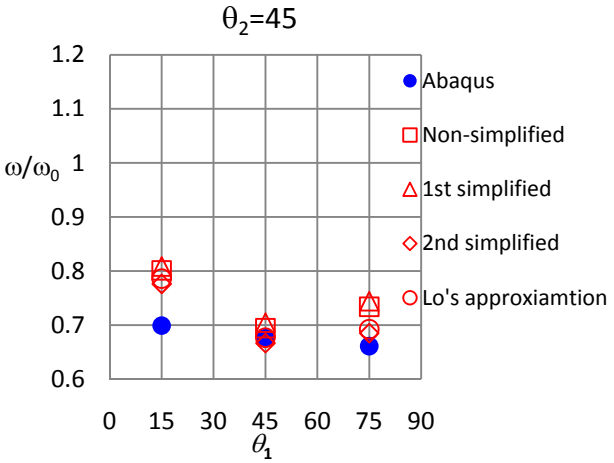

(e) $[\pm\vartheta]_{4S}$

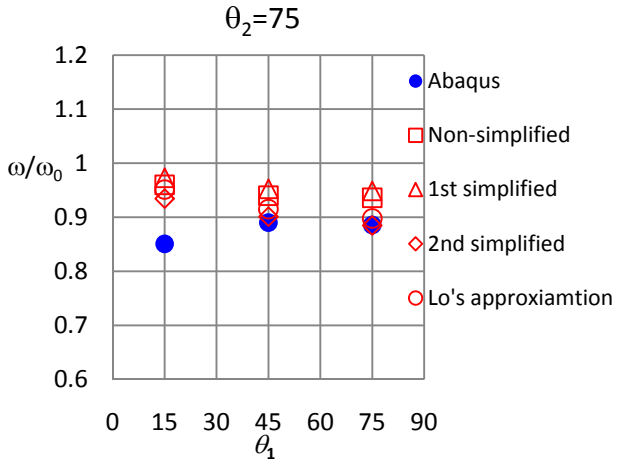

(c) $[\pm\vartheta/0/90]_{2S}$

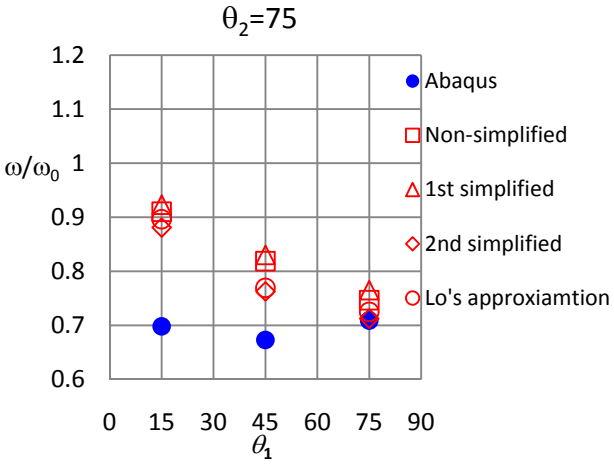

(f) $[\pm\vartheta]_{4S}$

Fig. 5- 4 Normalized fundamental frequency of large elliptical cylinders (b/a = 0.55) with linearly varying fiber angle

In Fig. 5- 5 is shown the normalized fundamental frequencies of small circular cylinders with linearly varying fiber angle. In Figs. 5- 5a, b, c the results for the $[\pm\vartheta/0/90]_S$ laminate are illustrated, whereas in Figs. 5- 5d, e, f the results for the $[\pm\vartheta]_{2S}$ laminate are presented. In each case the result from Abaqus is the lowest one and the result from the simplified equation is the highest one. The result from the non-simplified equation is between Abaqus and the simplified equation and 2~6% lower than the simplified equation, depending on the laminate. Though the predictions between the simplified equation and Abaqus for the $[\pm\vartheta/0/90]_S$ laminate family have a 12% difference for $\theta_2 = 75°$, $\theta_1 = 15°$ and $\theta_2 = 15°$, $\theta_1 = 75°$ cases, the trends in the three subfigures predicted by the non-simplified equation, by the simplified equation, and by Abaqus are generally the same. Compared to the large circular cylinders in Fig. 5- 3, for each value of θ_2 there is a more noticeable increasing trend of fundamental frequency with increasing θ_1. Comparing Figs. 5- 5d, e, f with Figs. 5- 3d, e, f, it can be stated that the sensitivity of the fundamental frequency of the small circular cylinders to increasing values of θ_1 and θ_2 is about the same as the sensitivity of the large circular cylinders. For the $[\pm\vartheta]_{2S}$ laminate family the maximum difference between Abaqus and the developed analysis occurs for the identical cases $\theta_2 = 15°$, $\theta_1 = 75°$ and $\theta_2 = 75°$, $\theta_1 = 15°$, where the difference is 26%. The second largest difference is 17% for the identical cases $\theta_2 = 45°$, $\theta_1 = 75°$ and $\theta_2 = 75°$, $\theta_1 = 45°$. The highest fundamental frequency occurs for constant fiber angle laminate $[\pm 75/0/90]_S$, independent of the method of prediction, and the lowest fundamental frequency occurs for constant fiber angle laminate $[\pm 15/0/90]_S$ or $[\pm 75]_{2S}$, depending on the method of prediction.

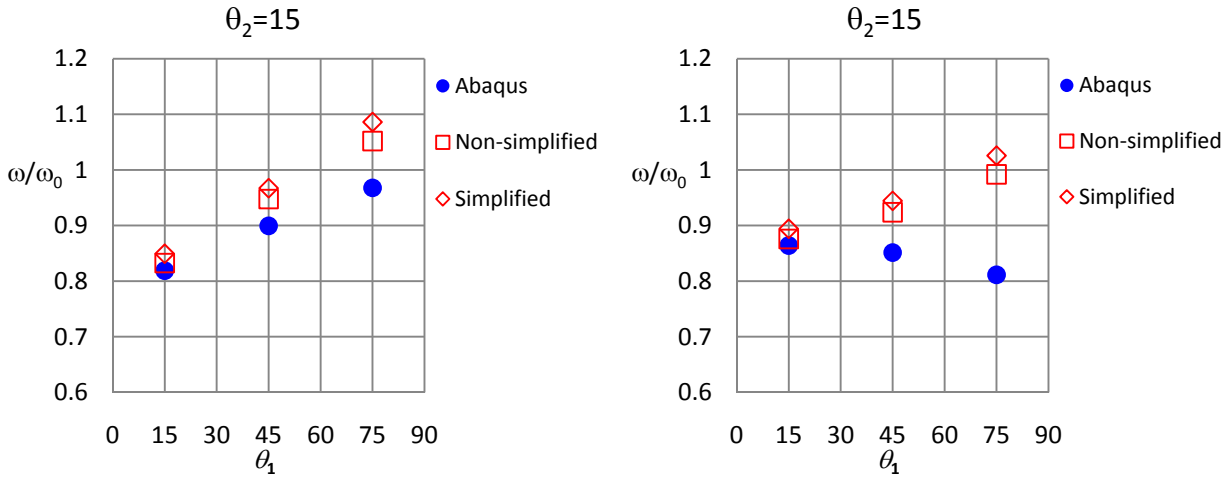

(a) $[\pm\vartheta/0/90]_S$

(d) $[\pm\vartheta]_{2S}$

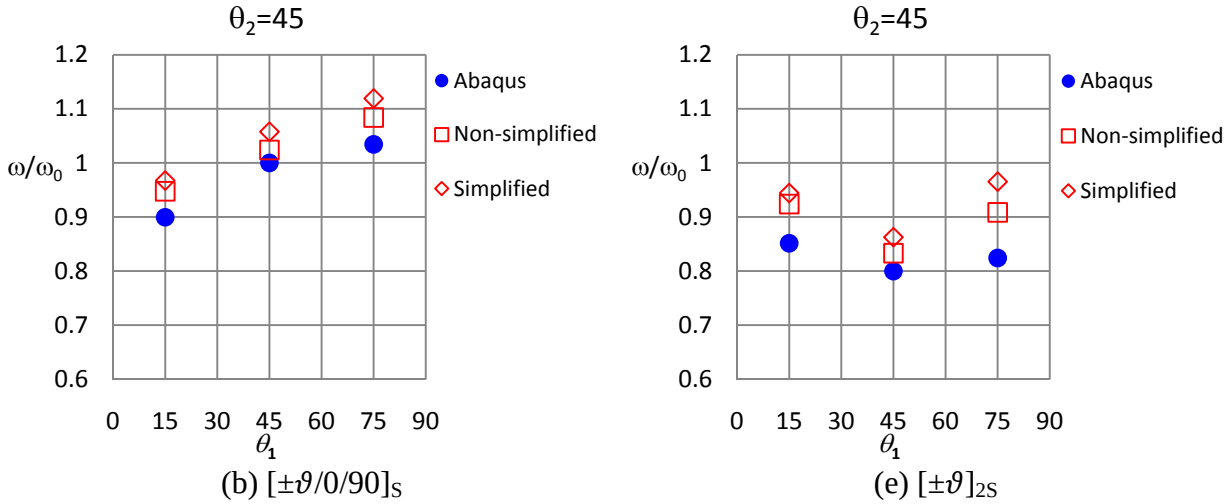

(b) $[\pm\vartheta/0/90]_S$

(e) $[\pm\vartheta]_{2S}$

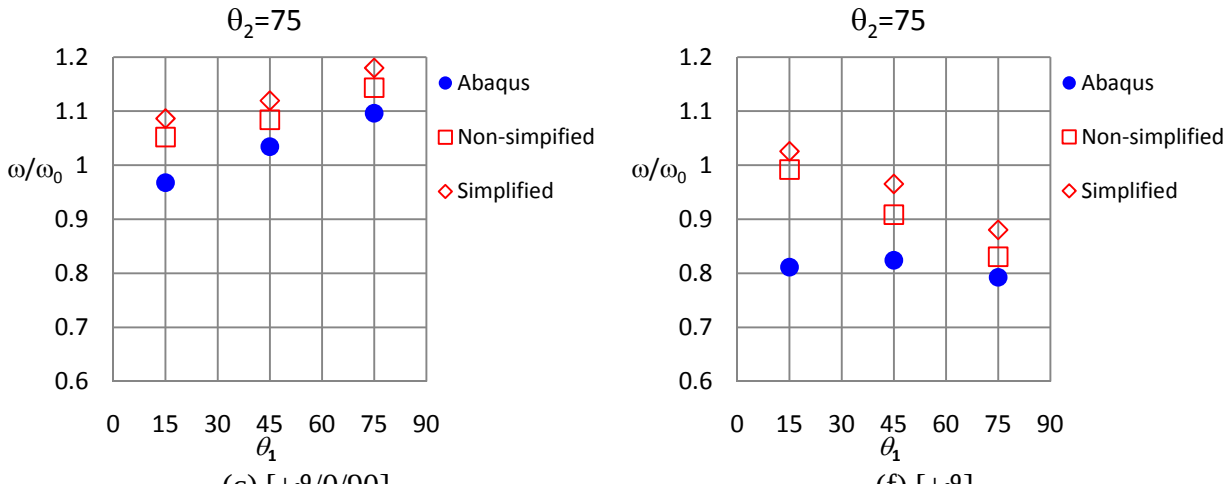

(c) $[\pm\vartheta/0/90]_S$

(f) $[\pm\vartheta]_{2S}$

Fig. 5- 5 Normalized fundamental frequency of small circular cylinders with linearly varying fiber angle

In Fig. 5- 6 the normalized fundamental frequencies of small elliptical cylinders are shown. The fundamental frequencies are predicted by Abaqus, the non-simplified equation, the first simplified equation, the second simplified equation, and Lo's approximation. Like the large elliptical cylinders, the prediction of the fundamental frequency from the non-simplified equation is very close but a little lower than that from the first simplified equation; the prediction of the fundamental frequency from the second simplified equation is very close but a little lower than that from Lo's approximate equation. Unlike the small circular cylinders, the predicted fundamental frequencies of the second simplified equation and Abaqus for most of the elliptical cylinders are close except for the $[\pm\vartheta]_{2S}$ laminate with $\theta_2 = 75°$, $\theta_1 = 15°$, a case for which the difference between the second simplified equation and Abaqus is 33%. The highest fundamental frequency occurs for varying fiber angle laminate $[\pm\vartheta/0/90]_S$ for $\theta_2 = 75°$, $\theta_1 = 45°$ (Lo's approximation,) or for $\theta_2 = 75°$, $\theta_1 = 45°$ (the non-simplified, the first simplified, or the second simplified equations,) or the constant fiber angle laminate $[\pm 75/0/90]_S$ (Abaqus), depending on the prediction tool. The lowest fundamental frequency occurs for the straight fiber laminate $[\pm 15/0/90]_S$ for both the simplified and Abaqus results. The sensitivities of the fundamental frequency to increasing values of θ_1 and θ_2 of the small elliptical $[\pm\vartheta/0/90]_S$ cylinders in Figs. 5- 6a, b, c are greater than for the corresponding large cylinders in Figs. 5- 4a, b, c. Considering only the Abaqus results, the lack of sensitivity of the small elliptical $[\pm\vartheta]_{2S}$ cylinders to values of θ_2 is about the same as for the large elliptical $[\pm\vartheta]_{4S}$ cylinders of Figs. 5- 4d, e, f. The same look of sensitivity holds for increasing values of θ_1.

Before considering further investigations into the effects of varying fiber angle, it might be better to determine the causes of the difference between the predictions of the developed equation and those of Abaqus. If those differences could be reduced, parameter studies as regards varying fiber angle would be much more efficient than with finite element analysis. In the next chapter some possible reasons for the discrepancies will be discussed.

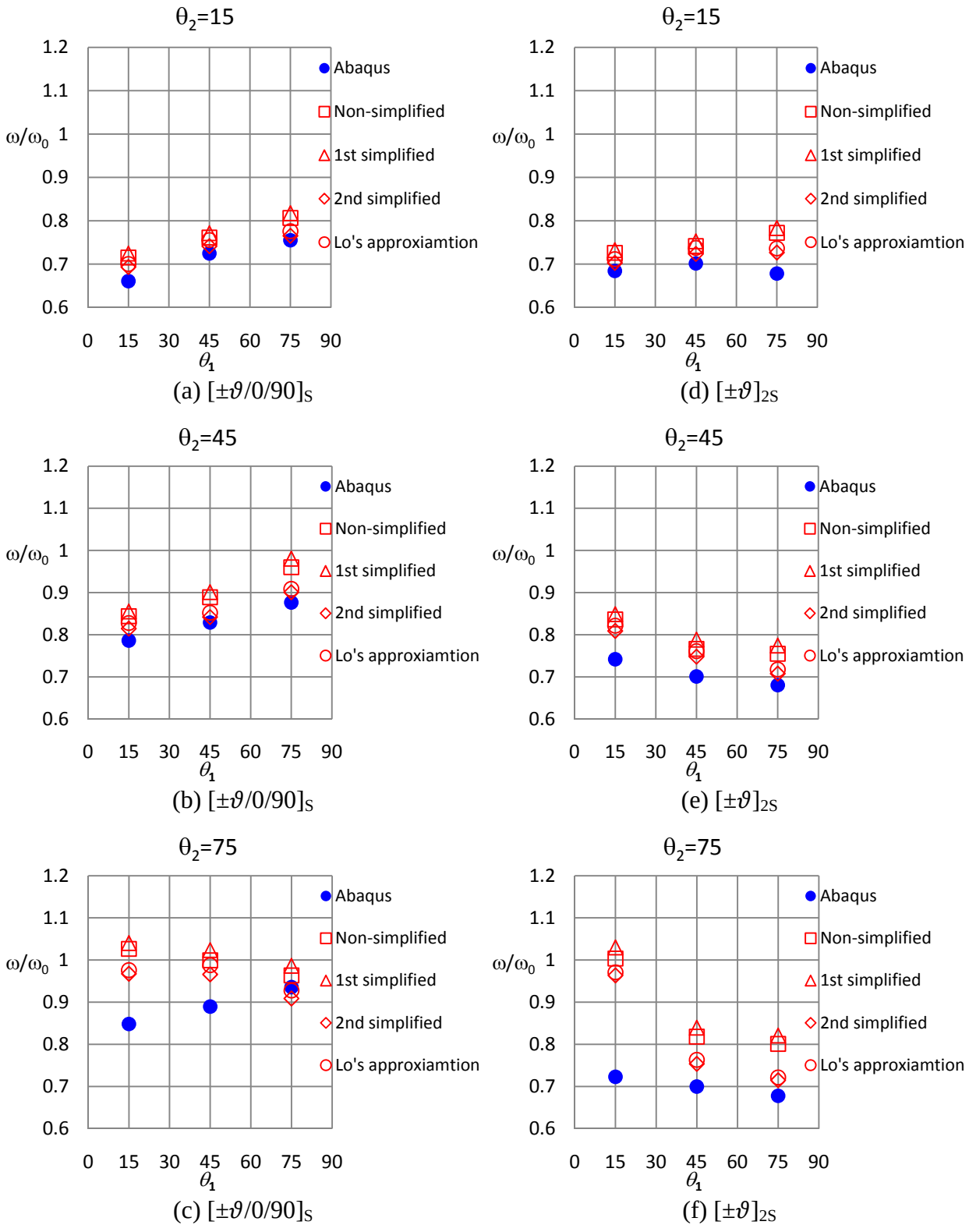

Fig. 5- 6 Normalized fundamental frequency of small elliptical cylinders (b/a = 0.55) with linearly varying fiber angle

Chapter 6 Discussion of Developed Analysis

As previously presented in the numerical results, for particular cases the differences between the fundamental frequency predictions using the developed analysis and the predictions using Abaqus are larger than desirable. There are two major cases that had errors of concerning levels and each of them is introduced in one the following sections. One case was the clamped support circular and elliptical cylinders with constant fiber orientation $\vartheta = 45°$ and lamination sequences $[\pm\vartheta]_{4S}$ and $[\pm\vartheta]_{2S}$, referred to as large and small cylinders, respectively (Figs. 4- 2e, 4- 4e, 4- 6e, and 4- 8e). Considering that for the most part large and small cylinders with similar lamination sequences have similar behaviors, only the large cylinders are discussed here (Figs. 4- 2e and 4- 6e). Further, considering that the developed analysis for circular cylinders with clamped supports with lamination sequences $[\pm15]_{4S}$ and $[\pm75]_{4S}$ had better agreement with Abaqus than the developed analysis for elliptical cylinders with the same boundary conditions and laminates, elliptical cylinders with clamped supports and lamination sequences $[\pm15]_{4S}$, $[\pm45]_{4S}$, and $[\pm75]_{4S}$ are selected for further discussion in the first subsection to follow (Figs. 4- 6d, e, f). The discussion will center on the variation with the axial coordinate of the normal displacement characteristics of the mode shapes. The other case with error levels of concern occurred with the simply-supported cylinders for lamination sequence $[\pm\vartheta]_{4S}$ and linearly varying fiber angle, with $\theta_1 = 15°$ and $\theta_2 = 75°$. Though the developed equations and Abaqus have the largest difference for elliptical cylinder with $\theta_1 = 15°$ and $\theta_2 = 75°$, by using a circular cylinder it is easier to explain why there is a difference. Therefore, in the second subsection to follow, the normal displacement characteristics of the mode shapes of circular cylinders with linearly varying fiber angle with $\theta_1 = 15°$, $\theta_2 = 75°$ and $\theta_1 = 75°$, $\theta_2 = 15°$ are discussed (Figs. 5- 3d, f). The discussion will focus on the difference between the circumferential variation of the normal displacement assumed in the developed analysis and that computed by Abaqus. Following is a discussion for varying fiber angle cylinders regarding the relation between the assumed function in the circumferential direction and agreement of Abaqus and the developed equation. In the last section of this chapter a discussion for Lo's approximation is presented.

6.1 Limit of Clamped Supported Cylinders

In terms of the mode shapes of the fundamental frequencies, each circumferential wave number n refers to two different vibration mode shapes. In Section 3.2 they were referred to as cosine- and sine-based vibration modes. Though in Abaqus there is nothing to specify particular functional forms of the mode shape, the variation of normal displacement around the circumferential direction appeared either cosine-like or sine-like in shape. In Fig. 6- 1 the circumferential location $s = 0$ is illustrated by the blue axial line and the red line illustrates the location $s = C/4$, a quarter way around the circumference. For fundamental frequencies with even n, the cosine-shape vibration mode has its largest amplitude of normal displacement at $s = 0$ and $s = C/2$, and the lowest amplitude of normal displacement is at $s = C/4$ and $s = 3C/4$. Considering odd n, the cosine-shape vibration mode also has its largest amplitude of normal displacement at $s = 0$ and $C/2$, but the normal displacements at $s = C/4$ and $s = 3C/4$ are zero. On the other hand, for odd n the sine-shape vibration mode has a nonzero amplitude of normal displacement at $s = C/4$ and $s = 3C/4$. Therefore, in this section, for odd n the normal displacement at $s = 0$ is discussed in relation to the cosine-shape vibration mode, and for even n the normal displacement at $s = C/4$ is discussed in relation to the sine-shape vibration mode. It is assumed that the cylinder length doesn't affect the shape of the normalized normal displacement.

Consider the normal displacement along $s = 0$ first. When the cylinder length is $0.5C$, the aspect ratio b/a is 0.55, and the lamination sequence is $[\pm 15]_{4S}$ (Fig. 4- 6d), a circumferential wave number of $n = 7$ for the fundamental frequency is predicted by both the developed analysis and Abaqus for the clamped support elliptical cylinder. So the correlation is good in that regard. The variation of the normal displacement in the axial direction, however, is a concern. For this case the normal displacement along $s = 0$ is normalized by the maximum displacement along $s = 0$ and is plotted in Fig. 6- 2. In Fig. 6- 2 the red line represents the assumed function in the developed analysis χ_0 in Section 3.1.2 and the green line is the displacement as computed by Abaqus. It can be observed that even though Abaqus is programmed to use clamped support boundary conditions at the cylinder ends, the slope of the normal displacement in the axial direction does not appear to be zero in the vicinity of $x = 0$ and $x = L$, whereas the assumed function χ_0 clearly shows a zero slope at the vicinity of the cylinder ends. This suggests that transverse shear deformations were more important than assumed for the calculation of the

fundamental frequency. To determine if indeed transverse shear deformations were more important than assumed, particularly at the cylinder ends, a large value of transverse shear modulus was used with Abaqus, but with no influence on the fundamental frequency calculated by Abaqus.

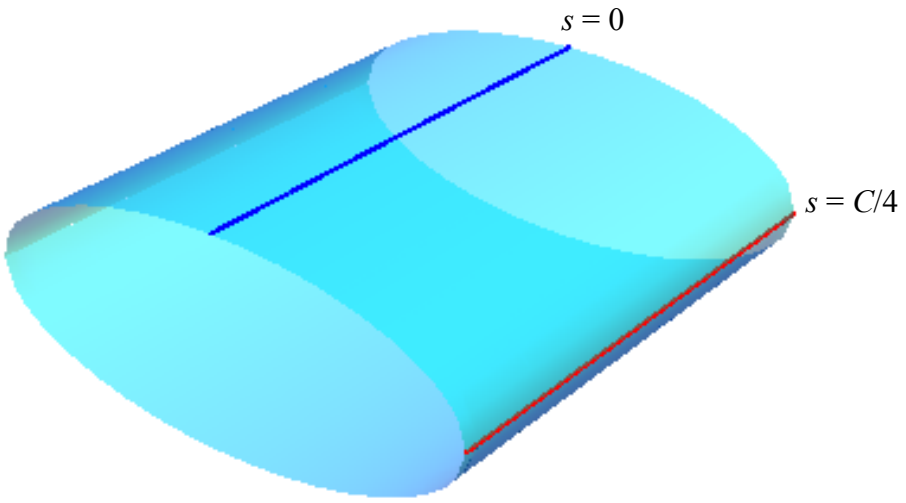

Fig. 6- 1 Circumferential positions of $s = 0$ (blue line) and $s = C/4$ (red line)

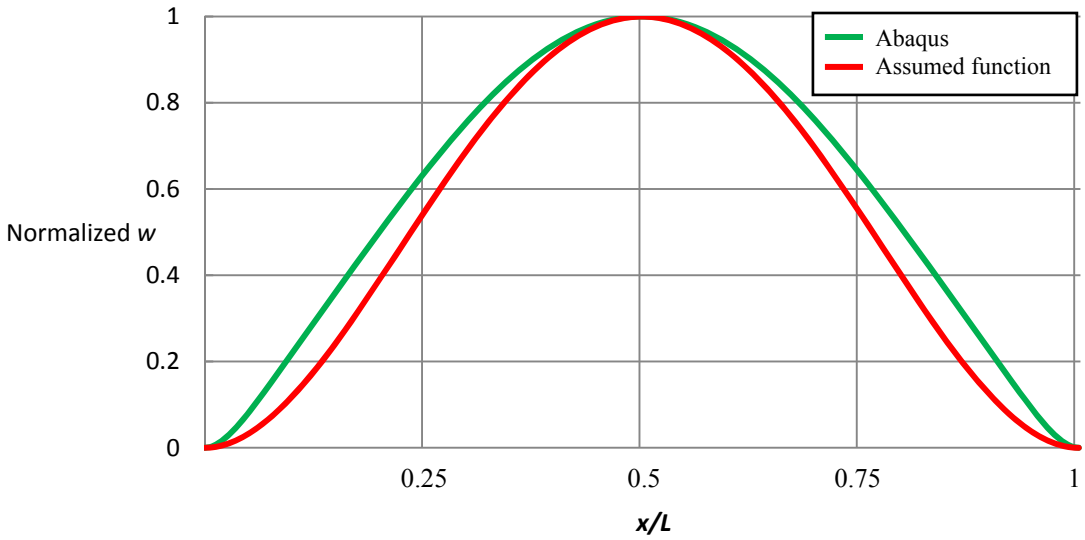

Fig. 6- 2 Normalized normal displacement of elliptical cylinders along $s = 0$ ($b/a = 0.55$, $L = 0.5C$, $[\pm 15]_{4S}$, clamped supports, Fig. 4- 6d)

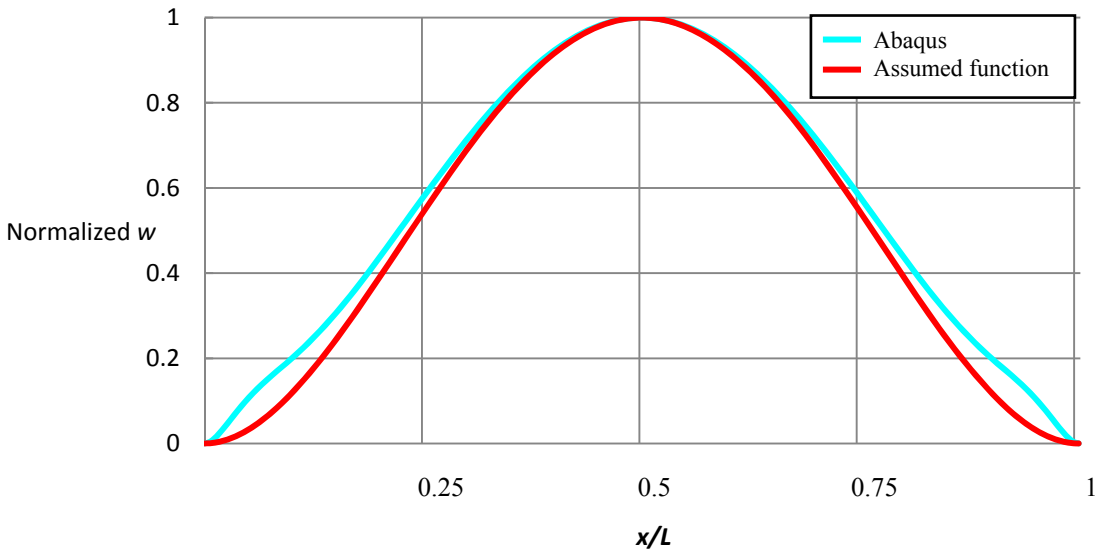

Fig. 6- 3 Normalized normal displacement of elliptical cylinders along $s = 0$ ($b/a = 0.55$, $L = 0.5C$, $[\pm 45]_{4S}$, clamped supports, Fig. 4- 6e)

Considering the same cylinder geometry as in Fig. 6- 2, that is, a cylinder length of $0.5C$, aspect ratio b/a =0.55, but with lamination sequence $[\pm 45]_{4S}$ (Fig. 4- 6e), the circumferential wave number of the fundamental frequency is n = 5. As in Fig. 6- 2 the normalized normal displacement is normalized by its maximum displacement along $s = 0$ for this case and is shown in Fig. 6- 3. In Fig. 6- 3 the red line again represents the assumed function χ_0 in Section 3.1.2 and the cyan line is the displacement computed by Abaqus. Again the displacement calculated by Abaqus shows little evidence of zero slope in the vicinity of the cylinder ends, and furthermore, close to each end the displacement computed by Abaqus has the local convex nature, which, when compared with Fig. 6- 2, suggests that the detailed characteristics of the axial variation of the normal displacement are dependent on the materials properties.

Considering the same elliptical cylinder, but with lamination sequence is $[\pm 75]_{4S}$ (Fig. 4- 6f), the circumferential wave number of the fundamental frequency is n = 4. In Fig. 6- 4 the red line again represents the assumed function χ_0 in Section 3.1.2 and the purple line is the displacement as computed by Abaqus. Compared with cases of $[\pm 15]_{4S}$ and $[\pm 45]_{4S}$, the results from the assumed function and results as computed by Abaqus have better overall agreement for the $[\pm 75]_{4S}$ laminate. This again suggests that the characteristics of the normal displacement depend on the material properties.

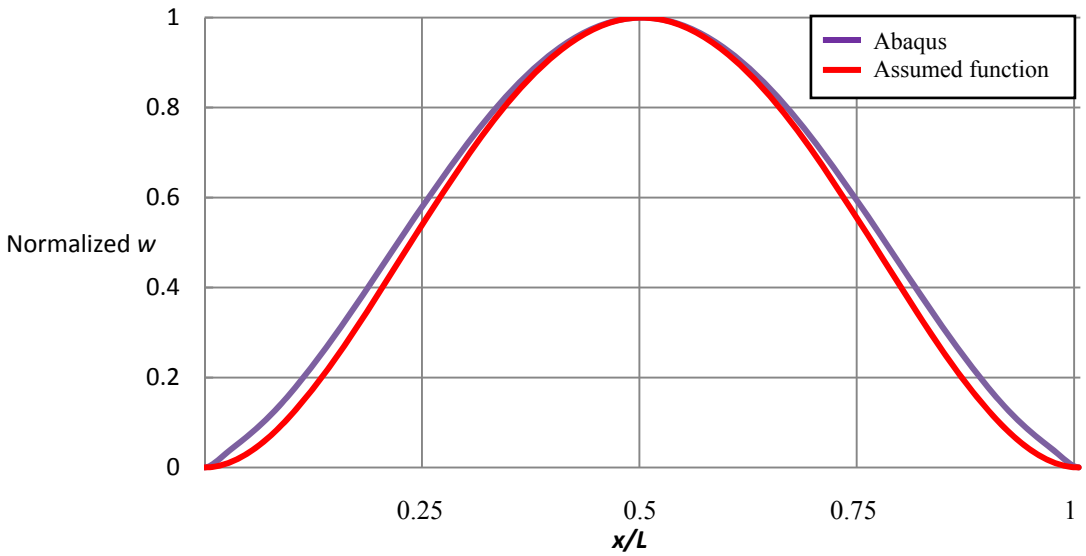

Fig. 6- 4 Normalized normal displacement of elliptical cylinders along $s = 0$ ($b/a = 0.55$, $L = 0.5C$, $[\pm 75]_{4S}$, clamped supports, Fig. 4- 6f)

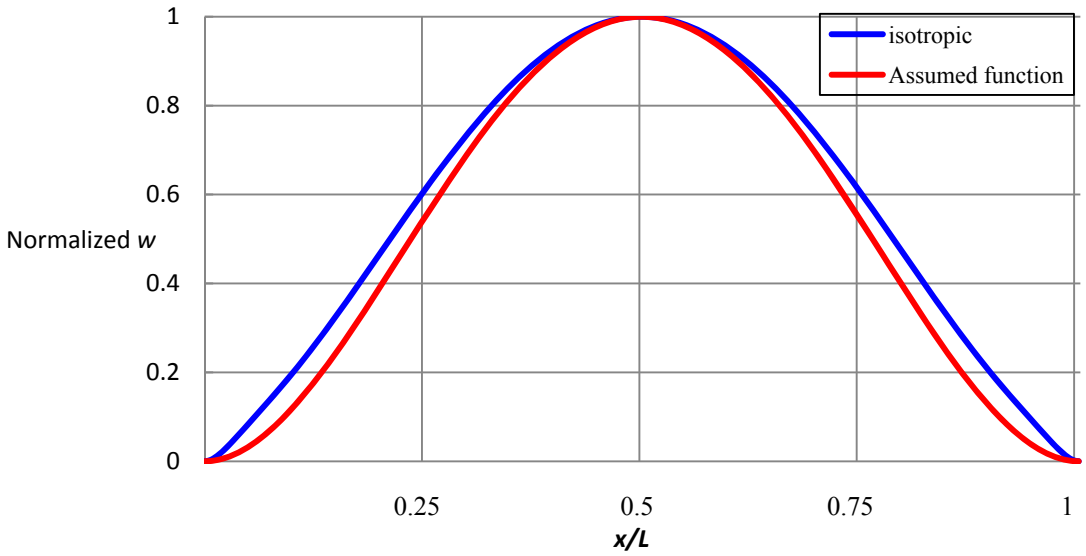

Fig. 6- 5 Normalized normal displacement of elliptical cylinders along $s = 0$ ($b/a = 0.55$, $L = 0.5C$, isotropic, clamped supports)

Considering the same geometry cylinder, but with an isotropic material with a Young's modulus of 130 GPa, which is the fiber-direction modulus for a layer of the composite material being considered (see Table 4- 5), and a Poisson's ratio of 0.3, the corresponding n is 6 and the

shape of the normalized displacement is also different from either $[\pm 15]_{4S}$, $[\pm 45]_{4S}$, or $[\pm 75]_{4S}$, as shown in Fig. 6- 5.

It is important to also consider the axial variation of the normal displacements of these same three cylinders along $s = C/4$. As mentioned, for the odd mode number n, which characterizes the $[\pm 15]_{4S}$ ($n = 7$) and the $[\pm 45]_{4S}$ ($n = 5$) cylinders, it is necessary to consider the sine-based developed analysis rather than the cosine-based analysis. The normalized normal displacements of the elliptical clamped supported cylinder with length $0.5C$, aspect ratio $b/a = 0.55$, and lamination sequence is $[\pm 15]_{4S}$ (Fig. B- 2d,) is illustrated in Fig. 6- 6. As before, in Fig. 6- 6 the red line represents the assumed function χ_0 in Section 3.1.2 and the green line is the displacement as computed by Abaqus. The characteristics of the normal displacement at $s = C/4$ based on Abaqus and the assumed function have a better agreement than the cases of $s = 0$, Fig. 6- 2. For the $[\pm 45]_{4S}$ cylinder, in Fig. 6- 7, though the locally convex regions still exist close to the boundaries of the cylinders, the agreement at $s = C/4$ between the normal displacements as computed by Abaqus and by the assumed function is better overall than at $s = 0$, Fig. 6- 3.

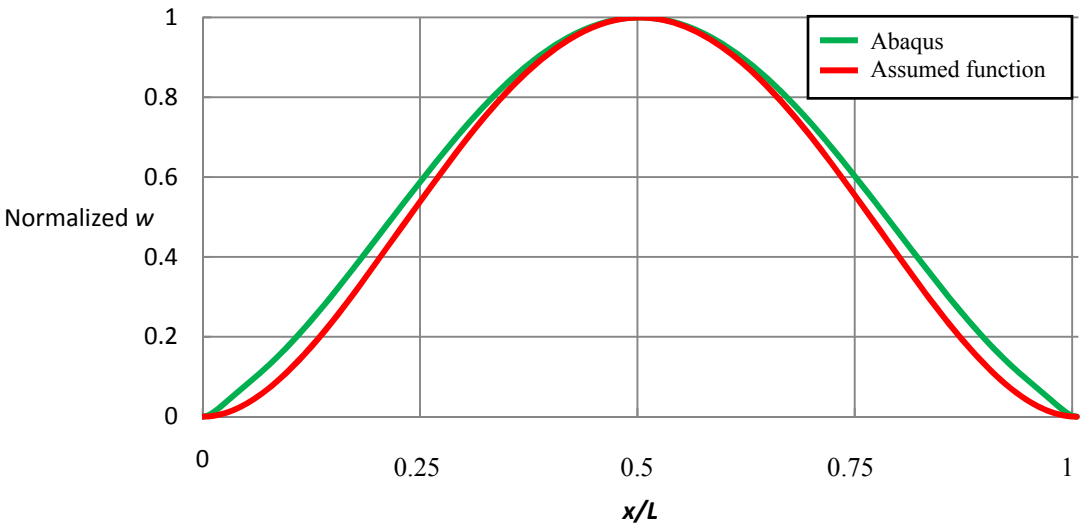

Fig. 6- 6 Normalized normal displacement of elliptical cylinders along $s = C/4$ ($b/a = 0.55$, $L = 0.5C$, $[\pm 15]_{4S}$, clamped supports, Fig. B- 2d)

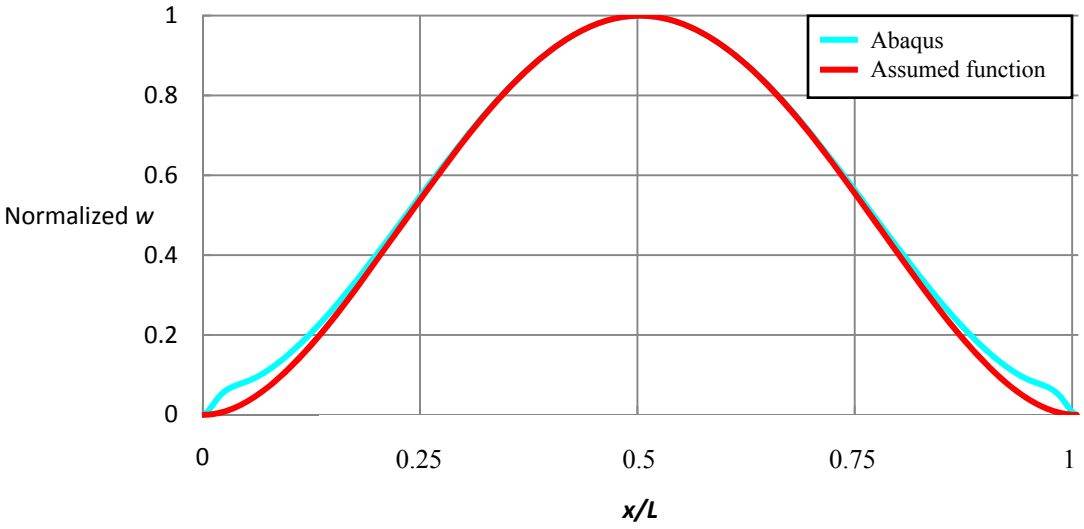

Fig. 6- 7 Normalized normal displacement of elliptical cylinders along $s = C/4$ ($b/a = 0.55$, $L = 0.5C$, $[\pm 45]_{4S}$, clamped supports, Fig. B- 2e)

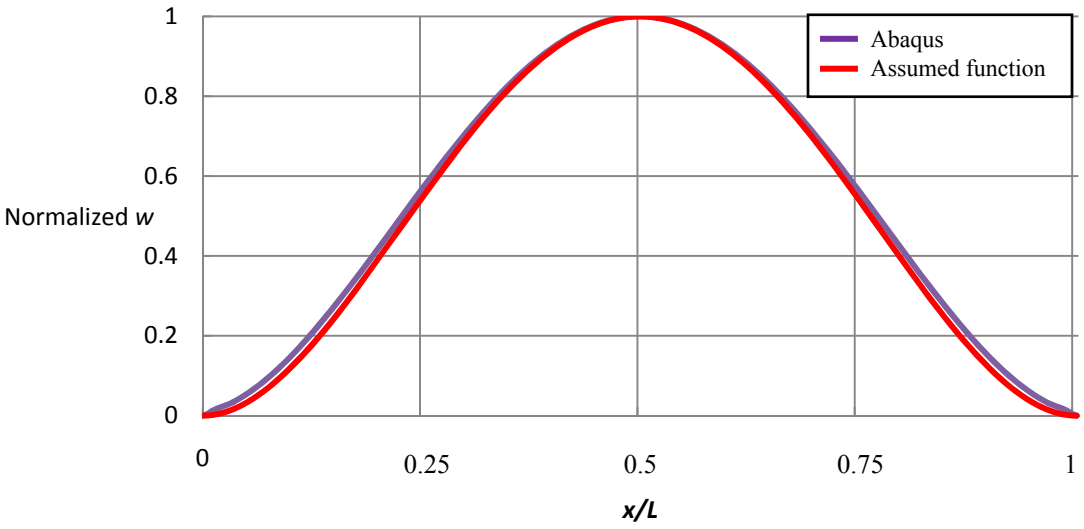

Fig. 6- 8 Normalized normal displacement of elliptical cylinders along $s = C/4$ ($b/a = 0.55$, $L = 0.5C$, $[\pm 75]_{4S}$, clamped supports, Fig. 4- 6f)

For the lamination sequence $[\pm 75]_{4S}$, since the mode number is even ($n = 4$), the cosine-based developed analysis is considered along with the results computed by Abaqus. In Fig. 6- 8 the red line represents the assumed function for the normal displacement and the purple line is

the normal displacement as computed by Abaqus. The agreement is better than at $s = 0$, Fig. 6- 4, even though upon close inspection the slopes in the vicinity of the ends do not match.

Considering a stiff isotropic cylinder (E =130GPa, ν =0.3), in Fig. 6- 9 the assumed normalized displacement at $s = C/4$ agrees quite well with the displacement computed by Abaqus, better than $s = 0$ in Fig. 6- 5.

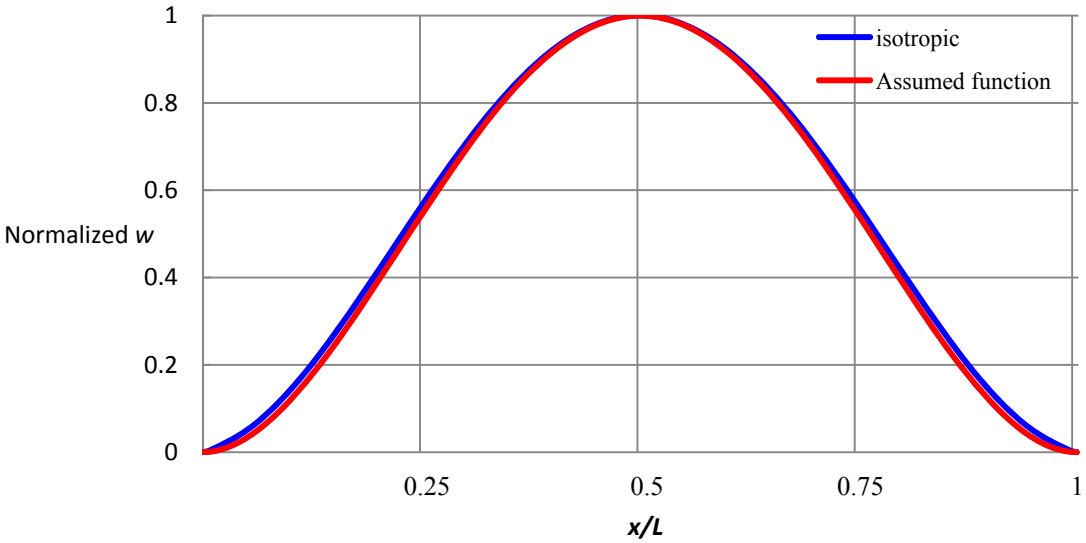

Fig. 6- 9 Normalized normal displacement of elliptical cylinders along $s = C/4$ ($b/a = 0.55$, $L = 0.5C$, isotropic, clamped supports)

As another comparison, the fundamental frequencies for the cylinders considered in Figs. 6- 2 through 6- 9 are listed in Table 6- 1. The frequencies have been normalized by ω_0=630 rad/s, as discussed relative to Table 4- 6. The fidelity of the axial variation of the normal displacement component is reflected in the frequency comparisons. As a reference, the fundamental frequencies of these same cylinders but for simple supports are listed in Table 6- 2. Interestingly, for the $[\pm 45]_{4S}$ case and simple supports, the error is the smallest of the four cylinders, in contrast to the clamped cylinders for which the $[\pm 45]_{4S}$ cylinder exhibits the largest error. So, it can be concluded that for the constant fiber angle case when the normal displacements as predicted by

assumed function χ_0 shown in Section 3.1.2 and those calculated by Abaqus have good agreement, the corresponding natural frequencies are close. When the function χ_0 does not correlate well with the normal displacement computed by Abaqus, the corresponding natural frequencies do not agree.

Table 6- 1 Normalized fundamental frequencies based on Abaqus and Lo's approximation, clamped supports

	Abaqus	Lo's approximation	$\%_{\text{difference}}$
$[\pm 15]_{4S}$	0.860	0.966	12.33
$[\pm 45]_{4S}$	0.986	1.164	18.05
$[\pm 75]_{4S}$	0.997	1.029	3.21
isotropic	1.901	2.04	7.31

$$\%_{\text{difference}} = \frac{\omega_{\text{Lo's approximation}} - \omega_{\text{Abaqus}}}{\omega_{\text{Abaqus}}} \times 100\%$$

Table 6- 2 Normalized fundamental frequencies based on Abaqus and Lo's approximation, simple supports

	Abaqus	Lo's approximation	$\%_{\text{difference}}$
$[\pm 15]_{4S}$	0.664	0.696	4.82
$[\pm 45]_{4S}$	0.676	0.678	0.296
$[\pm 75]_{4S}$	0.709	0.728	2.68
isotropic	1.381	1.460	7.27

$$\%_{\text{difference}} = \frac{\omega_{\text{Lo's approximation}} - \omega_{\text{Abaqus}}}{\omega_{\text{Abaqus}}} \times 100\%$$

6.2 Limit of Linear Fiber Angle Tailoring in Circular Cylinders with Simple Supports

Concerning the noticeable difference between the predictions of the developed analysis and the calculations from Abaqus for the case of a simply-supported circular cylinder with lamination sequence $[\pm\vartheta]_{4S}$ with ϑ varying linearly with circumferential position: In Fig. 6- 10 the axial variation of the normalized normal displacements (1) at $s = 0$ for $\theta_1 = 15°$, $\theta_2 = 75°$, (2) at $s = C/4$ for $\theta_1 = 15°$, $\theta_2 = 75°$, (3) at $s = 0$ for $\theta_1 = 75°$, $\theta_2 = 15°$, and (4) $s = C/4$ and $\theta_1 = 75°$, $\theta_2 = 15°$ as assumed in the developed analysis and as computed by Abaqus are presented. All the characteristics of the normalized normal displacements are normalized by their own maximum number respectively. It can be seen that all the normalized normal displacements, whether from Abaqus or from the assumed function, and independent of the values of θ_1 and θ_2, are identical, as they should be. Therefore, errors in the fundamental frequency predictions of the circular cylinders for the case of linearly varying fiber angle are not caused by the assumed axial function.

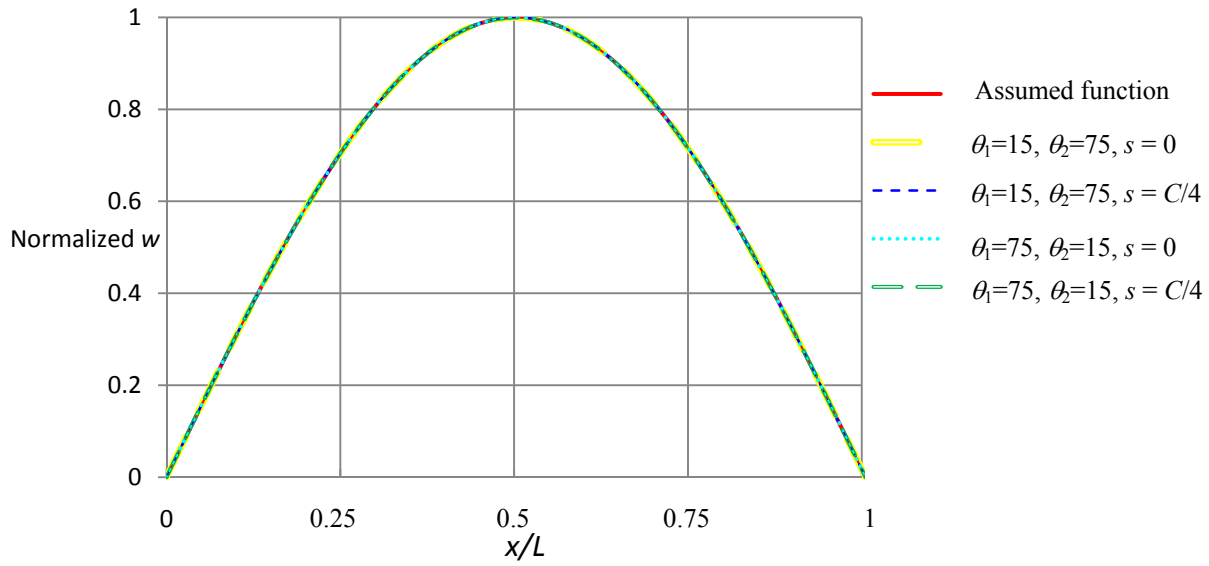

Fig. 6- 10 Normalized normal displacement of simply-supported circular cylinders with linearly varying $[\pm\vartheta]_{4S}$ laminate ($L = 0.5C$)

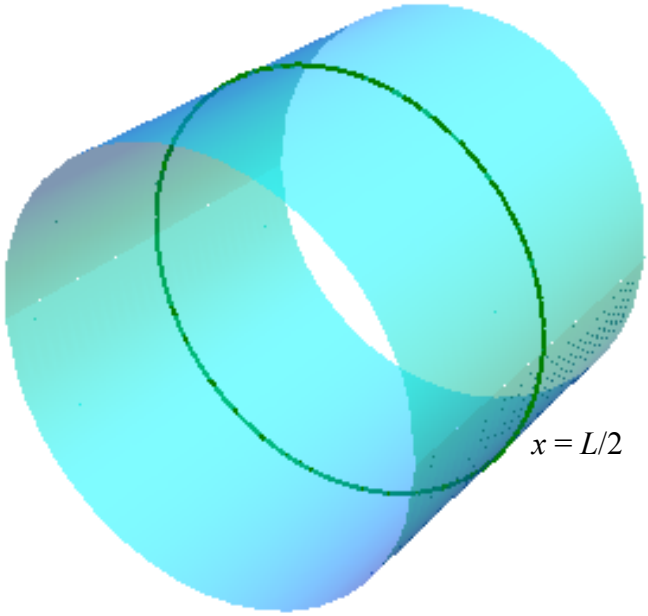

Fig. 6- 11 Positions of $x = 0.5L$

Considering, then, the variation of normal displacement with respect to the circumferential coordinate, the normal displacement around the cylinder at the location $x = L/2$, shown in Fig. 6-11, is discussed. Though there is no difference between the assumed circumferential variation of the normal displacement and the variation as computed by Abaqus for cosine- and sine-shapes and circular cylinders with constant fiber orientation, there is some difference for circular cylinder with varying fiber orientation. Considering the cosine-shape vibration mode as shown in Fig. 6- 12, where $\theta_1 = 75°$ and $\theta_2 = 15°$, it can be seen that the normalized displacement based on the assumed function does not totally agree with the results from Abaqus, where the normalized displacement is normalized by the maximum value from Abaqus. Whereas the assumed function is such that each wave has the same length, the displacement based on Abaqus shows a sense of varying wave length as the fiber orientation changes with circumferential location. Since $\vartheta = 15°$ at $s = 0$, $C/2$ and $\vartheta = 75°$ at $s = C/4$, $3C/4$, it can be observed the larger fiber angle, the longer wave length. Moreover, based on the Abaqus calculations, the amplitude of the normal displacement changes with the varying fiber angle as well. The lower ϑ, the larger the amplitude. In Fig. 6- 12 there are three values of the peaks of the normal displacement as computed by Abaqus. The smallest peak is about 92% of the next largest peak, which is also about 92% of the largest peak, and it should be noted that the normalized maximum amplitude is

unity. Regarding the change of wave length, there are also three different half lengths. Compared with the fixed wave length, the shortest one, the next shortest one, and the longest one become 78.7%, 92.6%, and 117.7%, respectively. In terms of the cosine-shape vibration mode as shown in Fig. 6- 13 where $\theta_1 = 15°$ and $\theta_2 = 75°$, though there is slight difference relative to Fig. 6- 12, it also shows the larger fiber angle, the longer wave length as well as the larger fiber angle, the smaller the amplitude.

As the varying fiber angle is considered, the normalized normal displacement based on Abaqus as shown in Fig. 6- 12 cannot be approached by shifting, inverting, or rotating that in Fig. 6- 13. However, because of the axisymmetric nature of the geometry of the circular cylinder, it could be expected that there exists a match for Fig. 6- 12. The reason a match cannot be made is the physical fact that the cosine mode vibration with odd n for $\theta_1 = 75°$ and $\theta_2 = 15°$ is the same as the sine mode vibration with the same n for $\theta_1 = 15°$ and $\theta_2 = 75°$. As shown in Fig. 6- 14, the phase shift between these two different vibration shapes is $C/4$.

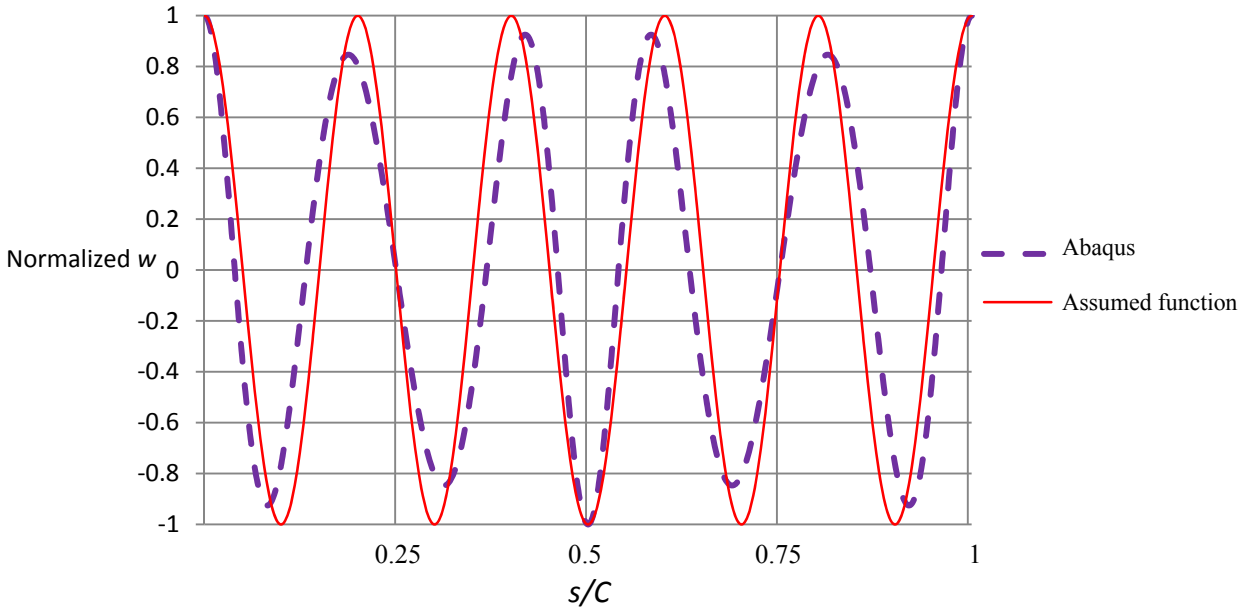

Fig. 6- 12 Normalized normal displacement of circular cylinders at $x/L = 0.5$ with linearly varying $[\pm\vartheta]_{4S}$ laminate where $\theta_1 = 75°$ and $\theta_2 = 15°$ based on cosine-shape ($L = 0.5C$, simple supports)

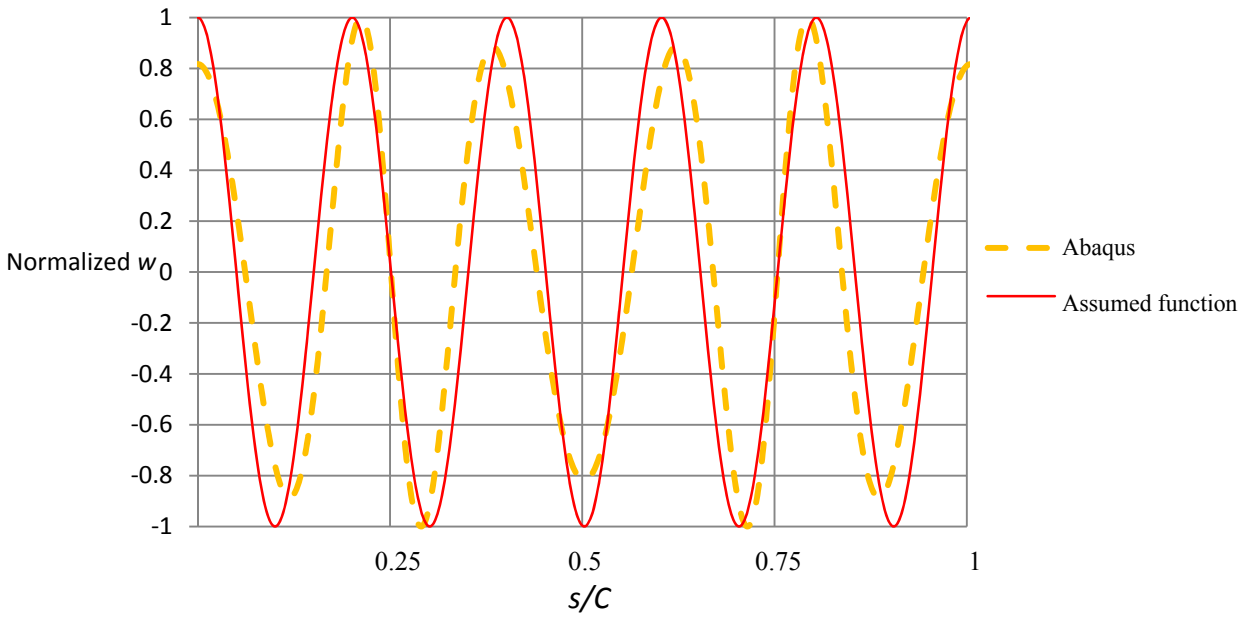

Fig. 6- 13 Normalized normal displacement of circular cylinders at $x/L = 0.5$ with linearly varying $[\pm\vartheta]_{4S}$ laminate where $\theta_1 = 15°$ and $\theta_2 = 75°$ based on cosine-shape ($L = 0.5C$, simple supports)

In summary, Abaqus calculations reflect (1) the variation of amplitude with circumferential position, (2) the variation of wave length with circumferential position, and (3) the phase shift of $\pi/2$ between the cosine-based functional dependence and the sine-based functional dependence. The developed analysis cannot characterize the variation of amplitude or the variation with wave length with circumferential position. Both the amplitude and wave length are constant with respect to circumferential position. The developed analysis can, however, reflect the phase shift of $\pi/2$ between the cosine-based functional dependence and the sine-based functional dependence, essentially only one of the three important characteristics. It is for this lack of the accurate representation of the variation of amplitude and wave length with the functions of the developed analysis that there is an error in the fundamental frequency predictions of the developed analysis.

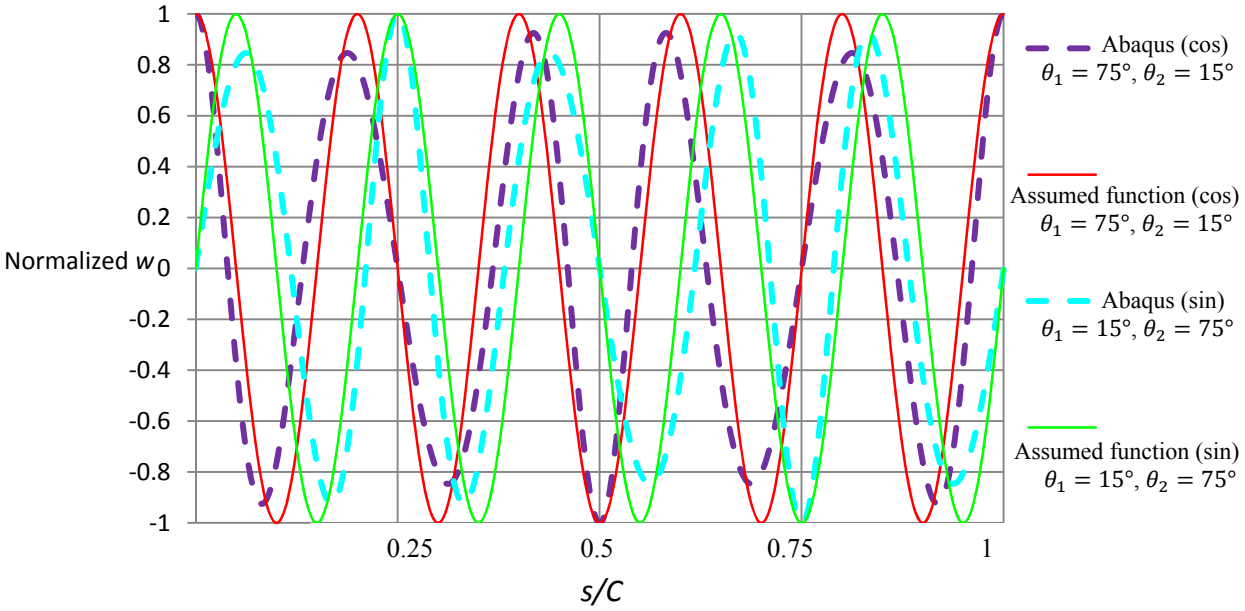

Fig. 6- 14 Normalized normal displacement of circular cylinders at $x/L = 0.5$ with linearly varying $[\pm\vartheta]_{4S}$ laminate ($L = 0.5C$, simple supports)

As can be seen in Figs. 6- 15, 6- 16, and 6- 17, which are provided for purposes of comparison, for the circular cylinders the assumed normal displacement function agrees well with the Abaqus calculations for constant fiber angle lamination sequences $[\pm 15]_{4S}$, $[\pm 45]_{4S}$, and $[\pm 75]_{4S}$, respectively, in contrast to the variable fiber angle orientation cases illustrated in the last three figures.

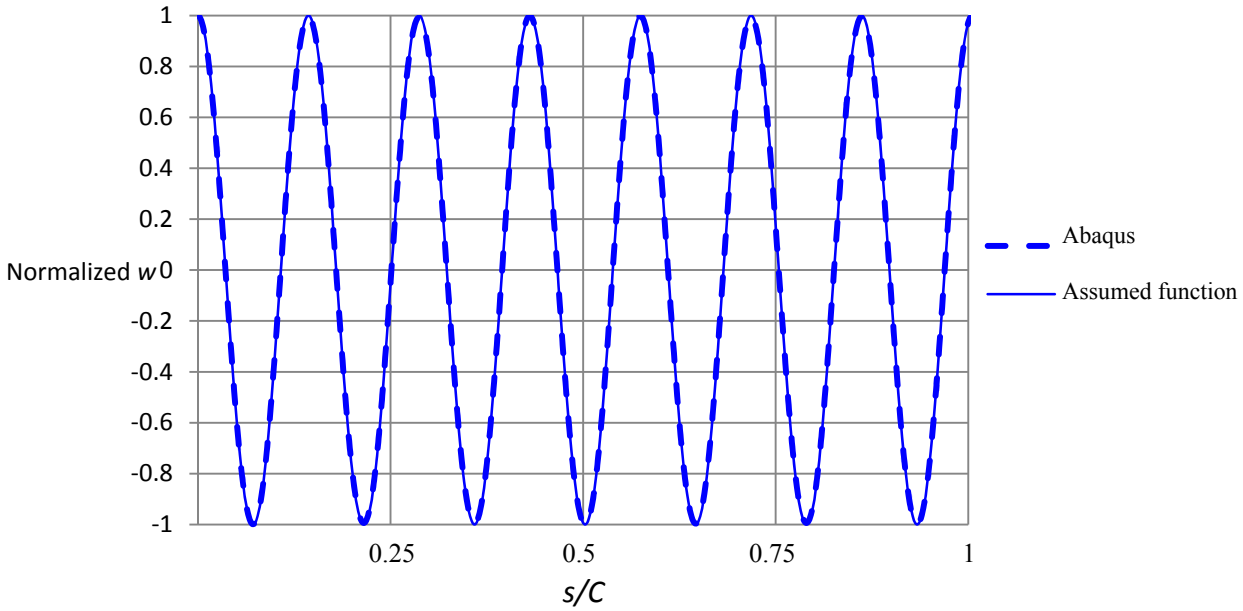

Fig. 6- 15 Normalized normal displacement of circular cylinders at $x/L = 0.5$ with $[\pm 15]_{4S}$ laminate based on cosine-shape ($L = 0.5C$, simple supports)

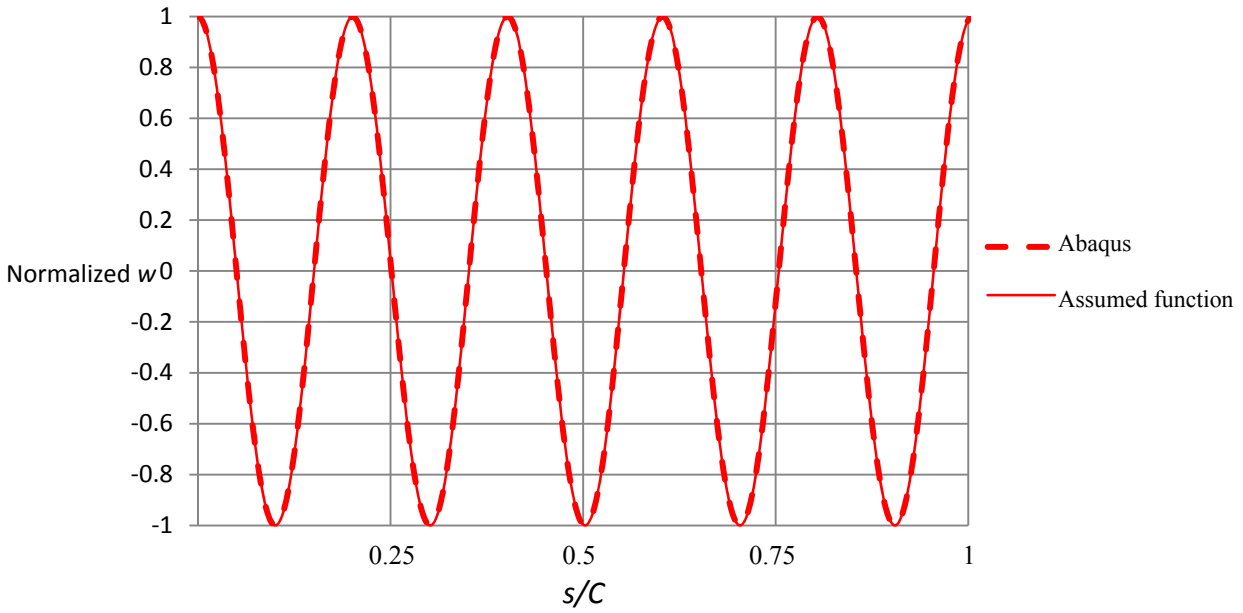

Fig. 6- 16 Normalized normal displacement of circular cylinders at $x/L = 0.5$ with $[\pm 45]_{4S}$ laminate based on cosine-shape ($L = 0.5C$, simple supports)

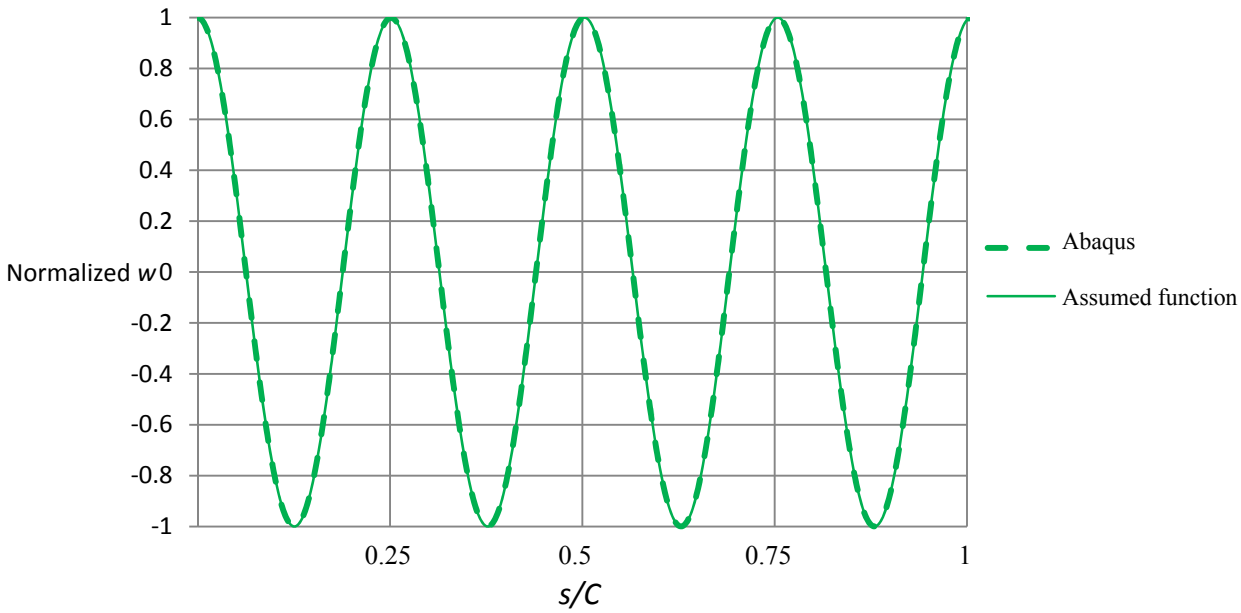

Fig. 6- 17 Normalized normal displacement of circular cylinders at $x/L = 0.5$ with $[\pm 75]_{4S}$ laminate based on cosine-shape ($L = 0.5C$, simple supports)

6.3 Discussion of Linear Fiber Angle Tailoring in Elliptical Cylinders with Simple Supports

As the prediction of the fundamental frequency from the developed analysis for varying fiber angle elliptical cylinders is sometimes better than that of the corresponding circular cylinders, it is worthwhile determining whether or not the discussion and conclusions in last section are applicable to elliptical cylinders.

In Figs. 6- 18, 6- 19 and 6- 20 the normalized normal displacements of large, simply-supported, elliptical cylinders with $b/a = 0.55$, $L = 0.5C$ at $x/L = 0.5$ with constant fiber angle laminates $[\pm 15]_{4S}$, $[\pm 45]_{4S}$, and $[\pm 75]_{4S}$, respectively, and based on the cosine-shape are illustrated. According to the study in Ch. 4, the difference of the prediction between the developed equation and Abaqus is smaller than 5% for these cases (Figs. 4- 5d, e, f). In Fig. 6-18, though in the circumferential direction the assumed function doesn't perfectly match the result of Abaqus, the general trend is represented in the sense that the amplitude of normal

displacement is high where the radius of curvature is large (s/C = 0, ½) and low where the radius of curvature is small (s/C = ¼ and ¾).

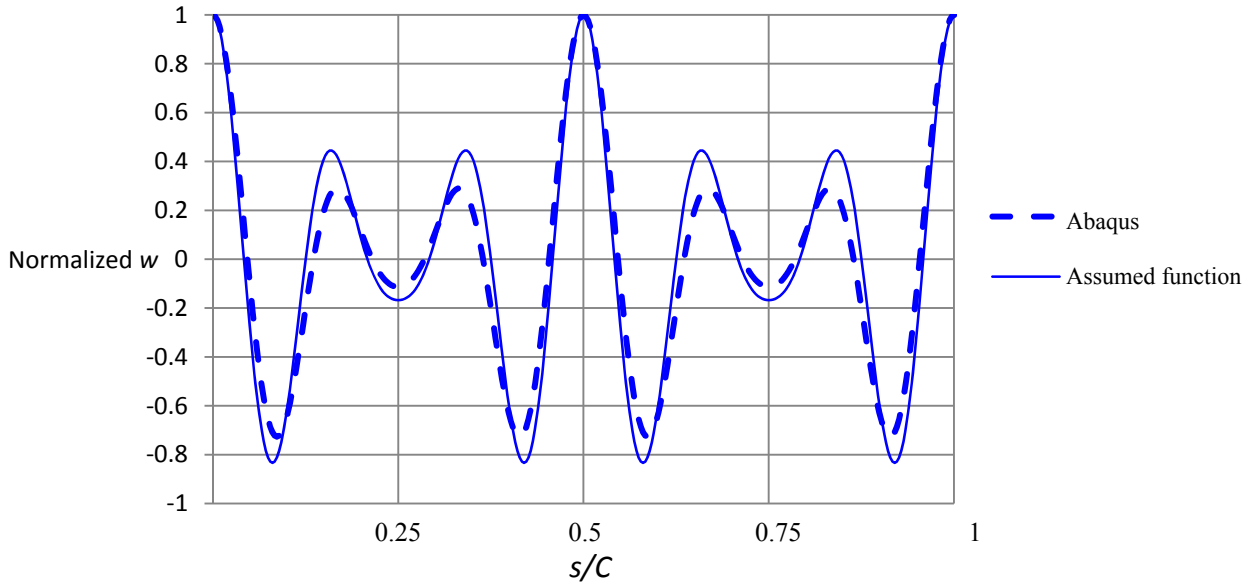

Fig. 6- 18 Normalized normal displacement of elliptical cylinders at x/L = 0.5 with $[\pm 15]_{4S}$ laminate based on cosine-shape ($L = 0.5C$, b/a = 0.55, simple supports)

In Figs. 6- 19 and 6- 20 the circumferential wave numbers of the fundamental frequency are both n = 4. It can be noticed that even if the assumed function for each case is the same, there are differences in the Abaqus results in the two figures due to the different laminates considered. The trends of the displacements in Figs. 6- 18, 6- 19, and 6- 20 show the sense of the shape factor introduced in Section 3.2. That the cases illustrated in Figs. 6- 18 through 6- 21 show good agreement between the prediction of Abaqus and those of the developed analysis is believed to be clear to the fact the locations of the peaks in normal displacement are aligned in the two predictions, and the major reaction in amplitude due to use of the shape factor is represented. Is this the situation for the linearly varying fiber angle cases? The next paragraph addresses this.

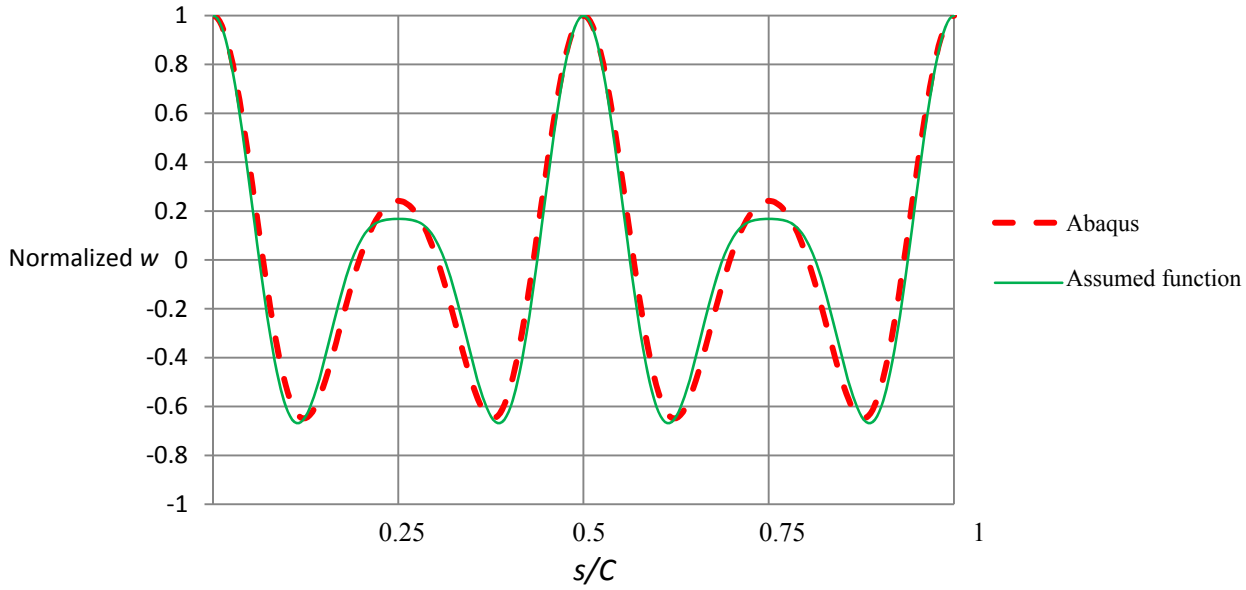

Fig. 6- 19 Normalized normal displacement of elliptical cylinders at $x/L = 0.5$ with $[\pm 45]_{4S}$ laminate based on cosine-shape ($L = 0.5C$, $b/a = 0.55$, simple supports)

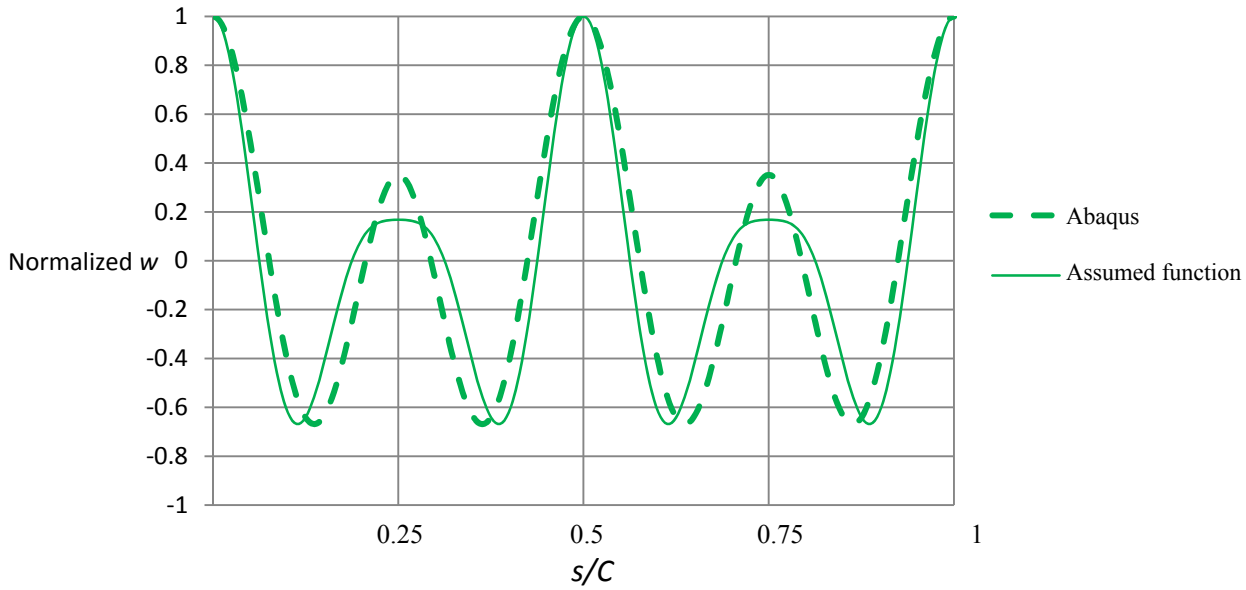

Fig. 6- 20 Normalized normal displacement of elliptical cylinders at $x/L = 0.5$ with $[\pm 75]_{4S}$ laminate based on cosine-shape ($L = 0.5C$, $b/a = 0.55$, simple supports)

The normalized normal displacement of elliptical cylinders with $L = 0.5C$, $b/a = 0.55$, simple supports, along $x/L = 0.5$, with linearly varying $[\pm\theta]_{4S}$ laminate where $\theta_1 = 75°$ and

$\theta_2 = 15°$ based on cosine-shape is presented in Fig. 6- 21. As mentioned in Ch. 5, while the difference of the prediction for fundamental frequency between Abaqus and developed equation for circular cylinders is as high as 25%, that for elliptical cylinder is only 5%. The assumed circumferential variation shown in Fig. 6- 21 leads to good agreement with the results of Abaqus. It appears that with a good assumed function in the circumferential direction the fundamental frequency as predicted by the developed formulation is close to the prediction of Abaqus.

In Fig. 6- 22 the normalized normal displacement of elliptical cylinders with $L = 0.5C$, $b/a = 0.55$, simple supports, along $x/L = 0.5$, with linearly varying $[\pm\vartheta]_{4S}$ laminate where $\theta_1 = 15°$ and $\theta_2 = 75°$ based on cosine-shape as shown. The assumed circumferential variation doesn't match the results from Abaqus as regards the variation of wavelength around the circumference, and as importantly, the locations in the local peak amplitudes of the normal displacement. In terms of the prediction of fundamental frequency, the difference between the developed equation and Abaqus is the largest case among all cases in this study.

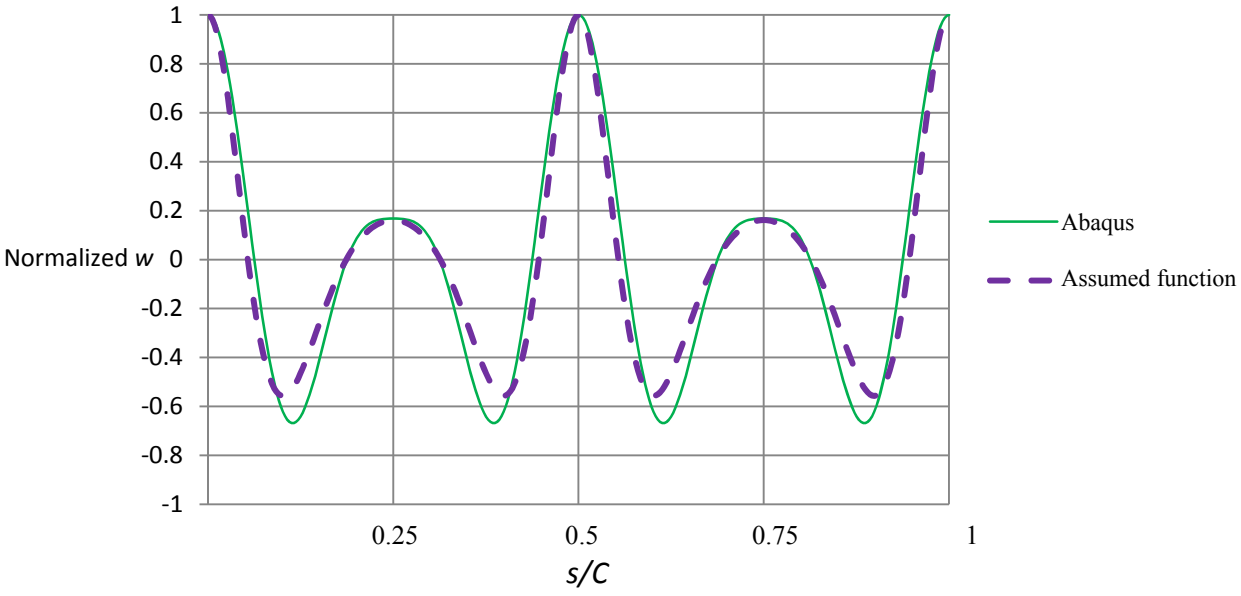

Fig. 6- 21 Normalized normal displacement of elliptical cylinders at $x/L = 0.5$ with linearly varying $[\pm\vartheta]_{4S}$ laminate where $\theta_1 = 75°$ and $\theta_2 = 15°$ based on cosine-shape ($L = 0.5C$, $b/a = 0.55$, simple supports)

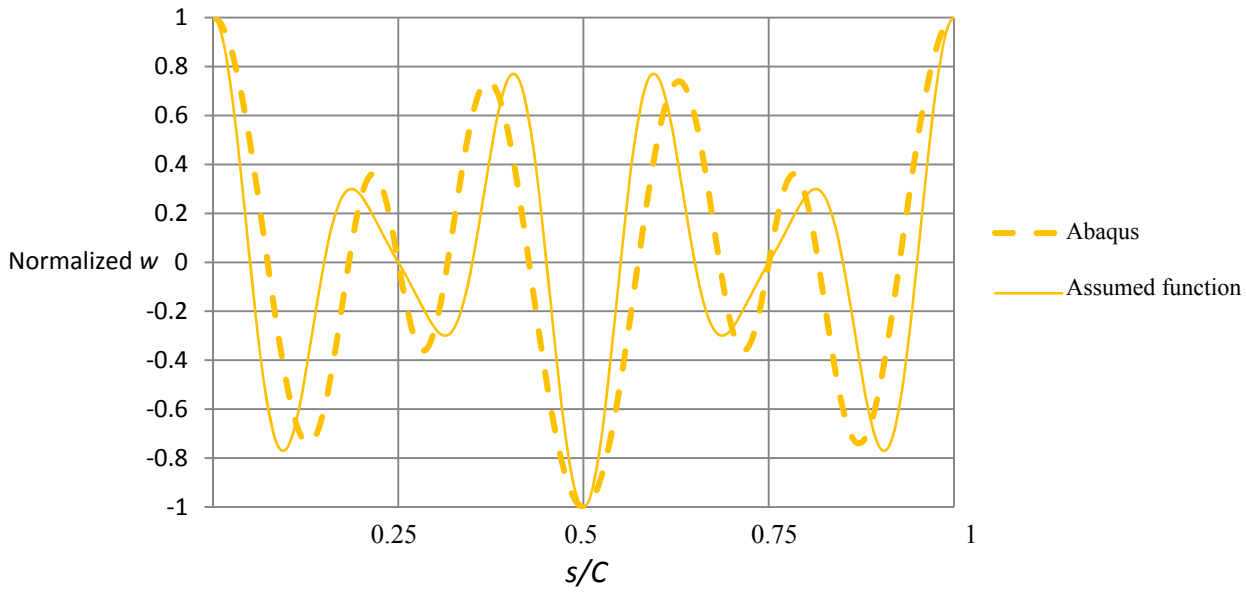

Fig. 6- 22 Normalized normal displacement of elliptical cylinders at $x/L = 0.5$ with linearly varying $[\pm\vartheta]_{4S}$ laminate where $\theta_1 = 15°$ and $\theta_2 = 75°$ based on cosine-shape ($L = 0.5C$, $b/a = 0.55$, simple supports)

It can be concluded that when the assumed circumferential function generally matches the normal displacement characteristics according to Abaqus, the corresponding fundamental frequencies predicted by developed equation and Abaqus have good agreement but if the assumed circumferential function and the displacement from Abaqus do not have good agreement, the fundamental frequencies of the developed equation and Abaqus do not have good agreement.

6.4 Discussion of Lo's Approximation

With the application of shape factor, developed equations without simplification, the first simplified equation, the second simplified equation, and Lo's approximate equation are presented. As with the simplification equation for circular cylinders, the first simplified equation for elliptical cylinders ignores the inertia in both axial and circumferential directions. The second simplification ignores not only the inertia as the first simplified equation, but also the higher-order terms caused by the shape factor, which also leads to $S_{1n} = S_{2n} = S_{3n} = S_{4n}$, where S_{1n} is

given by Eq. 3- 59. Through the deep observation, as shown in Fig. 6- 23, with b/a between 0.55 and 1.0, the maximum difference between R_{max}/R_0 and S_{1n} for $n \neq 1$ is around 18%. In Eqs. 3- 72, 3- 73, and 3- 74 the right hand sides can be treated as two parts: D-term part and A-term part. The D-term part is exactly the natural frequency equation for the plates that results from unrolling the corresponding cylinders. However, the value of D-term part increases with larger n, but the value of A-term part decreases with larger n. Therefore, for the fundamental frequency, the contribution from D-term part and that from A-term part are roughly close. Since only A-term part includes S_{1n}, in terms of the value in the right hand side of Eqs. 3- 72, 3- 73 and 3- 74, the maximum difference caused by replacing S_{1n} with R_{max}/R_0 reduces from 18% to 10%. Since in Eqs. 3- 72, 3- 73 and 3- 74 the frequency is with the form of square, the maximum influence for the fundamental frequency of the approximation reduces to only 5%. Moreover, considering the simplified equation for circular cylinder and the first and the second simplified equations lead to a higher value than Abaqus, in the region $0.6 < b/a < 1.0$ R_{max}/R_0 is generally larger than S_{1n} ($n \neq 1$) and it means Lo's approximate equation is somehow closer to Abaqus than the second simplified equation is with a specified b/a.

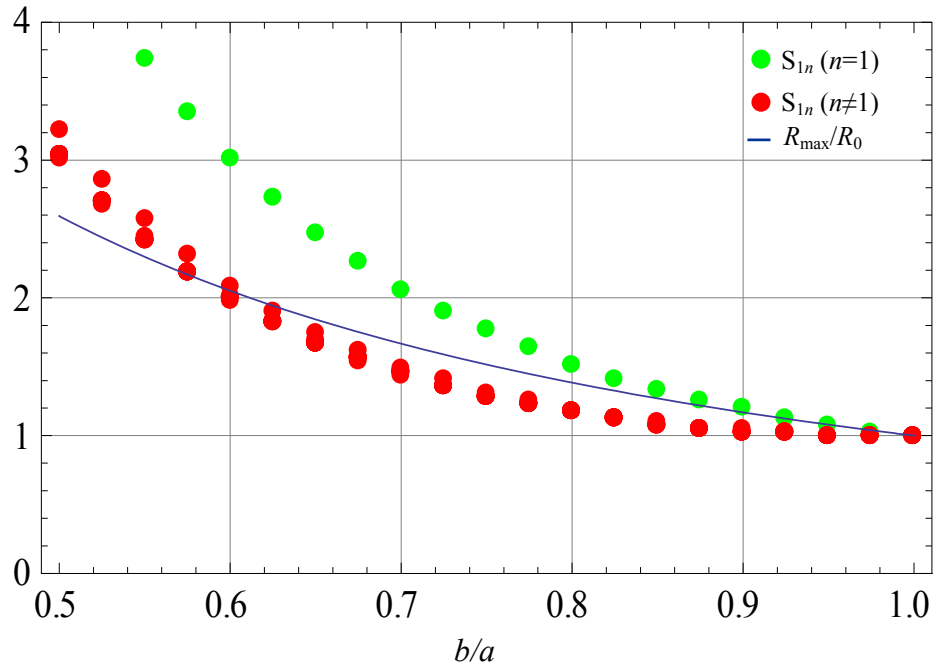

Fig. 6- 23 Difference between R_{max}/R_0 and S_{1n}

Even though for $n = 1$ cases the approximation can hardly match in most of the range of b/a, the numerical results have never shown the fundamental frequencies occur at $n = 1$ cases in the studied cylinders.

Chapter 7 Summary and Future Activities

Overview of the Chapters

Analyses to compute the fundamental vibration frequency of thin-walled cylinders constructed of fiber-reinforced composite material and with elliptical cross sections have been presented. Fiber reinforced materials with fiber angles that are constant with circumferential location, as well as materials with fiber angles which vary linearly with circumferential location were considered. The constant fiber angle case was considered in order to develop a comprehensive understanding of the role of fiber angle, wall lamination sequence, cylinder geometry, and boundary conditions on the fundamental frequency, in particular the differences between the fundamental frequency of an elliptical cylinder and that of a circular cylinder of the same circumference. The variable fiber angle case was considered to determine if there are any advantages or disadvantages to having the fiber angle vary with circumferential location, as the radius of curvature does for an elliptical cylinder. Through a series of simplifying assumptions, a hierarchy of expressions for computing the fundamental frequencies was developed for both the constant fiber angle case and the variable fiber angle case. The results of the analyses have been compared with results from finite element models, and the comparisons were generally good. For the few specific cases where the comparisons have not been good, the character of the vibratory deformation pattern has been studied by way of the finite element model and the short comings of the assumptions in the analysis identified. The simplest expression for computing the fundamental frequency has been identified as Lo's approximation and it has been demonstrated that the expression can be used with confidence for preliminary design and tradeoff studies.

Specifically, in Ch. 1 the problem of determining the fundamental vibration frequency of a thin-walled elliptical cylinder constructed of a fiber-reinforced composite material was introduced. Basic concepts regarding the geometry and nomenclature of an ellipse were presented. The geometry and nomenclature of the elliptical cylinders were also presented, as was the curvilinear analysis coordinate system used, and definitions of the reference surface displacements and rotations. A review of the relevant literature was presented, included past research on determining the natural frequencies of elliptical composite cylinders. Regarding the latter, much of what has been done has been for somewhat impractical laminates and cylinder geometries.

In Ch. 2 the surface geometry of a general shell was reviewed. Donnell shell theory was outlined and the relevant reference surface strains and curvatures defined. The assumed constitutive behaviors of a layer of fiber-reinforced composite material and a laminate made of a number of layers were reviewed. The Action Integral and Hamilton's principle, which utilize the potential and kinetic energies of the vibrating cylinder, was also reviewed. Accordingly, the expressions for the potential and kinetic energies were developed. Hamilton's principle was applied and the governing differential equations and boundary conditions for time-dependent behavior derived. The concept of using the Rayleigh-Ritz technique in conjunction with the Action Integral was discussed and the assumed forms of the displacements to be used with the Rayleigh-Ritz technique presented.

In Ch. 3 the focus was on the application of Hamilton's principle and the Rayleigh-Ritz technique for the derivation of the equations from which the fundamental frequencies could be calculated. Circular cylinders were first considered, with and without the consideration of axial and circumferential inertia, the latter resulting in a simplified form for the fundamental frequency equation, including Lo's approximation. Both simply-supported and clamped boundary conditions were considered. The concept of a shape factor was introduced for developing the frequency equation for an elliptical cylinder. The shape factor accounted for the fact that the amplitude of the normal component of vibration displacement would be larger near the circumferential locations where the radius of curvature of the cross section was largest, and would be smaller near the circumferential locations where the radius of curvature of the cross section was smallest. The argument for the need for a shape factor was based on the role of variable geometric stiffness of the elliptical cross section due to the changing radius of curvature. For simplicity in algebra, the shape factor was approximated as a four-term Fourier series derived based on the exact shape factor. Also, as the variation of the normal displacement with the circumferential coordinate was assume to be harmonic, the importance of considering both a sinusoidal-based variation and a cosinusoidal-based variation was illustrated. For the circular cylinders both variations led to the same frequency equation, but for the elliptical cylinder, the frequency equation depended on which harmonic variation was assumed. Non-simplified, first simplified, and second simplified equations and Lo's approximation were developed for these variations. Lo's approximation was actually the same for both variations.

Numerical results for so-called large and small circular and elliptical cylinders with a range of geometric parameters and multiple lamination sequences were presented and discussed in Ch. 4. Numerical results for the non-simplified frequency equation and the various simplified forms were presented along with finite element results to serve as a spot check on the developed analysis. Circular cylinders were first considered, mainly so the fundamental frequency response of circular cylinders, a subject which represents an established body of knowledge, could be discussed in the figure format to be used for elliptical cylinders, but also to provide a contrast to the findings for the elliptical cylinders. For large simply-supported circular cylinders agreement among the results from all methods of computing the fundamental frequency was very good. For large clamped support cylinders, except for the $[\pm 45]_{4S}$ cylinders, agreement among the results from all methods of computing the fundamental frequency was good. For small circular cylinders, except for the $[\pm 45]_{2S}$ case, simply-supported and clamped, the agreement among the various predictions from the non-simplified frequency equation and the various simplified forms and finite element results was good. The situations for the $[\pm 45]_{4S}$ and $[\pm 45]_{2S}$ clamped cylinders were investigated in more detail in Ch. 6, and it was concluded that the dependency of the normal displacement component on the axial coordinate, as computed by the finite element model, was strongly dependent on the cylinder wall lamination sequence. In contrast, for the developed analysis the assumed axial variation of the normal displacement was the same for all lamination sequences. Recall, the dependency of the normal displacement on the axial coordinate was derived from the fundamental mode shape of a clamped-clamped isotropic beam. Perhaps a fix for this problem is to use the fundamental mode shape of a beam with the same lamination sequence and value of ϑ of the cylinder of interest, i.e., $[\pm\vartheta/0/90]_{2S}$, $[\pm\vartheta/0/90]_{S}$, $[\pm\vartheta]_{4S}$, and $[\pm\vartheta]_{2S}$ laminates.

In Ch. 4 the fundamental frequencies of elliptical cylinders were then studied. Initially large and small simply-supported and clamped cylinders with an aspect ratio of b/a of 0.55 (e = 0.84) and ϑ = 15, 45, and 75° in the lamination sequences $[\pm\vartheta/0/90]_{2S}$, $[\pm\vartheta/0/90]_{S}$, $[\pm\vartheta]_{4S}$, and $[\pm\vartheta]_{2S}$ and a range of length to circumference ratios were discussed. This aspect ratio was considered first as it was the most challenging for the developed analysis, and results from the non-simplified and the various simplifications from the developed analysis were compared with finite element predictions. The results from the developed analysis and finite element results for the large simply supported elliptical cylinder agreed quite well, though not as well as for large simply-supported circular cylinders. For clamped supports the agreement was good, but, again, not as good as for the

simply-supported case. For small simply-supported cylinders Lo's approximation showed good agreement with finite element results, even for the $[\pm 45]_{2S}$ case. The non-simplified equation and the first and second simplified equations did not agree as well. The results for the small clamped elliptical cylinders were quite comparable for all lamination sequences except the $[\pm 45]_{2S}$ case. Overall, it was concluded that Lo's approximation could be used with confidence for design and tradeoff studies, studies which require relatively rapid evaluation of the sensitivity of various geometric and material parameters.

With the results for circular and elliptical cylinders with the most extreme cross section on hand, the decrease of fundamental frequency due to the cross section being noncircular could be evaluated. Though the specific percentage decrease depended on the cylinder size, laminate sequence, and boundary conditions, the largest decrease was about 30% which occurred for cylinders with ±15° layers and small values of L/C, while the smallest decrease in fundamental frequency was about 10% and occurred for cylinders with ±75° layers and large values of L/C.

Regarding differences in the predictions of a sine-based analysis and a cosine-based analysis, it was shown in Ch. 4 and Appendix A that for L/C in the range 0.8 to 1.0 and for circumferential wave number n=2 differences of 6-8% were found for selected cases. Generally, though, the differences were on the order of 1% or less.

Finally in Ch. 4 the fundamental frequencies for other aspect ratios were presented as a function of fiber angle, cylinder geometry, and boundary conditions. The insensitivity of the fundamental frequency to fiber angle, for fixed values of all the other parameters, was clearly demonstrated, though depending on particulars, fiber angles in the range 30 to 70° generally resulted in the maximum fundamental frequency.

In Ch. 5 the analysis was developed for computing the fundamental frequencies of large and small simply-supported circular and elliptical cylinders and for which ϑ varied linearly with circumferential location. While many of the details of the sensitivity of the fundamental frequency to the circumferential variation of fiber angle were discussed, the lack of sensitivity of the fundamental frequency was most apparent. This, of course, correlates well with the findings of Ch. 4.

In Ch. 6 the discrepancies between the predictions of the developed analysis and the finite element model were addressed. As mentioned above, it was shown that for the constant fiber angle cylinders, in particular the large circular $[\pm\vartheta]_{4S}$ clamped support cylinder, the character of the axial variation of the normal displacement as computed by the finite element model was dependent on the value of ϑ, whereas for the developed analysis the character of the axial variation was assumed to be independent of ϑ. This helped explain some of the differences between the predictions of the developed analysis and the predictions of the finite element model. In contrast, for variable fiber angle cylinders, for those cases for which there was considerable difference in the predictions, the axial variation of the normal displacement was not a problem. Rather, with a variable fiber angle around the circumference, based on the finite element results, the wavelength and amplitude of the periodic variation of the normal displacement varied with circumferential location. However, in the developed analysis it was assumed that the periodic variation was harmonic, so the wavelength and amplitude did not vary with location around the circumference. Finally, the circumferential variation of the normal displacement for the elliptical cylinders was examined for laminates for which there was poor correlation between the fundamental frequencies based on the developed analysis and those as computed by the finite element model. It was concluded that when the locations of the local peaks in the circumferential variation of the normal displacements in the developed analysis agreed with those of the finite element model, the fundamental frequency predictions compared well.

Major Contributions

The contributions of the work can be divided into two major categories. The first category consists of the analyses developed, and the second category consists of understanding the characteristics of the fundamental frequency of elliptical composite cylinders.

Analyses developed

A hierarchy of closed-form equations for computing the fundamental frequency of a thin-walled cylinder with an elliptical cross section constructed of a balanced and symmetric laminate with fiber angles which can vary linearly circumferential location was developed.

The simplest equation of the hierarchy, referred to as Lo's approximation, produces credible results, when compared with finite element calculations, and with the least amount of computation.

The use of the so-called shape factor is believed to be unique.

Sinusoidal-based and cosinusoidal-based analyses were developed. Lo's approximation was identical for both analyses.

Characteristics of the fundamental frequency of elliptical cylinders

Constant fiber angle

Within the context of the range of parameters considered, for a given cylinder length, circumference, boundary conditions, and wall laminate, the fundamental frequency of an elliptical cylinder is upwards of 30% less than a circular cylinder with the same length, circumference, boundary conditions, and wall laminate, depending on cross sectional geometric properties.

For all intents and purposes, there was little difference between the fundamental frequency predictions of the sinusoidal-based analysis and the cosinusoidal based analysis.

For the lamination sequences $[\pm\vartheta/0/90]_{2S}$, $[\pm\vartheta]_{4S}$ and $[\pm\vartheta/0/90]_{S}$, $[\pm\vartheta]_{2S}$ for large and small, respectively, elliptical and circular simply-supported cylinders, the fundamental frequency was insensitive to the fiber angle ϑ as it ranges from 0 to 90° The circumferential wave number does, however, depend strongly on the fiber angle. For clamped supports there was more sensitivity of the fundamental frequency, but not as much as might be expected for that range of fiber angle ϑ.

Linearly varying fiber angle

Allowing the fiber angle to change with circumferential location from 15 to 75° did not produce much change in fundamental frequency of large simply-supported *circular* cylinders as compared to a constant fiber angle cases. At most, a linear variation of fiber angle resulted in a 15% change, the sign of the change depending on the particular linear variation.

The fundamental frequency of small simply-supported *circular* cylinders was more sensitive to a linearly varying fiber angle than for large simply supported cylinders. Changes upward of 20% were computed.

Allowing the fiber angle to change with circumferential location from 15 to 75° produced little change in the fundamental frequency of large simply-supported *elliptical* cylinders as compared to a constant fiber angle cases. In some cases the change was close to 0%.

The fundamental frequency of small simply-supported *elliptical* cylinders was more sensitive to a linearly varying fiber angle than large simply supported cylinders. Changes upward of 15% were computed.

Future Activities

A natural next step in the study of the vibration of noncircular, in particular elliptical, cylinders would be the fabrication of cylinders both with constant fiber angles and with linearly varying fiber angles, and the testing thereof for natural frequencies. The former activity would be rather straightforward if mandrels or other hardware existed for fabricating the cylinders. The latter activity requires advanced tow placement equipment and the proper programming to achieve a linearly varying fiber angle on a noncircular cross section. It is expected that standard vibration testing techniques could be used to determine the fundamental frequency.

It has been mentioned repeatedly that particular cases did not exhibit as good agreement between the developed analysis and the finite element spot checks as other cases. As mentioned in Ch. 2, there are limitations to the application of Donnell shell theory, in particular the assumption that the circumferential displacement component is considerably smaller than the normal displacement component. Though quite involved, it would be worth considering using a shell theory with kinematics that can account for larger circumferential displacement, for example, Sanders shell theory.

Finally, the analysis could be extended to other non-circular cross sections, for example oval cross sections. However, it is expected that the general results obtained for elliptical cross sections would apply to oval cross sections.

References

[1] Sun, M., Hyer, M.W. (2008), Use of Material Tailoring to Improve Buckling Capacity of Elliptical Composite Cylinders, AIAA J. 46, 770-782

[2] Hyer, M.W., Vogl, G.A. (2001), Response of Elliptical Composite Cylinders to a Spatially Uniform Temperature Change, Compos. Struct. 51, 169-179

[3] Almroth, B. O. (1966), Influence of Edge Conditions on the Stability of Axially Compressed Cylindrical Shells, AIAA J. 4, 134-140

[4] Leissa, A.W. (1973), Vibration of Shells, NASA SP-288

[5] Sharama, C.B., Johns, D.J. (1972), Natural Frequencies of Clamped-Free Circular Cylindrical Shells, J. Sound Vibr. 21, 317-327

[6] Sharama, C.B., Johns, D.J. (1972), Free Vibration of Cantilever Circular Cylindrical Shells—A Comparative Study, J. Sound Vibr. 25, 433-449

[7] Soedel, W. (1980), A New Frequency Formula for Closed Circular Cylindrical Shell for a Large Variety of Boundary Conditions, J. Sound Vibr. 70, 309-317

[8] Soedel, W. (1981), Vibration of Shells and Plates, Marcel-Dekker, New York

[9] Callahan, J., Baruh, H. (1999), A Closed-Form Solution Procedure for Circular Cylindrical Shell Vibrations, Int. J. Solid Struct. 36, 2973-3013

[10] Soldatos, K.P. (1999), Mechanics of Cylindrical Shells with Noncircular Cross-section: A Survey, J. Appl. Mech. Rev. 52(8) 237-274

[11] Herrman, G., Mirsky, I. (1957), Three-Dimensional and Shell-Theory Analysis of Axially Symmetric Montions of Cylinders, J. Appl. Mech. 23, 563-568

[12] Klosner, J.M. and Pohle, F.V. (1958), Natural Frequency of An Infinitely Long Noncircular Cylindrical Shell, PIBAL Rept. 476, Polytech Inst., Brooklyn, N.Y.

[13] Klosner, J.M. (1959), Frequencies of An Infinitely Long Noncircular Cylindrical Shell. Part II—Plane Strain, Torsional and Flexural Modes, PIBAL Rept. 552, Polytech Inst., Brooklyn, N.Y.

[14] Klosner, J.M. (1960), Free and Forced Vibrations of A Long Noncircular Cylindrical Shell, PIBAL Rept. 561, Polytech Inst., Brooklyn, N.Y.

[15] Sewall, J.L., Thompson, Jr. W.M., Pusey, C.G. (1971), An Experimental and Analytical Vibration Study of Elliptical Cylindrical Shells, NASA TN D-6089

[16] Culberson, L.D. and Boyd, D.E. (1971), Free Vibration of Freely Supported Oval Cylinders, AIAA J. 9, 1474-1480
[17] Bergman, R.M. (1973), Investigation of the Free Vibrations of Noncircular Cylindrical Shells, J. Math Mech. 37, 1068-1077
[18] Shirakawa, K., Morita, M. (1982), Vibration and Buckling of Cylinders with elliptical cross section, J. Sound Vibr. 84, 121-131
[19] Boyd, D., Rao, K.P. (1973), A Theoretical Analysis of Ring and/or Stringer Stiffened Elliptical Cylinders with Arbitrary End Conditions. Volume I—Analytical Derivation and Applications, NASA CR-1251
[20] Chen, Y.N., Kempner, J. (1978), Model method for Free Vibration of Oval Cylindrical Shells with Simply Supported or Clamped Ends, J. Appl. Mech. 45,142-148
[21] Suzuki, K., Takahashi, S., Ishiyama, H. (1983), Vibrations of Noncircular Cylindrical Shells, Bull JSME 26, 818-826
[22] Suzuki, K., Leissa, A.W. (1985), Free Vibrations of Noncircular Cylindrical Shells Having Circumferential Varying Thickness, J. Appl. Mech. 52, 149-154
[23] Koumousis, V.K., Armenàkas, A.E. (1983), Free Vibration of Simply Supported Cylindrical Shells of Oval Cross Section, AIAA J. 21, 1017-1027
[24] Koumousis, V.K., Armenàkas, A.E. (1986), Vibrations of Infinitely Long Cylindrical Shells of Noncircular Cross Section, AIAA J. 24, 536-539
[25] Kumar, V., Singh, A.V. (1992), Approximate Vibration Analysis of Noncircular Cylinders Having Varying Thickness, AIAA J. 30, 1929-1931
[26] Kumar, V., Singh, A.V. (1993), Vibration Analysis of Noncircular Cylindrical Shells Using Bezier Functions, J. Sound Vibr. 161, 333-354
[27] Yamada, G., Irie, T., Tagawa, Y. (1984), Free Vibration of Noncircular Cylindrical Shells with Vabiable Circumferential Profile, J. Sound Vibr. 95, 117-126
[28] Irie, T., Yamada, G., Kobayashi, Y. (1984), Free Vibration of Noncircular Cylindrical Shells with Longitudinal Interior Partitions, J. Sound Vibr. 96, 133-142
[29] Chueng, Y.K., Yuan, C.Z., Xiong, Z.J. (1991), Transient Response of Cylindrical Shells with Arbitrary Shaped Sections, Thin-Walled Struct. 11, 305-318
[30] Baker, E.H., Kovalevsky, L., Rish, F.L. (1972), Structural Analysis of Shells. McGraw Hill, NY

[31] Kumar, V., Singh, A.V. (1993), Vibration Analysis of Noncircular Cylindrical Shells Using Bezier functions, J. Sound Vibr. 161, 333-354
[32] Dong, S.B. (1968), Free Vibrations of Laminated Orthotropic Cylindrical Shells, J. Acoust. Soc. Am. 44, 1628-1635
[33] Jones, R.M., Morgan, H.S. (1975), Buckling and Vibration of Cross-Ply Laminated Circular Cylindrical Shells, AIAA J. 13, 664-671
[34] Bert, C.W., Baker, J.L., Egle, D.M. (1969), Free Vibrations of Multilayer Anisotropic Cylindrical Shells, J. Compos. Mater. 3, 480-499
[35] Stavsky, Y., Loewy, R. (1971), On Vibrations of Heterogeneous Orthotropic Cylindrical Shells, J. Sound Vibr. 15, 235-256
[36] Greenberg, J.B., Stavsky, Y. (1981), Vibrations of Laminated Filament-Wound Cylindrical Shells, AIAA J. 19, 1055-1062
[37] Soedel, W. (1983), Simplified Equation and Solutions for the Vibration of Orthotropic Cylindrical Shells, J. Sound Vibr,=. 87, 555-566
[38] Bert, C.W., Kumar, M. (1982), Vibration of Cylindrical Shells of Bimodulus Composite Materials, J. Sound Vibr. 81, 107-121
[39] Sadasiva Rao, Y.V.K. (1983), Vibration of Layered Shells with Transverse Shear and Rotary Inertia Effects, J. Sound Vibr. 86, 147-150
[40] Ramesh Kumar, R., Sadasiva Rao, Y.V.K. (1988), Free Vibrations of Multilayered Thick Composite Shells, Computers and Structures 28, 717-722
[41] Lakshminarayana, H.V., Dwarakanath, K. (1992), Free Vibration Characteristics of Cylindrical Shells Made of Composite Materials, J. Sound Vibr. 154, 431-439
[42] Nosier, A., Reddy, J.N. (1992), Vibration and Stability Analyses of Cross-Ply Laminated Circular Cylindrical Shells, J. Sound Vibr. 157, 139-159
[43] Ye., J.Q., Soldatos, K.P. (1997), Three-Dimensional Vibrations of Cross-Ply Laminated Hollow Cylinders with Clamped Edge Boundaries, J. Vibr. Acou. 119, 317-323
[44] Tizzi, S. (1999), Free Frequencies and Modal Shapes of Cylindrical Vibrating Composite Structures, Computers and Structures 73, 629-653
[45] Tizzi, S. (2006), A Ritz procedure for Optimization of Cylindrical Shells, Formed by a Nearly Symmetric and Balanced Angle-Ply Composite Laminate, with fixed Minimum Frequency, Computers and Structures 84, 2159-2173

[46] Blom, A.W., Rassaian, M., Stickler, P.B., Gürdal, Z. (2009), Modal Testing of a Composite Cylinder with Circumferentially Varying Stiffness, 50th AIAA/ASME/ASCE/AHS/ASC Structures, Structural Dynamics, and Materials Conference, 4-7 May 2009, Palm Springs, CA
[47] Soldatos, K.P., Tzivanidis, G.J. (1982), Buckling and Vibration of Cross-Ply Laminated Noncircular Cylindrical Shells, Appl. Mech. Rev. 47, 501-516
[48] Soldatos, K.P. (1984), A Flügge-Type Theory for the Analysis of Anisotropic Laminated Noncircular Cylindrical Shells, Int. J. Solids Struct. 20, 107-120
[49] Hui, D., Du, H.Y. (1986), Effects of Axial Imperfections on Vibrations of Anti-Symmetric Cross-Ply, Oval Cylindrical Shells, J. Appl. Mech. 53, 675-680
[50] Suzuki, K., Shikanai, Leissa, A.W. (1994), Free Vibrations of Laminated Composite Noncircular Thin Cylindrical Shells, J. Appl. Mech. 61, 861-871
[51] Suzuki, K., Shikanai, Leissa, A.W. (1996), Free Vibrations of Laminated Composite Noncircular Thick Cylindrical Shells, Int. J. Solid Struct. 33, 4079-4100
[52] Kumar, V., Singh, A.V. (1995), Vibrations of Composite Noncircular Cylindrical Shells, J. Vibr. Acou. 117, 470-476
[53] Ganapathi, M., Patel, B.P., Patel, H.G., Pawargi, D.S. (2003), Vibration Analysis of Laminated Cross-Ply Oval Cylindrical Shells, J. Sound Vibr. 262, 65-86
[54] Ganapathi, M., Haboussi, M., (2003), Free Vibrations of Thick Laminated Anisotropic Non-circular Cylindrical Shells, Compos. Struct. 60, 125-133
[55] Ganapathi, M., Patel, B.P., Patel, H.G. (2004), Free Flexural Vibration Behavior of Laminated Angle-Ply Elliptical Cylindrical Shells, Computers and Structures 82, 509-518
[56] Dym, C.L. (1974), Introduction to the Theory of Shells, Pergamon Press Ltd., Headington Hill Hall, Oxford
[57] Donnell, L.H. (1976), Beams, Plates, and Shells, McGraw-Hill, Inc.
[58] Yamaki, N. (1984), Elastic Stability of Circular Cylindrical Shells, North-Holland, Amsterdam; New York, N.Y.
[59] Hyer, M.W. (2009), Stress Analysis of Fiber-Reinforced Composite Materials, DEStech Publications, Inc, Lancaster, P.A.
[60] Gürdal, Z., Olmedo, R. (1993), In-Plane Response of Laminates with Spatially Varying Fiber Orientations: Variable Stiffness Concept, AIAA J. 31, 751-758

[61] Abdalla, M.M., Setoodeh, S., Gürdal, Z.(2007), Design of Variable Stiffness Composite Panels for Maximum Fundamental Frequency Using Lamination Parameters, Compos. Struct. 81, 283-291
[62] Setoodeh, S., Abdalla, M.M., IJsselmuiden, S.T., Gürdal, Z.(2009), Design of Variable-Stiffness Composite Panels for Maximum Buckling Load, Compos. Struct. 87, 109-117
[63] Jones, R.M. (1999), Mechanics of Composite Materials, Taylor & Franics, Inc., Philadelphia, PA

Appendix A Finite Element Convergence Studies

The finite element method is commonly used for solving engineering problems. There is a variety of mature commercial software available nowadays. The commercial software Abaqus® is used in this study to spot-check the results obtained from the developed formulation, which is based on Donnell shell theory, Hamilton's principle, and the Rayleigh-Ritz approach. An issue with finite element models is whether or not they represent a converged solution to the problem. The finite element model used here and its convergence characteristic are discussed in this Appendix. The particular cases considered for these convergence studies are quasi-isotropic thin-walled elliptical composite cylinders with various lengths and wall thicknesses. Of interest are the first four vibration frequencies and mode shapes. In the main text of this dissertation results from the finite element model described here are compared with results from the developed formulation for other selected cylinders to assess the accuracy of the developed formulation.

The geometry and nomenclature of an elliptical cylinder is illustrated in Fig. A- 1. The major and minor axes $2a$ and $2b$, respectively, are illustrated, as are the cylinder circumference C, length L, and wall thickness H. The radius of a circular cylinder with the same circumference is $R_o = C/(2\pi)$. The global XYZ Cartesian coordinate system is shown, as the local xsz axial-circumferential-wall-normal coordinate system. The fiber angle in the wall laminate with respect to the axial direction is θ, as shown. Cylinder size is considered by the investigation of so-called small cylinders, $R_o/H = 100$, and large, $R_o/H = 200$ cylinders. For laminated composite walls, H is controlled by the number of layers in the wall, here eight for small cylinders and 16 for large cylinders. Cylinder length is varied by varying the ratio L/C, and cylinder lengths $L/C = 0.3$ and 1.0 are studied. Considering a circular cylinder with these dimensions would result in cylinders with L/D ratios of approximately 1 and 3, where D is cylinder diameter, $2R$, and $L/C = L/(\pi D)$. For circular cylinders these lengths would be considered short and quite long. Also, results are shown for elliptical cylinders with the most extreme cross-sectional aspect ratio considered in this study, $b/a = 0.55$ (eccentricity $e = 0.84$) and with a quasi-isotropic lamination sequences $[\pm 45/0/90]_{2S}$ and $[\pm 45/0/90]_S$ for $R_o/H = 200$ and 100, respectively.

For the finite element model the linear quadrilateral reduced integration shell element S4R from the Abaqus element library is employed, where S stands for shell and R stands for reduced integration through the thickness of the shell. The S4R element is a shear-deformable element that satisfies the Kirchhoff hypothesis as the element becomes thin, which is the case here. As shown in the local coordinate system in Fig. A- 1, each node has six degrees of freedom, where $u°$, $v°$ and $w°$ are the displacements in the axial, circumferential, and normal directions, and $\phi_x°$, $\phi_s°$ and $\phi_z°$ are the rotations about the local axial, circumferential, and normal coordinate directions.

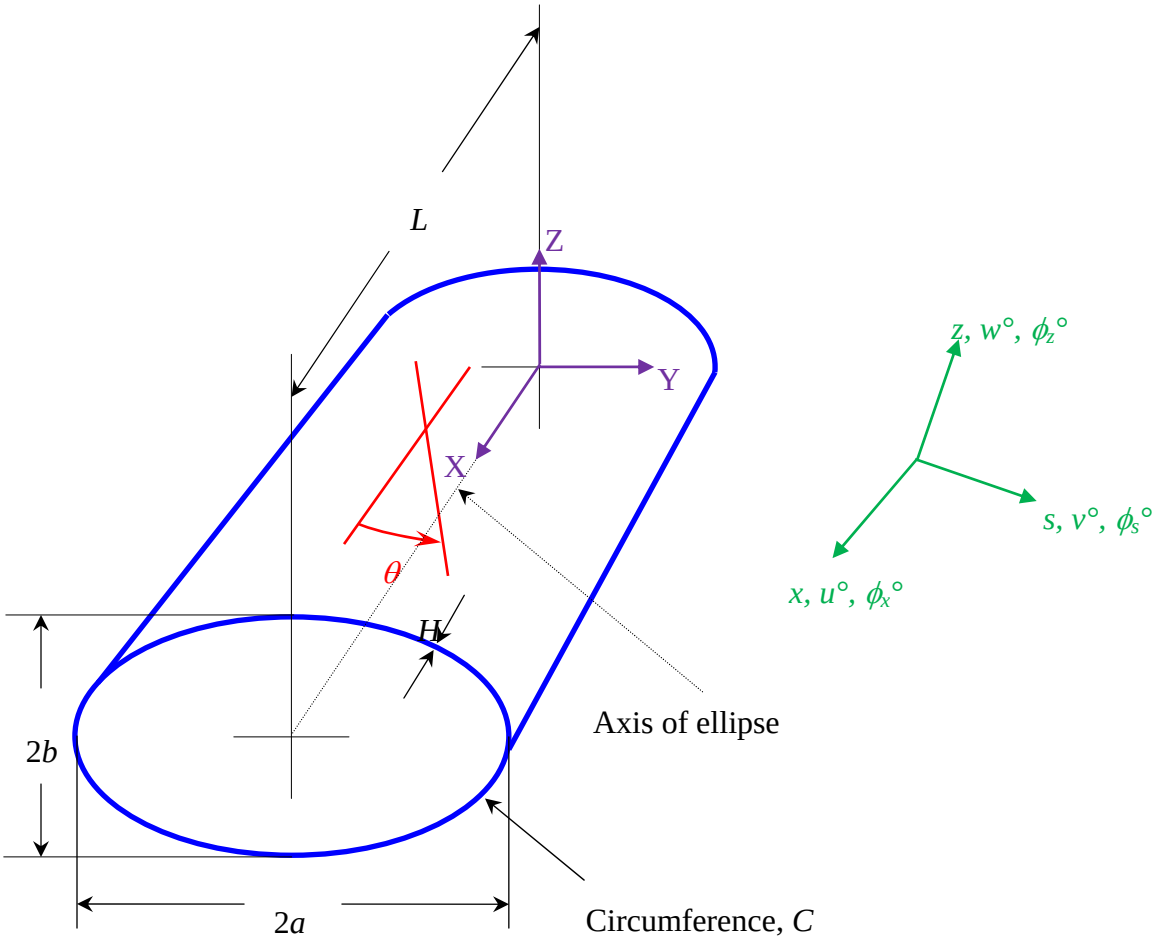

Fig. A-1 Cylinder geometry and nomenclature

For simply supported cylinders on the two cylinder ends displacements $v°$ and $w°$ are restrained to be zero and the other four degrees of freedom are unrestrained. That is

$$v°(0,s) = 0, \qquad v°(L,s) = 0 \qquad \text{Eq. A- 1}$$

$$w°(0,s) = 0, \qquad w°(L,s) = 0 \qquad \text{Eq. A- 2}$$

An extra condition

$$u°\left(\frac{L}{2}, s\right) = 0 \qquad \text{Eq. A- 3}$$

is applied to eliminate rigid body translation in the x-direction. No force resultants or moment resultants are not applied on the boundary $x = 0, L$. For clamped support cylinders, the boundary conditions at the two ends are restraint of all six degrees of freedom, $u°$, $v°$, $w°$, $\phi_x°$, $\phi_s°$, and $\phi_z°$. That is,

$$u°(0,s) = 0, \qquad u°(L,s) = 0 \qquad \text{Eq. A- 4}$$

$$v°(0,s) = 0, \qquad v°(L,s) = 0 \qquad \text{Eq. A- 5}$$

$$w°(0,s) = 0, \qquad w°(L,s) = 0 \qquad \text{Eq. A- 6}$$

$$\phi_x°(0,s) = 0, \qquad \phi_x°(L,s) = 0 \qquad \text{Eq. A- 7}$$

$$\phi_s°(0,s) = 0, \qquad \phi_s°(L,s) = 0 \qquad \text{Eq. A- 8}$$

$$\phi_z°(0,s) = 0, \qquad \phi_z°(L,s) = 0 \qquad \text{Eq. A- 9}$$

Six different mesh densities are considered, as will be shown below, and each mesh is designed so each element is approximately square. An overall conclusion reached during the convergence study is that for all meshes considered for a particular cylinder, the fundamental frequencies calculated are within 3% of each other. However, to accommodate changing fiber angles with circumferential position, as is necessary when addressing the second objective of this study, and to avoid problems with other lamination sequences or boundary conditions, which may exhibit different convergence characteristics, in the main text results from the developed

formulation are compared with the case of using 336 elements in the circumferential direction. The material properties are consistent with Table 4- 5.

The values of the first four frequencies for four specific cylinders are shown in Table A- 1, Table A- 2, Table A- 3, and Table A- 4, namely, quasi-isotropic elliptical cylinders that are large and long, small and long, large and short, and small and short. The mesh density is indicated at the left, and the first four vibration mode shapes displayed left to right with increasing frequency. As with linear buckling analysis, the first four vibration frequencies and close in value. Besides the frequency values, another characteristic to consider is the variation of mode shape with increasing mesh density. The color contouring of each mode shape subfigure aids in interpreting the mode shape characteristic, with red representing maximum outward normal displacement and green representing maximum inward normal displacement. For some modes there are two locations with a maximum outward displacement on, say, the upper surface of the cylinder, which others have just one location on the upper surface, where the outward displacement is a maximum. And as the mesh density increases, which frequency has two outward maxima and which frequency has one outward maximums changes. For example, in Table A- 1, comparing the mode shapes for mesh density 504 × 500 with mesh density 756 × 760, it is seen that for the second and the third frequencies, the mode shapes interchange, the mode shape with one outward maximum changing from being associated with the third frequency for the lower density mesh to being associated with the second frequency for the higher density mesh. There are other cases where this switching also occurs. That said, it is important to realize that for the work here material properties are input with three digits of accuracy. Therefore, citing frequencies to more than three digits of accuracy is meaningless. So considering three digits, for the 756 × 760 mesh the first three frequencies are identical (275 rad/s) and the fourth frequency is but 0.7% higher (277 rad/s).

A letter and a number are used as a descriptor for the mode shape. Letter “C” means that the vibration mode shape of the deformed cross section is similar to the cosine-based vibration mode mentioned in Ch. 3 and letter “S” means that the vibration mode shape of the deformed cross section is similar to the sine-based. The number is the wave number n in the circumferential direction.

Table A-1 Convergence of frequencies for large simply supported elliptical (b/a = 0.55, e = 0.84) cylinder with lamination sequence $[\pm 45/0/90]_{2S}$ and length $L = C$

Mesh density CxL	Mode shape and natural frequency (rad/s)	Mode shape and natural frequency (rad/s)	Mode shape and natural frequency (rad/s)	Mode shape and natural frequency (rad/s)
100 x100	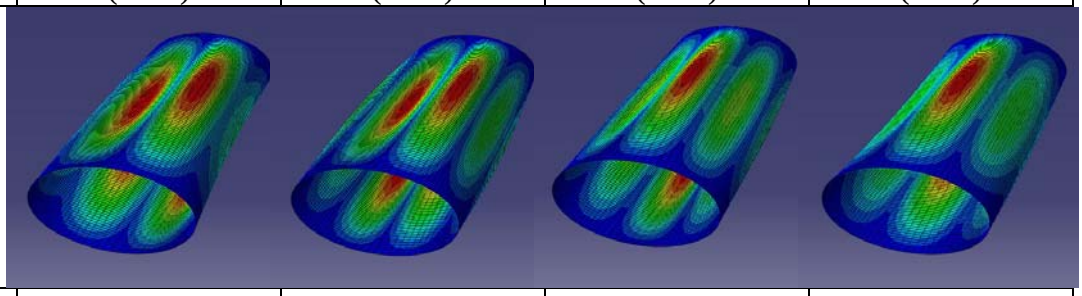			
	S3 277	S4 278	C4 278	C3 278
148 x140	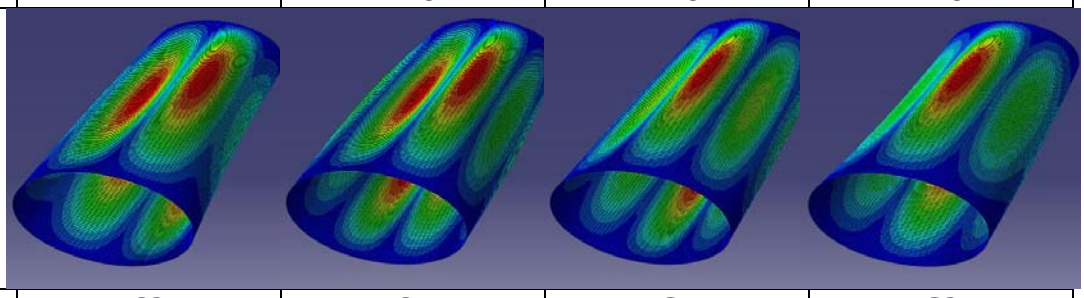			
	S3 276	S4 276	C4 276	C3 278
224 x220	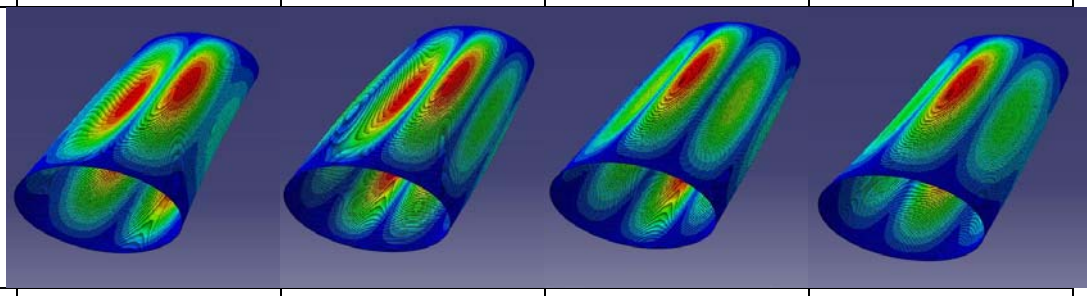			
	S3 275	S4 276	C4 276	C3 277
336 x340	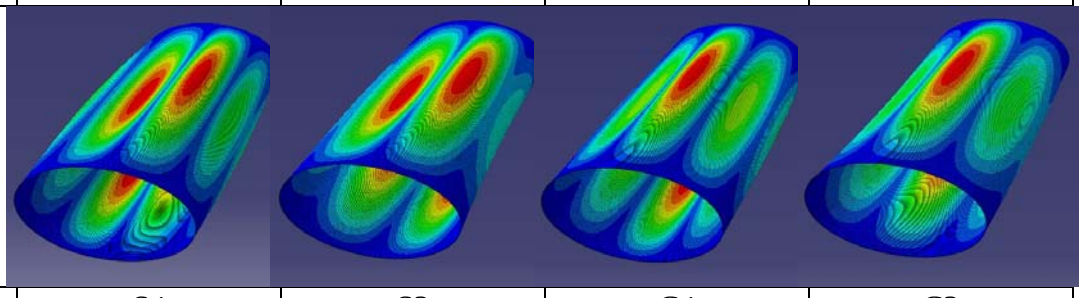			
	S4 275	S3 275	C4 275	C3 277

504 x500	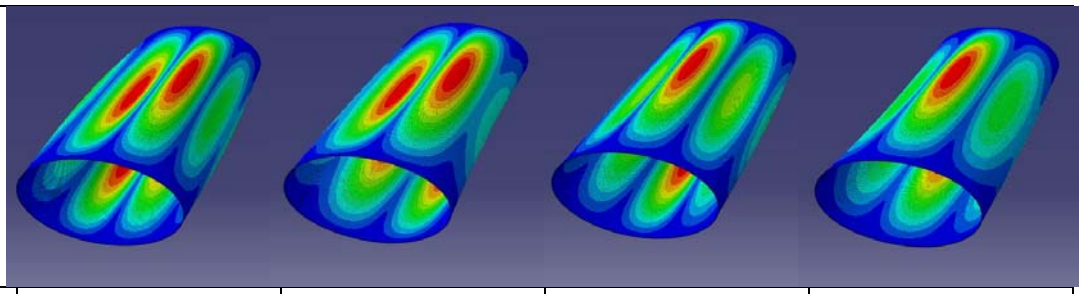			
	S4 275	S3 275	C4 275	C3 277
756 x760	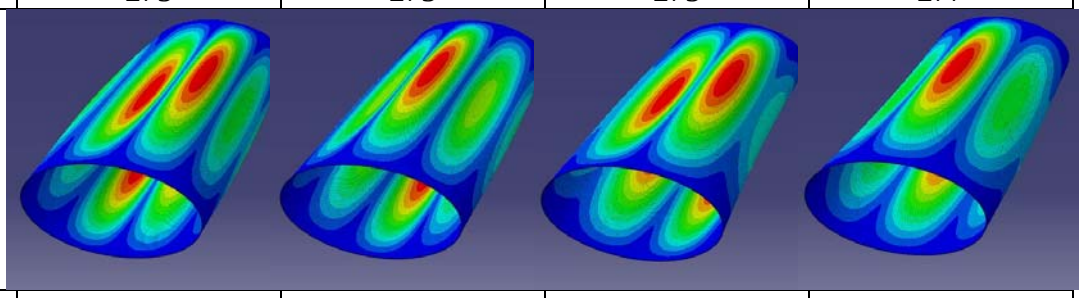			
	S4 275	C4 275	S3 275	C3 277

Table A-2 Convergence of frequencies for small simply supported elliptical (b/a = 0.55, e = 0.84) cylinder with lamination sequence $[\pm 45/0/90]_S$ and length $L = C$

Mesh density CxL	Mode shape and natural frequency (rad/s)	Mode shape and natural frequency (rad/s)	Mode shape and natural frequency (rad/s)	Mode shape and natural frequency (rad/s)
100 x100	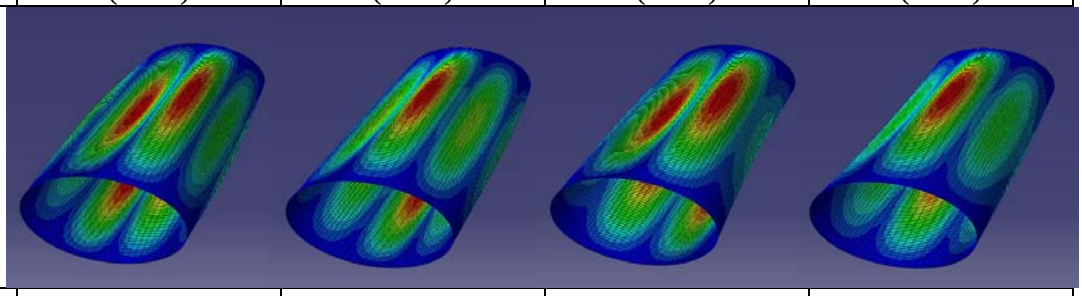			
	S4 529	C4 530	S3 543	C3 546
148 x140	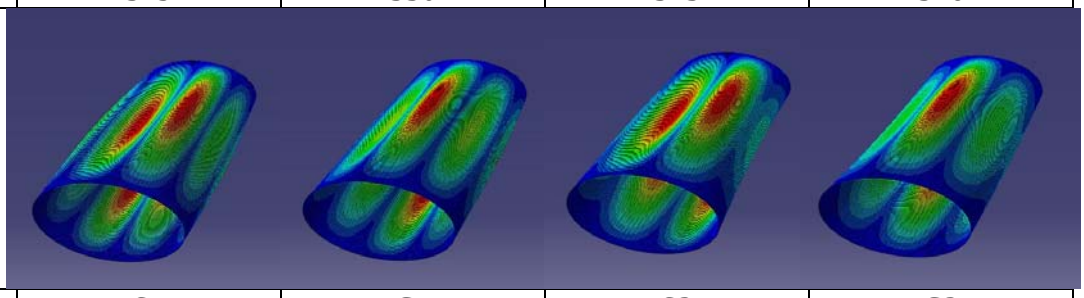			
	S4 526	C4 527	S3 541	C3 544
224 x220	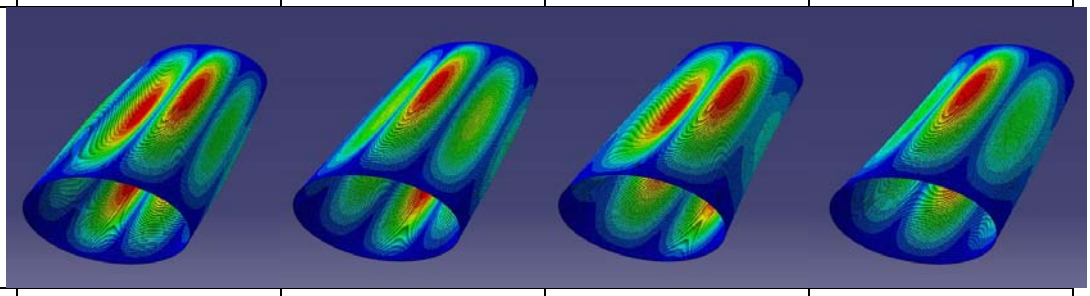			
	S4 525	C4 525	S3 540	C3 544
336 x340	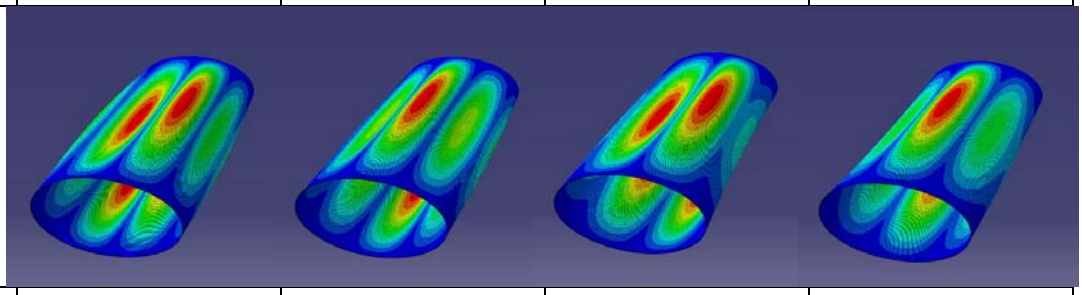			
	S4 524	C4 525	S3 540	C3 543

504 x500	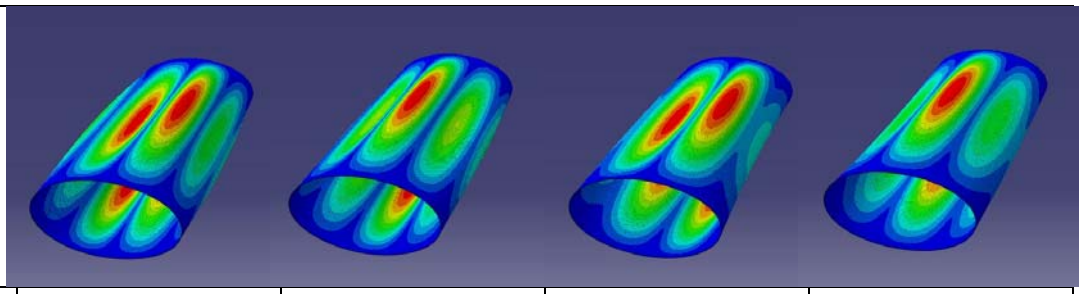			
	S4 524	C4 525	S3 540	C3 543
756 x760	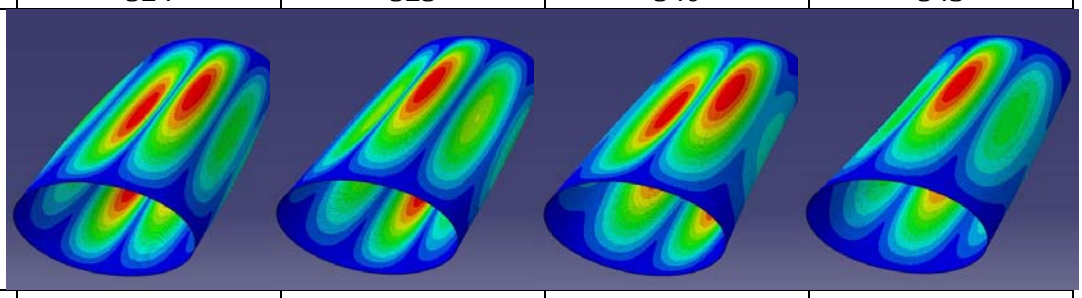			
	S4 524	C4 524	S3 540	C3 543

Table A-3 Convergence of frequencies for large simply supported elliptical (b/a = 0.55, e = 0.84) cylinder with lamination sequence $[\pm 45/0/90]_{2S}$ and length $L = 0.3C$

Mesh density CxL	Mode shape and natural frequency (rad/s)	Mode shape and natural frequency (rad/s)	Mode shape and natural frequency (rad/s)	Mode shape and natural frequency (rad/s)
100 x30	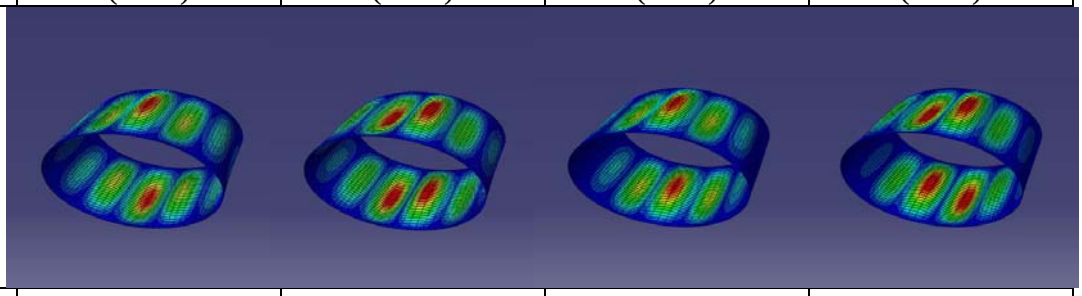			
	C6 876	S6 876	C7 890	S7 890
148 x42	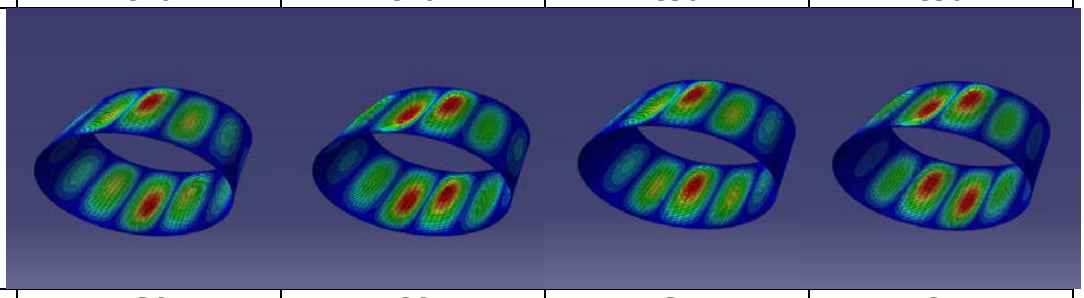			
	C6 864	S6 864	C7 877	S7 877
224 x66	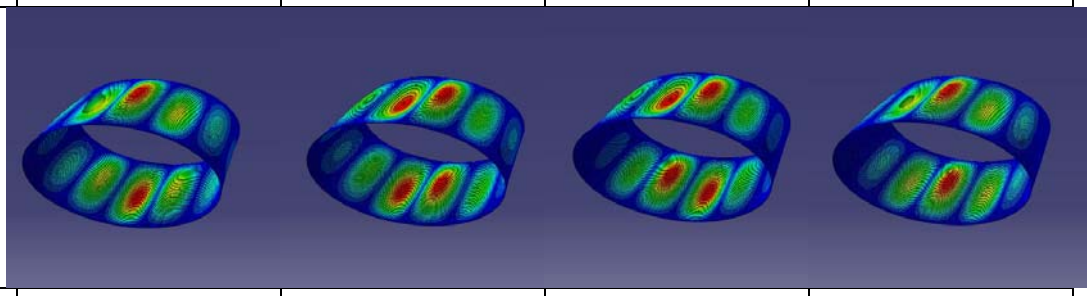			
	C6 859	S6 859	S7 870	C7 870
336 x102	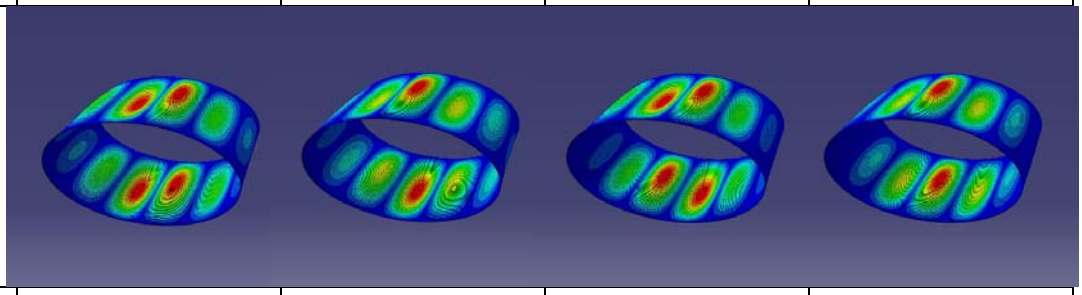			
	S6 856	C6 856	S7 867	C7 867

504 x150	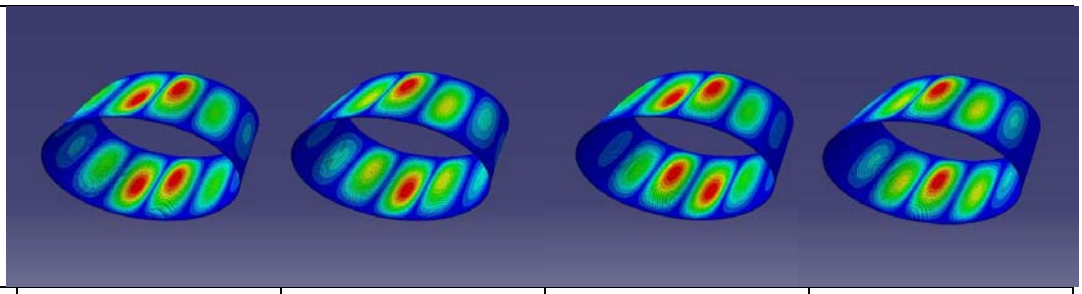			
	S6 855	C6 855	S7 866	C7 866
756 x228	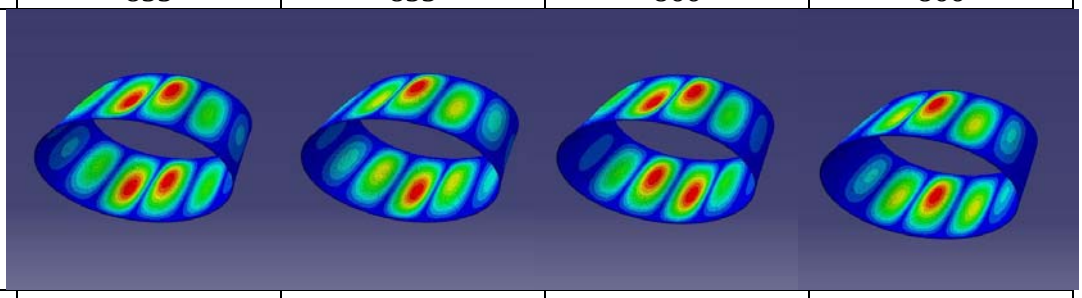			
	S6 855	C6 855	S7 866	C7 866

Table A-4 Convergence of frequencies for small simply supported elliptical (b/a = 0.55, e = 0.84) cylinder with lamination sequence $[\pm 45/0/90]_S$ and length $L = 0.3C$

Mesh density CxL	Mode shape and natural frequency (rad/s)	Mode shape and natural frequency (rad/s)	Mode shape and natural frequency (rad/s)	Mode shape and natural frequency (rad/s)
100 x30	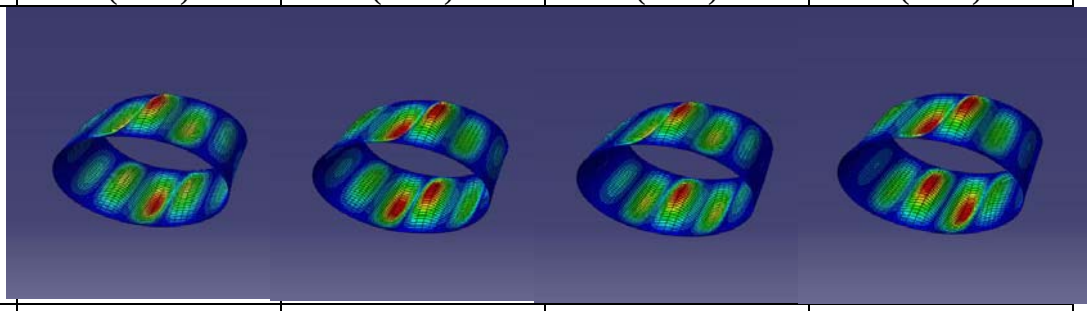			
	C6 1717	S6 1717	C7 1734	S7 1734
148 x42	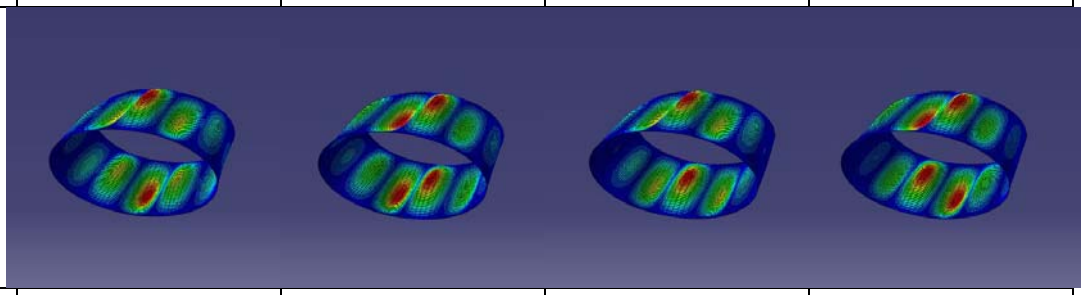			
	C6 1693	S6 1693	C7 1711	S7 1711
224 x66	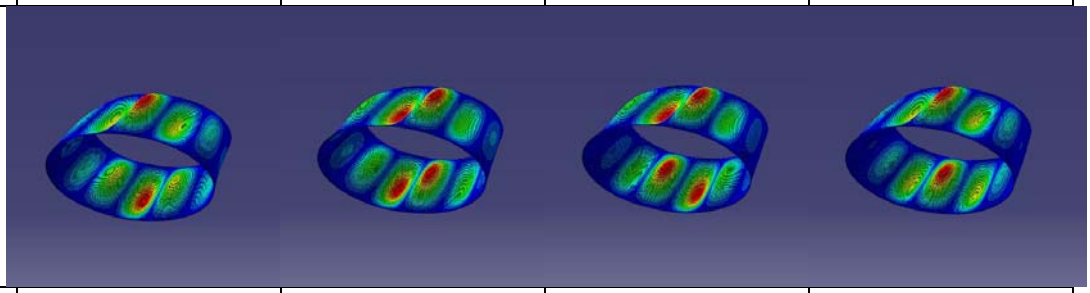			
	C6 1682	S6 1682	S7 1698	C7 1698
336 x102	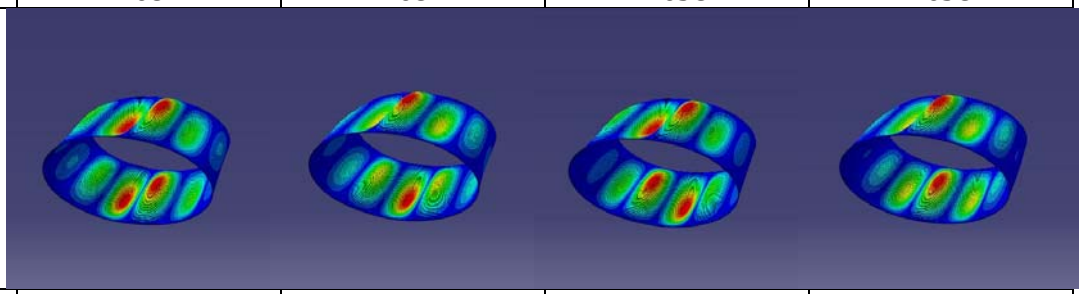			
	S6 1677	C6 1677	S7 1693	C7 1693

504 x150	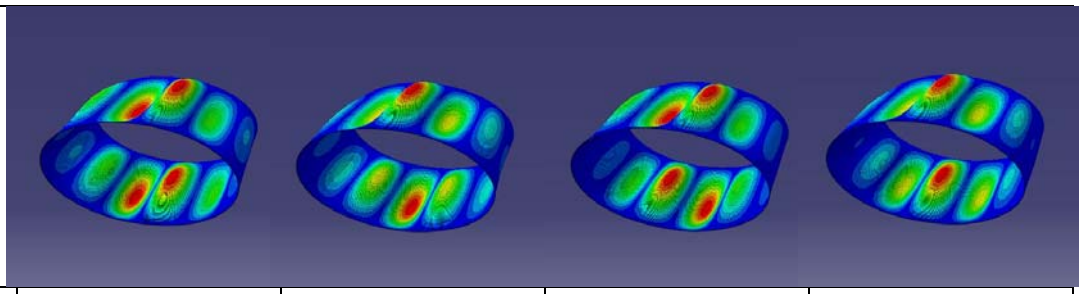			
	S6 1674	C6 1674	S7 1691	C7 1691
756 x228	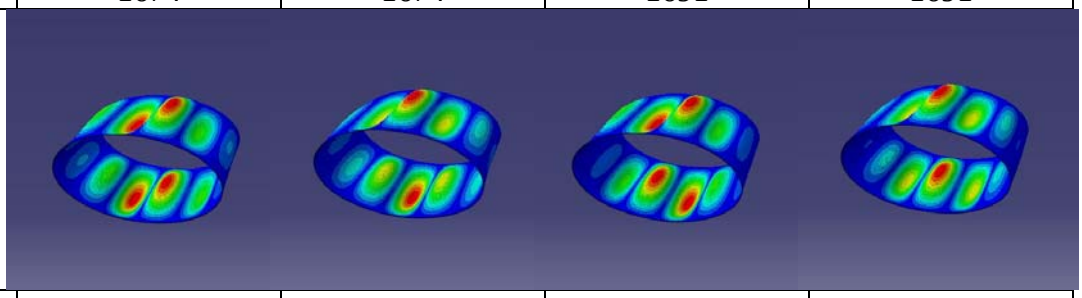			
	S6 1673	C6 1673	S7 1689	C7 1689

Appendix B Sine-based Fundamental Frequency of Elliptical Cylinders

In this appendix, the calculations from the developed formulations have been computed by using the sine-based functional form for $\Phi_n^w(s)$ and the corresponding forms for $\Phi_n^u(s)$ and $\Phi_n^v(s)$ as discussed in Table 3- 1. For Lo's approximation, Eq. 3- 74 and Eq. 3- 97, referring to simply-supported and clamped support cylinders, respectively, there are no separate cosine-based and sine-based equations. They are one and the same. For Abaqus calculation, even though cosine- and sine-based vibration modes sometimes refer to different frequencies, only the lower frequency between these two is the fundamental frequency. Hence, the results of Lo's approximation and Abaqus in this appendix are exactly the same as those in Ch. 4. The developed formulations without simplifications refer to Eq. 3- 68 and Eq. 3- 91 for simple supports and clamped supports, respectively. The 1st simplified formulations refer to Eq. 3- 71 and Eq. 3- 94 for simple supports and clamped supports, respectively. The 2nd simplified formulations refer to Eq. 3- 73 and Eq. 3- 96 for simple supports and clamped supports, respectively.

The figures in this appendix are analogs to Figs. 4- 5 through 4- 8, illustrating the fundamental frequencies for large and small simply-supported and clamped support cylinders with three laminates each from the two laminate families and L/C ranging from 0.30 to 1.0 with the most severe elliptical geometry (b/a = 0.55, or e = 0.85) in this study. The fundamental frequencies of large cylinders are normalized by 630 rad/s whereas those of small cylinders are normalized by 3490 rad/s.

The variations of the normalized fundamental frequencies of large elliptical cylinders with simple supports and clamped supports are illustrated in Figs. B- 1 and B- 2, respectively. The normalized fundamental frequencies of small elliptical cylinders with simple and clamped supports are illustrated in Figs. B- 3 and B- 4, respectively.

The comments made in chapter 4 regarding the cosine-based analysis results apply to the sine-based analysis results shown in this appendix.

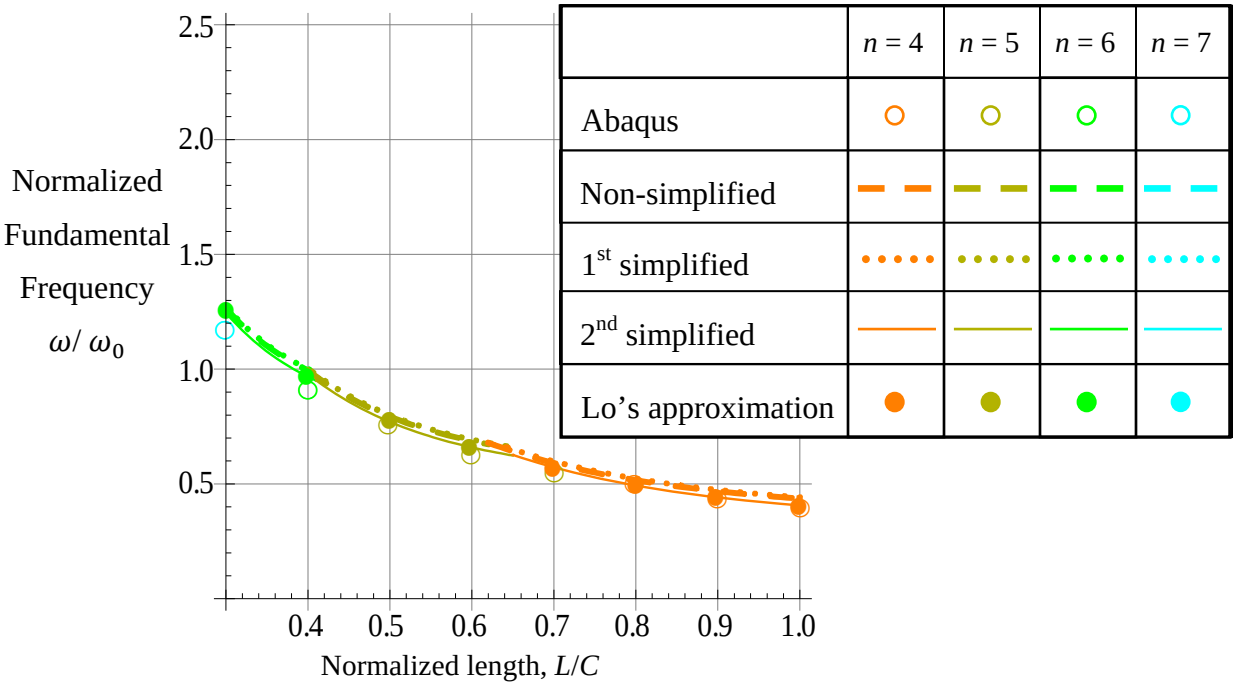

(a) Lamination sequences $[\pm 15/0/90]_{2S}$

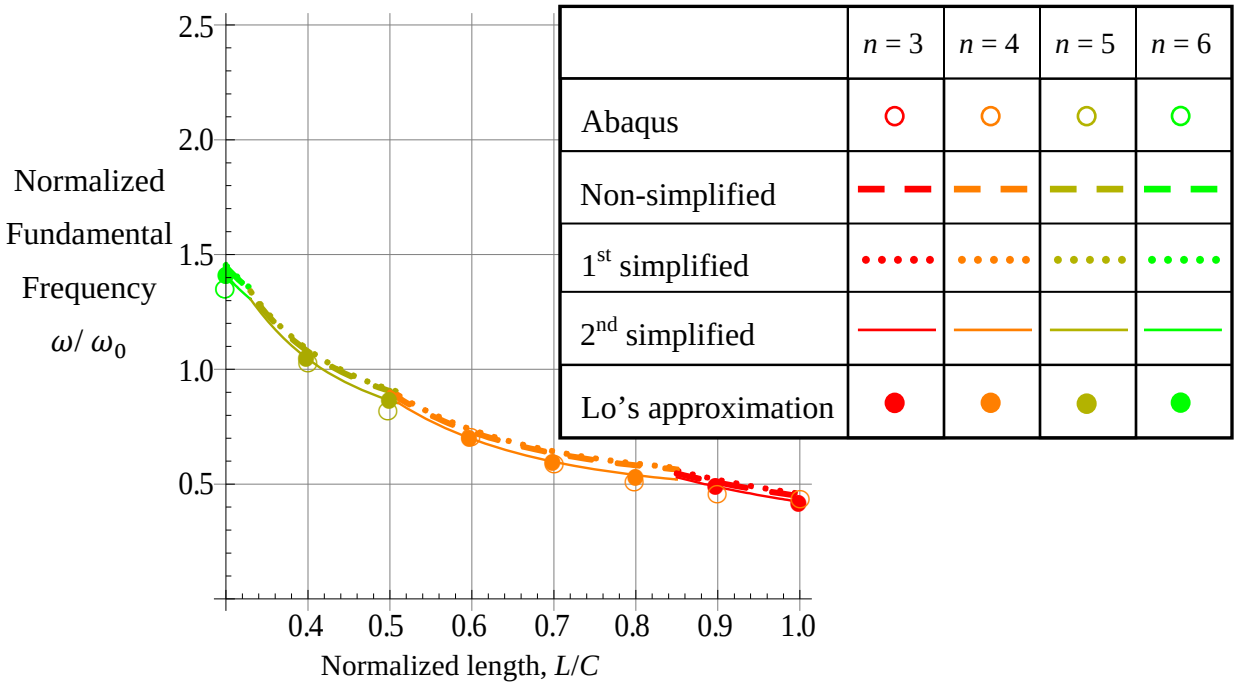

(b) Lamination sequences $[\pm 45/0/90]_{2S}$

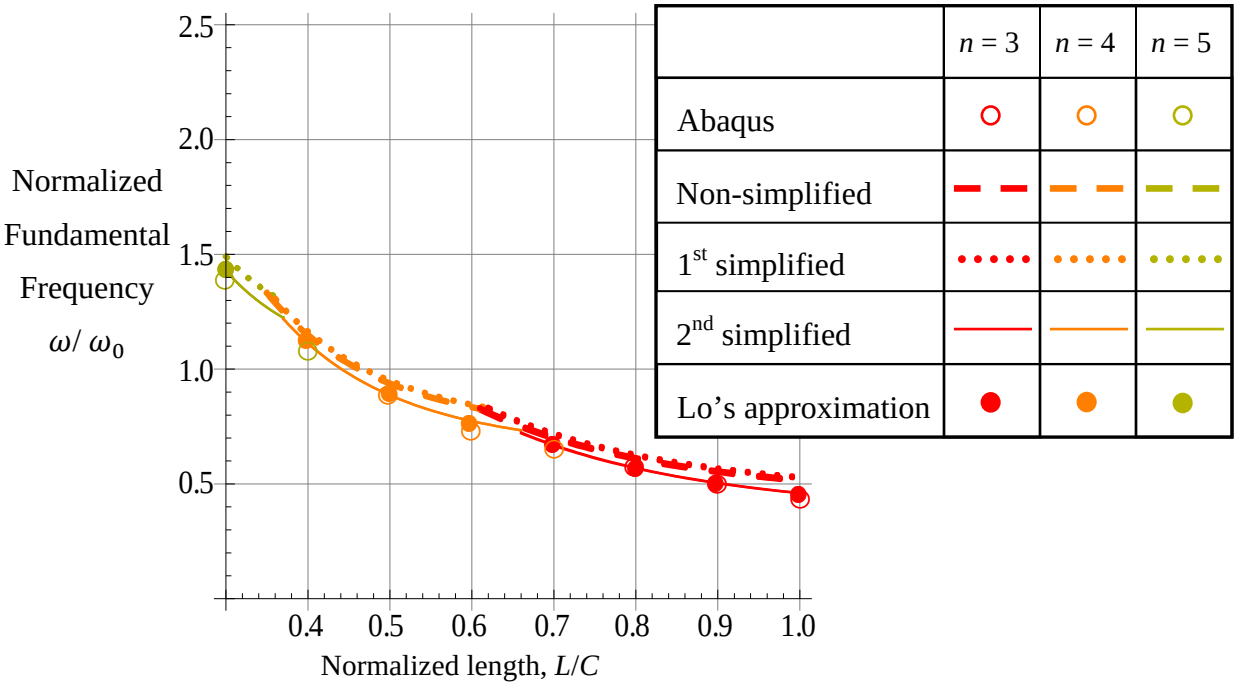

(c) Lamination sequences $[\pm 75/0/90]_{2S}$

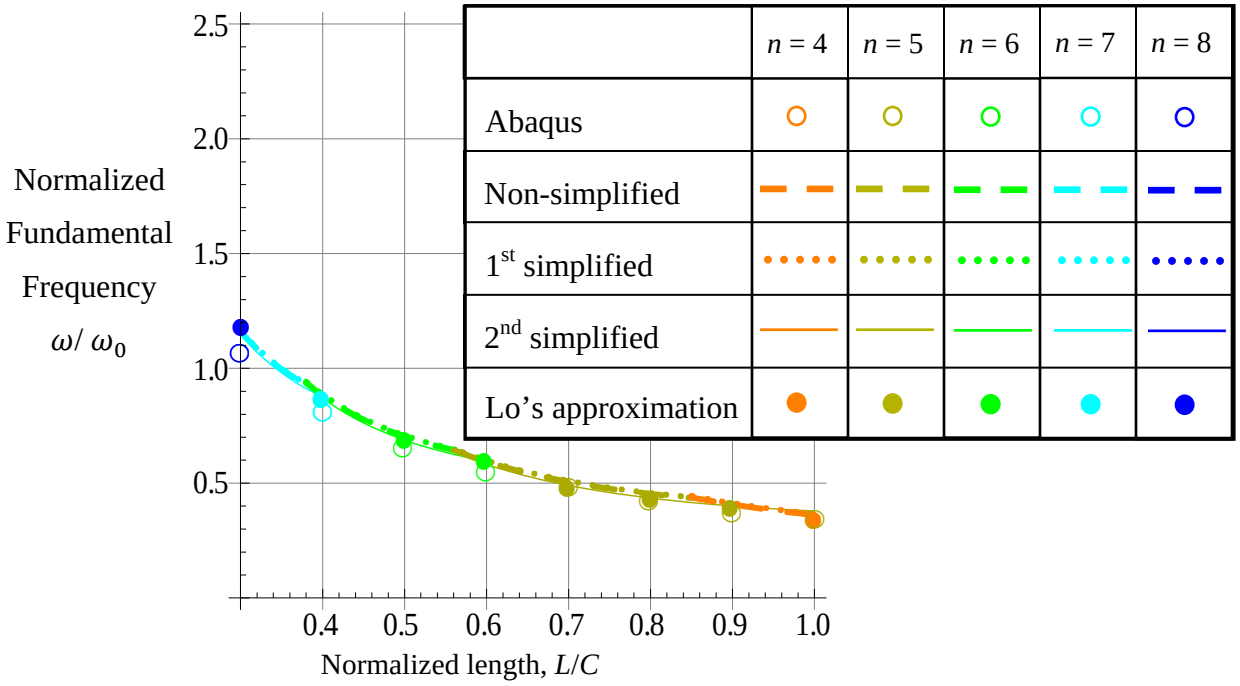

(d) Lamination sequences $[\pm 15]_{4S}$

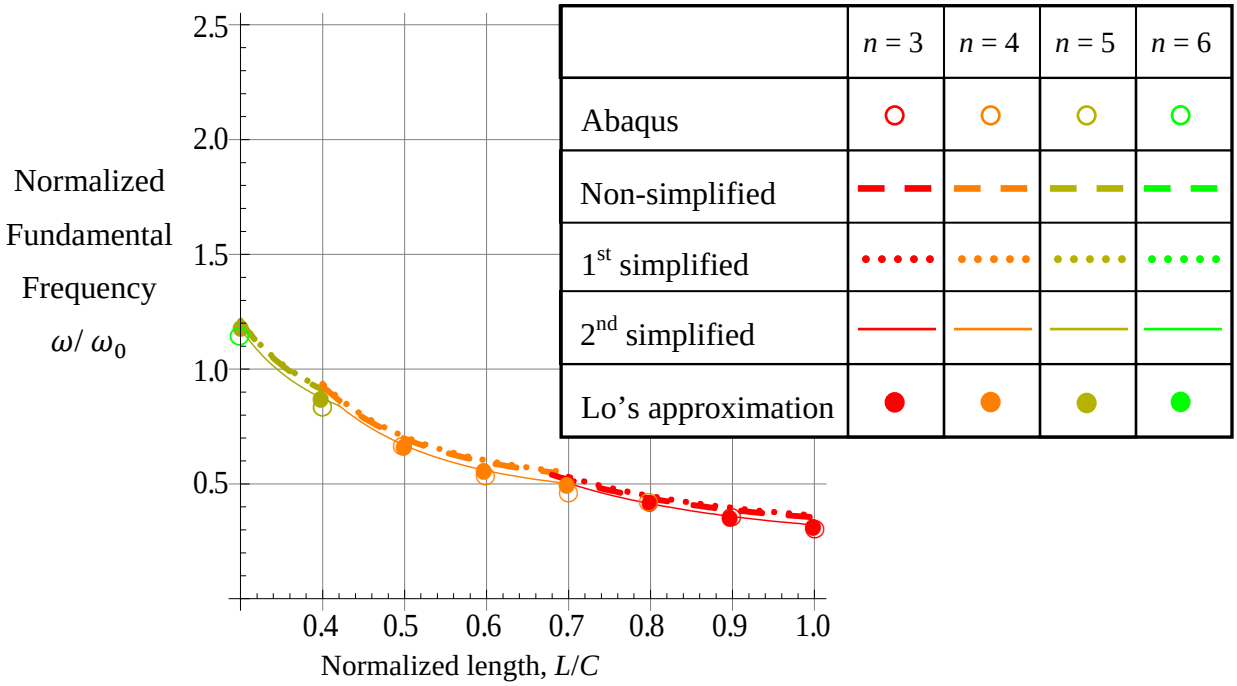

(e) Lamination sequences $[\pm 45]_{4S}$

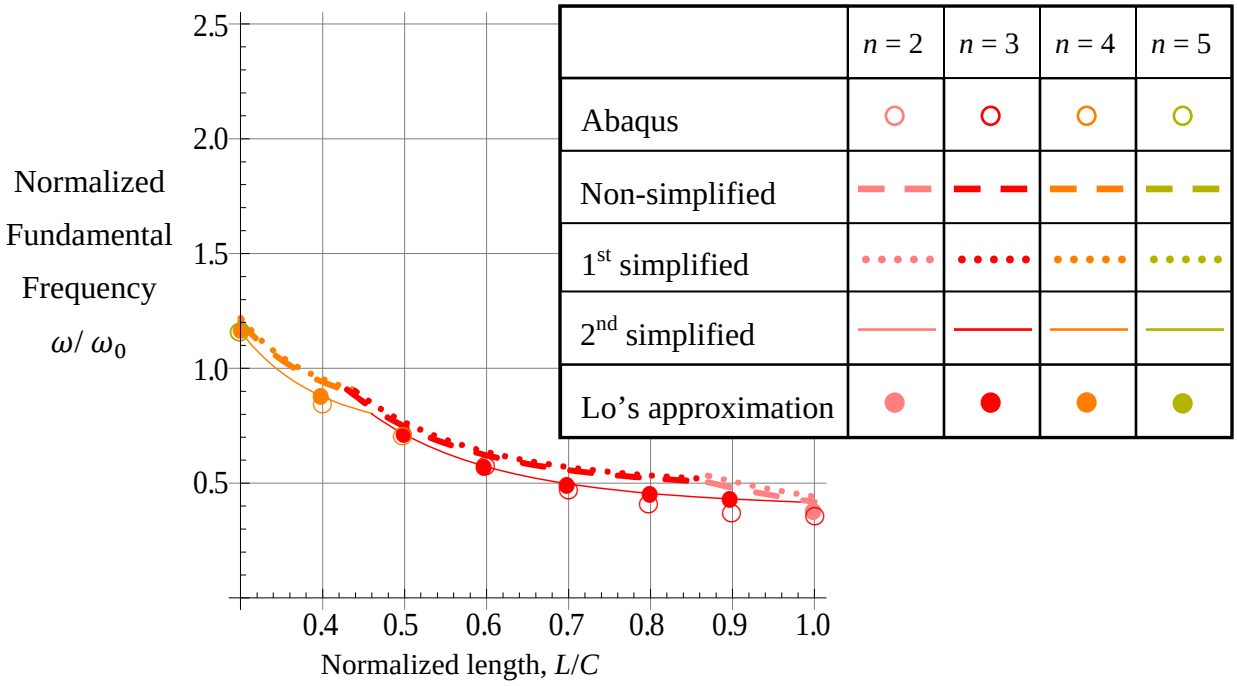

(f) Lamination sequences $[\pm 75]_{4S}$

Fig. B- 1 Normalized fundamental frequency of large elliptical cylinders, $b/a = 0.55$ ($e = 0.84$), simple supports, sine-based

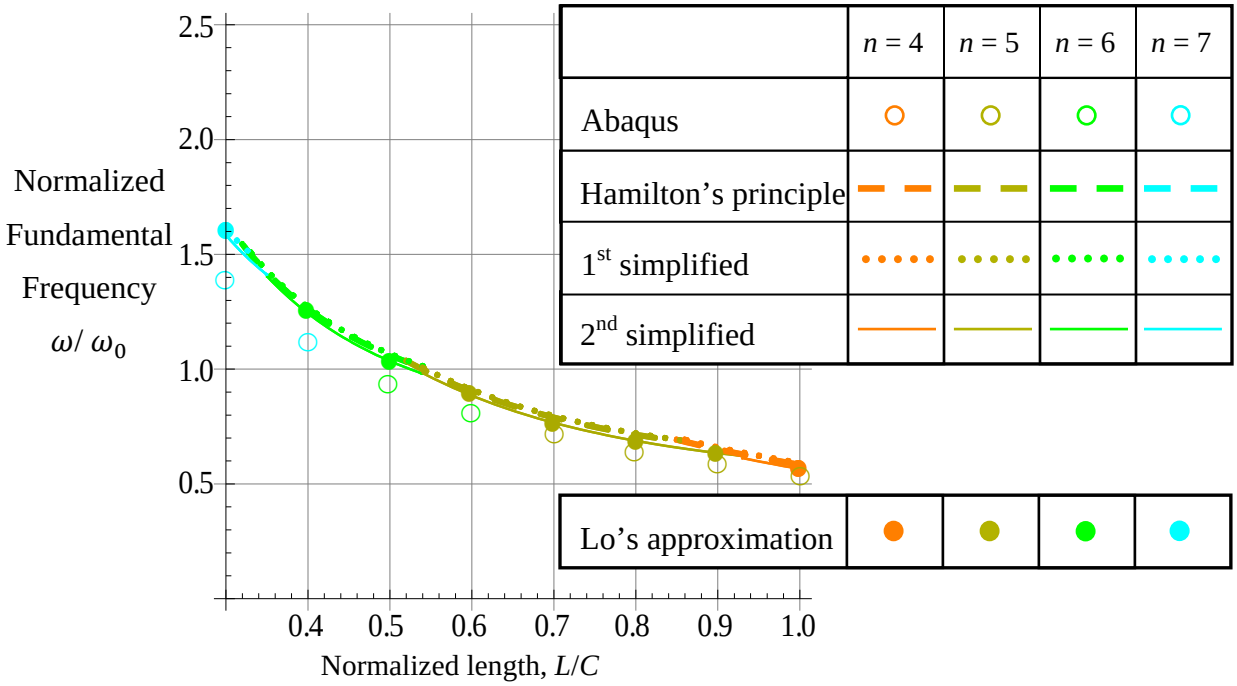

(a) Lamination sequences $[\pm 15/0/90]_{2S}$

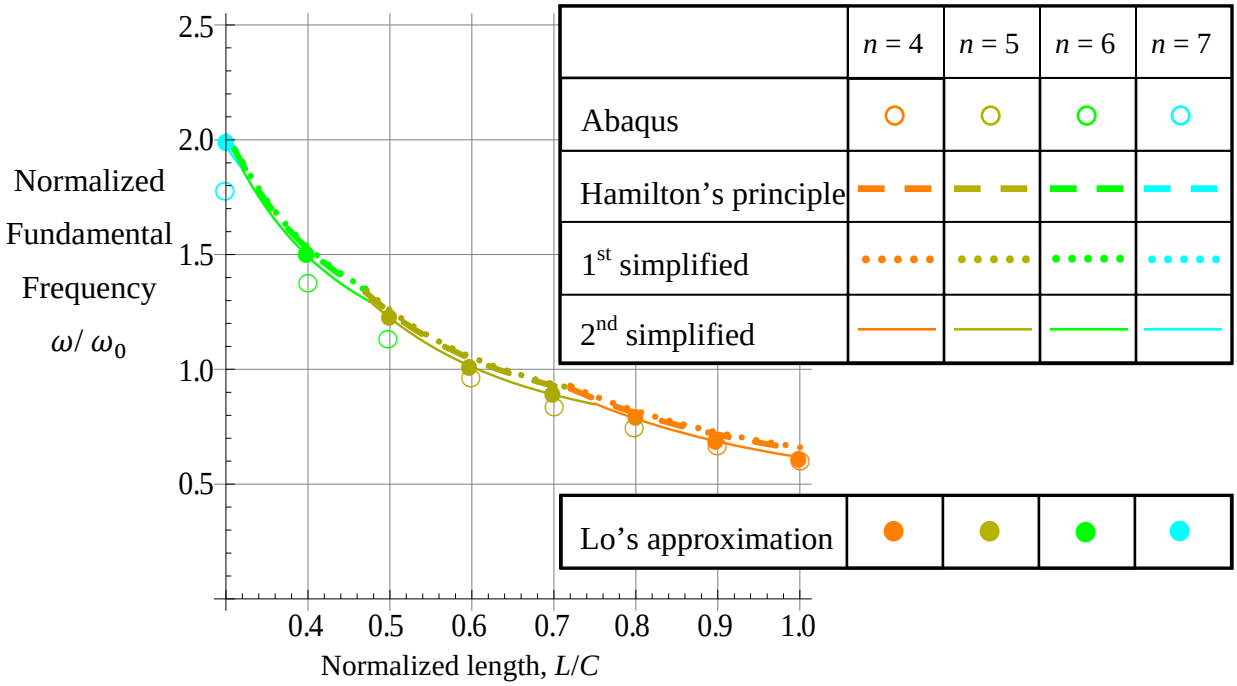

(b) Lamination sequences $[\pm 45/0/90]_{2S}$

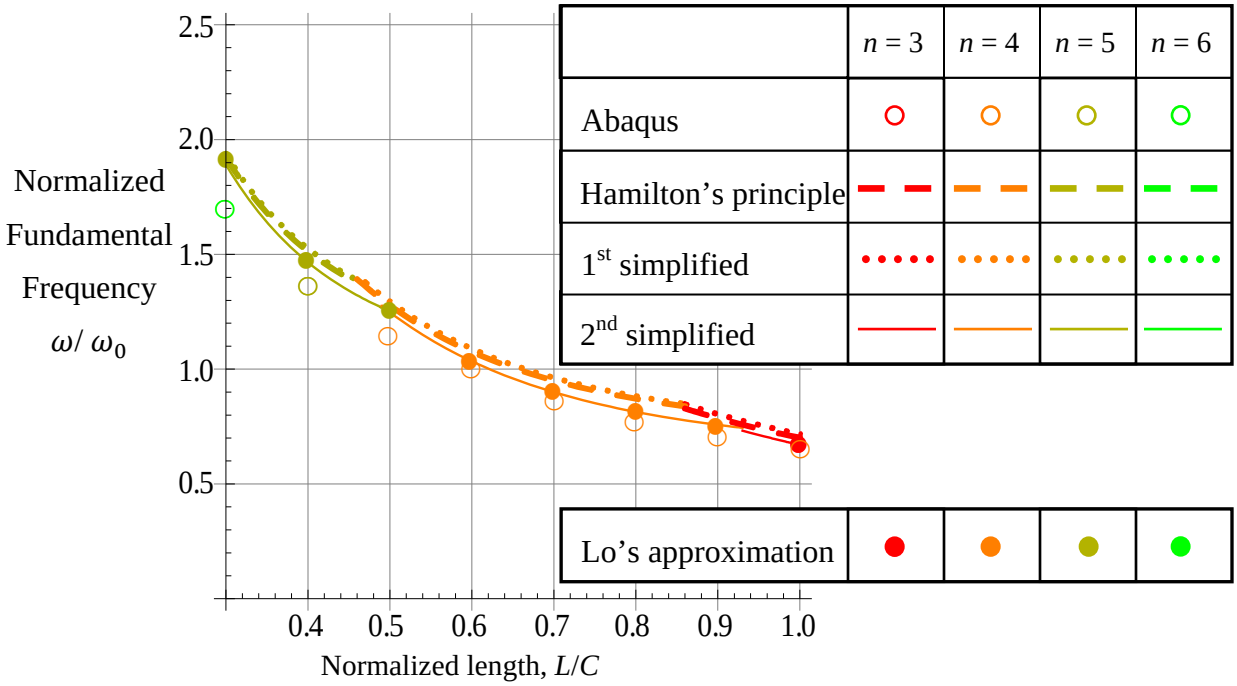

(c) Lamination sequences $[\pm 75/0/90]_{2S}$

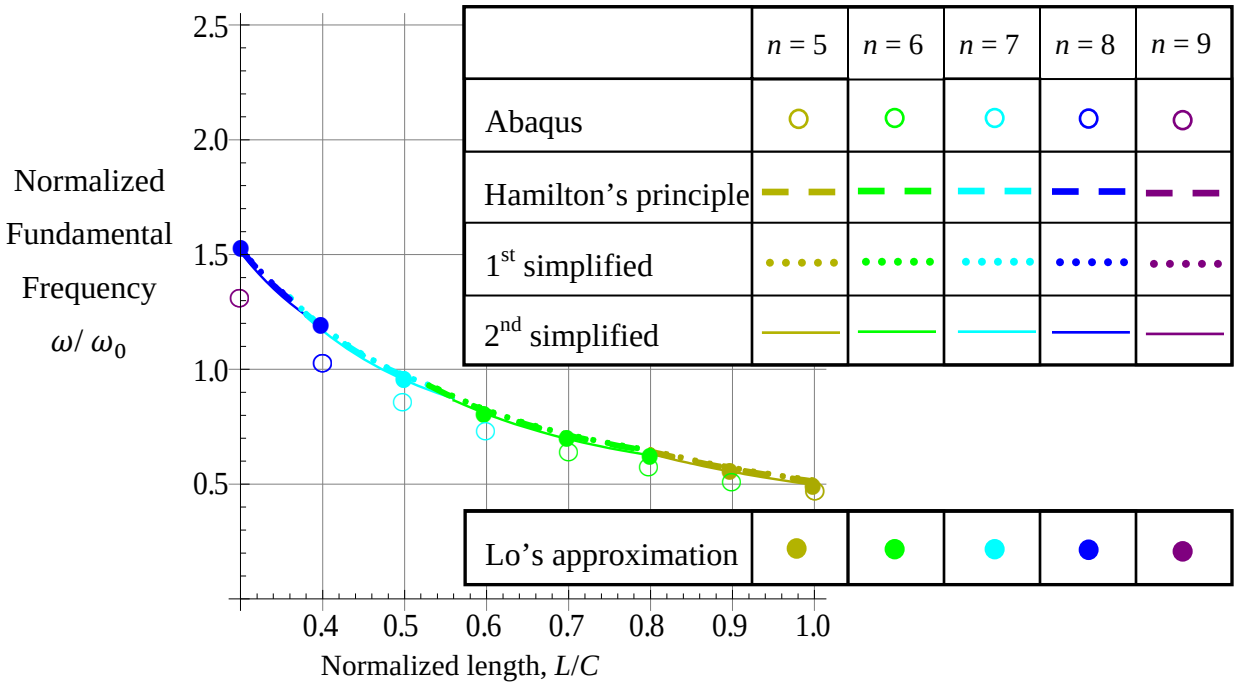

(d) Lamination sequences $[\pm 15]_{4S}$

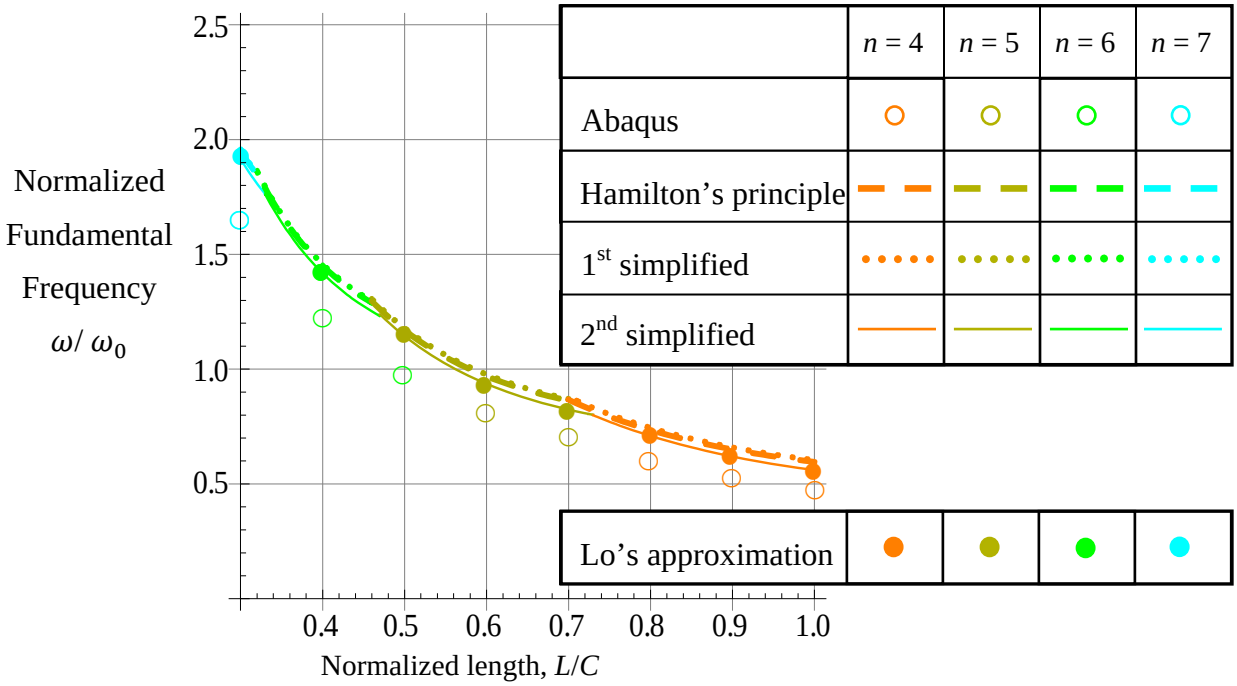

(e) Lamination sequences $[\pm 45]_{4S}$

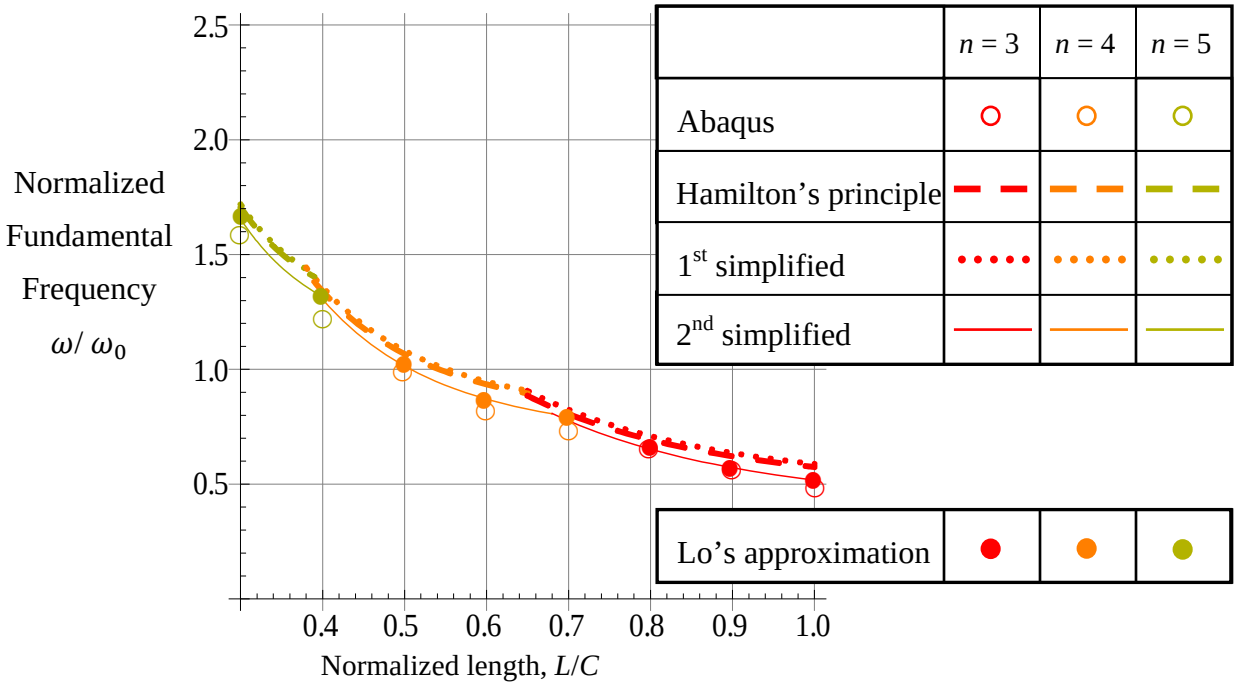

(f) Lamination sequences $[\pm 75]_{4S}$

Fig. B- 2 Normalized fundamental frequency of large elliptical cylinders, $b/a = 0.55$ ($e = 0.84$), clamped supports, sine-based

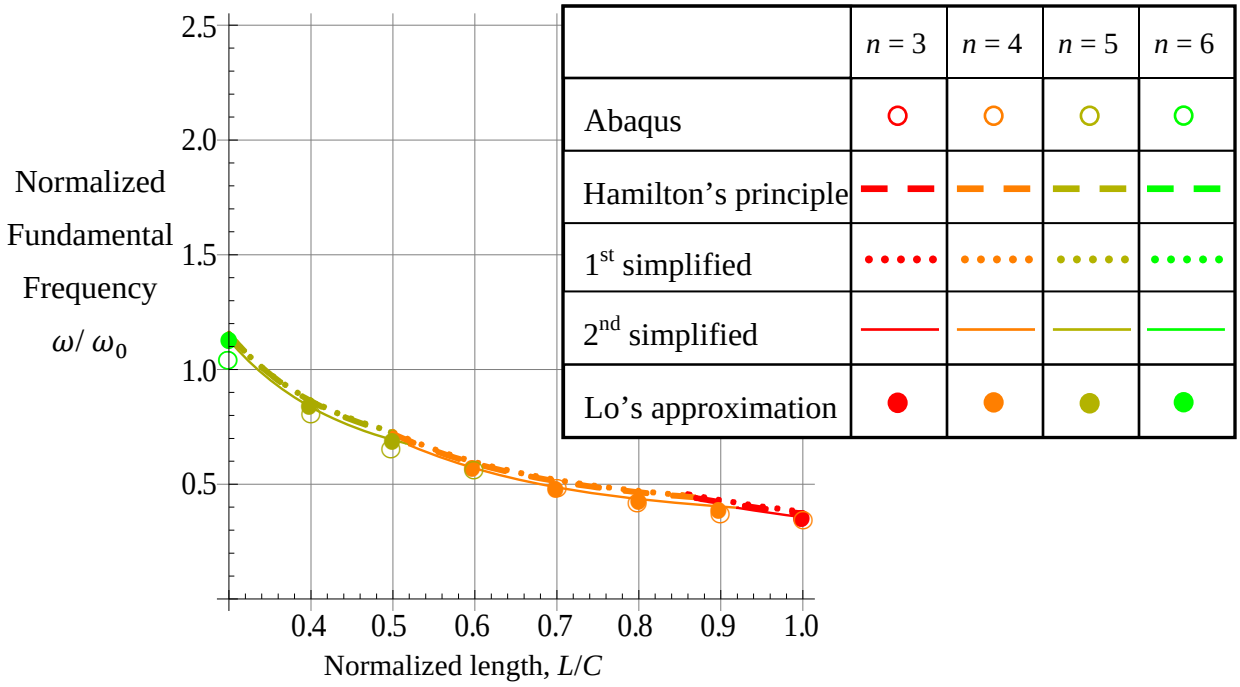

(a) Lamination sequences $[\pm 15/0/90]_S$

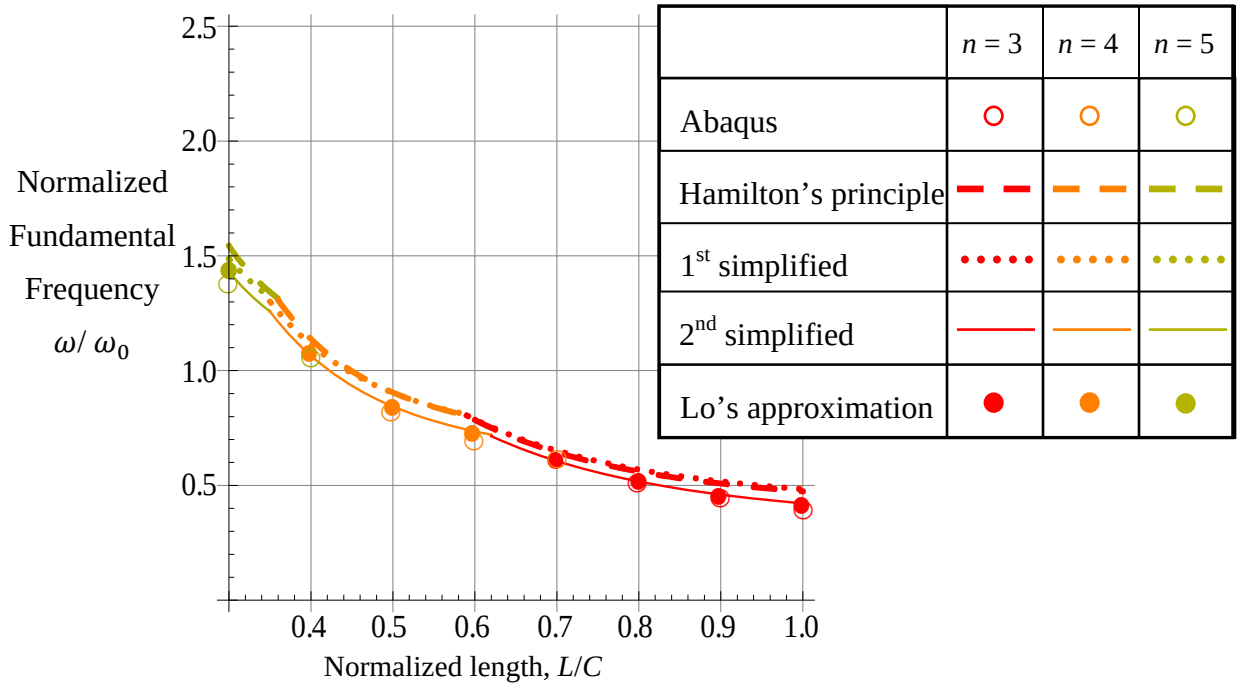

(b) Lamination sequences $[\pm 45/0/90]_S$

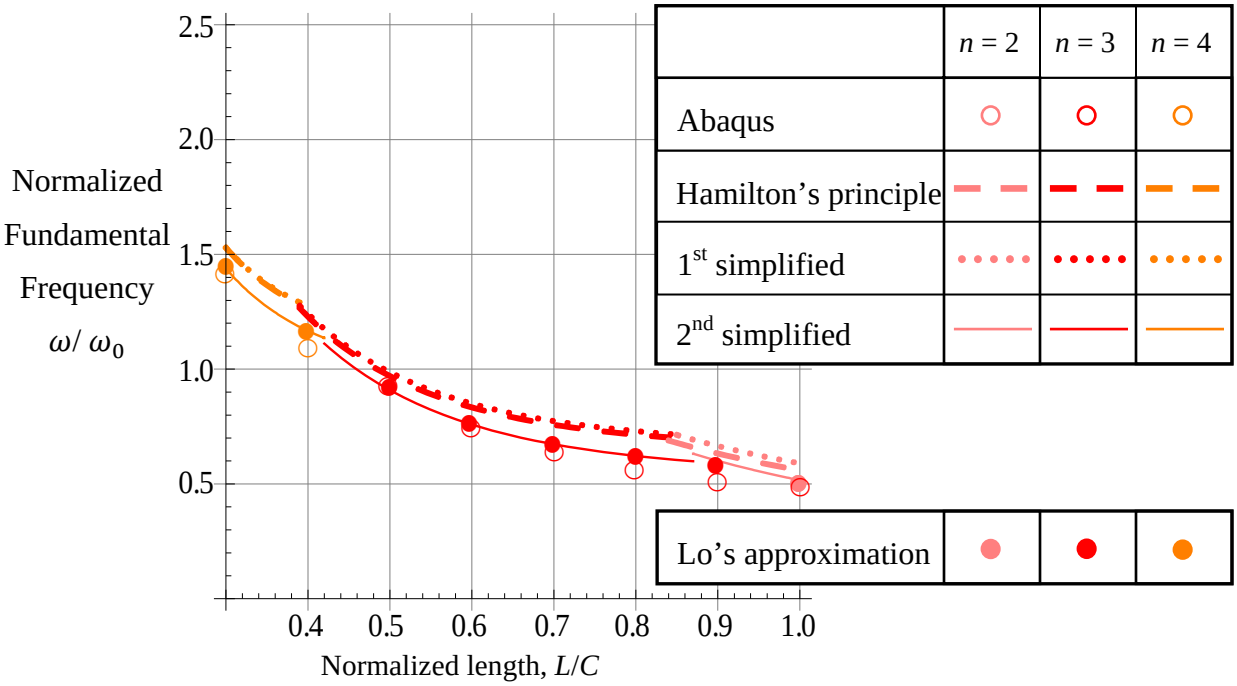

(c) Lamination sequences $[\pm 75/0/90]_S$

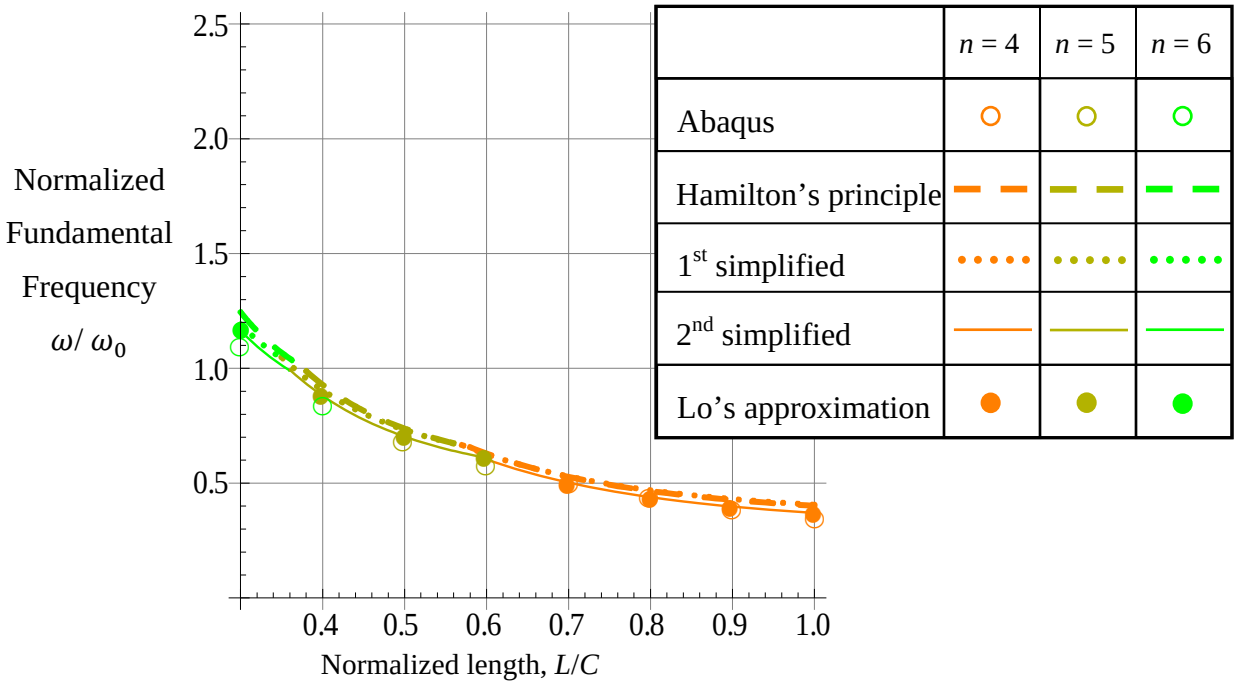

(d) Lamination sequences $[\pm 15]_{2S}$

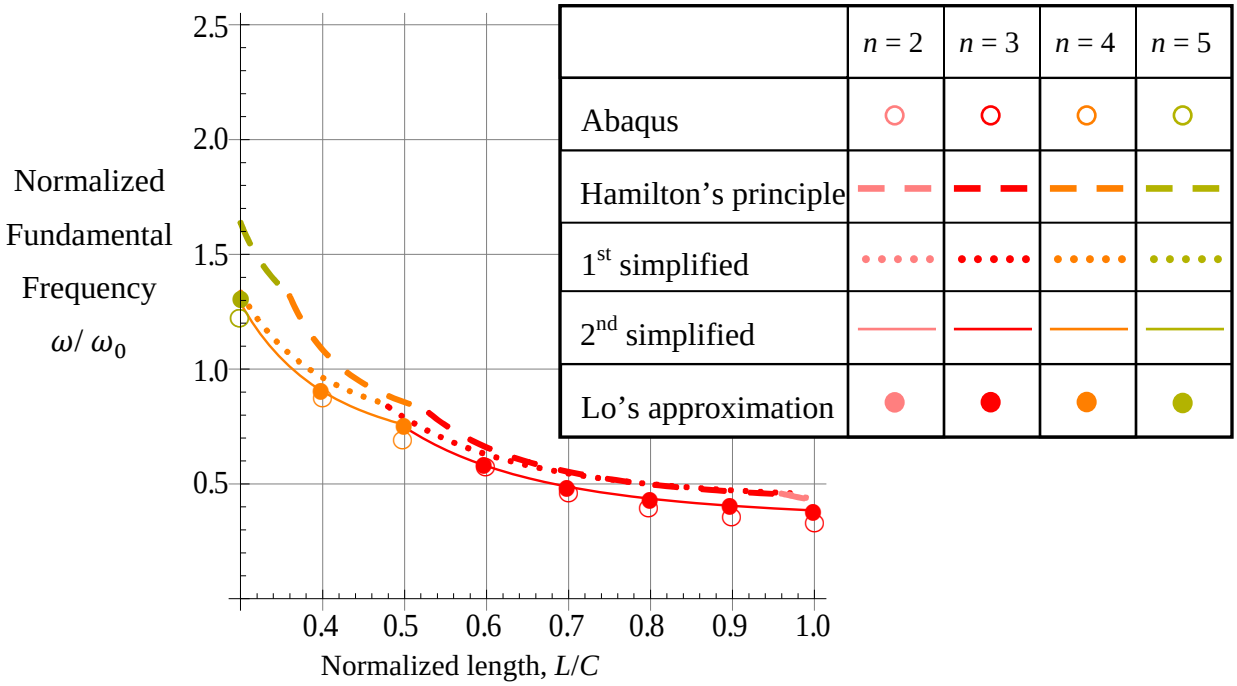

(e) Lamination sequences $[\pm 45]_{2S}$

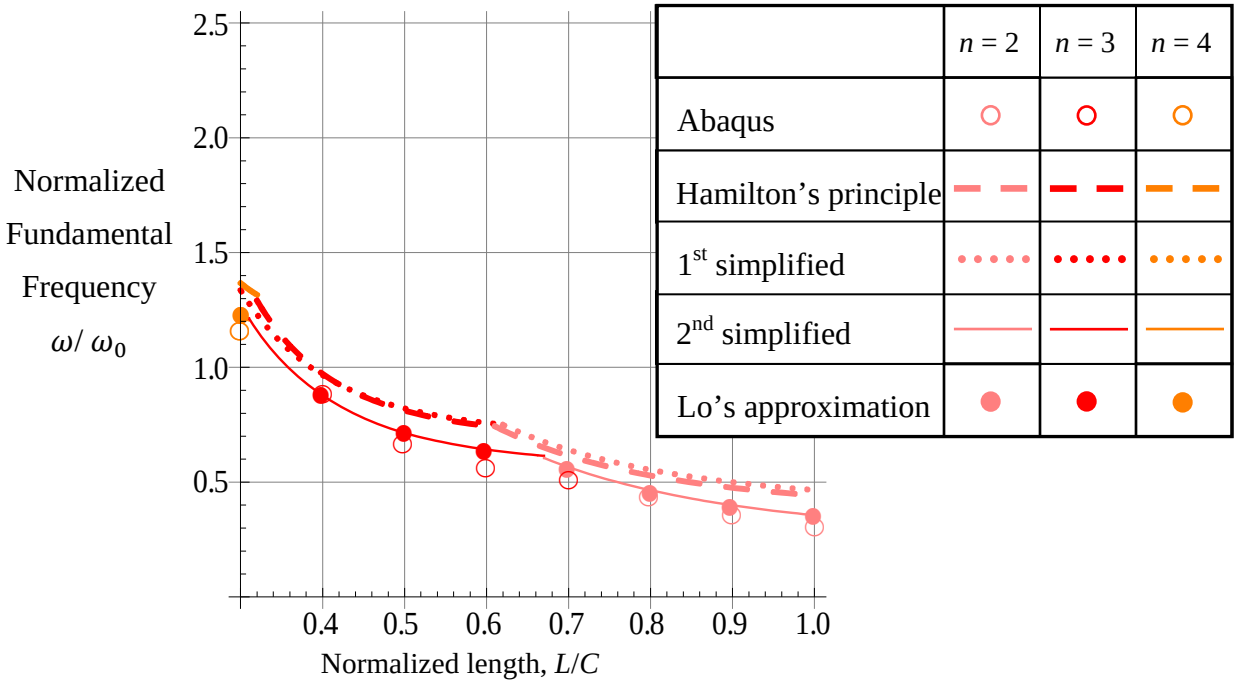

(f) Lamination sequences $[\pm 75]_{2S}$

Fig. B- 3 Normalized fundamental frequency of small elliptical cylinders, $b/a = 0.55$ ($e = 0.84$), simple supports, sine-based

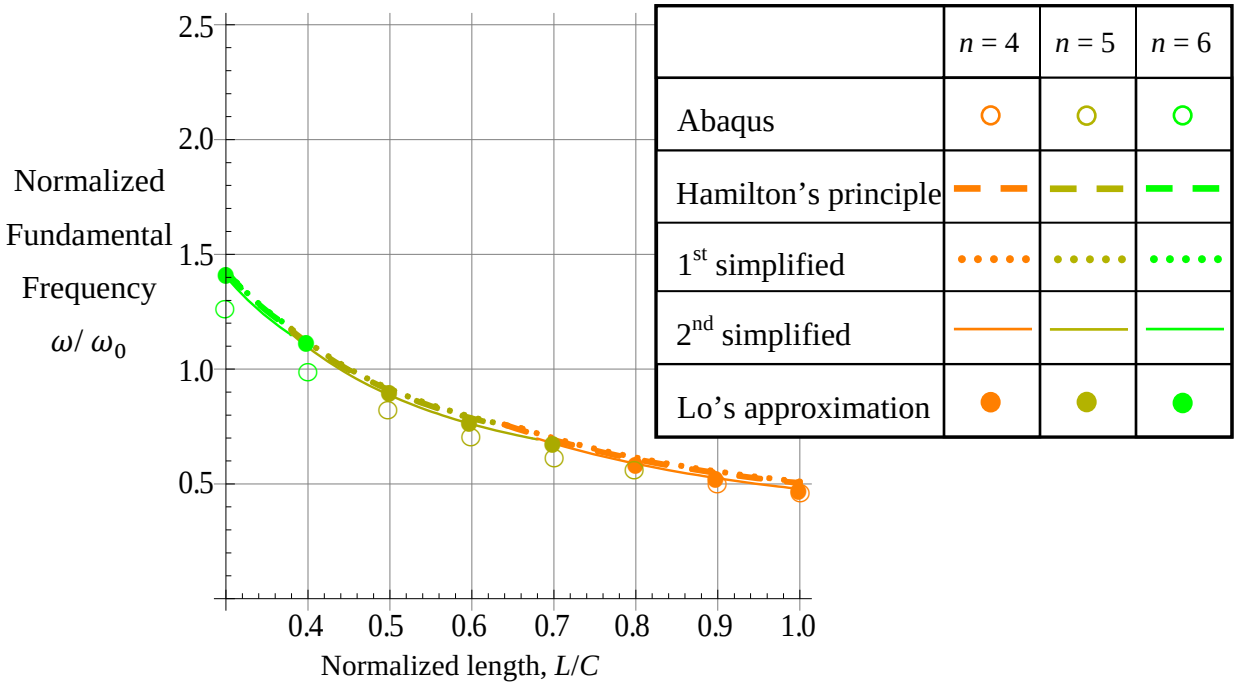

(a) Lamination sequences $[\pm 15/0/90]_S$

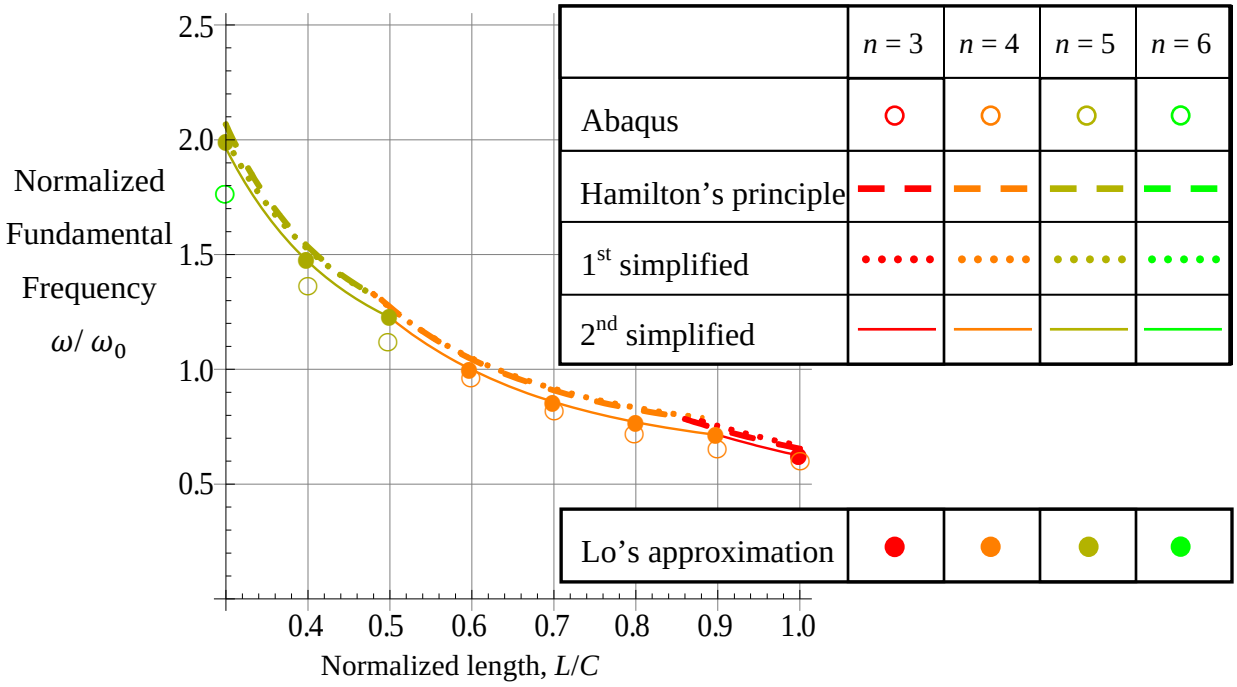

(b) Lamination sequences $[\pm 45/0/90]_S$

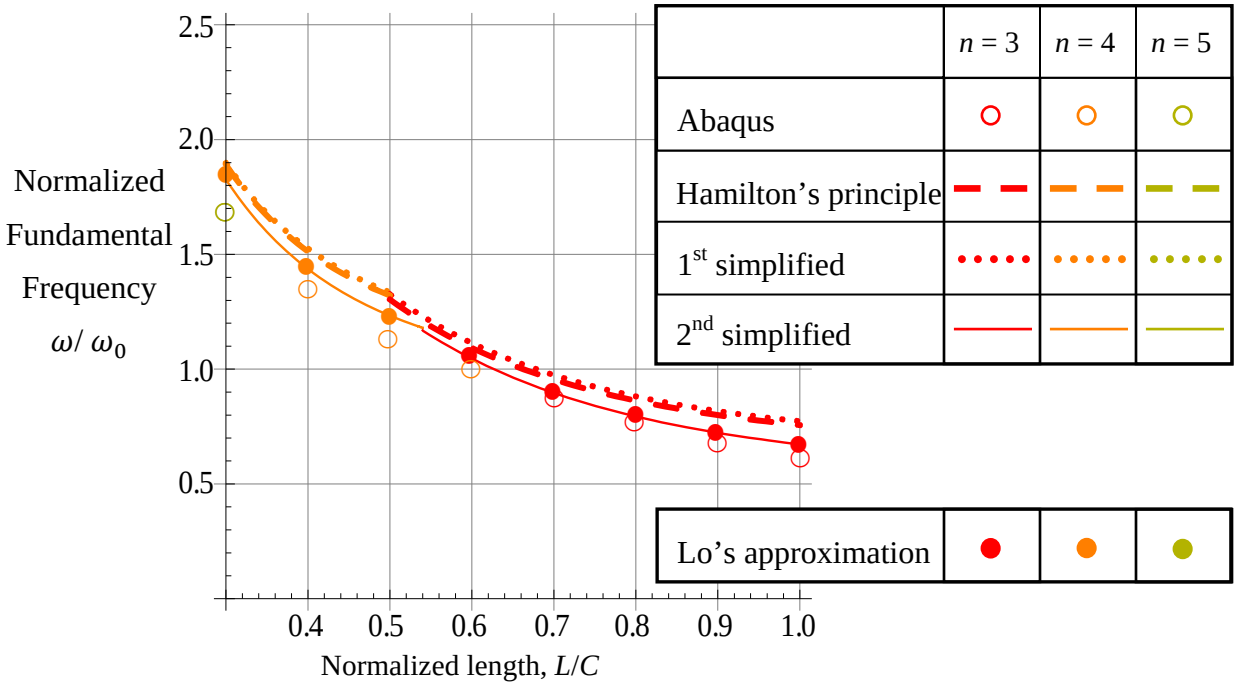

(c) Lamination sequences $[\pm 75/0/90]_S$

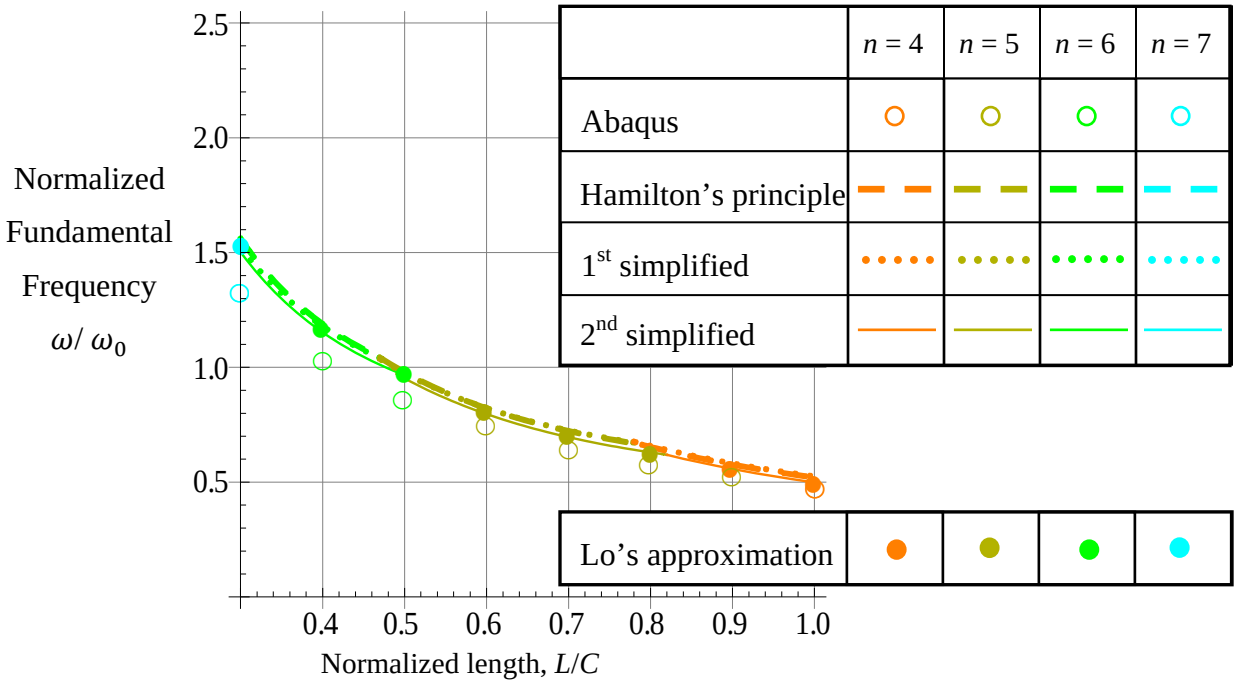

(d) Lamination sequences $[\pm 15]_{2S}$

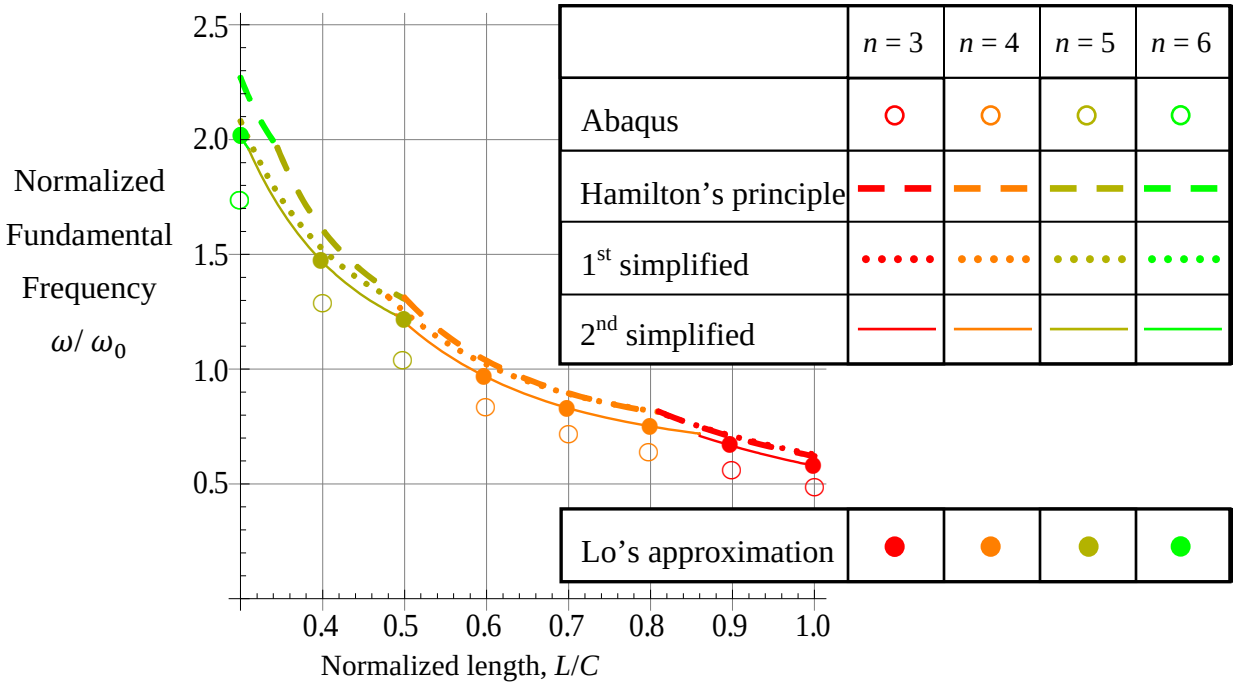

(e) Lamination sequences $[\pm 45]_{2S}$

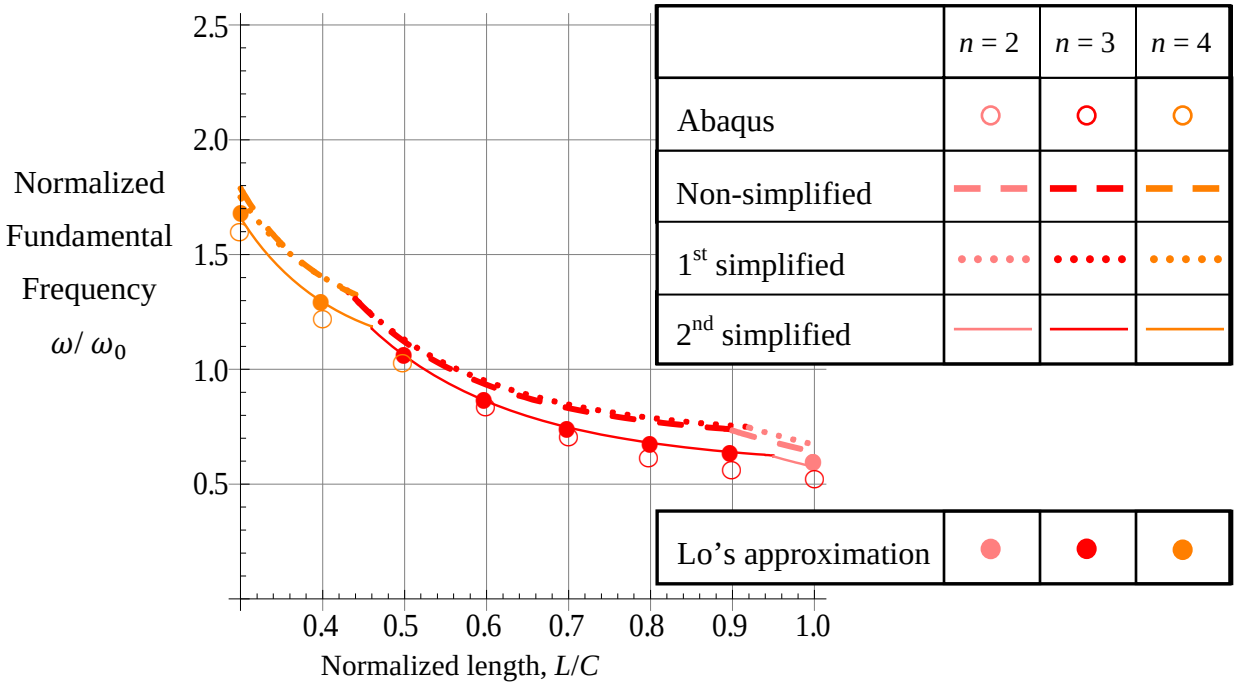

(f) Lamination sequences $[\pm 75]_{2S}$

Fig. B- 4 Normalized fundamental frequency of small elliptical cylinders, $b/a = 0.55$ ($e = 0.84$), clamped supports, sine-based